



HAL
open science

Chemoenzymatic synthesis of glycosphingolipid analogues and biological evaluation of their anticancer activities

Fang Liu

► **To cite this version:**

Fang Liu. Chemoenzymatic synthesis of glycosphingolipid analogues and biological evaluation of their anticancer activities. Organic chemistry. Sorbonne Université, 2023. English. NNT : 2023SORUS150 . tel-04497389

HAL Id: tel-04497389

<https://theses.hal.science/tel-04497389v1>

Submitted on 10 Mar 2024

HAL is a multi-disciplinary open access archive for the deposit and dissemination of scientific research documents, whether they are published or not. The documents may come from teaching and research institutions in France or abroad, or from public or private research centers.

L'archive ouverte pluridisciplinaire **HAL**, est destinée au dépôt et à la diffusion de documents scientifiques de niveau recherche, publiés ou non, émanant des établissements d'enseignement et de recherche français ou étrangers, des laboratoires publics ou privés.



THÈSE DE DOCTORAT DE SORBONNE UNIVERSITÉ

(ÉCOLE DOCTORALE: Chimie Moléculaire de Paris Centre – ED 406)

Spécialité : **Chimie Organique**

Présentée par **Mme. Fang LIU**

Pour obtenir le grade de

Docteur de Sorbonne Université

**Chemoenzymatic synthesis of glycosphingolipid analogues and
biological evaluation of their anticancer activities**

Directeur de recherches : **Dr. Yongmin ZHANG**

Soutenance prévue le : **09/03/2023**

Devant un jury composé de :

Madame	Laurence MULARD	Directeur de Recherche	Rapportrice
Monsieur	Boris VAUZEILLES	Directeur de Recherche	Rapporteur
Monsieur	Christian CAVÉ	Professeur	Examinateur
Madame	Virginie MOURIÈS-MANSUY	Professeure	Examinatrice
Monsieur	Matthieu SOLLOGOUB	Professeur	Co-Directeur de thèse
Monsieur	Yongmin ZHANG	Directeur de Recherche	Directeur de thèse

To my family

Contents

Acknowledgments	7
Abbreviations	9
Abstract	13
Résumé	15
Chapter I Introduction	17
1.1. Glycosphingolipids	21
1.1.1. The family of glycosphingolipids	21
1.1.2. Biological functions of glycosphingolipids	22
1.2. Gangliosides	25
1.2.1. Structure and function of sialic acid	25
1.2.2. Structure and classification of gangliosides	26
1.2.3. Biological functions of gangliosides	27
1.3. Ganglioside GM3	30
1.3.1. Structure of ganglioside GM3	30
1.3.2. Biological functions of ganglioside GM3	30
1.4. Synthesis of ganglioside GM3 analogues	38
1.4.1. Modification of sialic acid block	39
1.4.2. Modification of lactose block	40
1.4.3. Modification of ceramide block	41
1.5. Multivalent ligand effect	42
1.6. Background of this project	44
Chapter II Synthesis of mannose-containing GM3 analogue monomer	47
2.1. Introduction	49
2.2. Retrosynthetic analysis	49
2.3. Preparation of sialic acid donor block	50
2.4. Preparation of mannose glycosyl receptor block	51
2.5. Preparation of azidosphingosine block	52
2.6. Synthesis of mannose-containing GM3 analogue	54
Chapter III Synthesis of mannose-containing GM3 analogue oligomers with small molecule skeletons based on "click chemistry"	59
3.1. Introduction	61
3.2. Retrosynthetic analysis	61
3.3. Preparation of small molecular skeletons	62

3.4. Synthesis of dimer, trimer and tetramer of mannose-containing GM3 analogues	63
Chapter IV Biological evaluation of oligomers of mannose-containing GM3 analogues based on small molecular skeletons	67
4.1. Introduction.....	69
4.2. Experimental methods	69
4.2.1. Cell culture	69
4.2.2. MTT cytotoxicity assay	70
4.2.3. Cell colony formation assay	70
4.2.4. Wound healing test	71
4.2.5. Transwell migration and invasion assay	71
4.2.6. Western blot assay.....	72
4.3. Results and discussion	73
4.3.1. M1, M2, M3, and M4 inhibited tumor cell growth.....	73
4.3.2. M1, M2, M3, and M4 inhibited tumor cell migration and invasion.	76
4.3.3. M1, M2, M3, and M4 inhibited EMT via EGFR/VEGFR- β -catenin signaling pathway.....	83
Chapter V Synthesis of mannose-containing GM3 analogue oligomers with macromolecular skeletons based on "click chemistry"	87
5.1. Introduction.....	89
5.2. Retrosynthetic analysis	89
5.3. Preparation of macromolecular skeletons.....	91
5.4. Synthesis of hexamer and heptamer of mannose-containing GM3 analogues	94
Chapter VI Synthesis of GM3	97
6.1. Introduction.....	99
6.1.1. Retrosynthetic analysis of chemoenzymatic synthesis of GM3.....	99
6.1.2. Preparation of the per-acetylated lactosyl trichloroacetimidate block	100
6.1.3. Preparation of the lactosyl sphingosine	101
6.1.4. Chemoenzymatic synthesis of GM3.....	102
6.1.5. Retrosynthetic analysis of chemical synthesis of GM3	104
6.1.6. Preparation of the lactoside block.....	105
6.2. Construction of the GM3 by glycosylation of these three sugar units.....	105
Summary and Perspective	108
Experimental section	111
Bibliography.....	186

Acknowledgments

I am very happy that there is an “acknowledgement” section in the thesis, which allows me to write down what I would like to say as a thank you, even though I am not very expressive.

Firstly, I would like to sincerely thank all the members of the jury for your willingness to take the time to read my manuscript and attend my defense, as well as for your efforts.

Looking back on my four years of study, I am particularly grateful to my supervisor, Dr. Yongmin ZHANG, for giving me the opportunity to study in the GOBS team, for his patient teaching and professional help in my research, for his encouragement and support whenever I was not confident, and for his kind care and concern in my daily life.

Many thanks to Prof. Matthieu SOLLOGOUB for his guidance and help during the learning process, and for his tolerance and kindness towards me.

I am deeply grateful to Prof. Jianhua XU and Dr. Yan LIU from Fujian Medical University for their dedication to this part of the experiment on bioactivity testing. The effective communication between us has made my learning in the biological experiments very rewarding. I also want to thank Prof. Marco TERRENI from the University of Pavia for providing the CRL enzyme and guidance on enzymatic hydrolysis studies. I would like to thank Dr. Xin MENG from Tianjin University of Science and Technology for providing the enzymes NmCSS and PmST1 and for guidance on the "one pot, multiple enzyme" synthesis method.

Sincere thanks to Mickaël MÉNAND for providing us with a well-organized laboratory environment. Whenever there is a breakdown of equipment, he is always there like a superhero to fix it as soon as he can so that our experiments can always run smoothly. I would like to thank Guillaume VIVÈS for being with us every time we work overtime, as he makes it possible for us to do our experiments without worrying about the sudden appearance of the safety wardens. Speaking of safety, I would like to thank Sylvain ROLAND for always supervising me to put on my glasses and lab coat before working, as his presence makes our safety more secure.

I would like to thank Dr. Changping ZHENG for his guidance on my project, Dr. Zhihao LI for taking me through the experiments together so that I could avoid a lot of errors in details that are easily overlooked, and Jiayu ZHANG for helping me in the field of molecular biology. I would like to thank Thanaphon KHRUEAWATTHANAWET, who is in the same lab room with me, for bringing me a lot of pleasure. I would like to thank Dr. Jiang LIU, Dr. Wenting HU, Dr. Guangcan XU, Dr. Zhonghang WEN, Dr. Lisa TANZI, Enxu LIU, Jinge CAO, Yupeng FU, He WANG, Clara TESTARD, Hugo MADEC, Laora BOULO, Rebecca CHURAMANI and all those who are not mentioned here for their care and help in my study and life.

I would like to express my appreciation to Omar KHALED for teaching me how to use HRMS and data processing. I want to thank Claire TROUFFLARD, Régina MARUCHENKO and Aurélie BERNARD for training me in the use of NMR and for not hesitating to help me when I needed them. I am grateful to Sylvie PALLER-JAMMES, Christel VENTURINI and Dominique BENVENT-RANGUIN for their assistance and help.

Thanks for meeting, for the experience and for the wonderful memories made in Paris.

Last but not least, I would like to thank my father Guojun LIU, my mother Yuxia CAO, my father-in-law Zhanwu LIU, my mother-in-law Qingling XIA, my sister Yang LIU, my brother-in-law Xuchen ZOU, my nephew Yinuo ZOU, my husband Haipeng LIU and other family members for their support and for your love along the way.

Abbreviations

Ac	Acetyl
AgOTf	Silver trifluoromethanesulfonate
BHK	Baby hamster kidney
BF ₃ ·Et ₂ O	Boron trifluoride diethyl etherate
Bz	Benzoyl
Bn	Benzyl
calcd	Calculated value
C	Concentration
CCI	Carbohydrate-to-carbohydrate interaction
Cer	Ceramide
CD	Cyclodextrin
COSY	Correlation spectroscopy
Cy	Cyclohexane
CTP	Cytidine triphosphate
CMAH	Cytidine monophosphate N-acetylneuraminic acid hydroxylase
c-Met	tyrosine-protein kinase Met or hepatocyte growth factor receptor
c-Src	Cellular Src kinase
Csk	C-terminal Src kinase
d	Doublet
DCM	Dichloromethane
dd	doublet of doublet
DTBP	2,6-di(tert-butyl)pyridine
DMF	<i>N, N</i> --Dimethylformamide
DMSO	Dimethyl sulfoxide
DBU	1,8-diazabicyclo[5.4.0]undec-7-ene
DMAP	4-dimethylaminopyridine
eq	Equivalent
EMT	Epithelial-mesenchymal transition

ESI	Electro--Spray Ionisation
EtOAc	Ethyl acetate
EGF	Estimated growth factor
EGFR	Estimated growth factor receptor
ECD	Extracellular structural domain
FAK	Focal adhesion kinase
FGFR	Fibroblast growth factor receptor
GFRs	Growth factor receptors
h	Hour
HRMS	High-resolution mass spectrometry
Hz	Hertz
HGF	Hepatocyte growth factor
<i>J</i>	Coupling constant
Kdn	Keto-deoxynonanulonic acid
Lac	Lactose
LacCer	Lactosylceramide
Ln5	Laminin-5
PDGFR	Platelet-derived growth factor receptor
<i>m/z</i>	Isotopic mass--to charge ratio
min	Minutes
MS	Mass spectrometry
Me	Methyl
MAPK	Mitogen-Activated Protein Kinase
NMR	Nuclear magnetic resonance
NGFR	Nerve Growth Factor Receptor
Neu	Neuraminic acid
Neu5Ac	N-acetylneuraminic acid
Neu5Gc	N-glycolylneuraminic acid
Ph	Phenyl

PhSCl	Benzenesulfonyl chloride
ppm	Parts per million
PTSA	<i>P</i> -toluenesulfonic acid
Py	2-formylpyridine
PMCA	Plasma membrane Ca ²⁺ ATPase
q	Quadruplet
quant	Quantitative
r. t.	Room temperature
s	Singlet
t	Triplet
TBDMSCl	<i>Tert</i> -butyldimethylsilyl chloride
TFA	Trifluoroacetic acid
THF	Tetrahydrofuran
TLC	Thin layer chromatography
TSPs	Tetraspanins
VEGF	Vascular endothelial growth factor
VEGFR	Vascular endothelial growth factor receptor
δ	Chemical shift

Abstract

Glycosphingolipids were first found in nerve tissue and later found to be widespread in the membranes of various cells in animals and plants. They are important for maintaining the structure and function of cell membranes, participating in intercellular information transfer and adhesion, controlling cell growth and in the process of differentiation. Ganglioside GM3 (NeuAc α 3Gal β 4Glc β 1Cer) is the first and simplest member of the sialic acid-containing glycosphingolipid family to contain a single sialic acid. GM3 is a physiological substance secreted by tumor cells and is a tumor-associated carbohydrate antigen on several types of cancer, with a high tolerance and low toxicity profile unmatched by other exogenous drugs. GM3 has a wide range of biological functions, and previous studies have shown that GM3 and its analogues can inhibit tumor growth through a variety of pathways and play an important role in many physiological and pathological processes. Based on the theory of multivalent effect, we screened mannose-containing GM3 analogues from previously synthesized GM3 analogues with relatively better anticancer activity and modified it multivalently.

In this thesis, we report on concise protocols that can provide for the preparation of a range of oligomers of mannose-containing GM3 analogues, including the dimer, trimer and tetramer with a small molecule skeleton, and the hexamer and heptamer with a macromolecular skeleton, which cover a variety of synthetic approaches such as regioselective enzymatic hydrolysis for the preparation of mannose blocks with free 6-OH, highly regioselective and stereoselective α -sialylation of mannose residue acceptors with sialyl xanthate and multivalent modifications on monomer to multivalent backbones based on click chemistry. All the new compounds were purified by chromatography and their structures were characterized by nuclear magnetic resonance and high-resolution mass spectrometry.

We further evaluated the biological activity of synthesized compounds M1, M2, M3 and M4 by a number of in vitro experiments. In the MTT cytotoxicity assay, cell colony assay and morphology assay, the oligomers showed stronger cytotoxicity than the monomer, indicating that they could have more potent anti-proliferative activity, and the anti-proliferative effect on B16F10 and HCT116 cells was stronger than that of K562 and BXPC-3 cells. In the wound healing test and transwell migration/invasion assay, both M2 and M4 showed significant anti-migration and anti-invasion activities on B16F10 and BXPC-3 cells. From the results of the western blot assay, M1, M2, M3 and M4 may inhibit the movement of tumor cells by inhibiting the EGFR/VEGFR- β -catenin signaling pathway and thus the EMT process. And in the B16F10 and BXPC-3 cells, the expression levels of EMT-related proteins were more strongly inhibited by M2 and M4, further suggesting that M2 and M4 could have more potent anti-migration and anti-

invasion activities. This study provides valid information for the development of GM3 analogues-related oligomeric anticancer drugs.

Keywords: glycosphingolipid, ganglioside GM3, sialic acid, multivalent effect, synthesis, tumor, biological evaluation.

Résumé

Les glycosphingolipides ont été découverts pour la première fois dans les tissus nerveux, puis se sont révélés très répandus dans les membranes de diverses cellules animales et végétales. Ils sont importants pour le maintien de la structure et de la fonction des membranes cellulaires, participent au transfert d'informations intercellulaires et à l'adhésion, contrôlent la croissance cellulaire et le processus de différenciation. Le ganglioside GM3 (NeuAc α 3Gal β 4Glc β 1Cer) est le premier et le plus simple membre de la famille des glycosphingolipides contenant des acides sialiques à contenir un seul acide sialique. Le GM3 est une substance physiologique sécrétée par les cellules tumorales et constitue un antigène glucidique associé aux tumeurs sur plusieurs types de cancer, avec un profil de haute tolérance et de faible toxicité inégalé par d'autres médicaments exogènes. GM3 a un large éventail de fonctions biologiques, et des études antérieures ont montré que GM3 et ses analogues peuvent inhiber la croissance tumorale par diverses voies et jouer un rôle important dans de nombreux processus physiologiques et pathologiques. En basant sur la théorie de l'effet multivalent, nous avons criblé des analogues de GM3 contenant du mannose parmi les analogues de GM3 précédemment synthétisés au laboratoire avec une activité anticancéreuse relativement meilleure et nous les avons modifiés de manière multivalente.

Dans cette thèse, nous présentons des protocoles concis qui permettent la préparation d'une gamme d'oligomères d'analogues de GM3 contenant du mannose, y compris le dimère, le trimère et le tétramère avec un squelette de petite molécule, et l'hexamère et l'heptamère avec un squelette macromoléculaire, qui couvrent une variété d'approches synthétiques telles que l'hydrolyse enzymatique régiosélective pour la préparation de blocs de mannose avec 6-OH libre, l' α -sialylation hautement régiosélective et stéréosélective des accepteurs de résidus de mannose avec le xanthate de sialyle et les modifications multivalentes sur le monomère en squelettes multivalents basés sur la chimie click. Tous les nouveaux composés ont été purifiés par chromatographie et leurs structures ont été caractérisées par résonance magnétique nucléaire et spectrométrie de masse à haute résolution.

Nous avons ensuite évalué l'activité biologique des composés synthétisés M1, M2, M3 et M4 par un certain nombre d'expériences *in vitro*. Dans le test de cytotoxicité MTT, le test de colonie cellulaire et le test de morphologie, les oligomères ont montré une cytotoxicité plus forte que le monomère, indiquant qu'ils pourraient avoir une activité anti-proliférative plus puissante, et l'effet anti-prolifératif sur les cellules B16F10 et HCT116 était plus fort que celui des cellules K562 et BXPC-3. Dans le test de cicatrisation et le test de migration/invasion transwell, M2 et M4 ont montré des activités anti-migration et anti-invasion significatives sur les cellules B16F10 et BXPC-3. D'après les résultats du test

western blot, M1, M2, M3 et M4 peuvent inhiber le mouvement des cellules tumorales en inhibant la voie de signalisation EGFR/VEGFR- β -caténine et donc le processus EMT. Et dans les cellules B16F10 et BXPC-3, les niveaux d'expression des protéines liées à l'EMT ont été plus fortement inhibés par M2 et M4, ce qui suggère que M2 et M4 pourraient avoir des activités anti-migration et anti-invasion plus puissantes. Cette étude fournit des informations valables pour le développement de médicaments anticancéreux oligomères liés aux analogues de GM3.

Mots-clés : glycosphingolipide, ganglioside GM3, acide sialique, effet multivalent, synthèse, tumeur, évaluation biologique.

Chapter I
Introduction

Cells are the basic units of life, whether prokaryotes or eukaryotes, for a living individual, all living organisms are composed of one or more cells. No matter where the cells are located, they all share common properties and processes. Almost all cells are composed of four basic biomolecules: carbohydrates, proteins, nucleic acids, and lipids, and their main functions are shown in **Table I-1**. In addition, the above biomolecules can be combined together to form biomolecular complexes that perform certain functions of the cell and constitute certain structures of the cell (**Figure I-1**). For example, as we can observe from the following diagram of the cell membrane, in addition to the phospholipid bilayer structure, the cell membrane also contains a large number of proteins and sugar chains. On the outer surface of the cell membrane, the sugar chains can bind to proteins and RNA to form glycoproteins and glycoRNAs, respectively, which have important functions in cellular life activities. Besides glycoproteins and glycoRNAs, there are glycolipids on the surface of cell membranes that are combined with carbohydrates and lipid molecules, which can maintain the stability of the membrane and promote cell recognition [1].

Table I-1. Four types of biomolecular functions.

Carbohydrates	Proteins	Nucleic acids	Lipids
Major energy sources	Structure of the cell membrane	DNA is the main material basis for the storage, replication and transmission of genetic information	Formation of biomembrane
Provide structure	Cellular transport		Fats can be stored as energy source
Communication	Biocatalysts or enzymes	RNA plays an important role in protein synthesis	Steroid hormones regulate cellular activity by altering gene expression
Cellular attachment	Maintaining cell contact		
Defends against and removes foreign substances	Control cellular activity Transmitting signals		

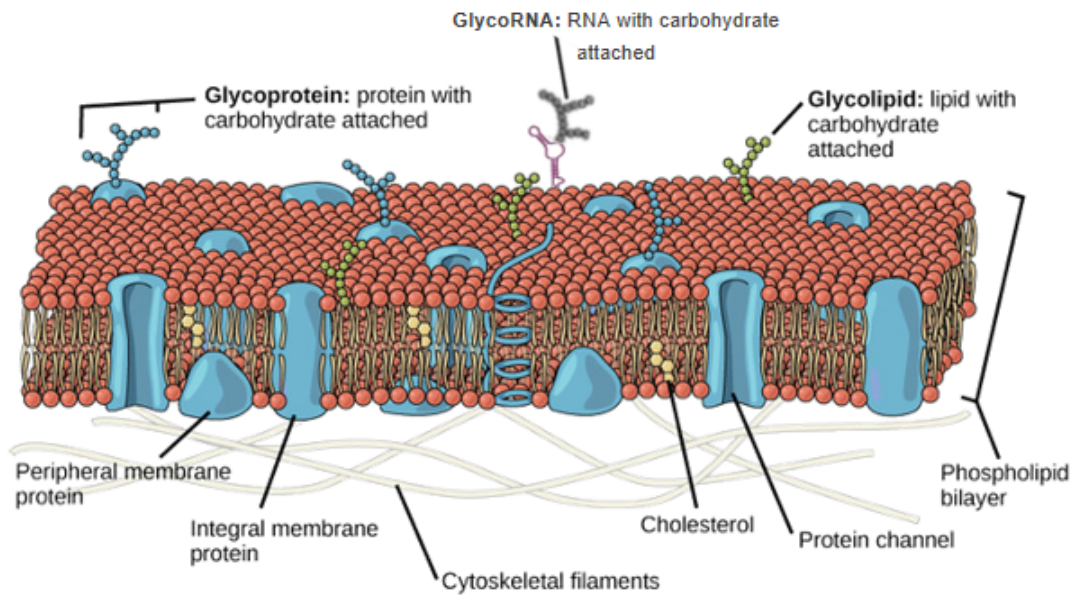


Figure I-1. The cell membrane of the cell is a phospholipid bilayer containing many different molecular components, including proteins, RNA and lipid, some with carbohydrate groups attached [1].

Glycolipids are widely distributed and diverse in living organisms, and their main components are alcohols, fatty acids and sugars, which are amphiphilic (i.e. hydrophilic and hydrophobic). The roles of glycolipids include (1) cells obtain energy from glycolipids; (2) glycolipids are components of cell membranes; (3) human blood type can be determined by glycolipids; (4) glycolipids also help the immune system by destroying and eliminating pathogens in the body, etc. It can be mainly divided into two categories: glycosphingolipids and glyco glycerolipids according to the types of alcohol groups in glycolipids components. The alcohol of glyco glycerolipids is propanetriol (glycerol), which forms ester bonds with fatty acids. The alcohol of glycosphingolipids is sphingosine (neurosphingosine), which forms amide bonds with fatty acids with its C-2 amino group, resulting in N-lipoyl sphingosine, also known as ceramide. Each of them has two long non-polar hydrophobic "tails", the former provided by two fatty acyls and the latter by one each of sphingosine and fatty acyl, and the special structure of these two long hydrophobic "tails" allows them to be more stably embedded in the lipid bilayer of the cell membrane structure. The hydrophilic portion of the glycosyl moiety is generally composed of straight or branched sugar chains, with the polar 'head' portion of the glycosyl moiety extending outside the cytoplasmic membrane to act as a cell surface marker or recognition part of an antigenic determinant cluster or receptor that carries out a range of life activities. The sugar chains are mostly linked to the hydroxyl groups of the alcohols by glycosidic bonds, forming glyco glycerolipids or glycosphingolipids, respectively. Glycosphingolipids are widely found in higher plants and microorganisms, and to a lesser extent in nerve tissue. Glycosphingolipids were first found in nerve tissue and later found to be widespread in various cell membranes of animals and plants. Since the biological functions of glycosphingolipids are much more complex than glycerolipids, the former has been more intensively studied. The structure of glycolipids as shown in **Figure I-2**.

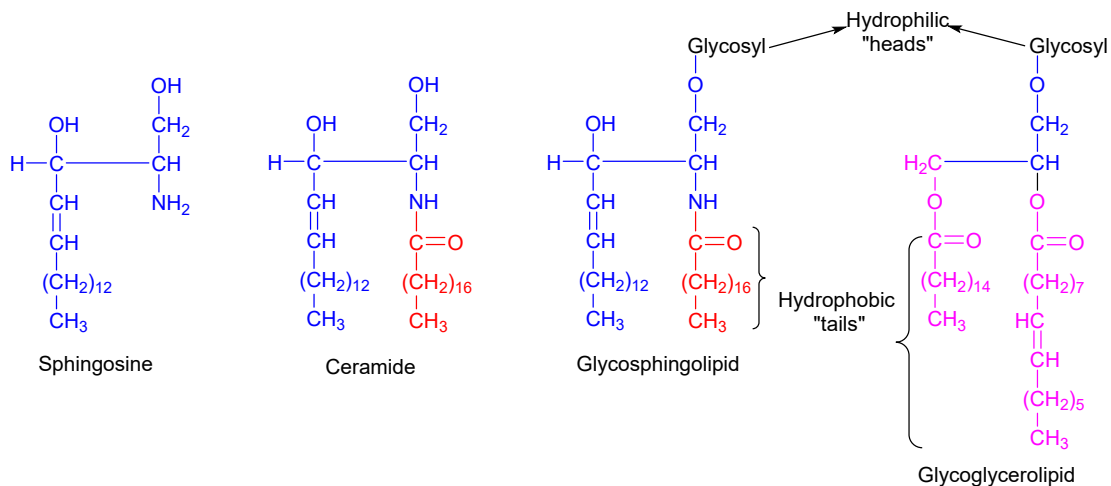


Figure I-2. The structure of glycolipids.

1.1. Glycosphingolipids

1.1.1. The family of glycosphingolipids

The discovery of glycolipids is generally attributed to Johan L. W. Thudichum, who published his article on the chemical composition of the brain in 1884 [2],[3]. Glycosphingolipids are glycosides formed by glycosylation of the 1-hydroxyl group of ceramides in the molecule. The general formula of its structure is as follows: the monosaccharides in the glycosphingolipid molecule are mainly D-glucose, D-galactose, N-acetylglucosamine, N-acetylgalactosamine, fucose and sialic acid; the fatty acid components are mainly saturated and low-saturated fatty acids with 16-24 carbon, in addition, there is a considerable amount of α -hydroxyl lipoic acid (**Figure I-3**) [4].

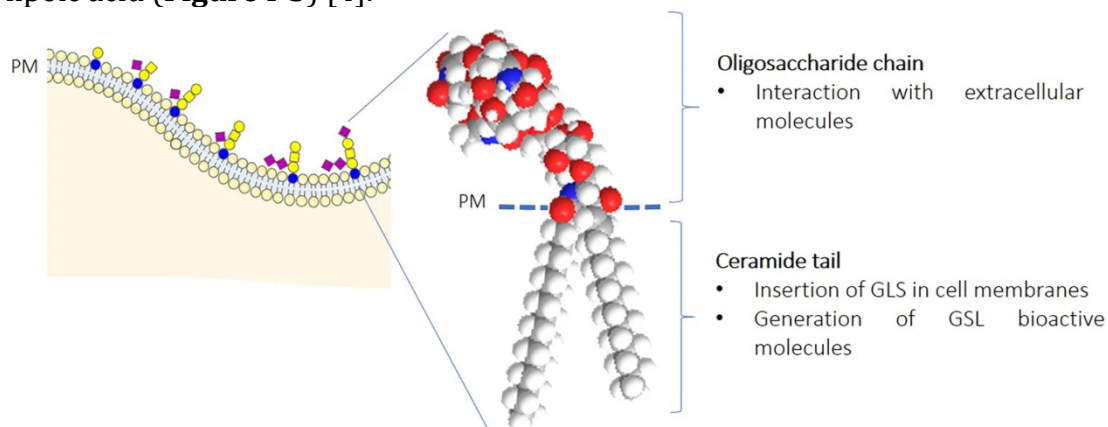


Figure I-3. Plasma membrane glycosphingolipid structure: the oligosaccharide head and the ceramide tail [4].

Glycosphingolipids can be divided into two categories: neutral glycosphingolipids and acidic glycosphingolipids, depending on whether the molecule contains sialic acid or sulfate group components. In recent years, due to the increasing number of glycosphingolipids with elucidated structures, glycosphingolipids have been further divided into the following series based on the composition and structure of several core glycosyl groups close to ceramide: Globo-series, Lacto-series, Neolacto-series, Ganglio-series, etc. (**Table I-2**).

Table I-2. Root Names, Symbols, and Root Structures for Glycosphingolipid Chains.

Root Name	Symbol	Root Structure IV III III I
Ganglio-	Gg	Galb3GalNAcb4Galb4Glc-
Lacto-	Lc	Galb3GlcNAcb3Galb4Glc-
Neolacto (Lactoneo)	nLc (Lcn)	Galb4GlcNAcb3Galb4Glc-
Globo-	Gb	GalNAcb3Gala4Galb4Glc-
Isoglobo-	iGb	GalNAcb3Gala3Galb4Glc-
Mollu-	Mu	GlcNAcb2Mana3Manb4Glc-
Arthro-	At	GalNAcb4GlcNAcb3Manb4Glc-

1.1.2. Biological functions of glycosphingolipids

The diversity of oligosaccharide chains, sphingosine bases and fatty acids makes the glycosphingolipid molecules exhibit a wide variety and complex structure. Studies have shown that glycosphingolipids are widely involved in intracellular and intercellular signalling, interacting with functionally important proteins and glycans in cells, and that there are interactions between glycosphingolipids, and have been found to exert biological effects through a variety of molecular mechanisms including organization of microdomains, direct regulation of receptors, signal transduction, and intercellular contacts, as shown in **Figure I-4** [5].

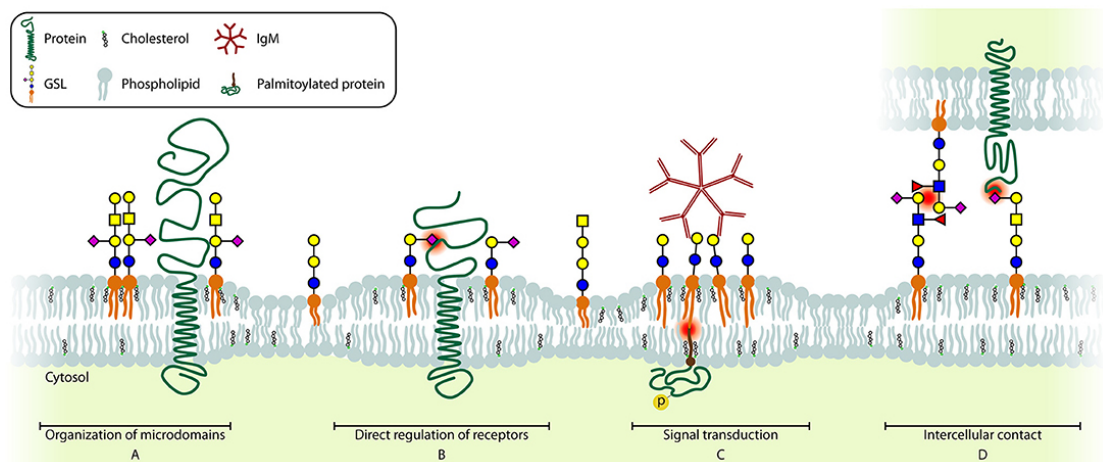


Figure I-4. Schematic model of the different GSL functions. Essential glycan-glycan, protein-glycan, and lipid interactions are highlighted (red dot). (A) GSLs are an essential component of membrane microdomains. (B) Several receptors can be directly regulated by GSLs present in the cell membrane. (C) Crosslinking of several GSLs can induce signaling across the membrane. (D) GSLs can interact with glycans (CCI, left) or with proteins (PCI, right) on other cells, contributing to cell-cell recognition and adhesion [5].


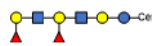

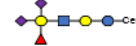
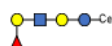
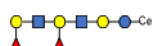
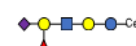
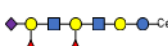



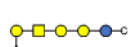

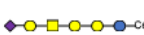

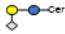
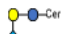





A number of scientific studies have shown that a group of glycosphingolipids have been found to interact with a number of signaling receptors located at the plasma membrane and regulate their activation: the gangliosides GM1, GM3, GD1A and GT1B inhibit EGFR phosphorylation. Gb4 promotes EGFR-induced activation of the ERK signaling pathway. GM3 directly or indirectly regulates FGFR function. GM1 and GM3 may regulate PDGFR function by affecting the extent of tyrosine phosphorylation. GM1 binds to Trk proteins and regulates NGFR function. GT1 mediates the interaction between NgR1 and LINGO-1. GM3 inhibits VEGF/VEGFR-2-mediated angiogenesis through a direct interaction with VEGFR-2. TGF- β 1-induced ganglioside GM3 regulates EMT through a potential interaction with TGF β R_s, etc. See **Table I-3** for more details [6].

Table I-3. Glycosphingolipids interact with a number of signalling receptors located in the plasma membrane.

Protein	Lipids	Reference
EGFR	GM1, GM3, GD1, GT1, Gb4	[7],[8],[9],[10],[11],[12],[13]
FGFR	GM3	[14],[15]
PDGFR	GM1, GM3, GD1, GT1	[16],[17]
NGFR/Trk	GM1	[18],[19]
NgR1	GT1	[20]
VEGFR	GM3	[21]
TGFB1R	Gb4, GM3	[10],[22]
IR	GM3	[23],[24]
Lyn/Cbp	GD3, GD1	[25]
Tetraspanins	GM3, GM2	[26],[27],[28]
CD11b/CD18	LacCer	[29]
α 5 β 1 integrin	GT1	[30]
Caveolin-1	GM3	[30],[31]
PMCA	GM3, GM2, GM1, GD1	[32]
Galectin-1	GM1	[33]
Galectin-3	GM1	[34]

Glycosphingolipids as functional regulators on the cell membrane surface are closely associated with the development of human diseases, and abnormal expression of specific glycosphingolipids and related enzymes can often influence tumorigenesis and malignant transformation, as shown in **Table I-4** regarding the expression of GSLs in tumor cells [35].

Table I-4. GSL molecules with altered expression in different types of cancer. Series, name and structure are listed for each GSL, along with the tumor type they are found to be altered.

Series	GSL name and structure	Tumor type
Lacto	Disialyl-Lc4 	Colon [36]
	Le ^a -Le ^a 	Gastric, Colon, breast, Hodgkin's lymphoma, bladder cancer [37]
	Sialyl Le ^a 	Colon, pancreatic and gastric cancer [38]
	Disialyl-Le ^a 	Colon [39]
NeoLacto	Le ^x 	Gastric, Colorectal [38] and breast cancer [40]
	Le ^x -Le ^x 	Lung [41], Colon and liver [42] cancer
	Sialyl Le ^x 	Colon [43] and bladder [44] cancer, T cell leukemia [45]
	Sialyl Le ^x -Le ^x 	Colon [42] and gastrointestinal, colorectal, breast and lung [46]
	Le ^y 	Gastric, colon [47], lung [48]
	Le ^y -Le ^x 	Colon [39], liver [43] and pancreatic [49] cancer
Globo	Gb3 	Burkitt lymphoma [50], ovarian cancer [51]
	Globo H 	Ovarian [52] and breast cancer [53], teratocarcinoma [54]
	Gb5 	Teratocarcinoma [54]
	Monosialosyl-Gb5 	Renal cell carcinoma [55]
	Disialosyl-Gb5 	Renal cell carcinoma [56]
Ganglio	De-N-acetyl GM3 	Melanoma [57]
	Neu5Gc-GM3 	Melanoma [58], colon [59], breast [60], retinoblastoma [61]
	GD3 	Melanoma [62], glioma [63]
	9-O-acetyl GD3 	Melanoma [64], glioblastoma [65]
	GM2 	Melanoma [62], neuroblastoma [66], medulloblastoma [67]
	GD2 	Melanoma [68], neuroblastoma [66], retinoblastoma [69]
	Fucosyl-GM1 	Small cell lung carcinoma [70]

● Gal ● Glc ■ GalNAc ■ GlcNAc ◆ Neu5Ac ◆ Neu5Gc ◇ Neu5NH₂ ▲ Fuc

The glycosyl portion of glycosphingolipids stretched on the surface of the cytosolic membrane has an immunogenic antigenic determinant cluster and is capable of inducing IgM antibody responses. Because it is overexpressed in a variety of tumor tissues, it is a target molecule for tumor vaccines and has become a hot topic in tumor vaccine research.

1.2. Gangliosides

1.2.1. Structure and function of sialic acid

Gangliosides belong to the Ganglio-series of glycosphingolipids, which were first discovered by E. Klenk in 1935 to accumulate in the brains of children with Tay-Sachs-type infantile amaurotic idiocy and are abundant in the grey and white matter of the brain, hence this kind of glycolipid is named ganglioside. Gangliosides are glycosphingolipids containing exclusively one or more sialic acid residues, which are widely present in the body's tissue cells as essential substances in most mammalian cell membranes.

Sialic acid is an acidic monosaccharide commonly found in higher animals and some microorganisms, and is a generic term for a group of derivatives of monosaccharides containing nine carbon atoms. It is an important component of glycoproteins and glycolipids in cell membranes and is widely distributed at the extremities of glycoprotein or glycolipid oligosaccharide chains on the surface of eukaryotic cells [71]. It was first isolated and named by Blix from the mucin of the submandibular gland in 1957 and established the nomenclature of sialic acid [72].

There are more than 50 different types of sialic acid, the core structures of which are keto-deoxynonanulonic acid (Kdn), neuraminic acid (Neu), N-acetylneuraminic acid (Neu5Ac or NANA) and N-glycolylneuraminic acid (Neu5Gc or NANG) as shown in **Figure I-5** [73]. The difference between the first two is the group attached to C5, while the latter two, Neu5Gc and Neu5Ac, differ structurally by the addition of an oxygen atom to the N-acyl group [58]. Neu5Ac can be converted to Neu5Gc in the cytoplasm by cytidine monophosphate N-acetylneuraminic acid hydroxylase (CMAH), but this enzyme activity was lost during human evolution, so that in human tissues it is mainly Neu5Ac, whereas Neu5Gc is widely synthesized in fish and most mammals, but not in normal human tissues [74], [75].

In general, sialic acid can be linked to C3, C6 or C8 of other sugars (galactose, N-acetylgalactosamine, etc.) via a glycosidic bond with its second carbon atom C2 in the presence of sialyltransferase, resulting in α 2,3, α 2,6 or α 2,8 linked sialoside, respectively [76]. The variety of linkage substrates, the different linkage modes and their spatial combinations constitute the diversity of sialylation modifications, which play a crucial role in many biological processes, for example, the content of sialic acid is closely related to tumor cell proliferation, metastasis, infiltration and evasion of immune surveillance by host cells [77].

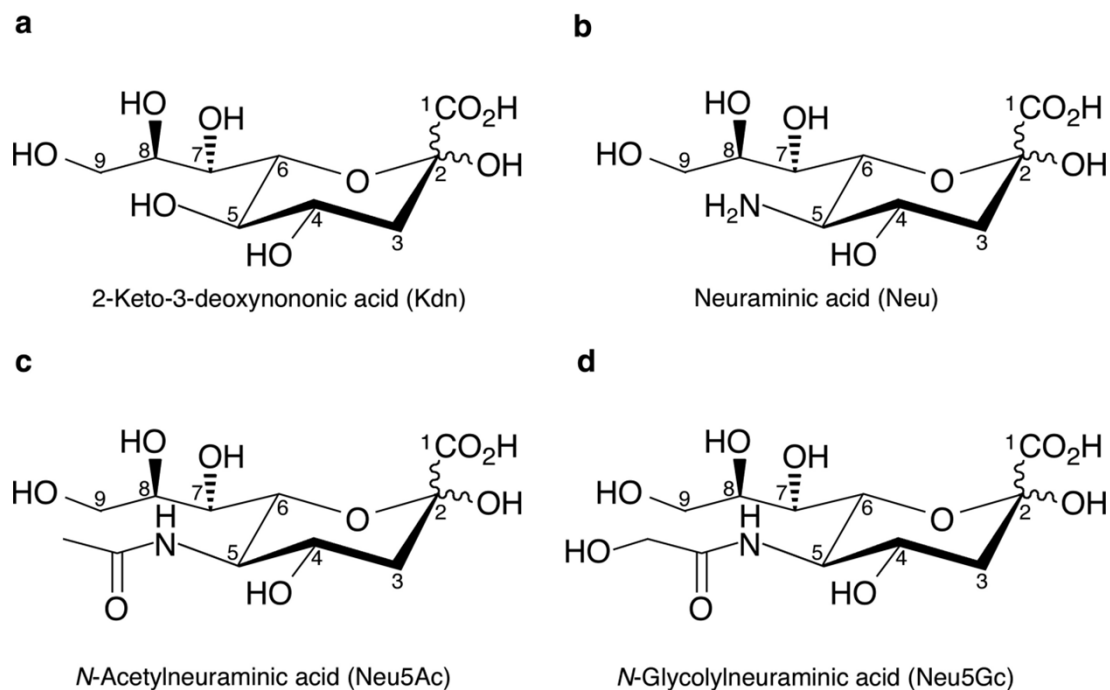


Figure I-5. The core structure of sialic acid [73].

1.2.2. Structure and classification of gangliosides

The structure of gangliosides consists mainly of hydrophobic ceramide lipids linked to hydrophilic sialic acid-containing glycan chains of different lengths and structures, which are both water-soluble and lipid-soluble. The ceramide is partially embedded in the lipid bilayer of the cell membrane, enhancing the stability of the cell membrane structure. Gangliosides are synthesized at the endoplasmic reticulum and the Golgi apparatus, where ceramide is first synthesized at the endoplasmic reticulum membrane, then transported to the Golgi apparatus to complete glycosylation modification, and final transported to the cytoplasmic membrane to play a role [78]. The biosynthesis of gangliosides is carried out in a glycosylation sequence and is divided into four series according to the number of sialic acid residues attached to the lactosylceramide (LacCer), with M, D and T denoting gangliosides containing 1, 2 and 3 sialic acids respectively, and their biosynthetic pathways are shown in **Figure I-6** [79],[80],[81],[82],[83].

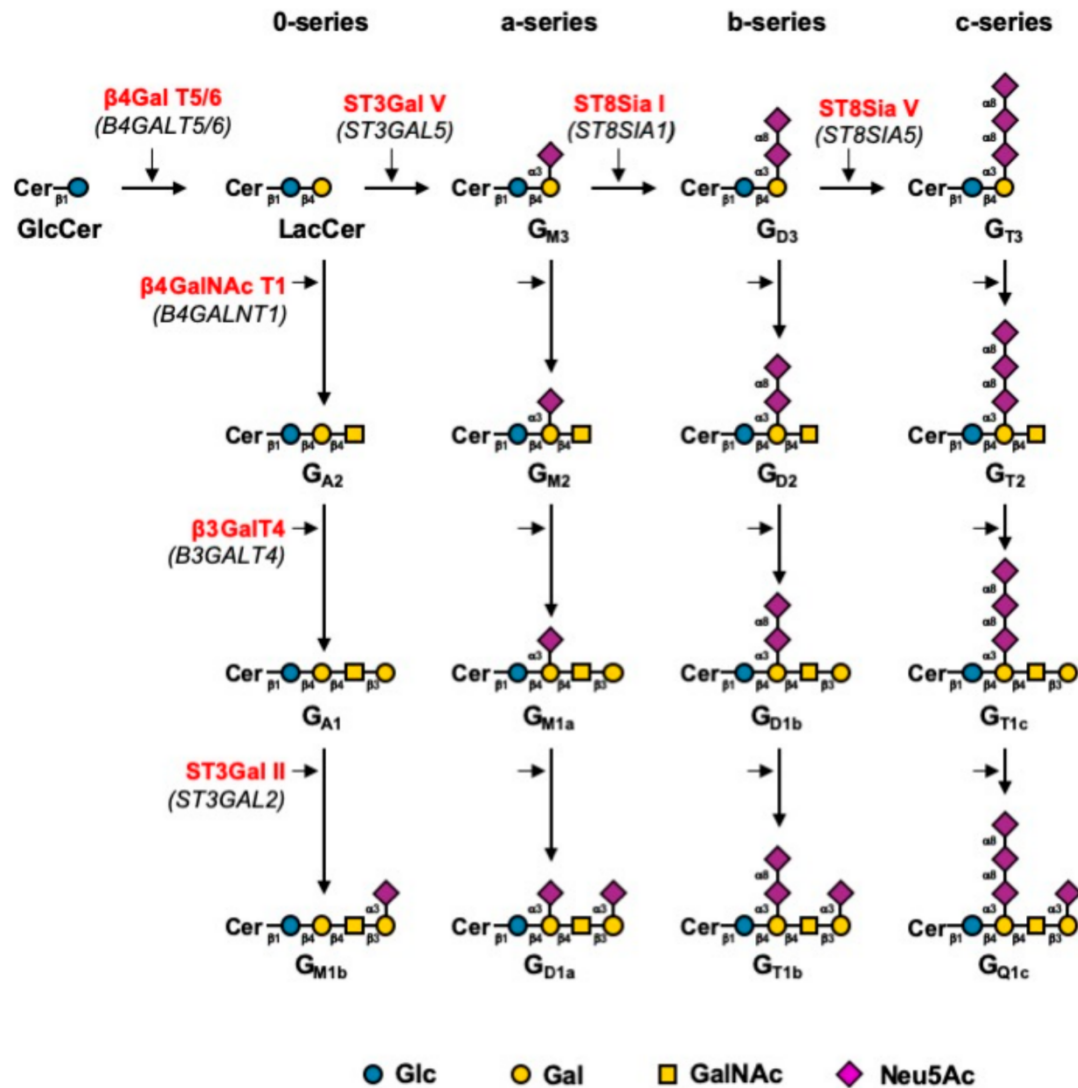


Figure I-6. Biosynthesis pathway for gangliosides. Gangliosides are synthesized by stepwise addition of monosaccharides to GlcCer. Extension of GlcCer occurs through the action of the UDP-Gal: GlcCer β1,4-galactosyltransferase to make LacCer. The action of the GM3 synthase, GD3 synthase, and GT3 synthase leads to the biosynthesis of the precursors of a-, b-, and c-series gangliosides, respectively. The 0-series gangliosides are directly synthesized from LacCer. Elongation is performed by the sequential action of β4GalNAc T1, β3Gal T4, and the sialyltransferases ST3Gal II and ST8Sia V. Genes encoding the different glycosyltransferases involved are indicated in italics between brackets [79].

1.2.3. Biological functions of gangliosides

Gangliosides play an important role in all stages of cell growth, differentiation, migration and death, and specific species of ganglioside molecules have also shown potential medicinal value against major diseases such as neurodegenerative diseases, diabetes, tumors and autoimmune diseases.

Long-standing research into cancer has shown that almost all human cancers are accompanied by aberrant glycosylation. In clinicopathological studies, abnormal expression of certain glycosylated epitopes of gangliosides affects the aggressiveness and distal metastatic ability of tumors, which often correlates closely with the survival rate of cancer patients. Abnormal accumulation of certain

gangliosides has been reported in a variety of cancers, such as neural and brain cancer, lung cancer, breast cancer, and hepatocellular carcinoma, among other types of cancer cells, as detailed in **Figure I-7** [84]. Gangliosides are mainly located in glycolipid-enriched domains, also called lipid rafts, on the outer leaflet of the plasma membrane bilayer. Raft domains are composed of cholesterol, phospholipids, and glycosphingolipids and enriched in specific proteins. Most cancers exhibit abnormalities in intracellular signal transduction systems, and gangliosides interact with signaling receptors in cells involved in related molecular mechanisms that are closely linked to the progression of cancer. As shown in **Figure I-8**, gangliosides typically form complexes with several types of tyrosine kinase receptors in the lipid rafts of cancer cells. These interactions contribute to the activation or inhibition of receptor tyrosine kinase signalling, leading to the inhibition or promotion of the malignant properties of cancer cells.

Gangliosides have been widely studied due to their diverse expression characteristics and important regulatory functions in tumor diseases. Reportedly, ganglioside GM1 promotes neuroblastoma cell differentiation by forming TrkA-GM1 oligosaccharide complexes on the cell surface to activate TrkA receptors [85]. GT1b down-regulates the expression of $\alpha 5\beta 1$ integrin, caveolin-1, fibronectin, FAK and ERK and up-regulates the expression of p53 and uPAR, leading to down-regulation of fibronectin- $\alpha 5\beta 1$ -integrin-ERK signalling in A549 lung adenocarcinoma cell lines [86]. In MDA-MB-231 breast cancer cells, predominantly expressed GD2 contributes to the activation of c-Met signalling, leading to a proliferative phenotype [87]. In human hepatocellular carcinoma HepG2 cells, HGF-induced phosphorylation of c-Met was inhibited after treatment with GD1a [88]. Inhibition of GM2 expression through MAPK inhibition also reduced TGF- $\beta 1$ signalling and inhibited the invasion of pancreatic cancer cells [89]. NEU3-silenced renal cell carcinoma with high GD1a expression showing reduced FAK/AKT signalling and reduced drug resistance, invasiveness and adhesion [90]. GD3 gangliosides mediate the propagation of apoptotic signals generated by CD95 in hematopoietic cells [91]. In human melanoma cells expressing GD3, Src family kinase yes protein is activated upon interaction with GD3, leading to a malignant phenotype of melanoma cells [92]. GD3/GD2-positive human osteosarcoma cells showed stronger tyrosine phosphorylation of p130Cas, FAK and paxillin following serum stimulation than GD3/GD2-negative cells, resulting in malignant properties [93].

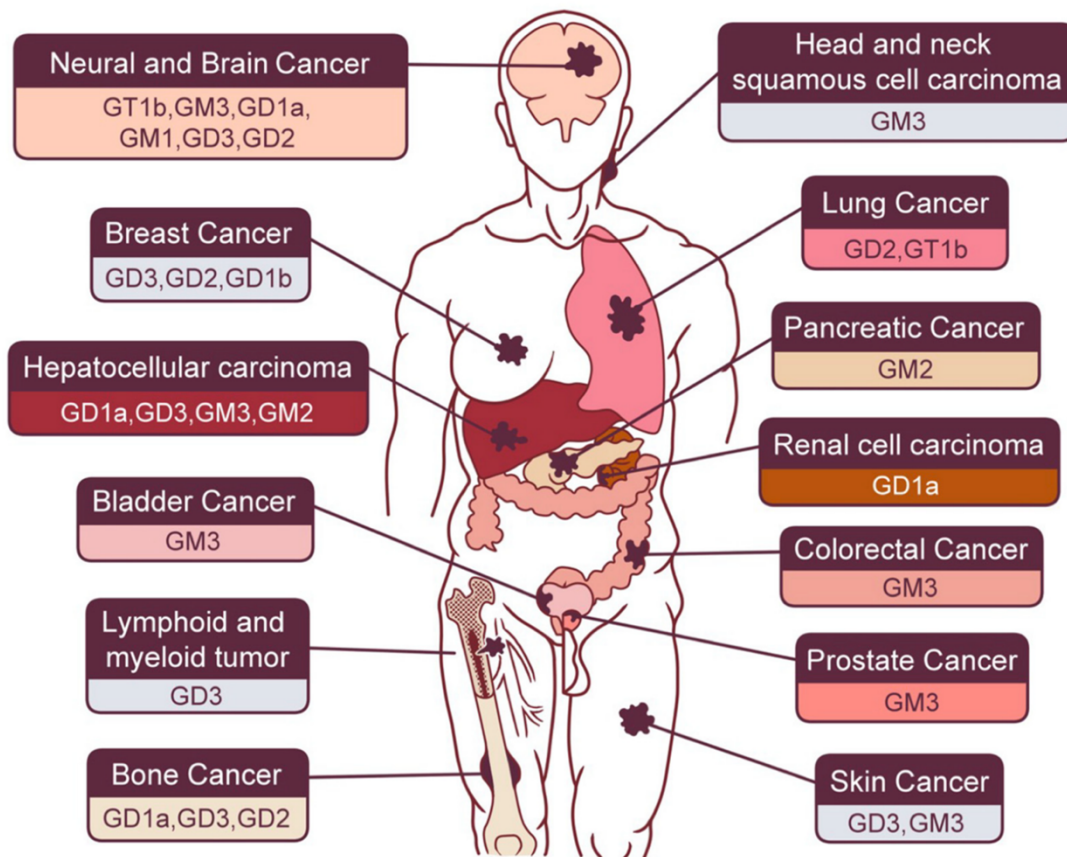
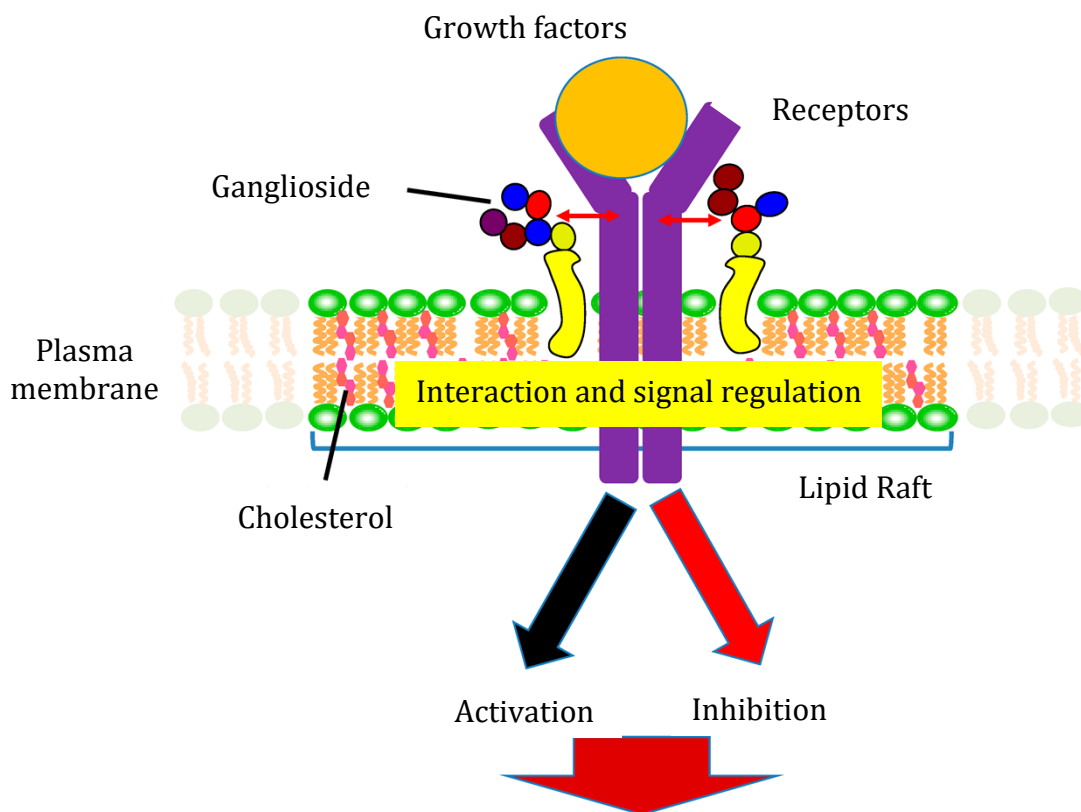


Figure I-7. Each species of cancer in the human body and related gangliosides [84].



Effect on malignant properties in cancer cells

Figure I-8. The effects of gangliosides on cancer cell signaling [84].

1.3. Ganglioside GM3

1.3.1. Structure of ganglioside GM3

GM3 is a ganglioside containing a single sialic acid and is the first and simplest member of the metabolic family of glycosphingolipids. It was first isolated from equine erythrocytes by Yamakawa et al. in 1952. Its chemical structure consists of one molecule of sialic acid, one molecule of lactose and ceramide (**Figure I-9**), which is synthesized in the cellular Golgi apparatus by GM3 synthase and is widely found in the cell membranes of mammalian tissues (**Figure I-10**) [94].

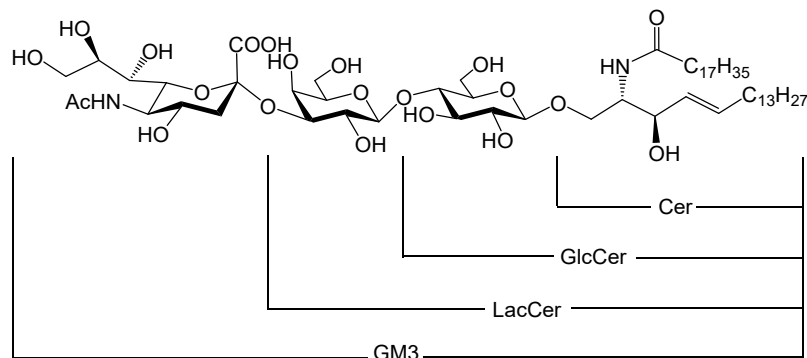


Figure I-9. Structure of ganglioside GM3.

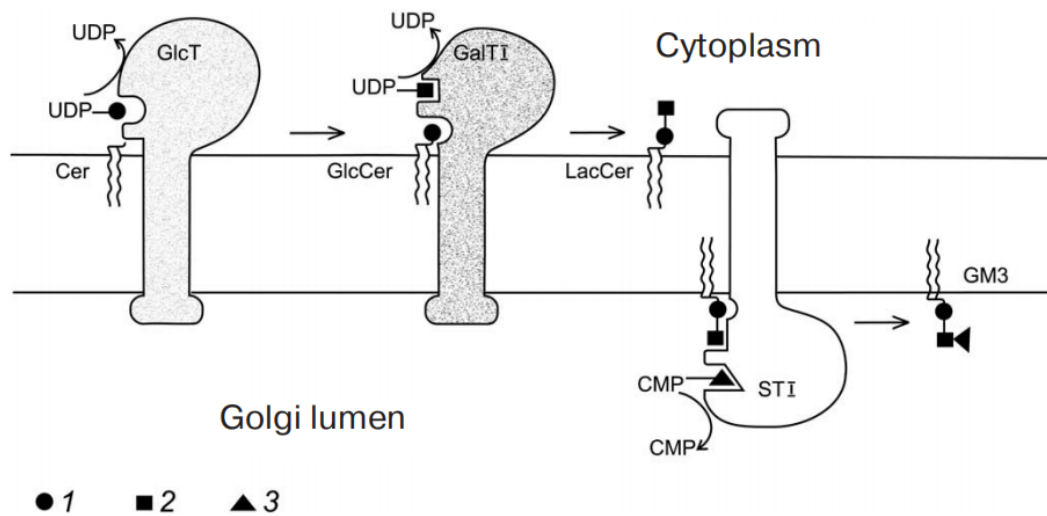


Figure I-10. Biosynthesis of ganglioside GM3 in the Golgi apparatus. 1- 3: glucose, galactose, and sialic acid, respectively [94].

1.3.2. Biological functions of ganglioside GM3

The ganglioside GM3 acts in an autocrine or paracrine manner on tumor or tumor-associated host cells, such as macrophages and endothelial cells, and is one of the most important gangliosides involved in intercellular recognition and adhesion, regulation of cell proliferation, growth, differentiation and signalling, as well as being involved in cell carcinogenesis and invasiveness. In cancer development, most gangliosides promote the formation and progression of cancer, but in some cancers, GM3 has an opposite inhibitory effect to most gangliosides.

1.3.2.1. Expression of ganglioside GM3 in tumor cells of different phenotypes

Exploration of the cellular and pathological phenotypes of GM3 was early and the expression of GM3 on cell membranes varies according to cell type, organ and species. As early as the 1960s, researchers found significantly reduced expression of ganglioside GM3 and enhanced expression of its precursor, LacCer in baby hamster kidney (BHK) cells transformed with the oncogenic virus polyomavirus [95]. In addition, reduced expression of disialo-ceramidetetrahexoside and monosialo-ceramidetetrahexoside was observed in mouse 3 T3 cell lines transformed by oncogenic SV40 virus (RNA virus) [96]. This was the beginning of the understanding of glycosphingolipid changes in the pathological phenotype of cancer cells, and further research continues along this line. Subsequently, GM3 expression was found to be reduced in chicken embryonic fibroblasts transformed by Rous sarcoma virus, and this reduction correlated closely with the transformed phenotype using a temperature-sensitive mutant of the virus. At the 'non-permissive temperature' (41 °C), GM3 expression was not reduced and the cells did not show a transformed phenotype, and at the 'permissive temperature' (35 °C), GM3 expression was reduced [97]. The ratio of ganglioside GM3:GD3 on the surface of normal melanocytes was 19:1 (based on LBSA%). When melanocytes were malignantly transformed into melanoma cells, the ratio of ganglioside components on the surface of the cells changed significantly: the ratio of GM3:GD3 ranged from 15:1 to 1:5, and patients with higher ratios had significantly longer survival than those with lower ratios [98]. In studies of human glioma cells [99] and human bladder tumor cells [100], GM3 expression was found to be inversely correlated with invasive potential, GM3 accumulated in large amounts in non-invasive tumors compared to infiltrating tumors, and the invasive capacity of tumor cell lines could be inhibited by exogenous supplementation of GM3. Similarly, in A2780 human ovarian cancer cells also exhibited low GM3 synthase activity and low ganglioside GM3 content, but high motility characteristics [101]. In the transformed phenotypes of mouse fibroblast line 10 T1/2 and chicken fibroblast line DF1 induced by v-Jun transfection, downregulation of GM3 and mRNA encoding GM3 synthase was detected, whereas artificially increasing the expression of GM3 synthase in these cells resulted in increased GM3 expression and reversal of the cancerous cells to the normal cell phenotype [26]. These results were consistent in the same colon cancer cell lines with low levels of GM3 expression [102]. The low level of ganglioside GM3 expression in chronic myeloid leukemia K562 cells is produced by the high expression of the sialidase Neu3, which removes sialic acid from gangliosides. Following silencing of Neu3 by small interfering RNA technology, ganglioside GM3 was significantly increased and K562 cells showed reduced proliferation, eliminating the barrier to differentiation of K562 cells and giving rise to a megakaryocytic phenotype [103]. In human multiple myeloma U266 cells, the inhibitory effect on U266 cells proliferation was also shown to increase with enhanced GM3 expression, among other features [104]. The evidence above shows that the expression level of ganglioside GM3 is negatively correlated with the malignancy of certain types of tumors.

1.3.2.2. Ganglioside GM3 and EGFR

There are many mechanisms by which GM3 inhibits tumor cell growth, including interaction with various growth factor receptors that affect cell proliferation. Growth factor receptors (GFRs) are transmembrane proteins that bind to specific growth factors and transmit information to the cell interior, where they are involved in many cellular functions. The binding of a growth factor to its receptor activates the receptor tyrosine kinase, which subsequently autophosphorylates certain tyrosine residues of the receptor itself and/or certain signal transducers involved in downstream cell signalling pathways. Over-activation of several GFRs, including the epidermal growth factor receptor (EGFR) and the vascular endothelial growth factor receptor (VEGFR), is known to be associated with tumor growth and development.

As early as 1986, Bremer EG et al. found that exogenous addition of GM3 inhibited epidermal growth factor (EGF)-induced tyrosine autophosphorylation of EGFR, thereby inhibiting the growth of human epidermal carcinoma A431 cells [105]. Subsequently, the gene encoding a soluble Mr 42,000 sialidase was transfected into the human epidermoid carcinoma cell line (A431), by which the level of endogenous GM3 was down-regulated by altering the level of terminal lipid-bound sialic acid on the cell surface. Transfected cells showed faster growth and enhanced tyrosine autophosphorylation of EGFR compared to controls [106]. Similarly, depletion of ganglioside GM3 induced by using the ceramide analogue [D]-PDMP results on EGFR-mediated autophosphorylation and A431 cell growth were consistent with previous studies. Furthermore, exogenous addition of GM3 to [D]-PDMP-treated cells restored EGF-induced proliferation and enhanced EGFR autophosphorylation back to normal levels, indicating that GM3 levels in cells can regulate EGFR activity in a reversible manner [107]. Some evidence suggests that GM3 inhibits EGFR activity by inhibiting EGFR autophosphorylation, but not by competing with EGF for receptor binding, and therefore the mechanism of inhibition cannot be explained by ligand-competitive binding [105],[108],[109]. Further studies showed that a site of direct interaction with ganglioside binding was identified on the extracellular structural domain (ECD) of EGFR and that the ECD interacted preferentially with GM3 over all other gangliosides tested, with the relative binding order of ECD to gangliosides being as follows: GM3 \gg GM2, GD3, GM4 > GM1, GD1a, GD1b, GT1b, GD2, GQ1b > lactosylceramide. as shown in **Table I-5**. These data suggest a further step in the study of the mechanism of EGFR inhibition by GM3 as a direct modulator of EGFR activity [110]. Mirkin BL et al. investigated the relationship between the inhibitory effects of several gangliosides on human neuroblastoma cell proliferation and EGFR phosphorylation and found that the inhibitory effect of GM3 on cell proliferation and on EGFR phosphorylation were almost equal compared to other gangliosides [111].

Table I-5. N.D.^a, not determined. Previous studies had indicated no inhibition of EGFR autophosphorylation by lactosyl ceramide. * Significantly different (p = 0.004) from EGF stimulated (100%) [105].

Ganglioside	Structure	Relative binding (%)	EGFR activity (%)
GM3		100	2.5*
Lactosyl Ceramide		11.6	N.D. ^a
GM2		29.9	79.3
GD3		49.0	153.1
GM4		43.5	104.7
GM1		12.1	133.2
GD1a		4.2	123.2
GT1b		17.2	157.6

NeuAc ▲ GalNac □ Gal ● Glc ◇ Cer

The results of the analysis of the effect of GM3 with other gangliosides on EGFR activity suggest that a highly specific interaction is involved. This molecular mechanism of interaction between GM3 and EGFR was further elucidated by Yoon SJ's team, which found that GM3 interacts with N-linked glycans with multiple GlcNAc-terminal residues on the EGFR receptor, where N-glycans with 5 or 6 GlcNAc termini (OS B1, B2) bind GM3 to the highest extent among the N-glycans tested, with this interaction was lower in structures with 2 GlcNAc termini (OS I). Furthermore, OS B1, B2 have so far shown no significant binding to other GSLs. These findings indicated the existence of a novel mechanism of specific carbohydrate-to-carbohydrate interaction (CCI), which occurs between the GlcNAc terminus of the N-linked glycan of EGFR and GM3 within the same cell membrane plane, termed 'cis-CCI'. These results demonstrated that activation, autophosphorylation and dimerization of EGFR were inhibited through specific lateral interactions between the GlcNAc terminus of the N-linked glycan of the EGFR receptor and the oligosaccharide chain of GM3 [112],[113],[114]. As

illustrated in **Figure I-11** [115]. In addition, under conditions of lateral action of GM3, EGFR shifts to GSL and caveolin-1 rich membrane domains and GM3 affects EGFR signalling through a second distinct molecular mechanism regulating EGFR/caveolin-1 binding, further regulating EGFR activity [30].

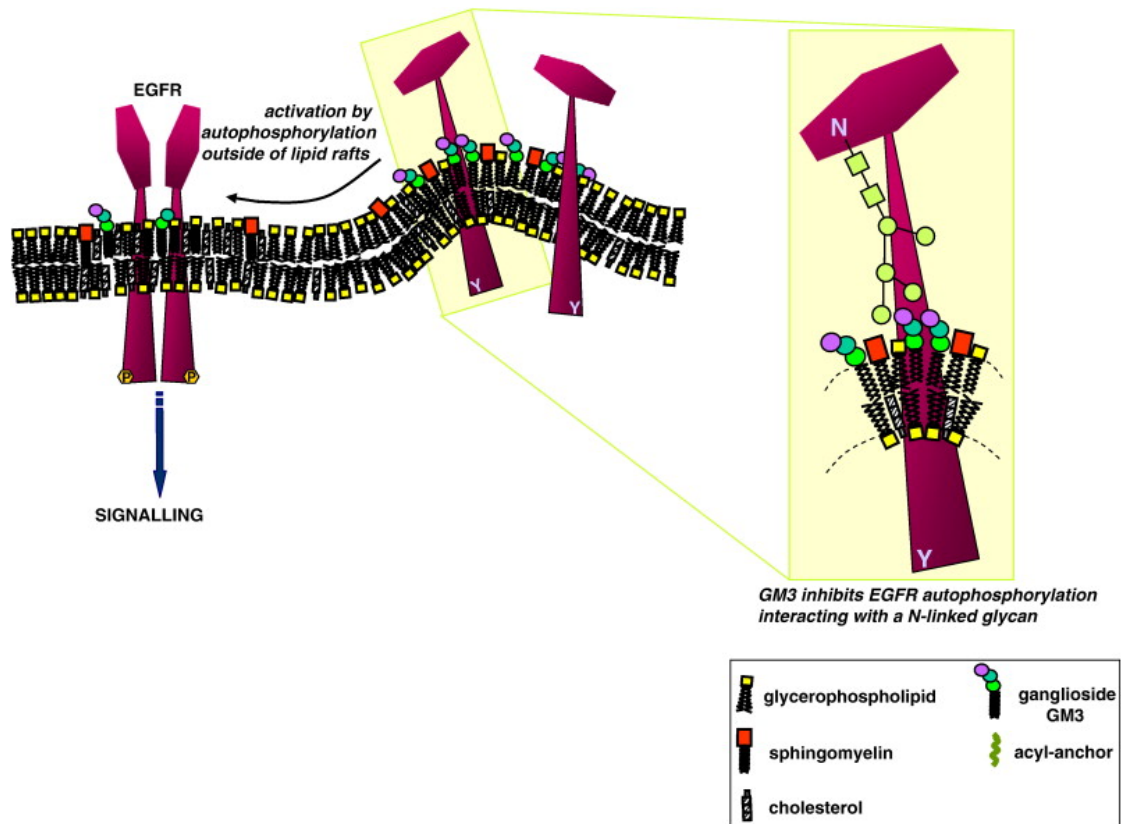


Figure I-11. GM3 and EGFR [115].

1.3.2.3. Ganglioside GM3 and VEGFR

Angiogenesis is one of the key aspects of malignant tumor growth. The role of angiogenesis in the process of tumor growth is shown in **Figure I-12**. When the tumor volume is less than 2 mm³, nutrition is provided to the tumor cells mainly through diffusion of oxygen into the tumor, and there are no blood vessels inside or on the surface of the tumor to provide nutrition for it, and there is actually no blood supply at this time; as the tumor volume becomes larger and larger, when it exceeds 2 mm³, the tumor cells will secrete vascular endothelial growth factor (VEGF), which specifically binds to the vascular endothelial growth factor receptor (VEGFR) on the surface of vascular endothelial cells to promote angiogenesis, thereby generating more blood supply to provide nutrients for tumor cell growth, which in turn supports the rapid growth of tumor cells and allows the tumor to develop and metastasise continuously. Regardless of the tumor type, angiogenesis is a key driver of tumor development [116],[117].

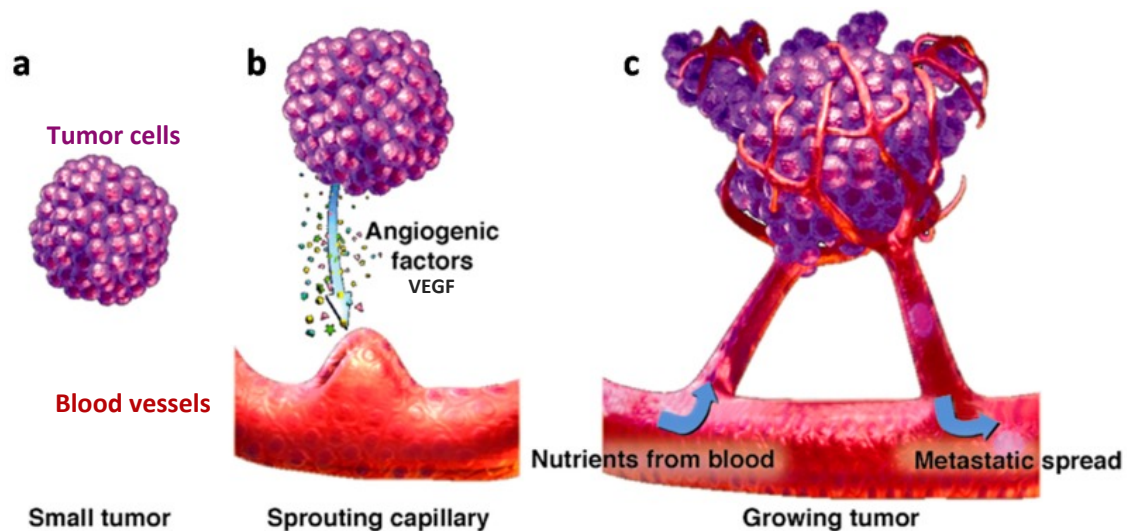


Figure I-12. Tumor expansion induced by the sprouting of blood vessels. (a) Small tumor. (b) Sprouting capillary. (c) Growing tumor [117].

In addition to tumor cells, the ganglioside GM3 also interacts with cell surface receptor molecules on vascular endothelial cells and there is growing evidence that GM3 can also regulate the angiogenic response of microvessels stimulated by angiogenic factors and is essential for the progression of the tumor-induced microenvironment. In the 1980s and 1990s, Gullino et al. induced new capillary formation in the rabbit cornea by optimal doses of angiogenic factors (e.g. prostaglandin E1, PGE1). The rabbit cornea was stimulated by angiogenesis with approximately twice the total ganglioside content of the unstimulated cornea, while the total concentration of GM3 produced a relative decrease compared to other gangliosides, suggesting that the optimal angiogenesis occurs in an environment with a low proportion of GM3 content [118]. Subsequent increases in GM3 content then revealed that angiogenesis was inhibited *in vivo* in a GM3-rich environment and also had an inhibitory effect on microvascular endothelial growth *in vitro*. This indicated that GM3 concentrations in the endothelial cell microenvironment had a decisive effect on the progression of tumor-induced angiogenesis [119]. Further experiments revealed that GM3 inhibited the proliferation of endothelial cells induced by human tumor cells from four (U 87, Filice, 166HT, SKNBE) different sources, indicating that in addition to animal experiments, the growth inhibitory effect of GM3 on vascular endothelial cells is also applicable to human vascular endothelial cells with tumors [120].

Furthermore, other studies have shown that after malignant mouse astrocytoma (CT-2A) was transfected with an antisense GalNAc-T plasmid, pcDNA3.1/TNG, into CT-2A/TNG cells, GM3 expression was upregulated and CT-2A/TNG tumor growth and angiogenesis and VEGF expression were significantly lower than in control CT-2A tumors, showing that GM3 may regulate the possible mechanism of tumor angiogenesis [121]. Further studies demonstrated that exogenous addition of GM3 significantly inhibited VEGF-induced proliferation and migration of human umbilical vein endothelial cells (HUVECs) and VEGF enhancer ganglioside GD1a-induced angiogenesis in severe combined immune deficiency (SCID) mice as shown in **Figure I-13**. Furthermore, the enrichment and depletion of GM3 was accompanied by a corresponding decrease and increase in

phosphorylation of VEGFR-2 and downstream Akt in HUVECs. These results are a further step forward in the analysis of the mechanism of action of GM3 in inhibiting angiogenesis [122],[123].

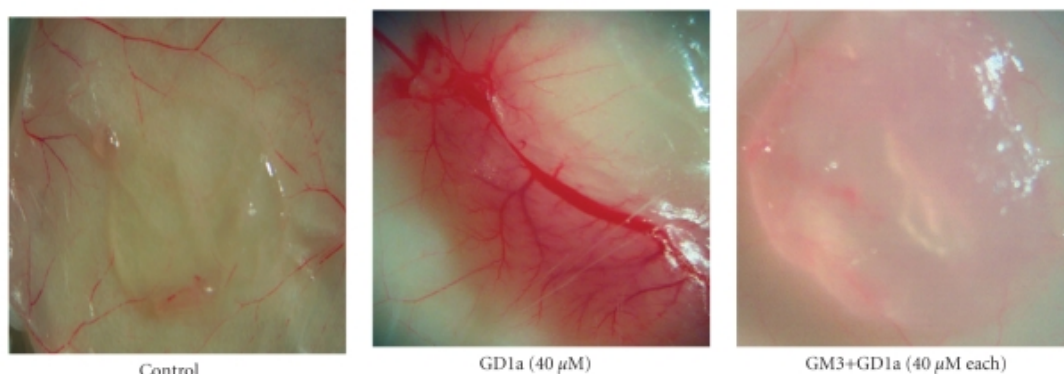


Figure I-13. GM3 inhibits the proangiogenic effects of GD1a in vivo Matrigel plug assay. Matrigel alone (control) or containing GD1a or GD1a with GM3 was injected subcutaneously in SCID mice. Plugs were photographed (12.5 \times) on day 7 after Matrigel injection [122], [123].

1.3.2.4. Ganglioside GM3 and tumor cell motility

Tumor cell migration and invasion are major factors affecting tumor metastasis and GM3 plays an important role in tumor cell motility. Low GM3 synthase activity, low GM3 content and high cell motility have been previously reported in A2780 human ovarian cancer cells, whereas cells overexpressing GM3 synthase and cells treated with exogenous GM3 showed strongly reduced cell motility [101]. In addition, histopathological examination showed that superficial bladder tumors showed a large accumulation of GM3 and infiltrating tumors showed a small amount of GM3, i.e. the expression of GM3 was inversely correlated with the invasive potential. In addition, exogenous supplementation of GM3 inhibited the invasive potential of human bladder tumor cell lines (T-24, KK-47) [100]. Similarly, when exogenous GM3 was incubated with glioma cells in vitro in an invasion assay, cell invasion was inhibited [99]. Further studies found that GM3 inhibition of tumor cell motility was associated with CD9, a member of the Tetraspanins (TSPs) family, and that haptotactic motility in the colorectal carcinoma cell lines SW480, SW620, and HRT18, which express CD9 at high levels, was inhibited by exogenous GM3, while motility in the gastric cancer cell line MKN74, which expresses CD9 at low levels, was not affected by exogenous GM3. When MKN74 cells expressed CD9 at high levels by transfection with CD9, its motility was inhibited by exogenous GM3. When mutant Chinese hamster ovary cell line Id1D cells were transfected with the CD9 gene (Id1D/CD9) and grown in galactose-containing medium, endogenous GM3 synthesis was observed and the motility of these Id1D/CD9 cells was greatly inhibited. In the mutant Chinese hamster ovary cell line Id1D cells transfected with the CD9 gene (Id1D/CD9) and grown in galactose-containing medium, endogenous GM3 synthesis was observed and the motility of these Id1D/CD9 cells was greatly inhibited. The above results revealed that the co-expression of CD9 and GM3 synergistically inhibited the motility of tumor cells. To test the association of GM3 with CD9 on the cell surface, the addition of photoactivatable (3)H-labelled GM3 to HRT18 cells followed by UV irradiation and (3)H labelling of CD9 was observed, indicating that exogenously

added GM3 interacted and cross-linked with CD9, cooperatively reducing the motility of tumor cells [102].

In-depth studies revealed that GM3 promoted the interaction of CD9 with $\alpha 3$ integrins in microdomains, thereby inhibiting laminin-5 (Ln5)-mediated cell motility [124]. Ln5 induces cell motility by interacting with integrin $\alpha 3\beta 1$ on the basal plasma membrane to activate relevant signalling pathways [125]. Results from Kawakami, Y.'s group showed that CD9 and integrin $\alpha 3$ co-immunoprecipitated in ldlD/CD9 cells under synthetic GM3 conditions (+Gal medium) but not under non-synthetic GM3 conditions (-Gal medium), and that by exogenous addition of GM3 to -Gal medium The co-immunoprecipitation of CD9 and $\alpha 3$ was enhanced. The surface expression of $\alpha 3$ was higher in cells grown under -Gal conditions than under +Gal conditions, suggesting that GM3 synthesized under +Gal conditions facilitated the interaction of $\alpha 3$ with CD9, thereby limiting the binding of $\alpha 3$ to antibodies. Furthermore Ln5/ $\alpha 3$ -dependent motility of ldlD/CD9 cells was greatly enhanced under -Gal conditions, but strongly inhibited under +Gal conditions. These results demonstrate the interaction of GM3 with CD9 and $\alpha 3$ [124]. The same results of action were obtained in human bladder cancer cell lines, where high or low GM3 levels promoted or inhibited the interaction of $\alpha 3$ with CD9 to stabilize or destabilize the $\alpha 3$ -CD9-GM3 complex within the microdomain. It was also found that in the highly aggressive and metastatic human bladder cancer cell line YTS1, where GM3 levels are low, c-Src (cellular Src kinase) was activated. Activation of c-Src was inhibited by exogenous addition of GM3 to translocate the C-terminal Src kinase (Csk) into the same microdomain [126]. It has been reported that $\alpha 3\beta 1$ interacts with Ln5 to activate Src kinase signaling to enhance cell motility, and that Csk phosphorylates and downregulates Src family tyrosine kinases to inhibit their activity [127],[128]. This effects of GM3 on the interaction of c-Src with Csk has also been reported by Toledo MS et al [129]. The above indicates that GM3 can inhibit tumor cell motility through two mechanisms of action: 1) The GM3/CD9 complex interacts with integrin $\alpha 3\beta 1$ to inhibit Ln5- $\alpha 3\beta 1$ -mediated activation of related signalling pathways or proteins (e.g. Src family kinases), thereby inhibiting tumor cell motility. 2) GM3 can also inhibit tumor cell motility by mediating the interaction of c-Src with Csk.

An additional study has shown that GM3 can form a complex with ganglioside GM2 and TSPs CD82 to exert an important inhibitory effect on hepatocyte growth factor (HGF)-induced activation of the receptor tyrosine kinase c-Met leading to cell motility [130]. HGF binding to c-Met activates c-Met, which then activates numerous downstream signalling pathways such as PI3K-Akt and Ras-MAPK, thereby exerting its effects on cell proliferation and motility [131],[132]. The Todeschini, AR team showed that GM2-GM3 forms a heterodimer in the presence of Ca^{2+} , and that c-Met activation and motility were strongly inhibited when bladder cancer cells high in CD82 expression, YTS-1 / CD82, were cultured with nanospheres coated with GM2/GM3 dimer. And activation of downstream effectors of the c-Met pathway, including c-Src and mitogen-activated protein kinase (MAPK), was also inhibited in the presence of GM2/GM3 dimers interacting with CD82. It was evidenced that the GM2 / GM3 / CD82 complex effectively inhibits cell motility by blocking the HGF-induced c-Met pathway in cells.

Furthermore, in the absence of HGF, YTS-1/CD82 cell adhesion to Ln5-coated plates resulted in c-Met activation and the GM2/GM3 dimer inhibited c-Met activation caused by Ln5-mediated $\alpha3\beta1$ activation and suppressed cell motility. Based on the above it is demonstrated that the GM2/GM3/CD82 complex inhibits HGF-induced c-Met kinase and Ln 5-mediated activation of $\alpha3\beta1$ and interaction of $\alpha3\beta1$ with c-Met tyrosine kinase ('crosstalk'), leading to inhibition of cell motility and growth [130]. Both $\alpha3\beta1$ and c-Met are important transmembrane receptors on the surface of tumor cells, and both can mediate signalling related to tumor invasion and metastasis, either independently or by interacting with each other. The possible mechanisms by which GM3 inhibits tumor cell motility through the inhibition of these two pathways are shown in **Figure I-14** [133],[134].

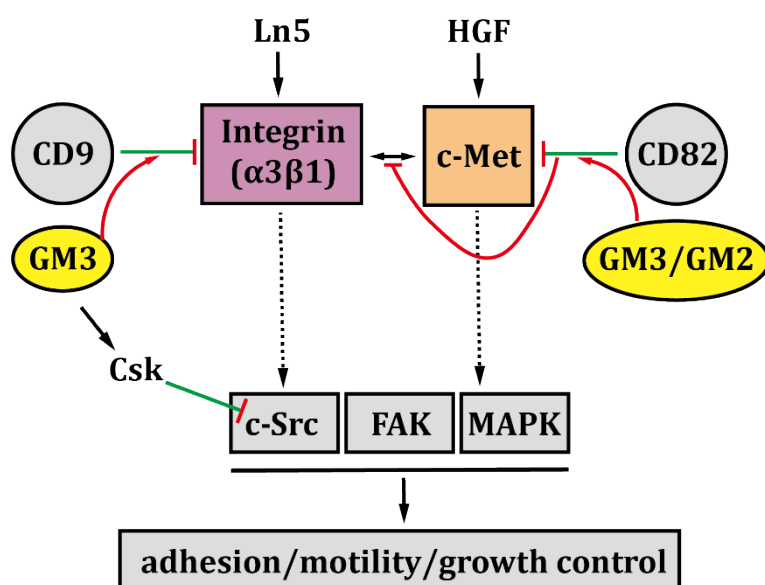


Figure I-14. Schematic representation of possible mechanisms by which GM3 inhibits tumor cell motility. (i) GM3 enhances the interaction of CD9 with integrin $\alpha3$ and inhibits c-Src activation following Ln5-induced integrin activation; it also inhibits c-Src activation via Csk. (ii) The GM2/GM3/CD82 complex inhibits HGF-induced activation of c-Met and cross-talk between c-Met and integrin $\alpha3\beta1$. (iii) Signalling (i) and (ii) involves various signal transduction molecules such as cellular Src kinase (Src), focal adhesion kinase (FAK) and mitogen-activated protein kinase (MAPK); and subsequently controls cell adhesion, motility or growth [133],[134].

1.4. Synthesis of ganglioside GM3 analogues

In recent years, with the development of biochemistry and molecular biology, great progress has been made in the study of the structure, function and application of the ganglioside GM3. The ganglioside GM3 is closely related to some tumors and its anti-tumor effects to a certain extent are encouraging. Meanwhile the synthetic studies of GM3 derivatives have also received extensive attention, and many studies have shown that GM3 derivatives display significant anti-tumor activity [109],[135]. In general, the usual procedure for the synthesis of GM3 is to construct a sialic acid block, a lactose block and a sphingosine block, each of which is linked by a glycosidic bond, and finally the fatty acid is introduced to the sphingosine to complete the synthesis of GM3 (**Figure I-15**) [136]. For GM3 derivatives, we will present some typical examples in the order of modification of

the blocks in the structure from left to right (sialic acid, lactose, ceramide).

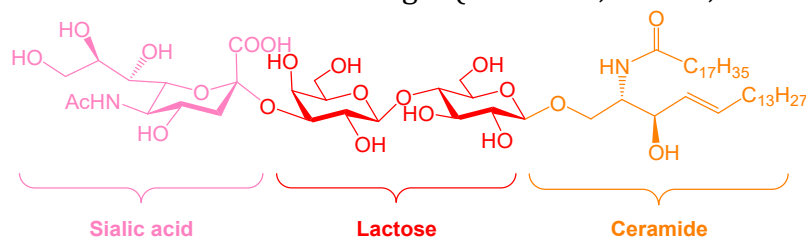


Figure I-15. Structures of the GM3.

1.4.1. Modification of sialic acid block

Ye et al. [137] reported the synthesis of three GM3 analogues with modifications on sialic acid, which provided two different N-modified GM3 analogues on the acetamino group in the sialic acid residue (**Figure I-16a, 16b, 16c**). In addition, another research group has synthesized compounds (**Figure I-16c**) based on the synthesis of GM3 once again in higher yields, as well as the new GM3 analogue (**Figure I-16d**) [135]. In the analysis of EGFR autophosphorylation and cell proliferation in human epidermoid carcinoma A431 cells, the inhibitory effect of two chloro-derivatives on EGFR activity was stronger than that of GM3. In particular the monochloro-GM3 (not GM3 or dichloro-GM3) has a significant inhibitory effect on Δ EGFR, which is a mutant form of EGFR, and is usually found in human glioblastomas.

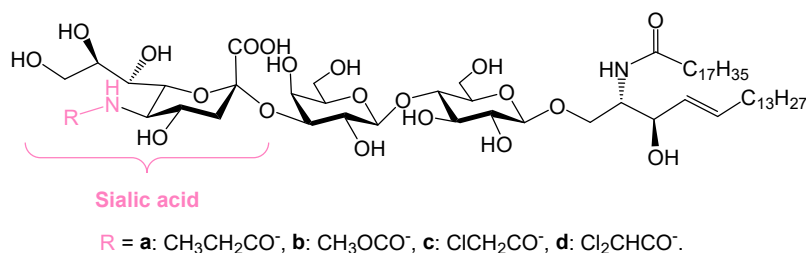


Figure I-16. GM3 analogues modified on acetamino position of sialic acid.

Meng and her colleagues describe a chemoenzymatic approach to synthesize Lyso-GM3 (Compound 1) and GM3 (Compound 4) and their derivatives (**Figure I-17**) [138]. This strategy catalyzes the sialylation of the Lac β Sph receptor by using bacterial salivary base-transferases. These compounds were further investigated for their activity on cancer cell proliferation and migration. Anti-proliferative activity studies showed that compounds 1-3 with sphingomyelin exhibited greater potency than the compounds 4-6 with ceramide. Anti-migration activity studies showed that all gangliosides GM3 and lysozyme GM3 were effective in inhibiting the migration of melanoma B16-F10 cells.

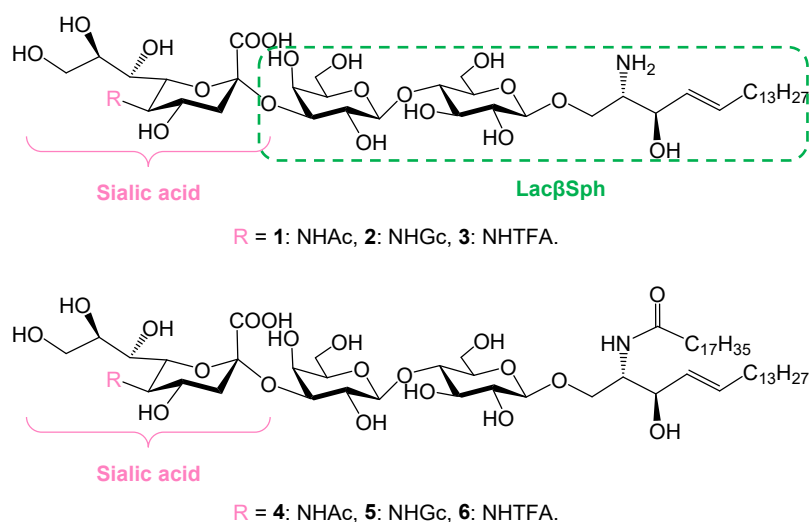


Figure I-17. GM3 analogues modified on acetylamino position of sialic acid.

1.4.2. Modification of lactose block

For the modification of the lactose block, Kiso et al. [139] described the synthesis of a positional isomer of GM3, which is a α -2,6 sialoside instead of α -2,6 sialoside (**Figure I-18**).

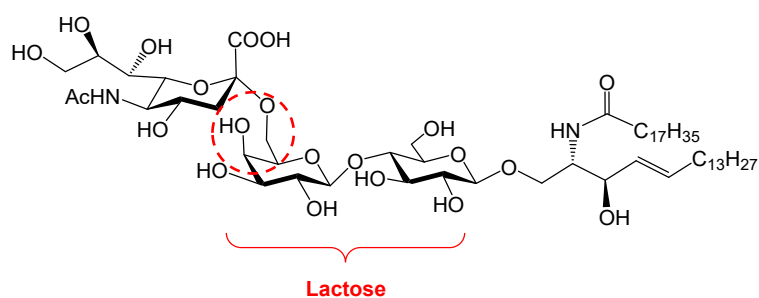


Figure I-18. The positional isomer of GM3.

Sodeoka et al. [140] reported four analogues of ganglioside GM3 that contain a C-sialoside linkage rather than the native O-sialoside linkage. These included two CHF-linked stereoisomers (**Figure I-19a, 19b**) as well as CF₂ and CH₂-linked GM3 analogues (**Figure I-19c, 19d**). Their biological functions are similar to those of the native GM3, the C-linked GM3 analogues inhibited EGF-induced autophosphorylation of the epidermal growth factor receptor (EGFR) in vitro. In addition, proliferative activity assays in Had-1 cells as well as NMR-based conformational analysis showed that the (*S*)-CHF-linked GM3 analogue with an *exo*-isomeric conformation was the most potent of the synthesized compounds. This may provide some inspiration for the design and synthesis of new GM3 analogues.

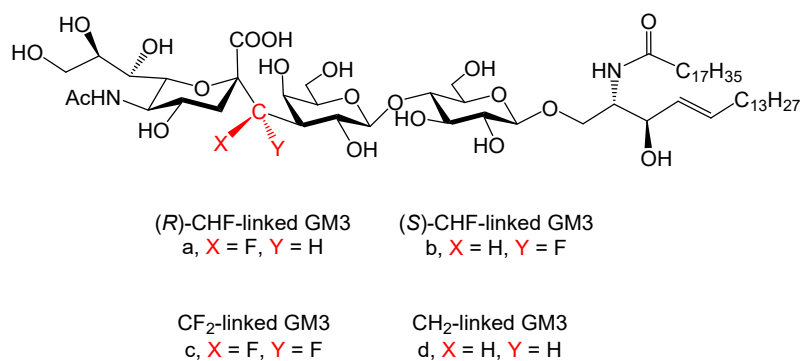


Figure I-19. C-sialoside linkage GM3 analogues.

1.4.3. Modification of ceramide block

The previous examples focused on the structures of the sialic acid and the lactose blocks. Next, we will show some structural modifications of the ceramide block. The GM3 analogues using sphingosine instead of the ceramide block was first synthesized which named Lyso-GM3. Furthermore, the amino group on sphingosine was further modified to synthesize a series of GM3 analogues, such as the introduction of a (C₁₇H₃₅CO-), b (CH₃CO-), c (CH₃OCOCH₂CH₂-), d (CF₃CO-), e (ClCH₂CO-) groups onto the amino group (**Figure I-20**) [137].

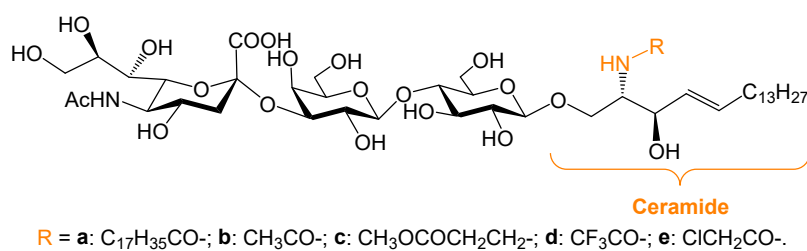


Figure I-20. Ceramide partially modified GM3 analogues.

Hakomori's [141],[142] group reported synthesis of lipid mimetics of GM3 (LM-GM3) and lyso-GM3, as well as LM-GM3 dimer and Lyso-GM3 dimer (**Figure I-21**). These compounds were used to study the effects on EGFR tyrosine kinase activity and the consequent changes in the phenotype of A431 cells. First, the LM-GM3 dimer showed comparable strong inhibition of EGF-induced EGFR tyrosine kinase activity and displayed similar low cytotoxicity to the Lyso-GM3 dimers. In addition, the LM-GM3 dimer inhibited tyrosine phosphorylation of EGFR or its dimer similarly to the lyso-GM3 dimer, but more potent than the LM-GM3 or GM3. Further studies revealed that the inhibitory effect of LM-dimers on EGF-induced EGFR kinase activity. Only Akt kinase activity was significantly inhibited, but kinases associated with other signal transducers were not affected.

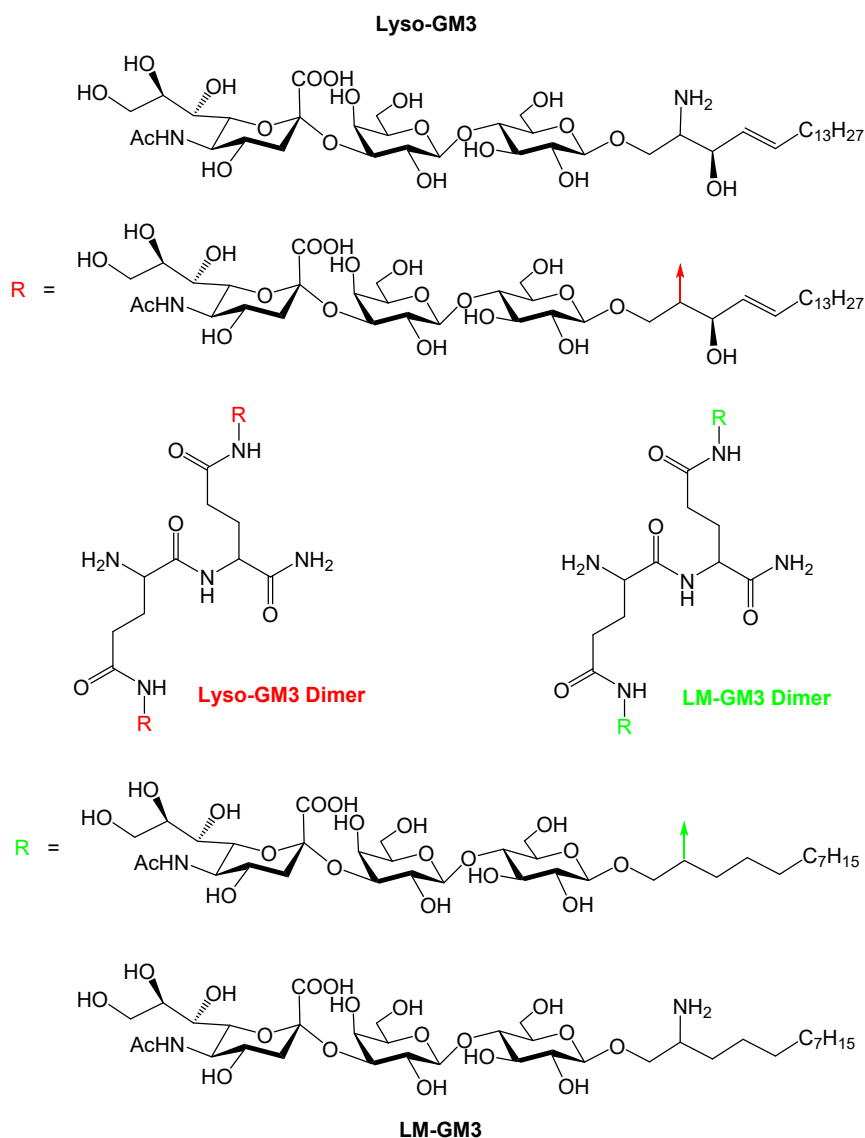


Figure I-21. Lyso-GM3, LM-GM3 and their dimers.

1.5. Multivalent ligand effect

The "multivalent ligand effect" can also be referred to as the "glycosyl cluster effect" [143],[144]. This theory suggests that glycosyl receptors are present in clusters on the cell surface and that the binding sites for glycans are multi-local. Numerous modelling studies have shown that the presence of a multivalent ligand effect can significantly increase the binding of ligand-receptor. Attempts have been made to explain the mechanism of the multivalency effect in five ways (**Figure I-22**) [145]. Including (A) Chelating effect: Multivalent ligands can bind oligomeric receptors by occupying multiple binding sites (1:1). (B) Clustering effect: multivalent ligands can cause receptors to aggregate on the cell surface, enhancing the multivalent interactions. (C) Statistical effect: The physical size and distribution of the multivalent ligand can prevent other competing ligands from binding to the receptor. (D) Subsite binding effect: Multivalent ligands can occupy primary and secondary binding sites on the receptor. (E) Statistical effect:

multivalent ligands show higher concentrations of local binding sites, which may lead to higher apparent affinity.

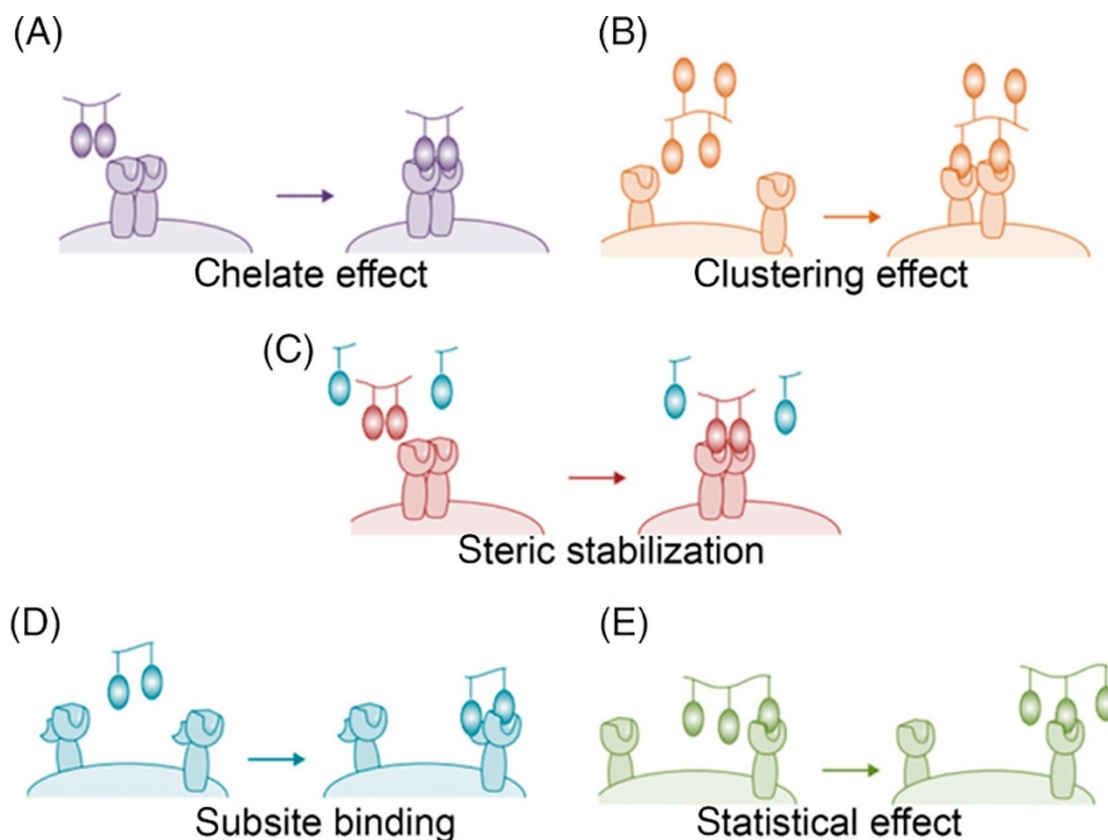


Figure I-22. potential mechanisms of multivalent ligand effects

In these circumstances, a multivalent ligand can bind to one or more receptors simultaneously to enhance ligand-receptor interactions for enhanced functional affinity compared to monovalent ligands. The multivalent effect has been widely developed and applied in the field of glycobiology, for example, the development of anti-cancer drugs containing glycoconjugate moieties, which are based on naturally occurring glycoproteins and glycolipids to design reasonable glycoconjugate mimics with similar or even better functions than natural glycoproteins and glycolipids in terms of bioactivity, thus obtaining glycodrugs with better binding power and selectivity [141],[142]. With the continuous research on glycoprotein and glycoglycan interactions and the in-depth understanding of receptor structure and function, new binding sites are constantly discovered, which will lead to the more rational design of multivalent ligand molecules and enable them to better satisfy the needs of drug design. Based on this concept, we believe that for improving the activity of glycolipid molecules, in addition to modifying their structures, using multivalent ligand effects to mimic the binding process of natural glycolipids to receptors is also an effective way to improve the activity of glycolipids [146].

1.6. Background of this project

The current study shows that GM3 acts in an autocrine or paracrine manner on tumors or tumor-associated host cells (e.g. endothelial cells), and that some tumors show their malignant nature by expressing GM3, but tumors with high GM3 expression are often non-invasive, while tumors with low GM3 expression are often more malignant. GM3 can influence the growth, invasion and metastasis of different tumor types through the regulation of various cytokines and cell signalling pathways, and is closely related to cellular carcinogenesis. GM3 is a physiological substance secreted by cells, which is highly tolerable and less toxic, and studies on GM3 derivatives have shown that they have similar safety profile as GM3, but also have the same or even stronger anti-tumor effects.

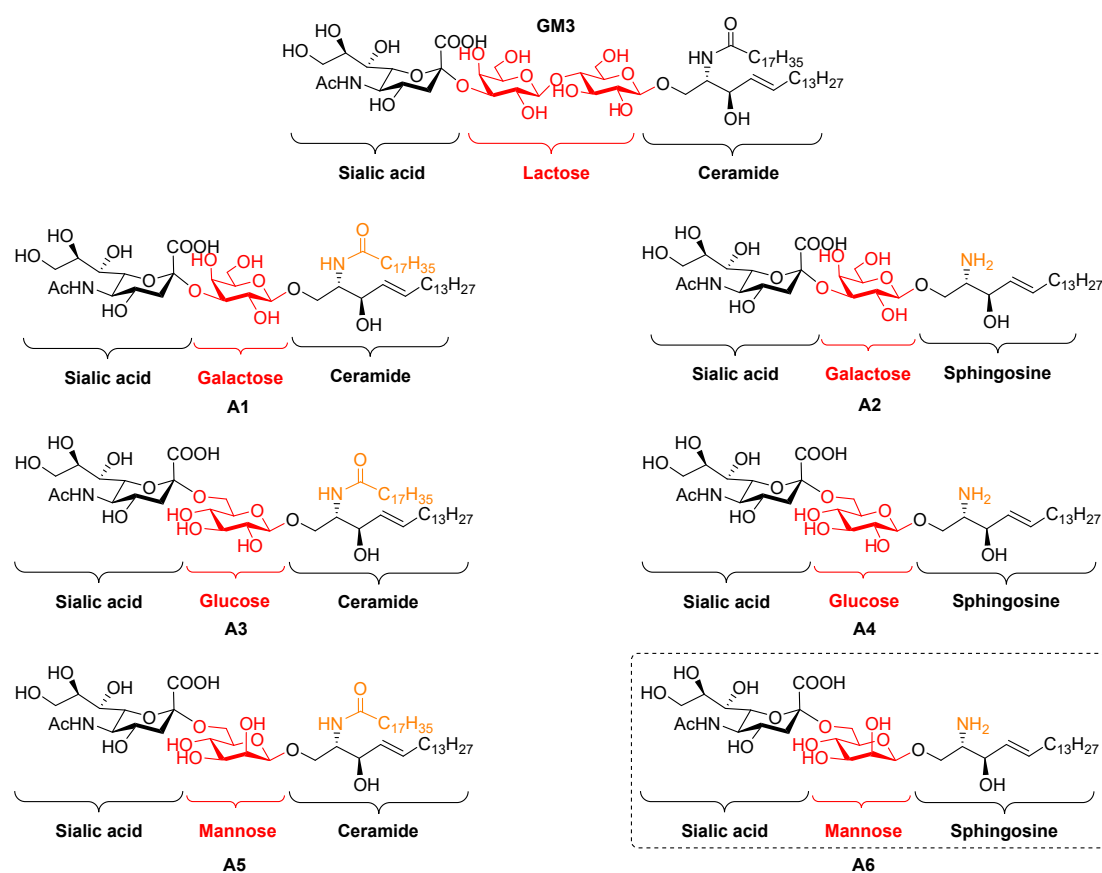


Figure I-23. GM3 and its analogues.

Previous work in our laboratory has synthesized a number of GM3 analogues. These analogues mainly focus on the replacement of the lactose residue block in the GM3 structure with other glycosyl groups (Figure I-23). These GM3 analogues show interesting anti-tumor activity and this activity is highly selective towards tumor cells [147],[148]. In particular, the mannose-containing GM3 analogue A6 showed a better ability to inhibit the proliferation and migration of tumor cells. In order to find anticancer agents with better biological activity than previously synthesized GM3 analogues, we expected to use the concept of multivalent effects to design synthetic oligomers based on GM3 analogue monomers to further improve their antitumor capacity. In this project, we designed and synthesized a series of oligomers containing the GM3 analogue A6, including dimer, trimer and

tetramer with a micromolecular skeleton. and hexamers and heptamers with a macromolecular skeleton, and evaluated the antitumor activity of these oligomers.

We believe that this work will provide a reference for the synthesis and purification of oligomers for the preparation of GM3-related anticancer agents on the one hand, and for the exploration of new and more potent anti-tumor agents. On the other hand, it provides a meaningful theoretical basis for the exploration of new GM3-related carbohydrate anticancer agents with stronger potency.

Chapter II
Synthesis of mannose-containing GM3 analogue monomer

2.1. Introduction

This chapter describes the synthesis of the mannose-containing GM3 analogue monomer. The target monomer structure contains three units, the structure is shown in **Figure II-1**.

O-(5-acetamido-3,5-dideoxy-D-glycero- α -D-galacto-2-nonulopyranosylonic acid)-(2 \rightarrow 6)-O-(α -D-mannopyranosyl)-(1 \rightarrow 1)-(2S,3R,4E)-2-amino-4-octadecene-1,3-diol.

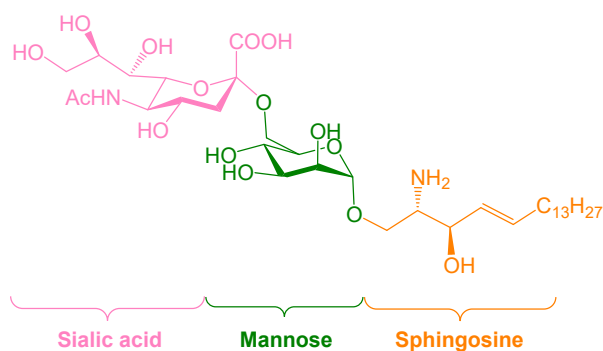


Figure II-1. Mannose-containing GM3 analogues.

2.2. Retrosynthetic analysis

The retrosynthetic analysis of the mannose-containing GM3 analogue monomer is shown in **Figure II-2**. Our synthetic strategy is divided into three parts: firstly, the three key building blocks are prepared; secondly, the sialylation of mannoside is completed with a sialic acid donor to construct the sialo-oligosaccharide; finally, the lipid precursor is incorporated into the sialo-oligosaccharide.

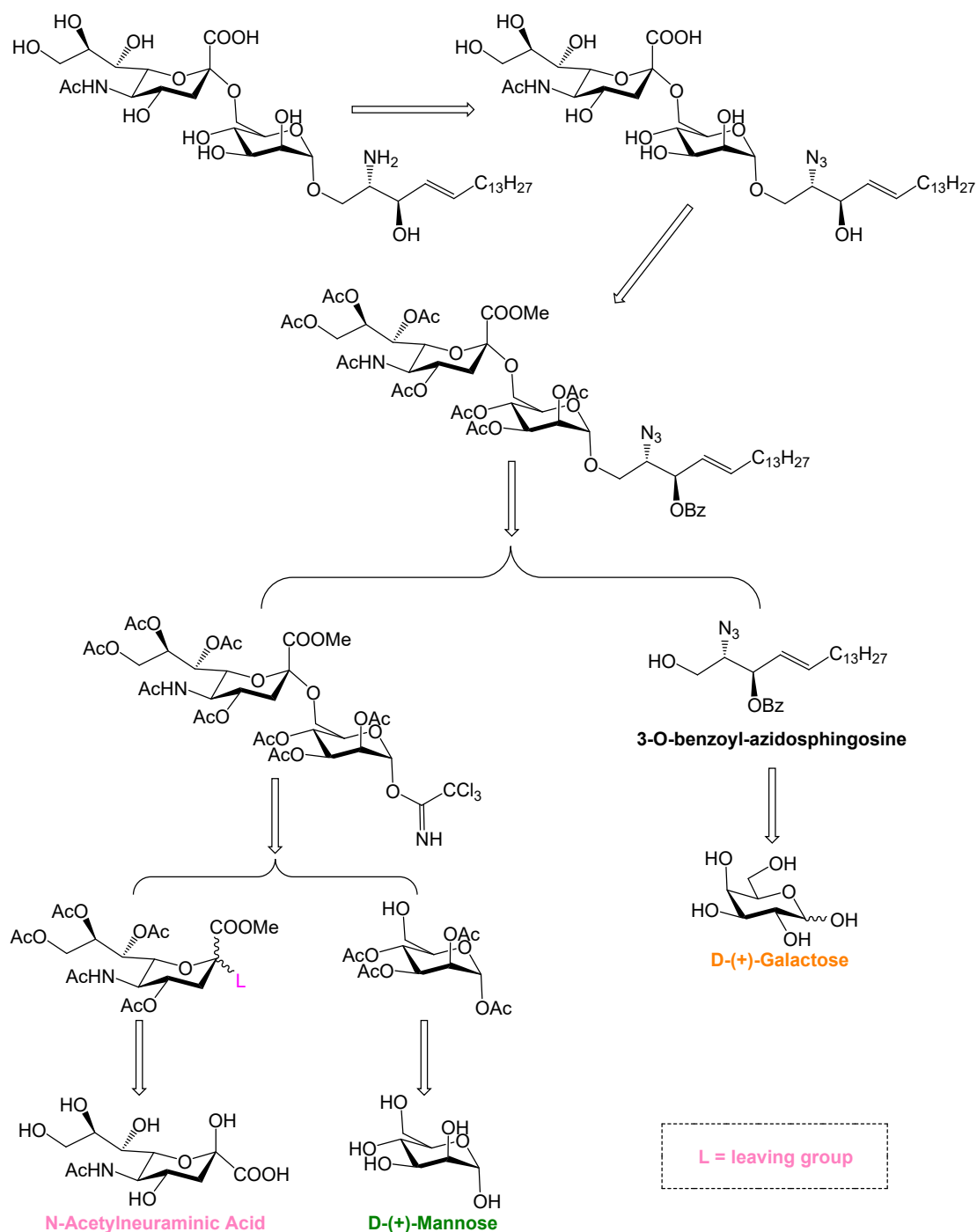
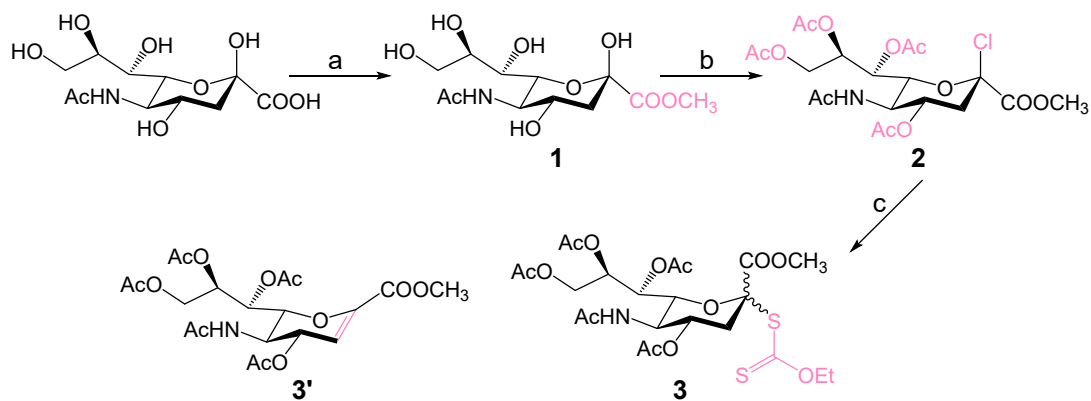


Figure II -2. Retrosynthetic plan for synthesis of the mannose-containing GM3 analogue.

2.3. Preparation of sialic acid donor block

The formation of chemical O-sialylation involves the coupling of a glycosyl acceptor with a free hydroxyl group to a sialosyl donor with an appropriate leaving group at the anomeric center (C-2). Therefore, we need to activate the sialic acid donor in the form of sialyl xanthate, and the synthesis of sialic acid donor **3** can be achieved as shown in **Scheme II-1** [149],[150].

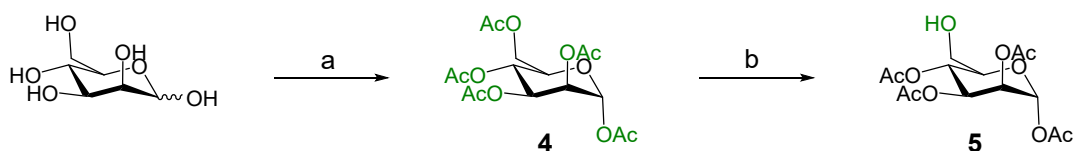


Scheme II-1. Reagents and conditions: (a) Amblyst-H⁺, MeOH, 45 °C, 12 h, 95%; (b) AcCl, 0 °C, MeOH, r.t., 72 h, 88%; (c) EtOH, 0 °C, K₂CO₃, 12 h, r.t., 12 h, 74% (for **3**), 15% (for **3'**).

The reaction of sialic acid with methanol under acidic conditions provided by an Amblyst-H⁺ resin was heated to 45 °C overnight to give a colorless clarified solution, and removal of the solvent gave methyl ester **1** in good yield, and compound **1** was pure enough to be used in the next reaction step without further purification. In this step of the reaction, we used the Amblyst-H⁺ resin, which can be removed by filtration, as an acidic catalyst to avoid liquid acid. Next, the crude methyl ester **1** was treated with acetyl chloride for three days and a small amount of methanol was added to further promote the formation of the fully acetylated chloroneuraminic acid methyl ester **2**. Although the reaction time for this step was relatively long, however, the yield of sialyl chloride **2** was excellent. Ultimately, sialyl chloride **2** was reacted with O-ethyl S-potassium dithiocarbonate in dry ethanol to give α- and β-sialyl xanthate **3** and glycal **3'** in a molar ratio of 16:1:3. Chromatographic separation yielded our target sialic acid donor **3**. Since α- or β-linked sialosides have very similar glycosyl donor properties, so the α/β-**3** mixture was used directly in the ensuing sialylation reaction without subjecting the anomers to further separation.

2.4. Preparation of mannose glycosyl receptor block

We have employed a simple and efficient chemoenzymatic approach for the preparation of monohydroxytetraacetylated monosaccharides as building blocks for oligosaccharide synthesis. The strategy is based on regioselective hydrolysis catalyzed by immobilized lipase. The most commonly used immobilized lipase for regioselective deacetylation is *Candida rugosa* lipase (CRL), which could specifically remove the C-6 acetyl group from the per-acetylated sugars and is particularly effective in the hydrolysis of the α anomer of the acetylated monosaccharide, while the hydrolysis of the β anomer is largely unresponsive [151],[152],[153].

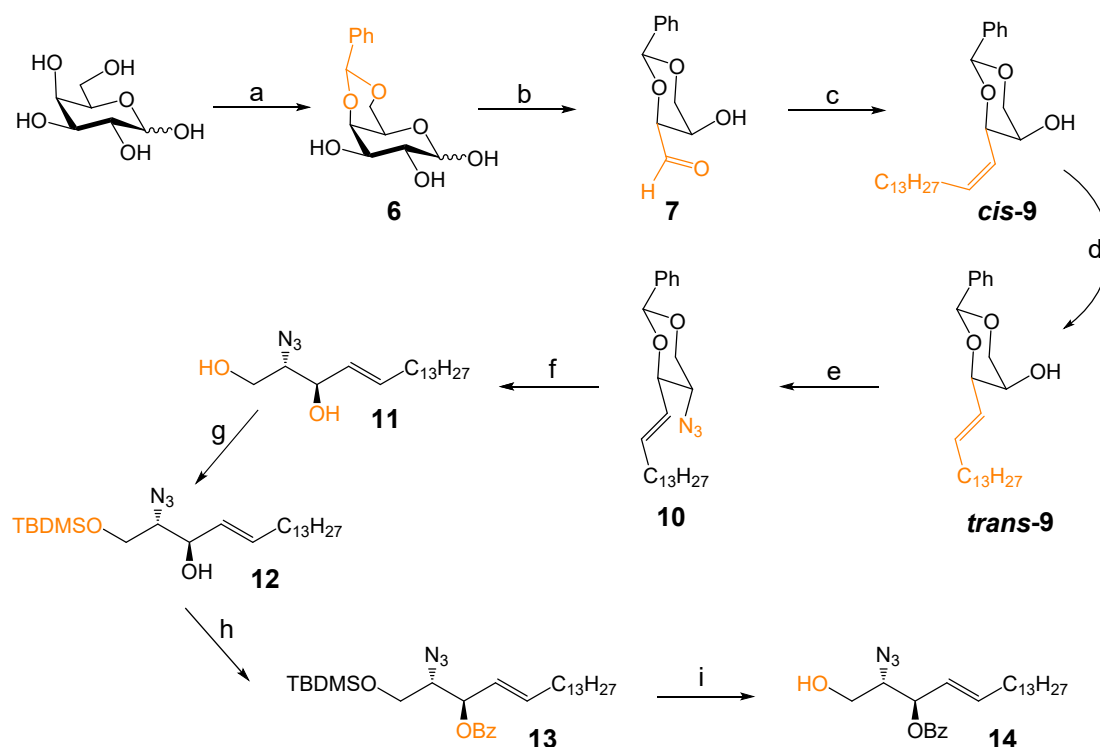


Scheme II-2. Reagents and conditions: (a) Ac₂O, pyridine, r.t., 12 h, 72%; (b) enzyme CRL, phosphate buffer, CH₃CN, r.t., 4 h, 78%.

Starting from commercially available D-(+)-mannose, mannose residues with a free 6-OH can be synthesized in high yield, as shown in **Scheme II-2**. Firstly, the exposed hydroxyl group in the D-(+)-mannose molecule reacted with anhydrous acetic anhydride in the presence of pyridine to form a per-acetylated mannose **4**, thus completing the protection of the hydroxyl groups. Compound **4** was then added into phosphate buffer containing 20% acetonitrile at pH 5, and biocatalyst CRL was added to initiate the reaction. After 4 h of the reaction, the enzyme was recovered by filtration and the mannose residue **5** with a free 6-OH was obtained in good yield as a glycosyl acceptor.

2.5. Preparation of azidosphingosine block

Sphingosine is a long-chain amino alcohol containing 18-20 carbon atoms, and the most common sphingosine in glycosphingolipids is C₁₈-sphingosine, of which 3-O-benzoyl azidosphingosine is the preferred glycosyl acceptor for the preparation of glycosphingolipids [154],[155],[156]. To date, many synthetic routes have been published for the synthesis of 3-O-benzoyl azidosphingosine [157],[158],[159],[160],[161],[162],[163] and in this section we have avoided the use of expensive and dangerous chemicals in favor of a simple and practical method for the synthesis of 3-O-benzoyl azidosphingosine [164].



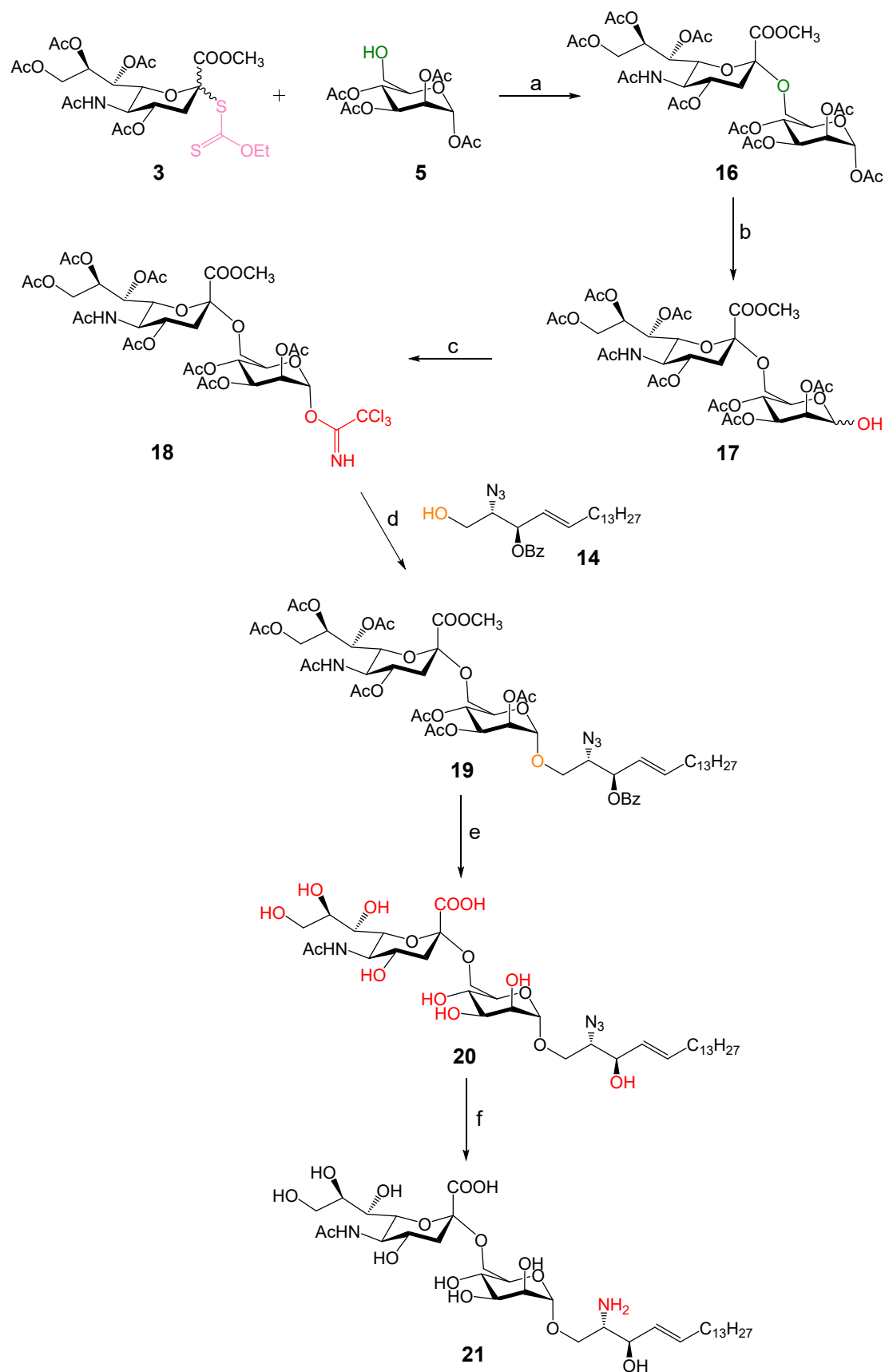
Scheme II-3. Reagents and conditions: (a) α,α -dimethoxytoluene, PTSA, DMF, 40 °C, 3 h, 79%; (b) NaIO_4 , phosphate buffer (pH = 7.6, 0.1 M), r.t., 2 h, 68%; (c) tetradecyltriphenylphosphonium bromide **8**, n-butyllithium, THF, -30 °C, 12 h, 46% (**trans-9**) and 16% (**cis-9**); (d) diphenyldisulfide, cycl ohexane, dioxane, high-pressure mercury lamp, 5 h, 48%; (e) Tf_2O , DCM, Pyr., -15 °C, 15 min; NaN_3 , DMF, r.t., 3 h, 78%; (f) PTSA, MeOH, DCM, r.t., 24 h, 92%; (g) TBDMSO, DCM, Pyr., r.t., 3 h, 94%; (h) BzCl , Pyr., r.t., 1 h, quant.; (i) $\text{BF}_3 \cdot \text{Et}_2\text{O}$, DCM, r.t., 4 h, 82%.

4,6-O-benzylidene was first introduced into the commercially available **D-(+)-galactose** by α,α -dimethoxytoluene in dry DMF in the presence of p-toluenesulfonic acid (PTSA). The methanol formed during the reaction was gradually evaporated at 40 °C to facilitate the reaction thus yielding compound **6** in good yield. Next, aldehyde **7** was obtained by treatment with sodium periodate in phosphate buffer (pH = 7.6, 0.1 M). Then, 1-bromotetradecane and PPh_3 were reacted at 140 °C for 7 h to prepare tetradecyltriphenylphosphonium bromide **8** [165] which reacted with aldehyde **7** and n-butyllithium in THF at -30 °C to afford a mixture of isomers with a ratio $\text{trans/cis} = 3/1$. After careful purification, the desired **trans-9** was obtained in 46% yield. The **cis-9** could be converted to the desired **trans-9** through an illumination reaction in the presence of diphenyldisulfide in 48% yield. According to the reported method, the azide group was carefully introduced into **trans-9** via the corresponding triflate intermediate [166] Notably, extraction and concentration of reaction mixtures containing sodium azide have been reported to be potentially explosive, so this procedure should be performed with caution [167]. Deprotection of azide **10** was carried out by acid-catalyzed transacetalation, which was quenched using Et_3N at the end of the reaction to give azidosphingosine **11** in a very high yield. Ultimately, the diol

11 underwent selective protection of the primary and secondary hydroxyl groups by TBDMSCl and benzoyl chloride, respectively, as well as deprotection of the TBDMS group to provide the desired azidosphingosine derivative 3-O-benzoyl azidosphingosine **14** (**Scheme II-3**), which will be used in the glycosidic coupling reactions.

2.6. Synthesis of mannose-containing GM3 analogues

The sialylation reaction is a key step in the synthesis of sialic acid conjugates. Because of the steric hindrance of the glycerol structure at the C6 position, the C3 position lacks a hydroxyl group, so it lacks neighbor participation effect to control the α/β configuration selectivity, and the presence of an electron-withdrawing carboxyl group in sialyl donors, the conditions of the sialylation reaction are harsher than the general glycosylation reaction [168],[169],[170] so the efficiency of obtaining α -glycosidic linkages in the sialylation reaction is one of the most important indicators for evaluating the merits of the reaction. According to our previous study, we optimized the α -sialylation reaction between the acceptor and the sialic acid donor by the following **Scheme II-4**.

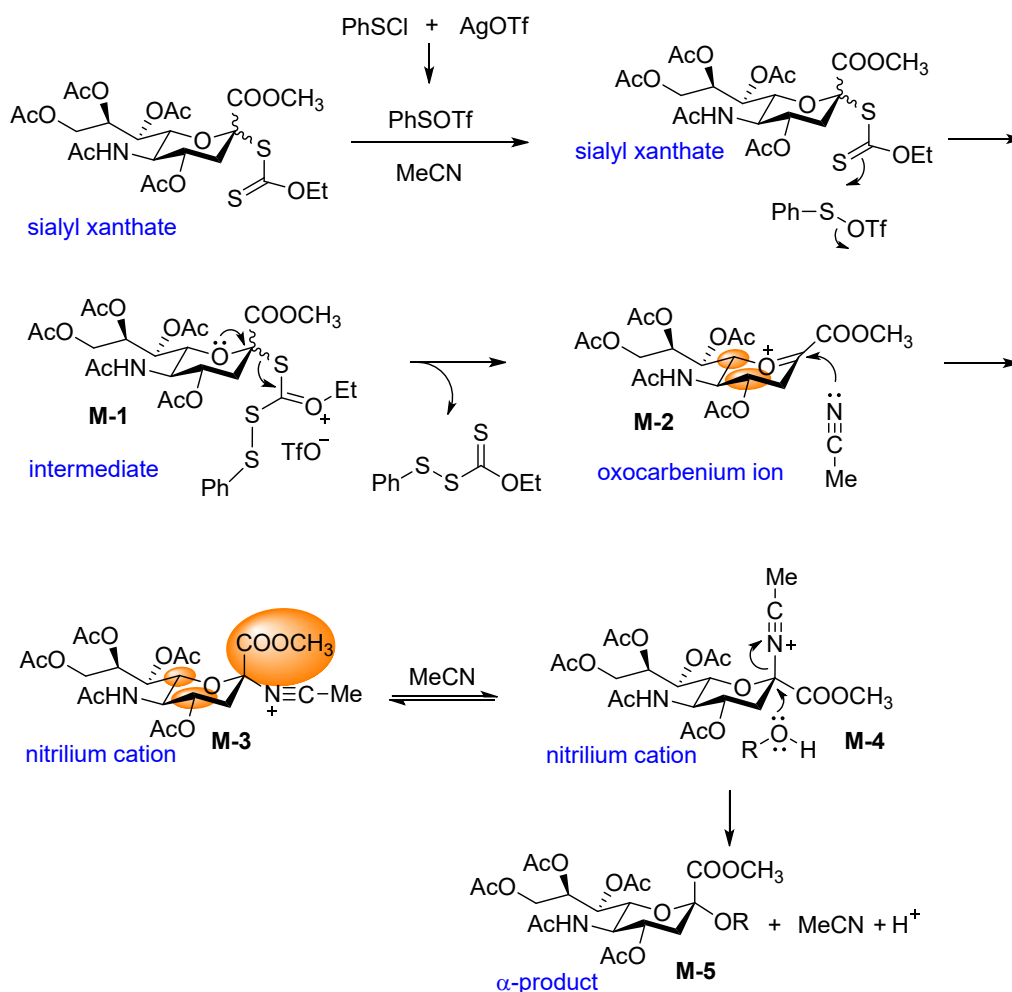


Scheme II-4. Reagents and conditions: (a) CH₃CN, CH₂Cl₂, molecular sieves, r.t., 1 h, AgOTf, DTBP, -68 °C, PhSCl, 3 h, 52%; (b) PhCH₂NH₂, THF, r.t., 12 h, 72%; (c) CCl₃CN, DBU, CH₂Cl₂, -5 °C - 0 °C, 12 h, 70%; (d) BF₃·Et₂O,

CH₂Cl₂, molecular sieves, -15 °C, 2.5 h, 54%; (e) NaOMe, MeOH, r.t., 14 h; H₂O, 0 °C - r.t., 2 h; (f) HS(CH₂)₃SH, Et₃N, pyridine-water (1:1 v/v), 50 °C, 12 h, 82%.

We used the Martichonok and Whitesides method for the α -sialylation reaction between the sialyl xanthate and the free 6-OH of per-acetylated mannose residue. PhSOTf formed by adding PhSCl and AgOTf as a promoter reacted in a mixture solvent of CH₂Cl₂:CH₃CN (1:2) for 3 h at a low temperature of (-68 °C) [147],[148].

In the reaction mechanism as shown in **Scheme II-5** [171], in the first step, sialyl xanthate reacts with PhSOTf to obtain the oxonium cation M-2 by forming the intermediate M-1. In the second step, the oxonium cation M-2 is stabilized by reacting with acetonitrile to form the nitrilium cations M-3 and M-4. Due to kinetic and thermodynamic control, the nitrilium cation M-3 may be formed first, and when acetonitrile is attacked from M-2, the formation of M-4 is hindered by unfavorable steric interactions with protons at C-4 and C-6 of the sialic acid, and the nitrilium cations M-3 and M-4 are in equilibrium in this step. In the third step, the receptor ROH reacts with the nitrilium cation M-4 to give the α -product M-5. The attack on the nitrilium cation M-3 is very hindered due to the protons at C-4 and C-6 and the CO₂Me group. A small amount of β -product is formed by the reaction of the receptor ROH with the oxonium cation M-2.



Scheme II-5. Proposed mechanism for α -sialylation reaction.

Because of the lack of anomeric hydrogen at the C-2 position of sialic acid, the anomeric configuration can be confirmed based on empirical rules, including δ H-3eq, δ H-4, $\Delta\delta$ {H-9a-H-9b}, $J_{\text{H-7,H-8}}$, $J_{\text{C-2,H-3ax}}$ and $J_{\text{C-1,H-3ax}}$. It was demonstrated that the chemical shift of H-3eq of the α isomer is shifted downfield (δ 2.67-2.72 ppm) compared to that of the β isomer (δ 2.25-2.40 ppm). And the chemical shift of H-4 of the α isomer is shifted upfield (δ 4.89-4.93 ppm) compared to that of the β isomer (δ 5.68-5.81 ppm). In addition, the anomeric configuration of sialic acid glycosides can be determined from the difference in chemical shifts between two vicinal protons at C-9 ($\Delta\delta$ {H-9a-H-9b} values), which is 0.5 ppm for α -glycosides and about 1.0 ppm for β -glycosides. Besides that, depending on the coupling constants, including the coupling constants $J_{\text{H-7,H-8}}$ between H7,H8 on the side chains of the sialic acid residues, the $J_{\text{H-7,H-8}}$ values of α -glycosides (6.2-8.5 Hz) are larger than those of β -isomers (1.5-2.6 Hz); furthermore, it was shown that the sialic acid residues within α -isomers (5.8-7.5 Hz) show larger $J_{\text{C-1,H-3ax}}$ values than those of β -isomers (1.0- 1.7 Hz); and $J_{\text{C-2,H-3ax}}$ values, which were found to be about 8.0 Hz for the α -isomer and about 4.0 Hz for the β -isomer [172],[173],[174],[175],[176],[177],[178].

Where PhSCl **15** was freshly prepared each time and the addition of DTBP to remove the proton could improve the yield. Finally, the α -sialoside **16** was obtained in satisfactory yield. The α -sialoside was then reacted overnight at room temperature in THF in the presence of benzylamine to selectively remove the acetyl group at the anomeric center to give the hemiacetal **17** as an α and β mixture. The reaction of trichloroacetonitrile with the hemiacetal in the presence of DBU gave trichloroacetimidate **18**. Next, the glycosylation of trichloroacetimidate and 3-O-benzoyl azidostigmine was carried out using $\text{BF}_3 \cdot \text{Et}_2\text{O}$ as a promoter. In this step, the α -configuration target monomer **19** of the newly introduced glycosidic linkage was obtained due to the acetyl group at C-2 position of mannose (neighboring participation effect). Subsequently, under Zemplén transesterification (NaOMe/MeOH) conditions, all protecting groups were removed and the resulting product was directly reduced for its azide group with propanedithiol/triethylamine without further purification to give the mannose-containing GM3 analogue monomer **21** (**Scheme II-4**).

To summarize: this section describes the synthesis of the mannose-containing GM3 analogue monomer M1.

Chapter III

Synthesis of mannose-containing GM3 analogue oligomers with small molecule skeletons based on "click chemistry"

3.1. Introduction

This chapter describes the synthesis of the dimer, trimer and tetramer of the mannose-containing GM3 analogues. The structures of these oligomers are shown in **Figure III-1**.

Dimer of mannose-containing GM3 analogues:

1,2-Di-{1-[O-(5-acetamido-3,5-dideoxy-D-glycero- α -D-galacto-2-nonulopyranosylonate) -(2 \rightarrow 6)-O-(α -D-mannosyl)-(1 \rightarrow 1)-(2S,3R,4E)-4-octadecene-1,3-diol]-1H-1,2,3-triazole-4-ylmethoxy} ethane.

Trimer of mannose-containing GM3 analogues:

1,3,5-Tri-{1-[O-(5-acetamido-3,5-dideoxy-D-glycero- α -D-galacto-2-nonulopyranosylonate) -(2 \rightarrow 6)-O-(α -D-mannosyl)-(1 \rightarrow 1)-(2S,3R,4E)-4-octadecene-1,3-diol]-1H-1,2,3-triazole-4-ylmethoxy} benzene.

Tetramer of mannose-containing GM3 analogues:

Tetrakis- {1-[O-(5-acetamido-3,5-dideoxy-D-glycero- α -D-galacto-2-nonulopyranosylonate) -(2 \rightarrow 6)-O-(α -D-mannosyl)-(1 \rightarrow 1)-(2S,3R,4E)-4-octadecene-1,3-diol]-1H-1,2,3-triazole-4-ylmethoxy} pentaerythritol.

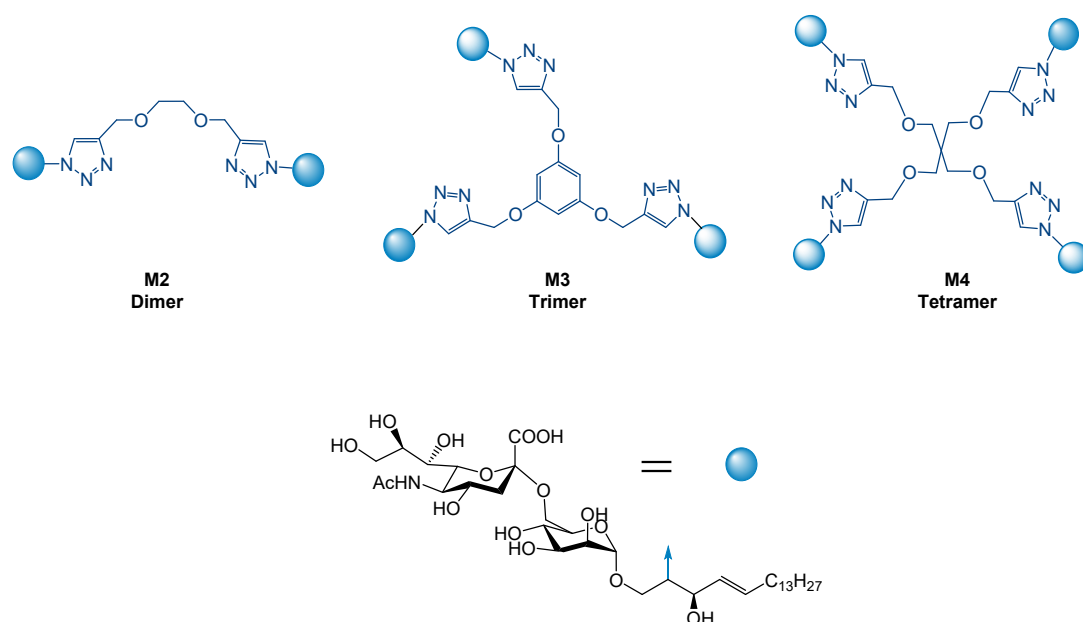


Figure III-1. Structures of the dimer, trimer and tetramer of mannose-containing GM3 analogues.

3.2. Retrosynthetic analysis

Retrosynthetic analysis of dimer, trimer, and tetramer of mannose-

containing GM3 analogues is shown in **Figure III-2**. The synthetic strategy of these oligomers is as follows: firstly, three small molecular skeletons containing alkyne groups were prepared and then tightly linked with the target monomers of mannose-containing GM3 analogues with azide groups by the "click reaction". Finally, the protecting groups were removed to obtain the desired oligomers.

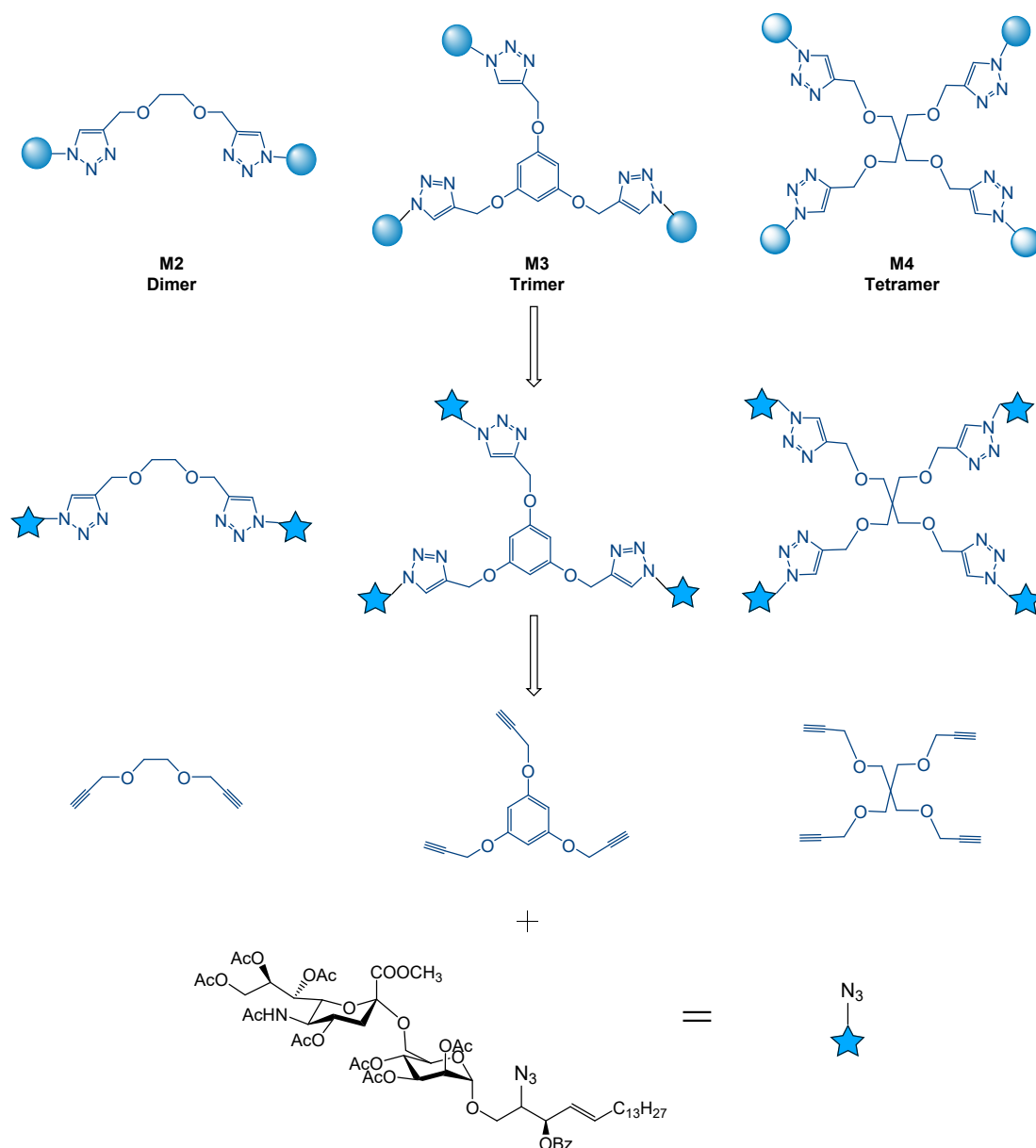
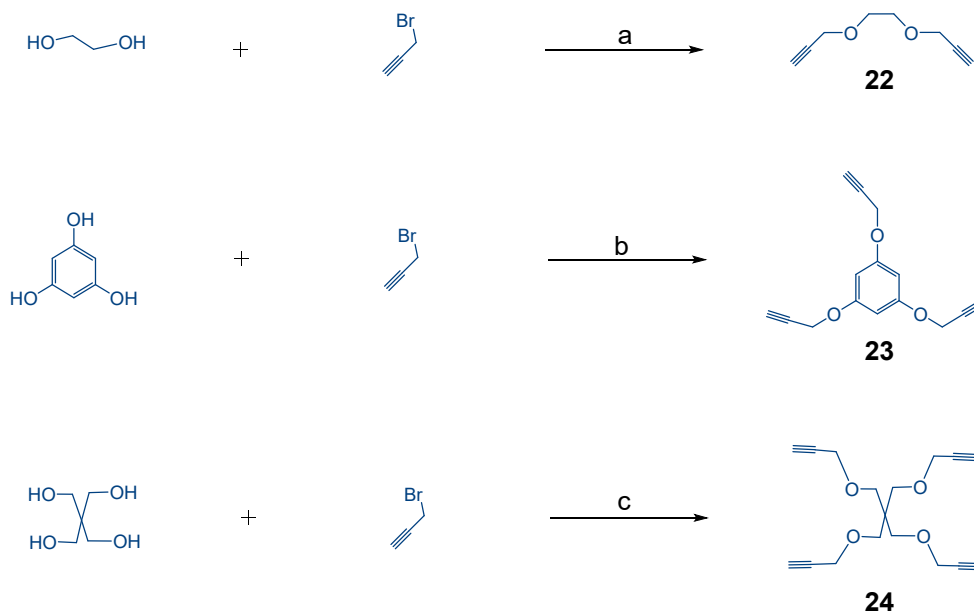


Figure III-2. Retrosynthetic plan for the synthesis of the dimer, trimer and tetramer of mannose-containing GM3 analogues.

3.3. Preparation of small molecular skeletons

The alkyne group is one of the least reactive functional groups in organic chemistry and is chemically inert with many common functional groups, making it highly compatible with many systems [179]. For the desired small molecule

skeletons, we obtained the corresponding divalent, trivalent and tetravalent skeletons by reacting bromopropyne with ethylene glycol, phloroglucinol and pentaerythritol under basic conditions provided by different bases, respectively, as shown in **Scheme III-1** [180],[181], [182].



Scheme III-1. Reagents and conditions: (a) KOH, DMF, 0 °C-r.t., 14 h, 48%; (b) K₂CO₃, DMF, 0 °C-r.t., 14 h, 75%; (c) NaH, DMF, 0 °C-r.t., 14 h, 65%.

3.4. Synthesis of dimer, trimer and tetramer of mannose-containing GM3 analogues

The term "click chemistry" was first coined by K. B. Sharpless in 2001, with the main idea being the fast and reliable construction of complex molecular structures through the stitching together of small units [183]. It particularly emphasizes the development of new approaches in combinatorial chemistry based on carbon-heteroatom linked units (C-X-C) to obtain a wider range of molecular diversity through simple, reliable and highly selective chemical transformations [185]. Because of its characteristics: easy availability of reaction raw materials; simple reaction conditions, the reaction process is insensitive to water and oxygen; high yield, no by-products or harmless by-products; and high stereoselectivity and stability of the product, etc. It is widely used in many fields such as drug development and biomedical material synthesis [179],[186],[187]. It has become one of the most attractive development directions in the pharmaceutical field and is also considered to be one of the most effective technologies to accelerate the research and development of new drugs in the future [188].

Click chemistry reactions can be divided into the following four main types: cycloaddition reactions; carbon-carbon multiple bond addition reactions;

nucleophilic ring opening reactions and mild condensation reactions of carbonyl compounds (**Figure III-3**) [189]. Among the cycloaddition reactions, the copper-catalyzed azide-alkyne 1,3-dipole cycloaddition (CuAAC) is the most classical system for click chemistry reactions. The click reaction originated from the Huisgen 1,3-dipole cycloaddition reaction, which requires high temperatures and yields a mixture of two isomers when using an asymmetric alkyne reaction [190]. In 2002, two research groups of Meldal and Sharpless independently reported that the 1,3-dipole cycloaddition reaction of azides with alkynes could be further enhanced under copper catalysis with the advantages of efficient reaction, mild conditions, high product yields and simple post-treatment, and the application of the terminal alkyne group could provide high regioselectivity [191],[192].

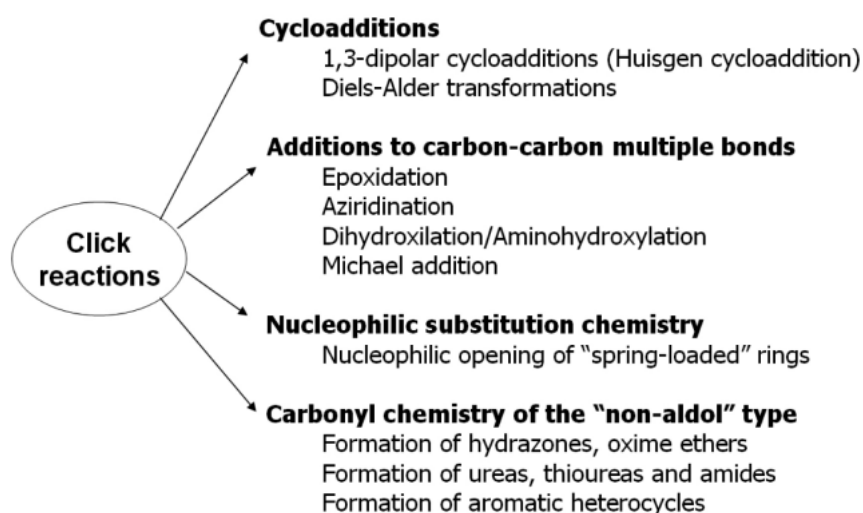


Figure III-3. Classification of click reactions [189].

Fokin and his co-workers described the mechanism of copper-catalyzed azide-alkyne cycloaddition (CuAAC) (**Figure III-4**) [193],[194],[195]. Click chemistry refers to the rapid reaction between an alkyne and an azide, with copper (I) ions as the catalyst in the process. The linkage of alkynes and azides results in the formation of a stable five-membered heterocyclic compound called the triazolide. Before the formal reaction, the alkyne functional group is first activated gradually by two copper (I) ions. The first copper(I) ion combines with an alkyne to form a monocopper acetylide. The monocopper alkynylide will form an activated bicopper alkynylide when it interacts with another copper(I) ion. During the click reaction, the copper(I) ion in the bicopper alkynylide first interacts with the third nitrogen atom in the azide functional group. Then the second carbon atom in the bicopper alkynylide forms a covalent bond with the first nitrogen atom in the azide to form a six-membered heterocyclic intermediate. Next, the third nitrogen atom in the azide forms another covalent bond with the first carbon atom in the alkyne, and the copper(I) ion that originally interacted with the nitrogen atom is removed in the process. In the last step, a proton replaces the remaining copper(I) ion to obtain the triazolide.

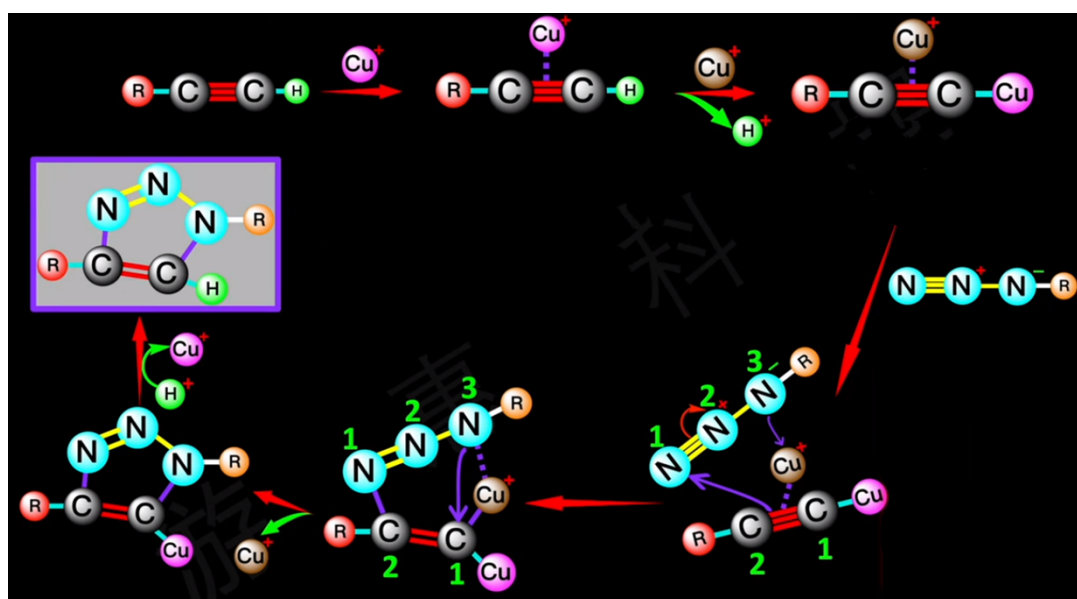
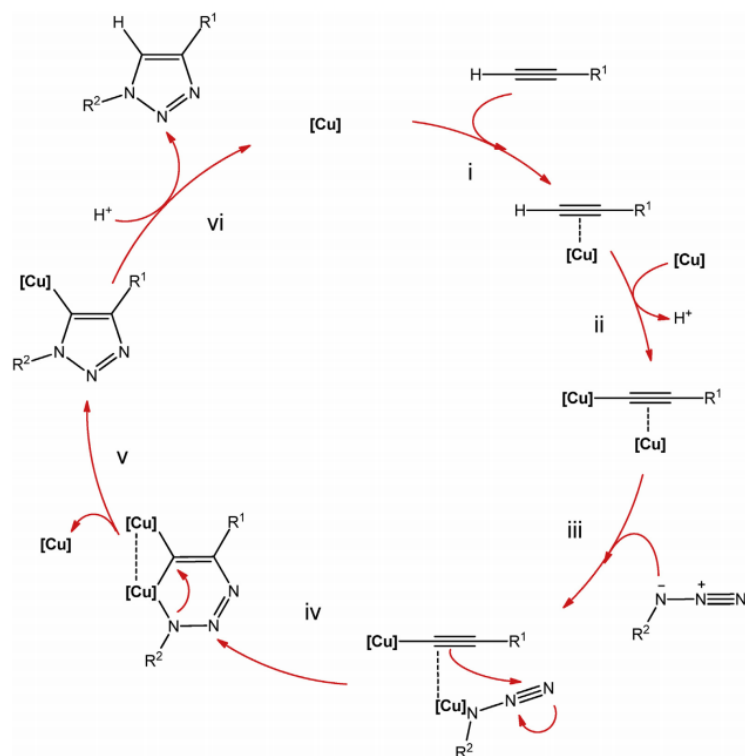
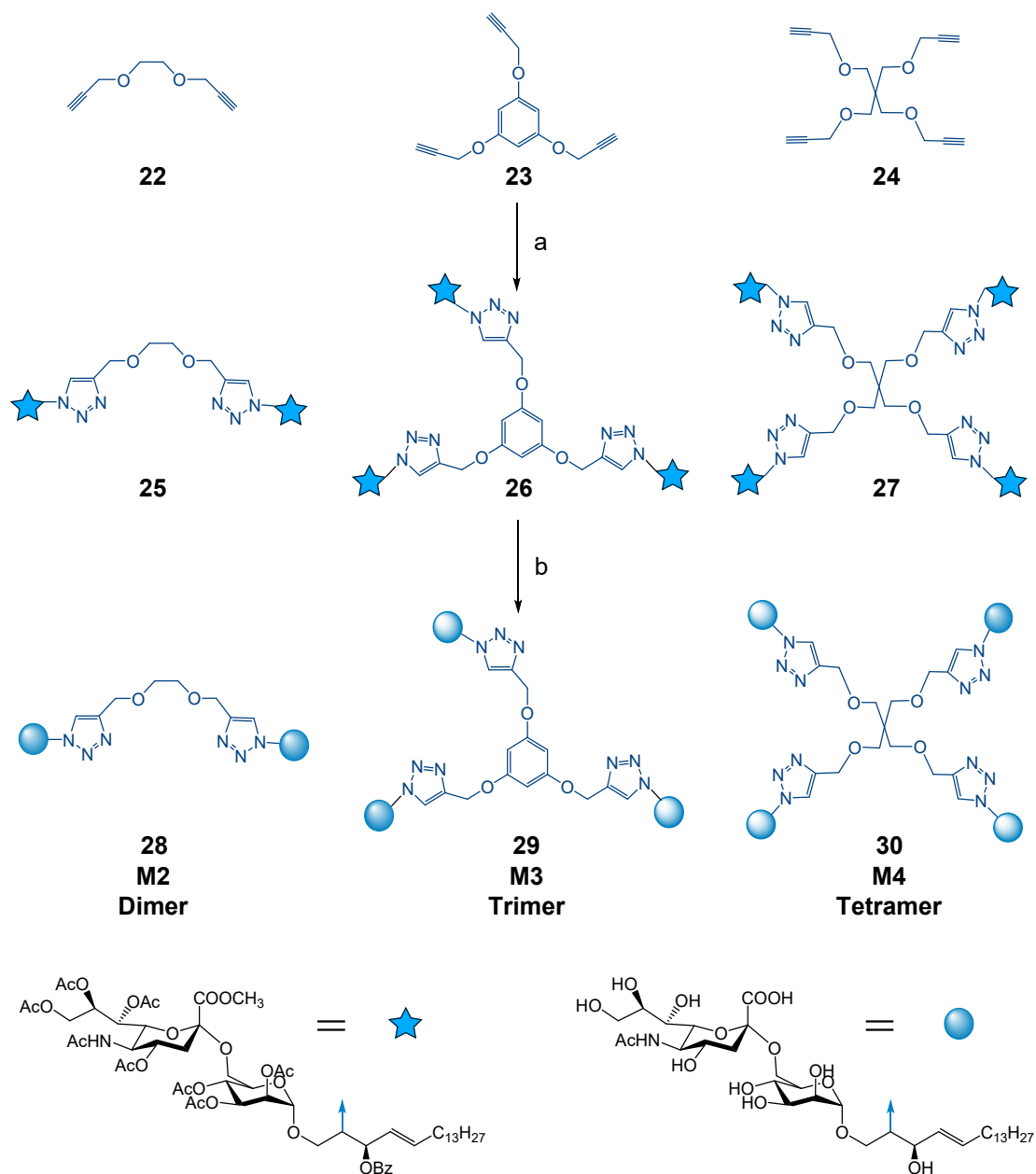


Figure III-4. Proposed mechanism of the CuAAC reaction (13).

Our synthetic strategy employed the copper-catalyzed cycloaddition reaction as shown in **Scheme III-2**, where the monomer **19** containing the azide moiety is linked to three small molecule alkyne skeletons by the click reaction, respectively. The azide monomer **19** and the alkyne skeleton were dissolved in a mixture of tetrahydrofuran and deionized water, and then copper sulfate pentahydrate and sodium ascorbate were added. Activated copper(I) catalysts can be catalyzed directly with monovalent copper salts, or by reducing divalent copper salts to monovalent copper salts using sodium ascorbate as the reducing agent. A slight

excess of sodium ascorbate is added to the reaction to prevent the formation of oxidative coupling products. The latter reduction scheme of Cu(II) salt is used in this step of the reaction. The reaction system was reacted at 56 °C for 24 h. The protected di-, tri- and tetramers (**25**, **26**, **27**) were then purified by extraction and column chromatography. Eventually, all protecting groups were removed under Zemplén transesterification (NaOMe/MeOH) conditions to achieve the target oligomers (**28**, **29**, **30**) in good yields.



Scheme III-2. Reagents and conditions: (a) **19**, CuSO₄·5H₂O, sodium ascorbate, THF, H₂O, 56 °C, 24 h, **25**-62%; **26**-55%; **27**-48%; (b) NaOMe/MeOH, H₂O, r.t., 12 h, **28**-83%; **29**-85%; **30**-84%.

To summarize: this section describes the synthesis of the dimer M2, trimer M3 and tetramer M4 of the mannose-containing GM3 analogue.

Chapter IV

Biological evaluation of oligomers of mannose-containing GM3 analogues based on small molecular skeletons

4.1. Introduction

Some studies have shown that GM3, in addition to being involved in a number of processes such as intercellular recognition, connectivity and information transmission, also has anti-tumor effects and has a significant impact on the proliferation and motility of tumor cells [196]. GM3 is easily penetrates various tissue barriers, and has high tolerability and low toxicity characteristics unmatched by other drugs, and can inhibit tumor growth through multiple pathways. GM3 affects the proliferation of tumor cells by interacting with various membrane receptors. For example, exogenous GM3 inhibits epidermal growth factor receptor phosphorylation, thereby inhibiting the growth of human epidermoid carcinoma A431 cells [107]. Furthermore, cell motility in tumor growth is crucial and represents one of the relevant factors in assessing the malignancy of cancer. Some studies have found that GM3 may regulate the expression of MMP-9 through the PI3K/Akt signal transduction pathway to regulate cell metastasis [197]. EMT is currently seen as the pathological process that leads to tumor progression. During the malignant evolution of tumors, EMT allows tumor cells to invade and metastasize, and inhibition of EMT may be an effective way to inhibit tumor cell migration or metastasis. Some studies have demonstrated that Src kinase inhibitors such as dasatinib can effectively inhibit the occurrence of EMT [198], thereby suppressing tumor growth. Therefore, investigating the effects of exogenous drugs on EMT-related proteins and signalling pathways provides a direction for the treatment of tumors and has become a strategy for the development of new clinical drugs.

To date, we have successfully synthesized a certain amount of small molecule backbone based on oligomers of mannose-containing GM3 analogues, including dimer M2, trimer M3 and tetramer M4. In this section, the anticancer activity of monomer and oligomers of mannose-containing GM3 analogues will be evaluated. The effect of the monomer and oligomers on the growth and motility of tumor cells was investigated through a series of bioactivity evaluation assays: MTT cytotoxicity assay, cell colony formation assay, cell morphology assay, wound healing assay, Transwell migration and invasion assay and Western blot assay. This work was done in collaboration with Pr. Jianhua XU and Dr. Yan LIU (School of Pharmacy, Fujian Medical University, Fuzhou, Fujian 350122, China).

4.2. Experimental methods

Statistical Analysis

Data are expressed as the mean \pm SD from at least three independent experiments.

4.2.1. Cell culture

Human colon cancer HCT116 cells, human leukemia K562 cells, highly

metastatic murine melanoma B16F10 cells, and highly metastatic human pancreatic adenocarcinoma BXPC-3 cells were originally obtained from Shanghai Institutes for Biological Sciences, Chinese Academy of Sciences (China), and maintained in RPMI-1640 supplemented with 10% fetal bovine serum (FBS, PVN) at 37 °C and 5% CO₂, as well as penicillin and streptomycin (100 mg/ml each).

4.2.2. MTT cytotoxicity assay

Cell viability was determined using MTT method (**Figure IV-1**). Briefly, cells were seeded at a density of 5×10^3 cells/well in a 96-well plate and allowed to adhere overnight. Cells were treated with GM3 analogues (M1, M2, M3, M4) with different concentrations or vehicle DMSO for 72 h, then added 20 μ L MTT solution (5 mg/mL) into each well of the 96-well plate and incubated at 37 °C for 4 h. After incubation, the supernatant was discarded, replaced with 150 μ L DMSO and then measured at a wavelength of 570 nm (Thermo Fischer). All experiments were tested in triplicate.

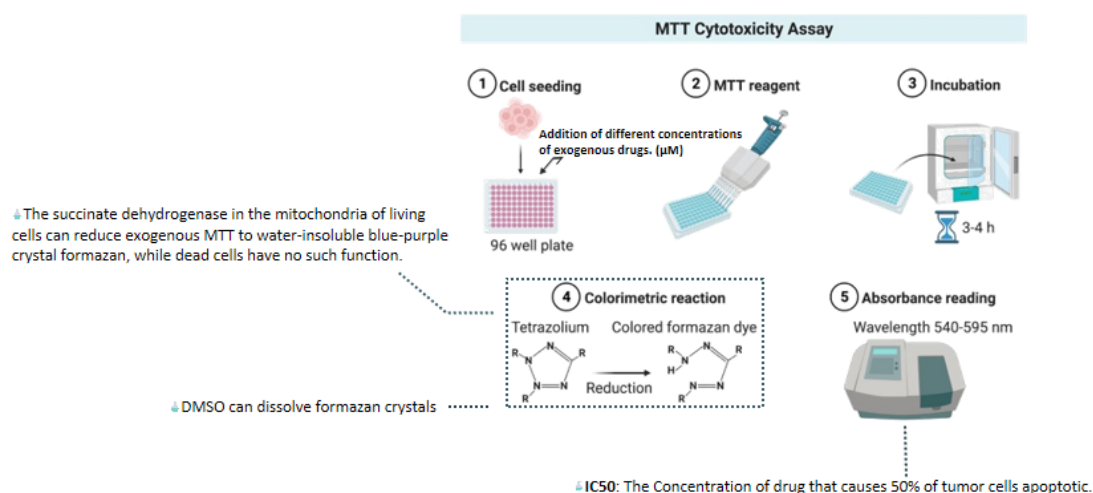


Figure IV-1. MTT cytotoxic assay procedure.

4.2.3. Cell colony formation assay

Cells were seeded in 12-well plates (700/well) and treated with different concentrations of GM3 analogues (M1, M2, M3, M4). After cultured for 24 h, cells were removed GM3 analogues, change fresh medium and cultured in a humidified 5% CO₂ atmosphere at 37 °C. After 7-14 days, removed the medium, colonies were fixed with methanol for 20 min, stained with crystal violet for 30 min and counted by light microscopy (**Figure IV-2**).

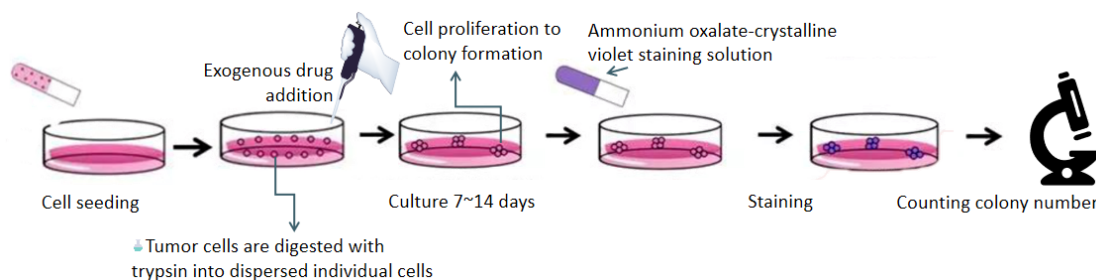


Figure IV-2. Cell colony formation assay procedure.

4.2.4. Wound healing test

B16F10 cells (5×10^4 cells/mL) were cultured into 24-well plates and grown in RPMI-1640 medium containing 10% FBS to nearly confluent cell monolayer, then used a 10 μ L plastic pipette tip to draw a “wound” in the cell monolayer of each well. The monolayer was then washed twice with PBS buffer to remove debris or detached cells, and GM3 analogues (M1, M2, M3, M4) were added at different concentrations in fresh RPMI-1640 medium without FBS, and subsequently cultured for 24 h or 36 h. The wound healing of the scratched cells was photographed under a microscope (Leica, Zeiss, Germany). The effect of GM3 analogues on tumor cell motility was expressed as migration % of control. The migration rate was calculated by formula $[(\text{wound width at 0 h} - \text{wound width at exposure time point}) / \text{wound width at 0 h}] \times 100 \%$, then the migration rate of control group was normalized to 100 %, and values were calculated as migration (%) of control group $[(\text{migration in treatment} / \text{migration in control}) \times 100 \%]$.

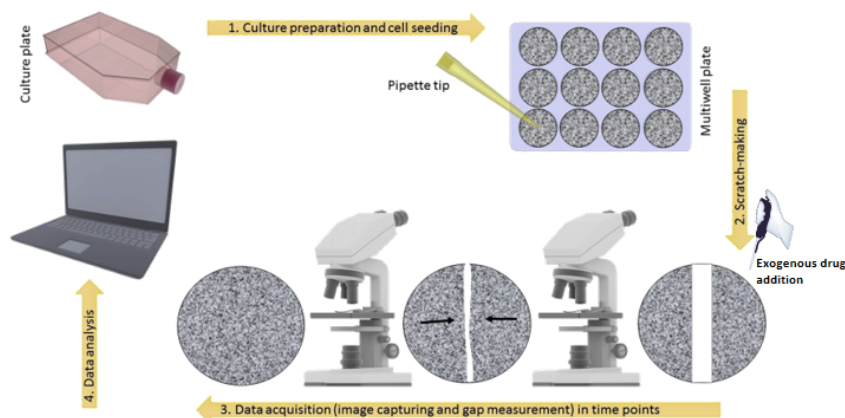


Figure IV-3. Wound healing test procedure.

4.2.5. Transwell migration and invasion assay

Cell migration or invasion was evaluated using Transwell pore polycarbonate membrane insert (8 mm) with or without Matrigel-coated invasion chambers, respectively (**Figure IV-4**) [199]. In brief, 1×10^5 cells which were untreated, or pretreated with GM3 analogues (M1, M2, M3, M4) at different concentrations were

seeded into the upper chamber for adhesion in a 100 μL of serum-free medium. The lower chamber was then supplemented with a 600 μL of RPMI-1640 culture medium containing 20% FBS. After 12 h or 24 h incubation, invasive cells that adhered to the lower chamber were fixed with methanol for 20 min, stained with 500 μL of 0.5% crystal violet solution for 30 min at room temperature, washed with PBS and observed under an optical microscope. Finally, the invasive cells were subjected to 33% acetic acid, and absorbance was measured at 570 nm using a microplate reader (Thermo Fischer).

The migration rate was calculated by formula $[(\text{Mean number of migrated cells in the experimental group (OD value)} / \text{Mean number of migrated cells in the control group (OD value)}) \times 100 \%$], then the migration rate of control group was normalized to 100 %, and values were calculated as migration (%) of control group $[(\text{migration in treatment} / \text{migration in control}) \times 100 \%$]. The experiment was repeated three times.

The invasion rate was calculated by formula $[(\text{Mean number of invasive cells in the experimental group (OD value)} / \text{Mean number of invasive cells in the control group (OD value)}) \times 100 \%$], then the invasion rate of control group was normalized to 100 %, and values were calculated as invasion (%) of control group $[(\text{invasion in treatment} / \text{invasion in control}) \times 100 \%$]. The experiment was repeated three times.

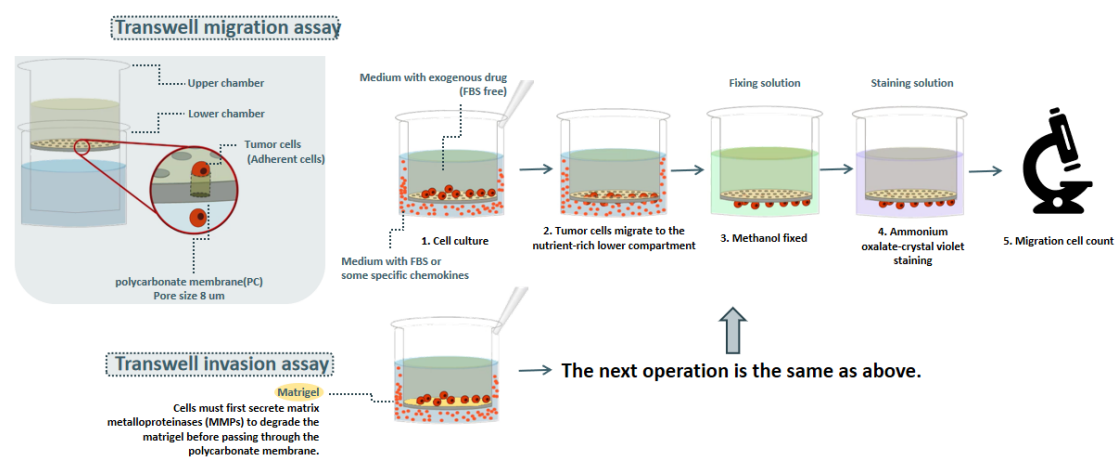


Figure IV-4. Transwell migration and invasion assay procedure.

4.2.6. Western blot assay

The cells (5×10^5 / well) were cultured into 10 cm culture dishes, the control group and different concentrations of GM3 analogues (M1, M2, M3, M4) were treated for 48h (**Figure IV-5**). Cells were then harvested and lysed in RIPA buffer containing protease inhibitors and phosphatase inhibitors, and protein was quantified using a BCA protein assay kit (Beyotime, China). Proteins were separated using 8% or 10% SDS-PAGE and electrotransferred onto the PVDF membranes (Roche, Switzerland). Blots were blocked with 5% skim milk and then subjected to incubation with the primary antibody overnight at 4 $^{\circ}\text{C}$. The

membrane was then washed with TBST buffer and incubated with horseradish peroxidase (HRP)-conjugated secondary antibodies: goat anti-mouse IgG (H + L) (Cat. #A16072, Thermo Fisher Scientific), and goat anti-rabbit IgG (H + L) (Cat. #A16110, Thermo Fisher Scientific). After washed with TBST for three times, the membranes were incubated with an enhanced chemiluminescence detection kit (Thermo Fisher Scientific) and visualized using a ChemiDoc™ imaging system (GE Healthcare, Uppsala, Sweden). Anti-GAPDH antibody was used as a loading control. The primary antibodies included GAPDH (#5174, CST), β -catenin (#8480, CST), N-cadherin (#13116, CST), Vimentin (#5741, CST), E-cadherin (#3195, CST), EGF Receptor (#4267, CST), VEGF Receptor 2 (#2479, CST), Gsk3 β (A2081, ABclonal) and C-myc (#18583, CST). All Western blots analyses were repeated at least three times.

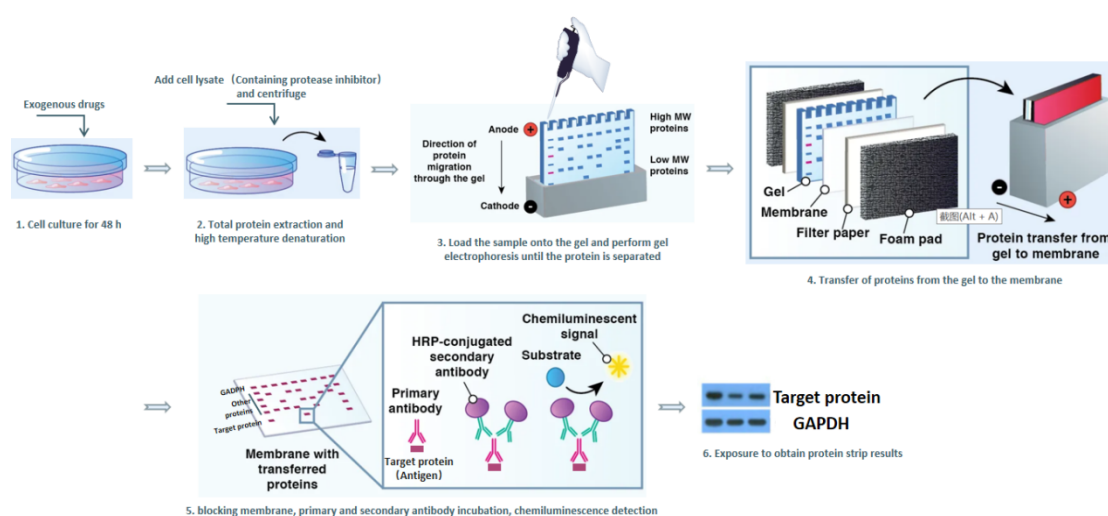


Figure IV-5. Transwell migration and invasion assay procedure.

4.3. Results and discussion

4.3.1. M1, M2, M3, and M4 inhibited tumor cell growth

4.3.1.1. Results and discussion of MTT cytotoxicity assay

MTT assay was used to measure the cytotoxicity of M1, M2, M3, and M4 on tumor cells. It was found that M1, M2, M3, and M4 could inhibit tumor cell lines HCT116, K562, B16F10, and BXPC viability in different degrees (**Figure IV-6**), and they had a stronger effect on HCT116 and B16F10 cell lines than that on K562 and BXPC-3. However, GM3 analogues showed weak antiproliferative activity on BXPC-3 cells, with IC₅₀ values greater than 200 μ M.

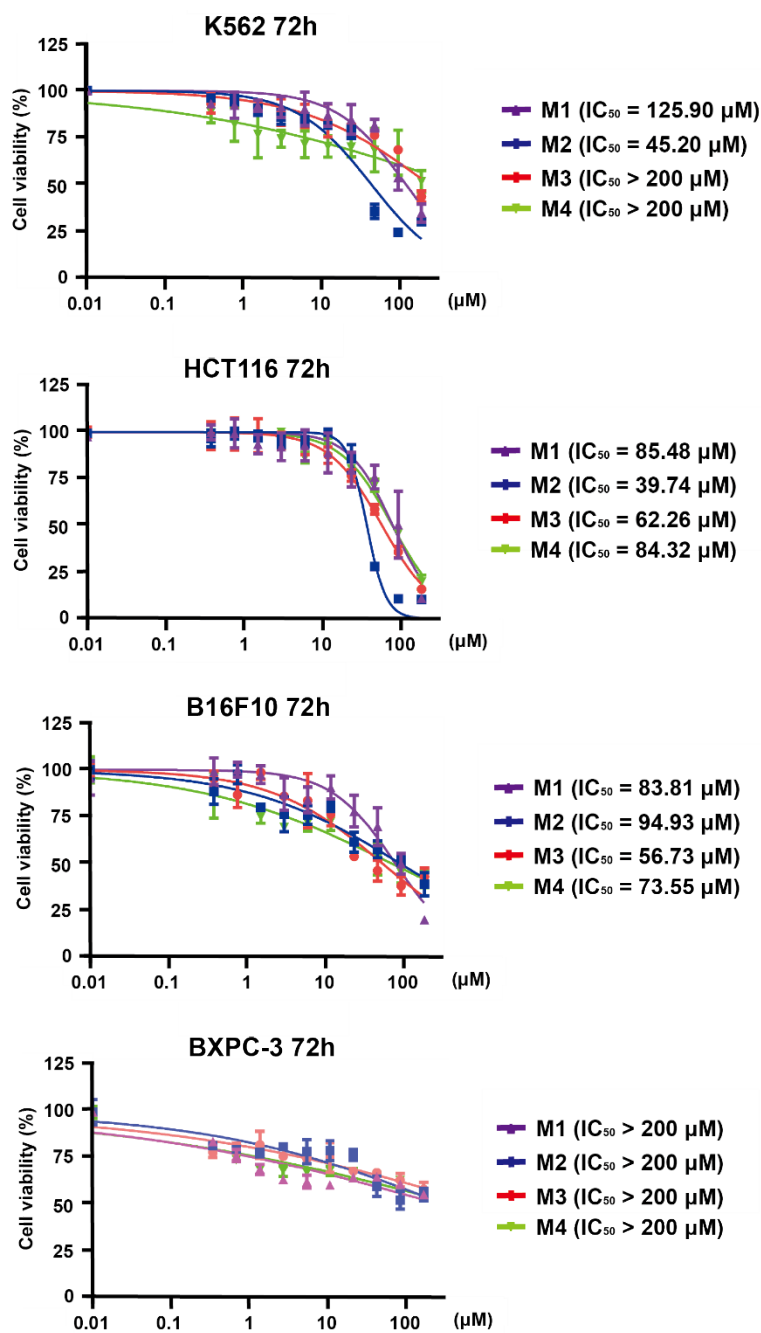


Figure IV-6. GM3 analogues inhibited cancer cell viability. HCT116, K562, B16F10 and BXP-3 cells were treated with GM3 derivatives (M1~M4) for 72 h. Cell viability was measured with MTT and expressed relative to vehicle-treated control. Results are presented as means \pm SD of three independent experiments.

4.3.1.2. Results and discussion of cell colony formation assay

The colony formation assay was used to evaluate the effect of M1, M2, M3, and M4 on the proliferation of tumor cells. As illustrated in **Figure IV-7**, M1, M2, M3 and M4 all suppressed the cell colony formation of B16F10 cells in a concentration-dependent manner. Among them, M2 and M4 were more cytotoxic than M1 and M3, which indicated that M2 and M4 could have more potent anti-

proliferative activity.

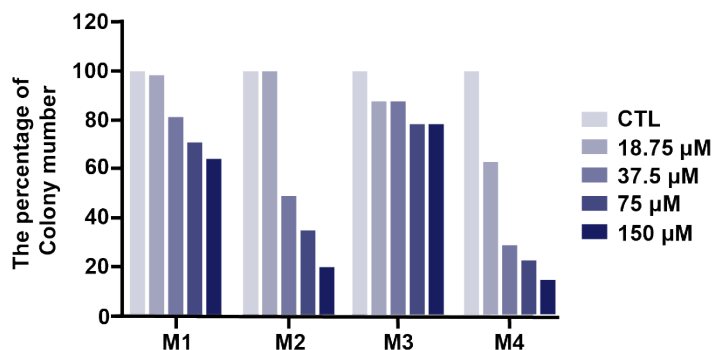
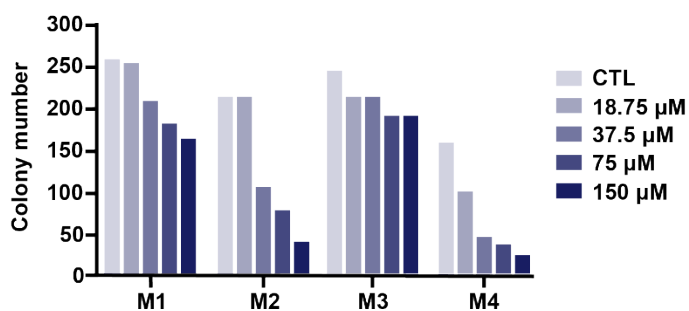
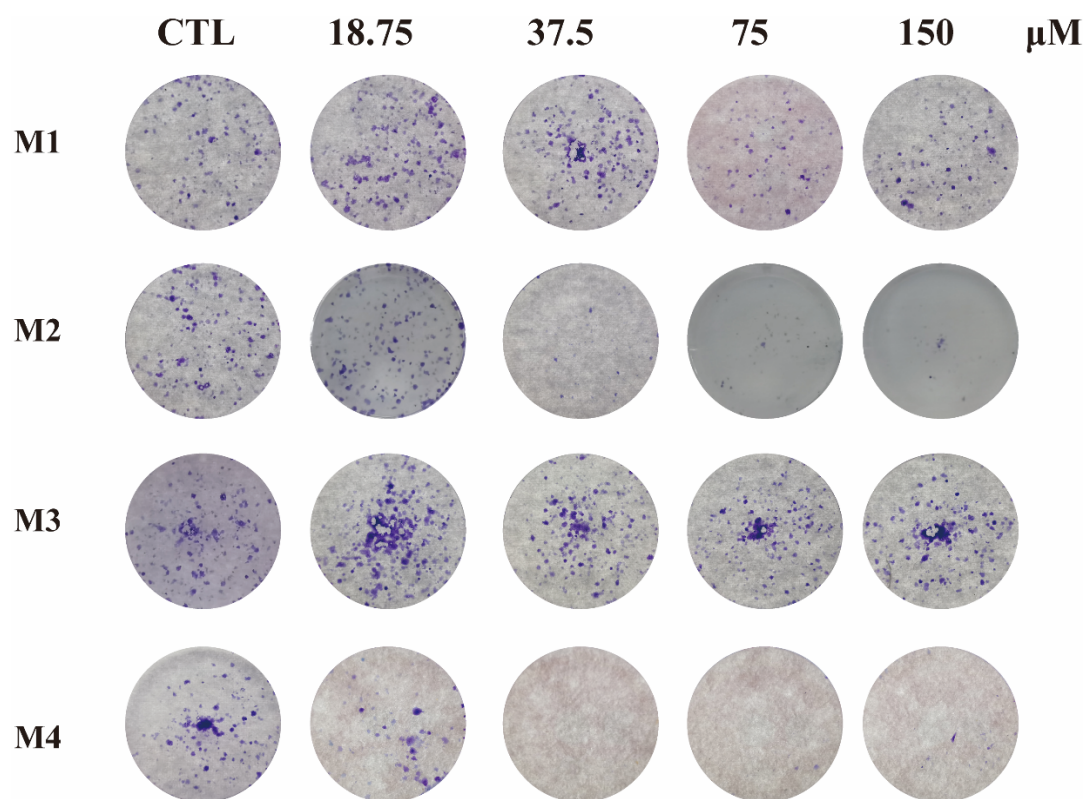


Figure IV-7. GM3 analogues inhibited cancer cell proliferation. Effect of M1, M2, M3 and M4 on colony formation of B16F10 cells. B16F10 cells were treated with GM3 derivatives (M1~M4) for 24 h, then cultured for 7-14 Days. Results are presented as means \pm SD of three independent experiments.

4.3.1.3. Results and discussion of cell morphology assay

By observing the morphological changes of B16F10 cells after 24 h of M1, M2, M3 and M4 effects, it was found that the cell antennae retracted and gradually became round at the concentration of 1.565 μM for M2 and M4. The above changes were observed for M1 and M3 at concentrations of 3.15 μM and 12.5 μM , respectively (**Figure IV-8**). That is, the toxicity of M2 and M4 on B16F10 cells was significantly stronger than that of M1 and M3, which was consistent with the results of the cell colony formation assay.

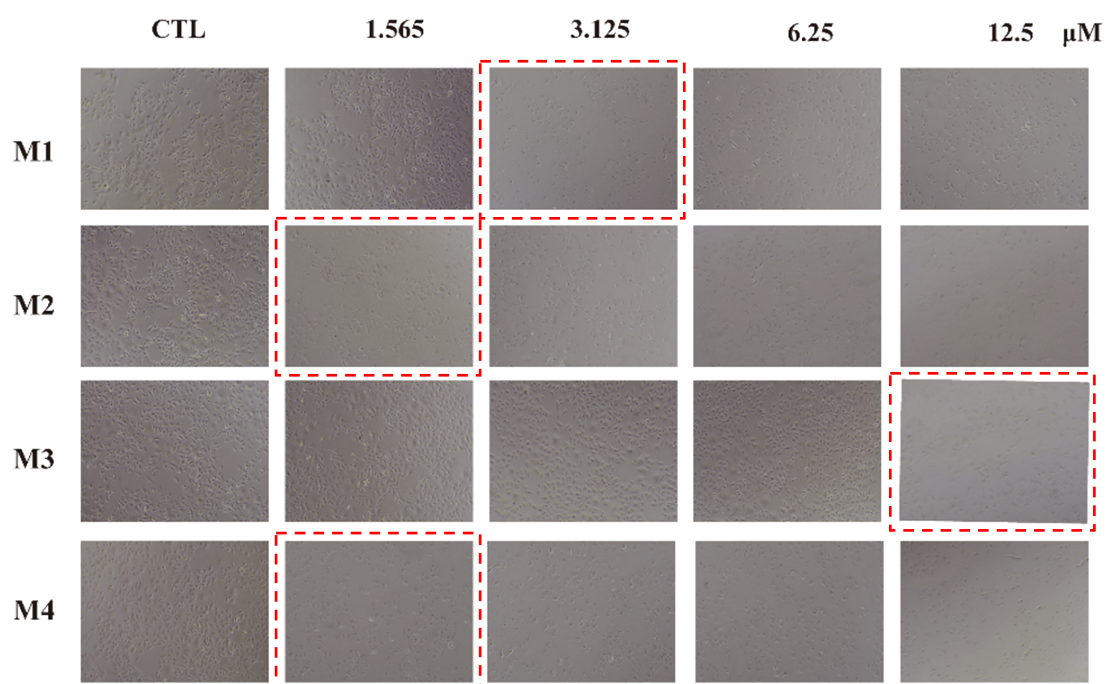


Figure IV-8. Effects of M1, M2, M3 and M4 treatments on morphological changes of B16F10 cells after 24 h.

4.3.2. M1, M2, M3, and M4 inhibited tumor cell migration and invasion.

4.3.2.1. Results and discussion of wound healing test

Given the low cytotoxicity of M1, M2, M3 and M4, wound healing tests were performed to assess their effect on the migration ability of highly metastatic B16F10 cells. As shown in **Figure IV-9** and **Figure IV-10**, the migration rates of B16F10 cells treated with 25 μM GM3 analogues M1, M2, M3, M4 for 24 h or 36 h were 45.7%, 7.6%, 32.2%, 2.1% and 53.8%, 20.2%, 63.7%, 17.7%, respectively. The results demonstrated that M1, M2, M3 and M4 had a significant inhibitory effect on migration for highly metastatic cell, M2 and M4 had a stronger anti-migration effect than M1 and M3.

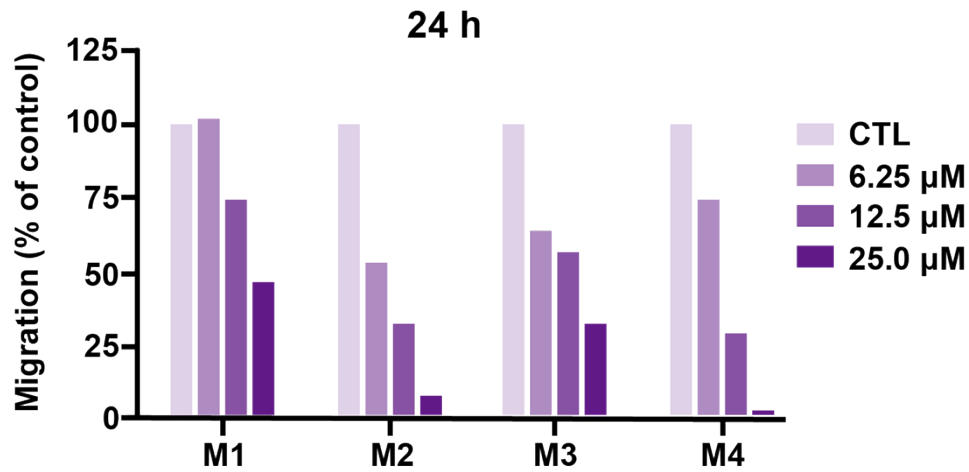
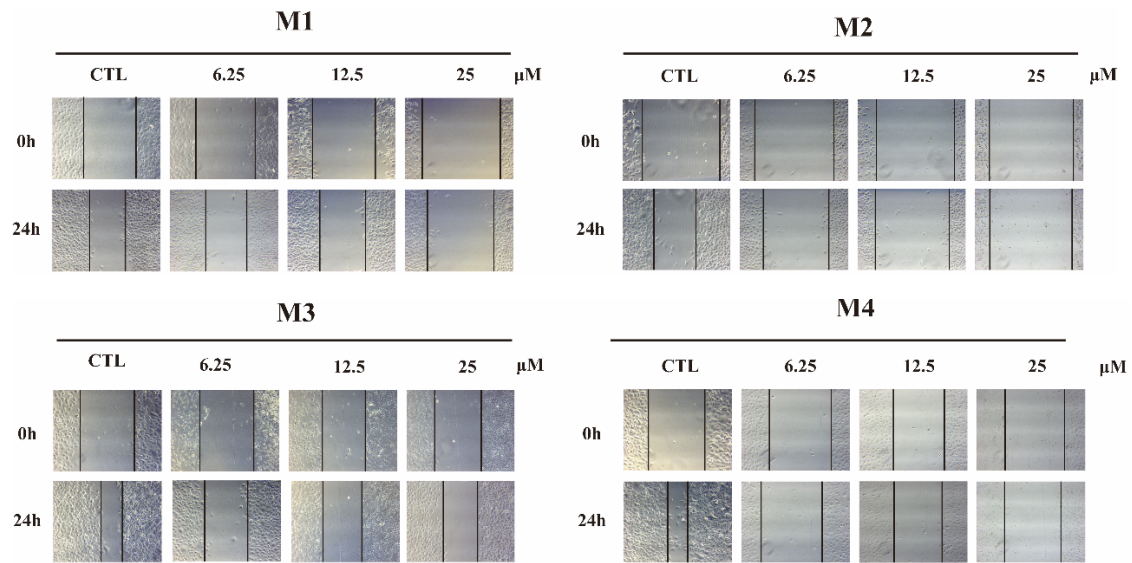
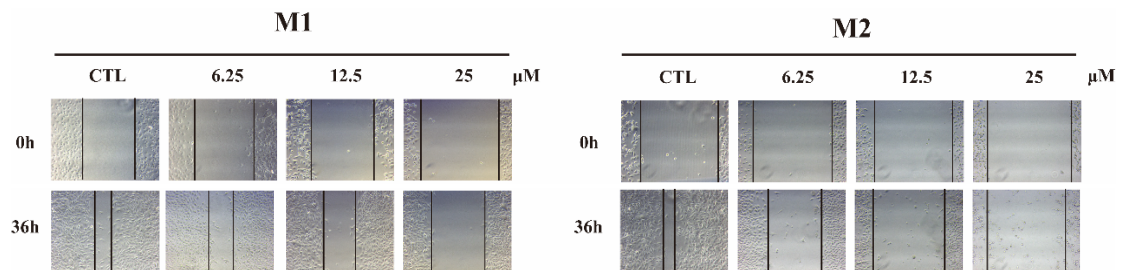


Figure IV-9. M1, M2, M3 and M4 inhibited tumor cell migration. Effect of M1, M2, M3 and M4 on B16F10 cell migration after 24 h of exposure was measured by Wound healing assay. The migration was calculated by formula $[(\text{wound width at 0 h} - \text{wound width at exposure time point}) / \text{wound width at 0 h}] \times 100 \%$, and values were calculated as migration % of control $[(\text{migration in treatment} / \text{migration in control}) \times 100 \%$]. Results are presented as means \pm SD of three independent experiments.



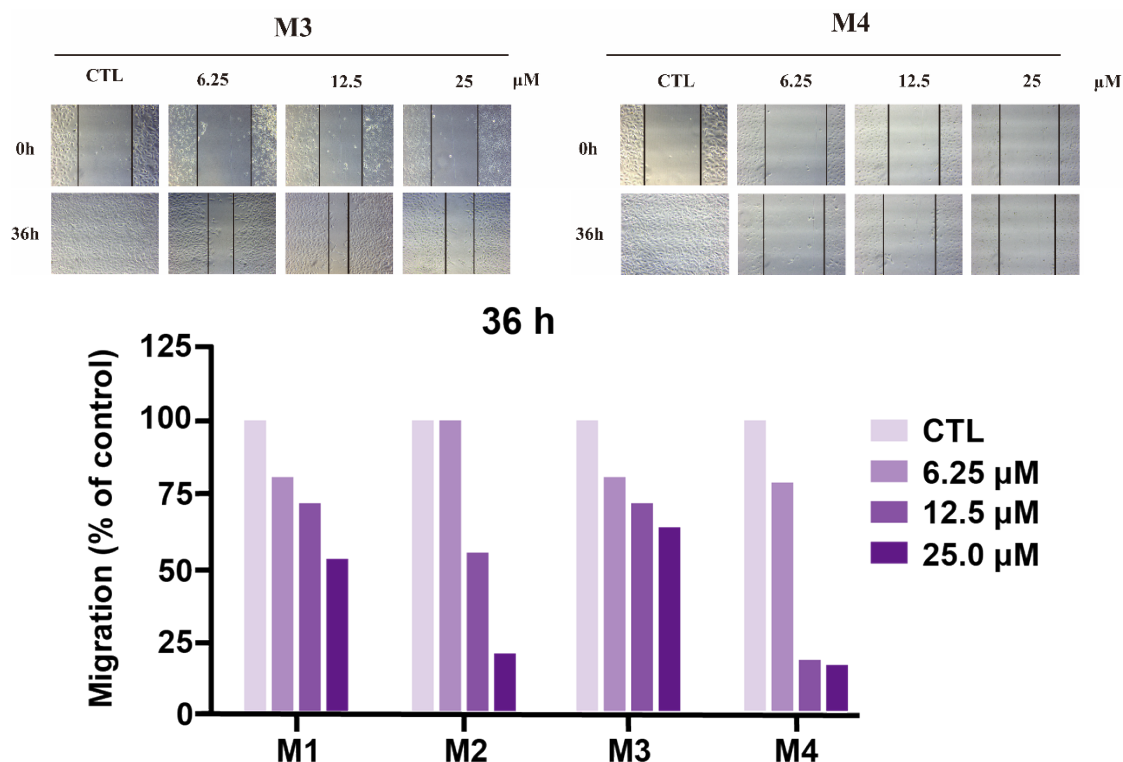


Figure IV-10. M1, M2, M3 and M4 inhibited tumor cell migration. Effect of M1, M2, M3 and M4 on B16F10 cell migration after 36 h of exposure was measured by Wound healing assay. The migration was calculated by formula $[(\text{wound width at 0 h} - \text{wound width at exposure time point}) / \text{wound width at 0 h}] \times 100 \%$, and values were calculated as migration % of control $[(\text{migration in treatment} / \text{migration in control}) \times 100 \%$]. Results are presented as means \pm SD of three independent experiments.

4.3.2.2. Results and discussion of transwell migration and invasion assay

Our previously synthesized GM3 analogues have been reported to inhibit tumor cell migration, but their effect on tumor cell invasion has not been investigated [147],[200]. Transwell assay can be used to analyze cell migration and invasion, based on the wound healing test to verify the ability of M1, M2, M3 and M4 to inhibit tumor cell migration, we further verified their ability to inhibit the migration and invasion of tumor cells by transwell migration and invasion assay.

When B16F10 cells were treated with M1, M2, M3 and M4, they inhibited the migration and invasion of tumor cells at concentrations lower than their cytotoxic doses (**Figure IV-11** and **Figure IV-12**). The migration and invasion rates in M2 and M4 dose groups were dose-dependent and relatively low at 25 μM compared with M1 and M3, suggesting that M2 and M4 had the most significant inhibitory effects on tumor cell migration and invasion.

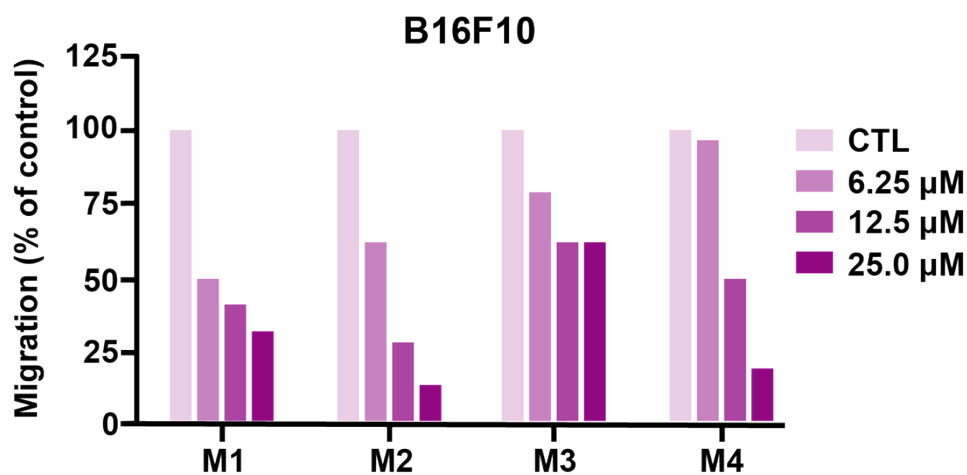
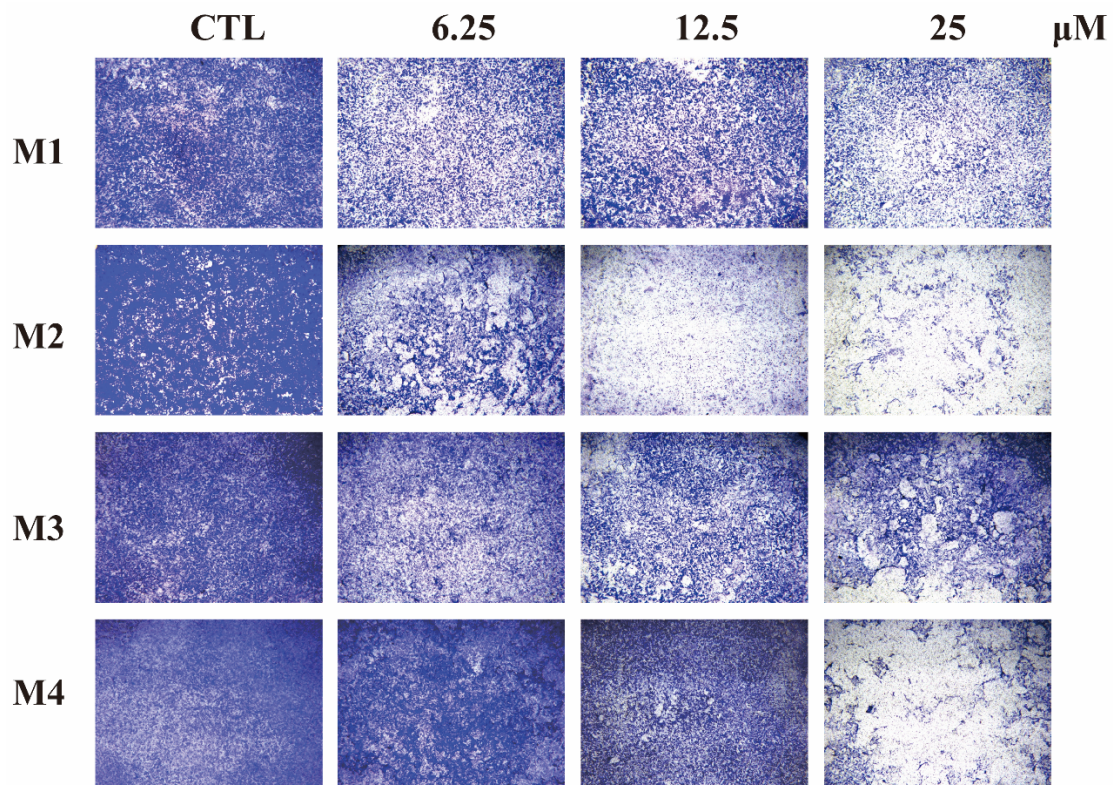


Figure IV-11. GM3 analogues inhibited tumor cell migration. Effect of M1, M2, M3 and M4 on B16F10 cell migration after exposure for 12 h by transwell migration assay. The migration rate was calculated by formula [(Mean number of migrated cells in the experimental group (OD value) / Mean number of migrated cells in the control group (OD value)) × 100 %], then the migration rate of control group was normalized to 100 %, and values were calculated as migration (%) of control group [(migration in treatment / migration in control) × 100 %]. Results are presented as means ± SD of three independent experiments.

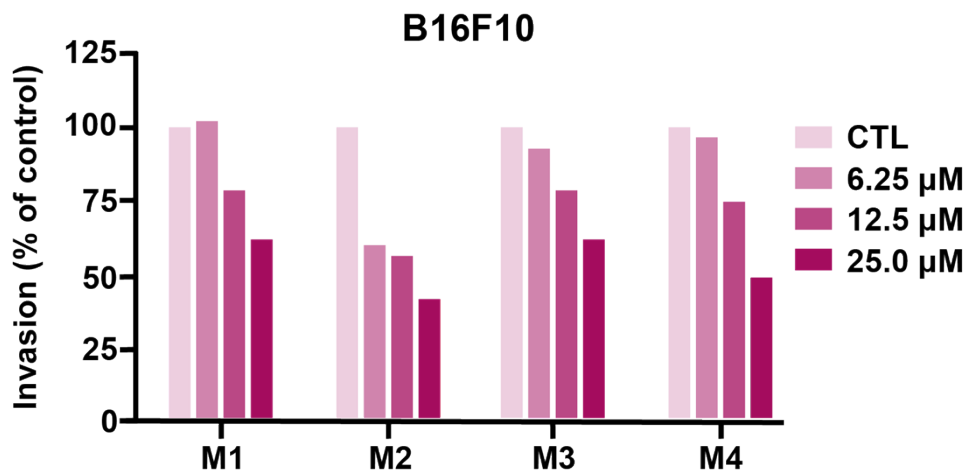
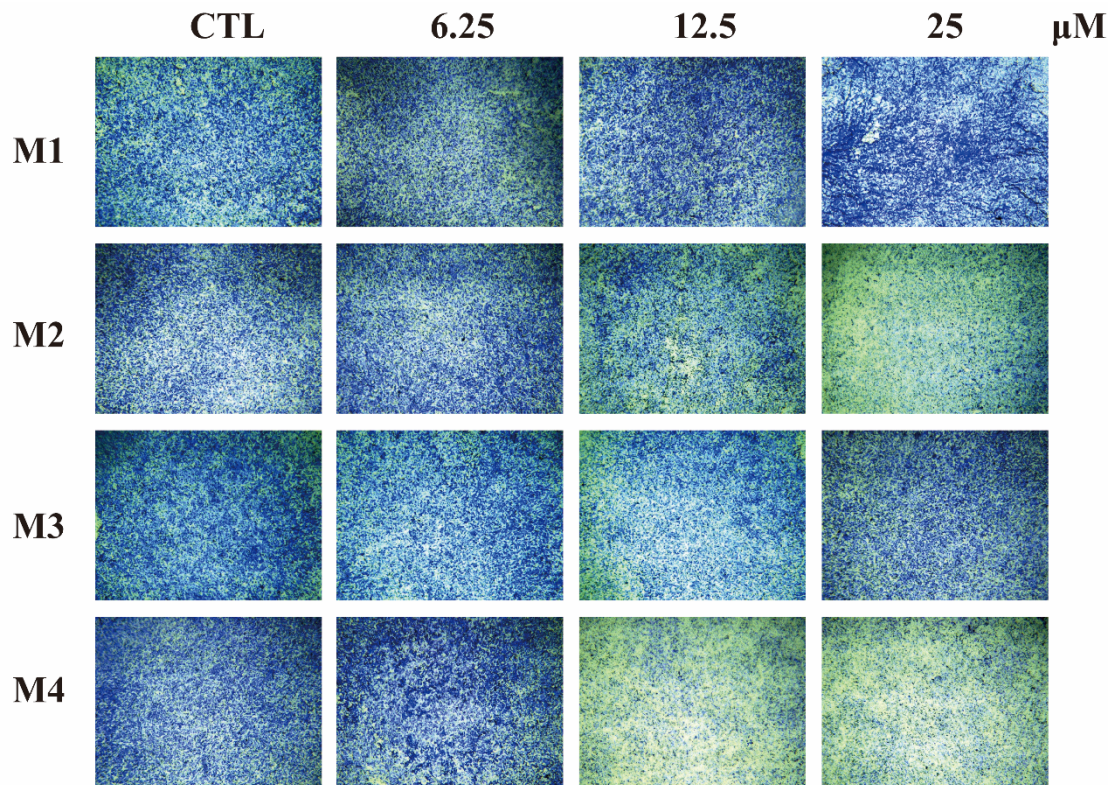


Figure IV-12. GM3 analogues inhibited tumor cell invasion. Effect of M1, M2, M3 and M4 on B16-F10 cell invasion after exposure for 24 h measured by transwell invasion assay. The invasion rate was calculated by formula [(Mean number of invasive cells in the experimental group (OD value) / Mean number of invasive cells in the control group (OD value)) × 100 %], then the invasion rate of control group was normalized to 100 %, and values were calculated as invasion (%) of control group [(invasion in treatment / invasion in control) × 100 %]. Results are presented as means ± SD of three independent experiments.

M1, M2, M3 and M4 had similar results on BXP-3 tumor cells (**Figure IV-13** and **Figure IV-14**). Similarly, M1, M2, M3 and M4 inhibited the migration and invasion ability of tumor cells at concentrations below their cytotoxic levels, and M2 and M4 inhibited the migration and invasion of tumor cells most significantly.

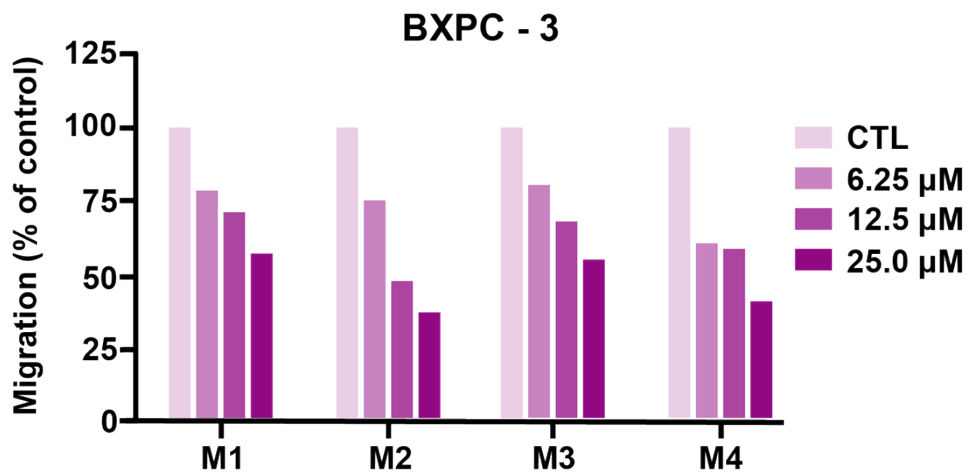
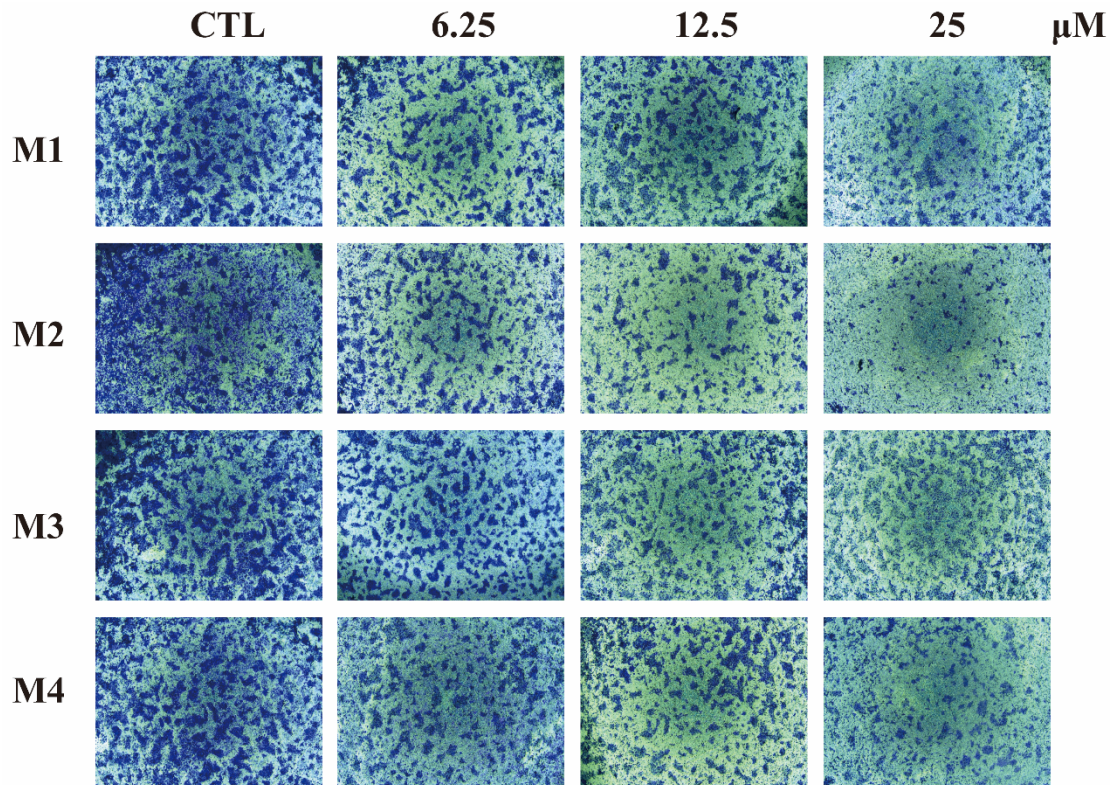


Figure IV-13. GM3 analogues inhibited tumor cell migration. Effect of M1, M2, M3 and M4 on BXPC-3 cell migration after exposure for 12 h by transwell migration assay. The migration rate was calculated by formula $[(\text{Mean number of migrated cells in the experimental group (OD value)} / \text{Mean number of migrated cells in the control group (OD value)}) \times 100 \%$], then the migration rate of control group was normalized to 100 %, and values were calculated as migration (%) of control group $[(\text{migration in treatment} / \text{migration in control}) \times 100 \%$]. Results are presented as means \pm SD of three independent experiments.

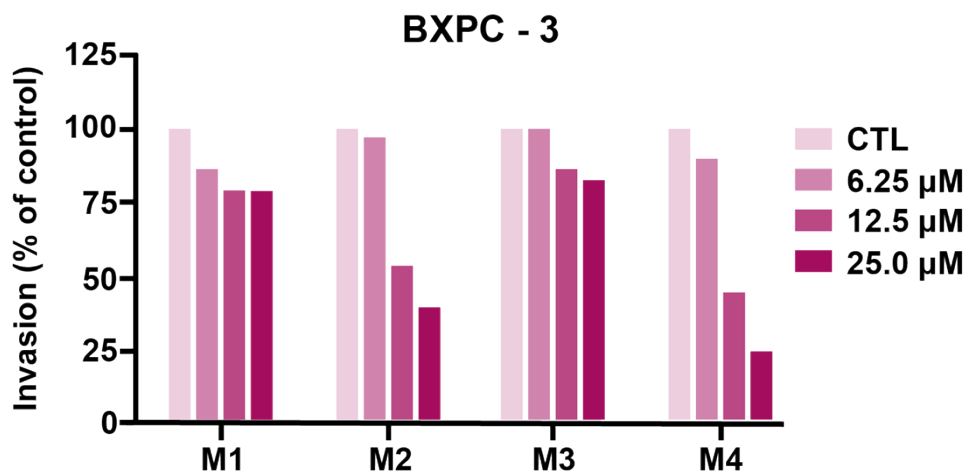
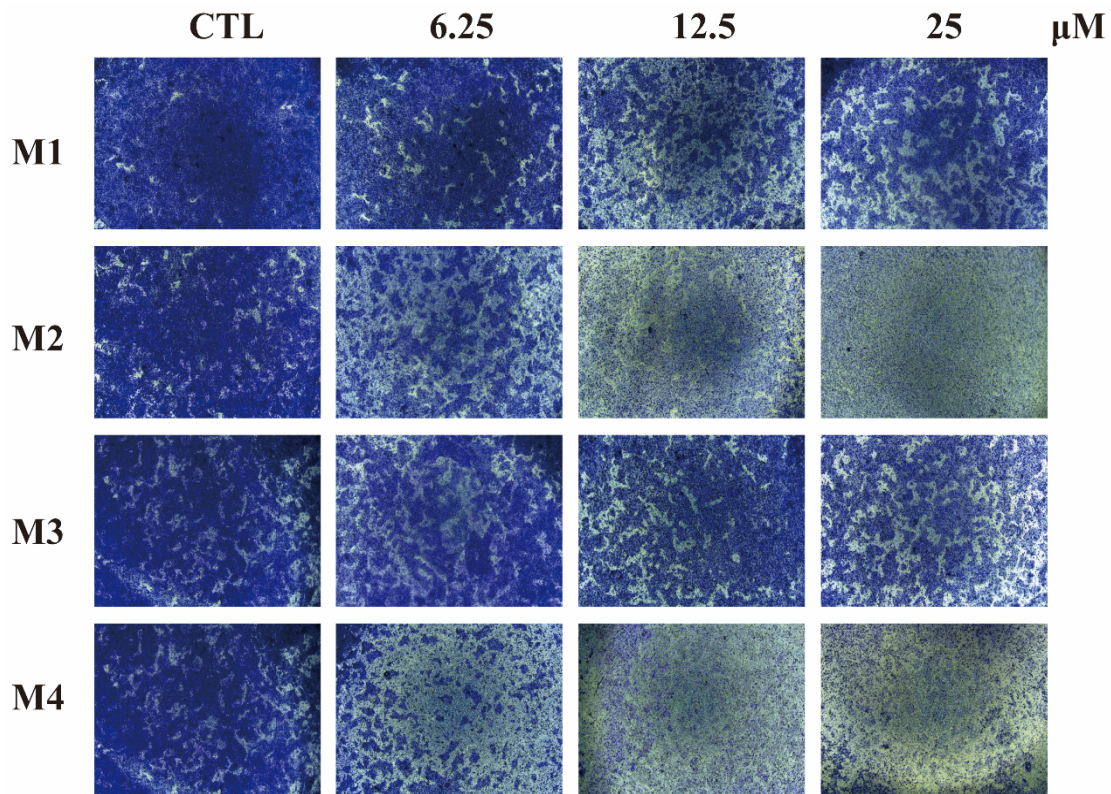


Figure IV-14. GM3 analogues inhibited tumor cell invasion. Effect of M1, M2, M3 and M4 on BXPC-3 cell invasion after exposure for 24 h measured by transwell invasion assay. The invasion rate was calculated by formula [(Mean number of invasive cells in the experimental group (OD value) / Mean number of invasive cells in the control group (OD value)) × 100 %], then the invasion rate of control group was normalized to 100 %, and values were calculated as invasion (%) of control group [(invasion in treatment / invasion in control) × 100 %]. Results are presented as means ± SD of three independent experiments.

4.3.3. M1, M2, M3, and M4 inhibited EMT via EGFR/VEGFR- β -catenin signaling pathway.

4.3.3.1 Results and discussion of western blot assay

Our statistics indicated that oligomers have a significant inhibitory effect on the migration and invasion of tumor cells, suggesting that they may have an effect on the EMT (Epithelial-mesenchymal transition) process of tumor cells. EMT is an important link in tumor development, allowing tumor cells to acquire migratory and aggressive characteristics [201],[202]. EMT is a process in which epithelial cells lose their morphology and function and gradually transform into mesenchymal-like cells. It is manifested as loss of cell polarity, reduced adhesion, migration and invasion ability, and abnormal expression of molecular markers, such as decreased expression of E-cadherin and increased expression of N-cadherin (**Figure IV-15**) [203]. Therefore, we investigated the effect of M1, M2, M3, and M4 on the expression of EMT-related proteins by western blot assay.

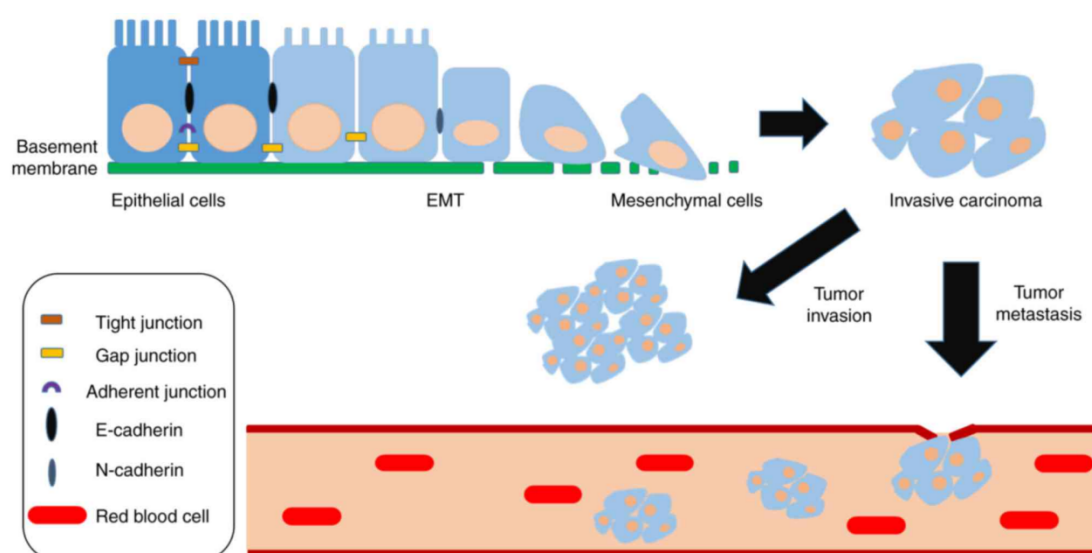


Figure IV-15. General characteristics of EMT [201].

The results showed that the protein levels of β -catenin, N-cadherin and Vimentin in tumor cells reduced and that of E-cadherin increased after treating B16F10 cells with M1, M2, M3 and M4 for 48 h (**Figure IV-16**), indicating M1, M2, M3 and M4 could inhibit tumor cell EMT process. In addition, M2 and M4 significantly inhibited the expression effect of EMT-related proteins and in a dose-dependent manner, which was consistent with the results of wound healing test and Transwell assay.

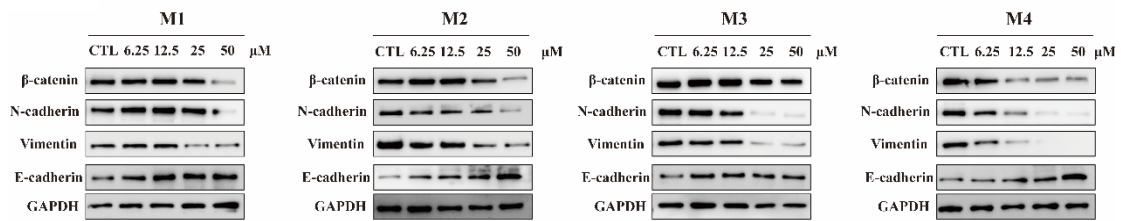


Figure IV-16. Protein levels of EMT-related molecules were detected by Western blotting in B16F10 tumor cell lines treated with M1, M2, M3 and M4. Whole cell lysates were resolved by SDS-PAGE and analyzed through immunoblotting antibodies against EMT-related molecular and GAPDH as a loading control.

Previous studies have proven that GM3 could inhibit tumor cell motility and proliferation by down-regulating EGFR and PI3K/AKT signaling pathways [12],[135]. EGFR and other growth factor receptors are mutated or overexpressed in various cancers. The EGFR/VEGFR-mediated PI3K/Akt signaling pathway phosphorylates and inactivates GSK3 β via Akt and then up-regulates β -catenin to activate the EMT process. As a negative regulator of EMT, GSK3 β promotes β -catenin phosphorylation, resulting in β -catenin degradation. In addition, activation of the β -catenin signaling pathway promotes the expression of other key proteins of EMT, such as C-myc [205],[206],[207],[208].

In order to explore the mechanism of M1, M2, M3 and M4 reducing EMT process, we observed the effects of M1, M2, M3 and M4 on the expression of EGFR, VEGFR, GSK-3 β , β -catenin, C-myc, N-cadherin and E-cadherin. After treating BXP3-3 cells with M1, M2, M3 and M4 for 48 h, the protein levels of EGFR and VEGFR reduced and that of GSK-3 β increased, resulting in decreased Wnt/ β -catenin pathway proteins β -catenin and C-myc, that in turn reduced N-cadherin and increased E-cadherin expression, resulting in the inhibition of EMT (**Figure IV-17**). The outcomes indicated that M1, M2, M3 and M4 could restrain the EMT process of tumor cells through inhibiting the EGFR/VEGFR- β -catenin signaling pathway, thus inhibit tumor cell migration and invasion.

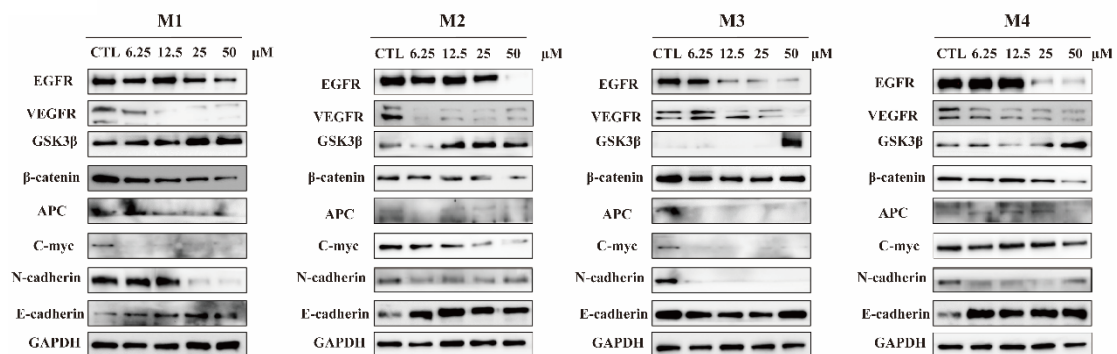


Figure IV-17. Protein levels of EGFR/VEGFR- β -catenin signal pathway and EMT-related molecules were detected by Western blotting in BXP3-3 tumor cell lines treated with M1, M2, M3 and M4. Whole cell lysates

were resolved by SDS-PAGE and analyzed through immunoblotting antibodies against EGFR/VEGFR- β -catenin signal pathway and EMT-related molecules and GAPDH as a loading control.

To summarize: this section describes the anti-tumor activity of M1, M2, M3 and M4. As M2 and M4 show good biological activity, it is logical to continue with the synthesis of higher valence oligomers.

Chapter V

Synthesis of mannose-containing GM3 analogue oligomers with macromolecular skeletons based on "click chemistry"

5.1. Introduction

This chapter describes the synthesis of the hexamer and heptamer of the mannose-containing GM3 analogue. The structures of these two oligomers are shown in **Figure V-1**.

Hexamer of mannose-containing GM3 analogues (M6).

Hexakis {2,3-di-O-methyl-6-[O-(5-acetamido-3,5-dideoxy-D-glycero- α -D-galacto-2-nonulopyranosylate)-(2 \rightarrow 6)-O-(α -D-mannosyl)-(1 \rightarrow 1)-(2S,3R,4E)-4-octadecene-1,3-diol.]-1H-1,2,3-triazole-4-ylmethoxy} cyclomaltohexaose

Heptamer of mannose-containing GM3 analogues (M7).

Heptakis {2,3-di-O-methyl-6-[O-(5-acetamido-3,5-dideoxy-D-glycero- α -D-galacto-2-nonulopyranosylate)-(2 \rightarrow 6)-O-(α -D-mannosyl)-(1 \rightarrow 1)-(2S,3R,4E)-4-octadecene-1,3-diol.]-1H-1,2,3-triazole-4-ylmethoxy} cyclomaltoheptaose

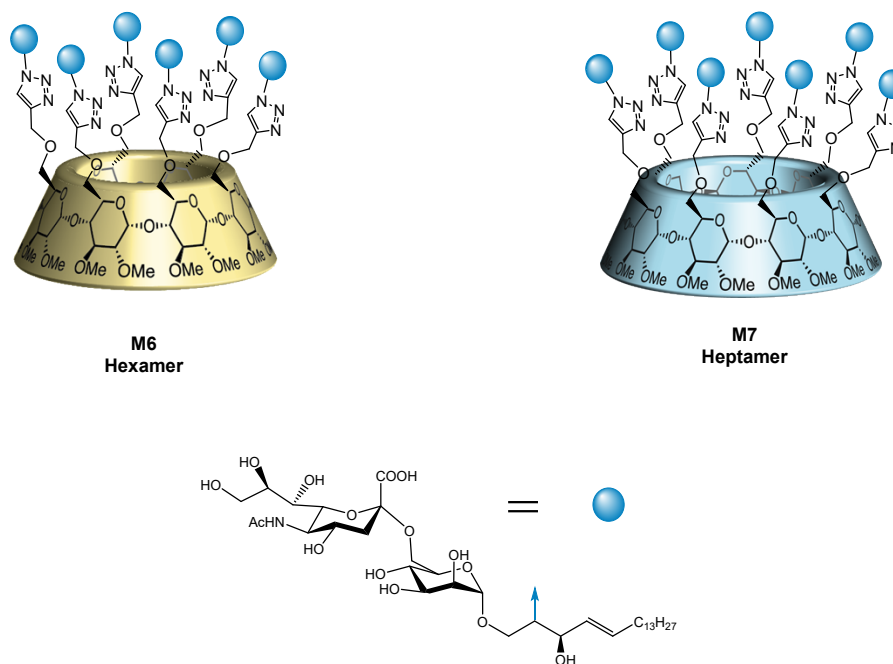


Figure V-1. Structures of the hexamer and heptamer of mannose-containing GM3 analogues.

5.2. Retrosynthetic analysis

Retrosynthetic analysis of hexamer and heptamer of mannose-containing GM3 analogues is shown in **Figure V-2** and **Figure V-3**. The synthetic strategy of these target oligomers is as follows: the hexavalent and heptavalent molecular skeletons containing alkyne groups were first prepared from α and β cyclodextrins as the raw material, respectively. Then the target monomers were introduced into these two skeletons by click reaction. Finally, the protecting groups were removed to obtain the desired target oligomers.

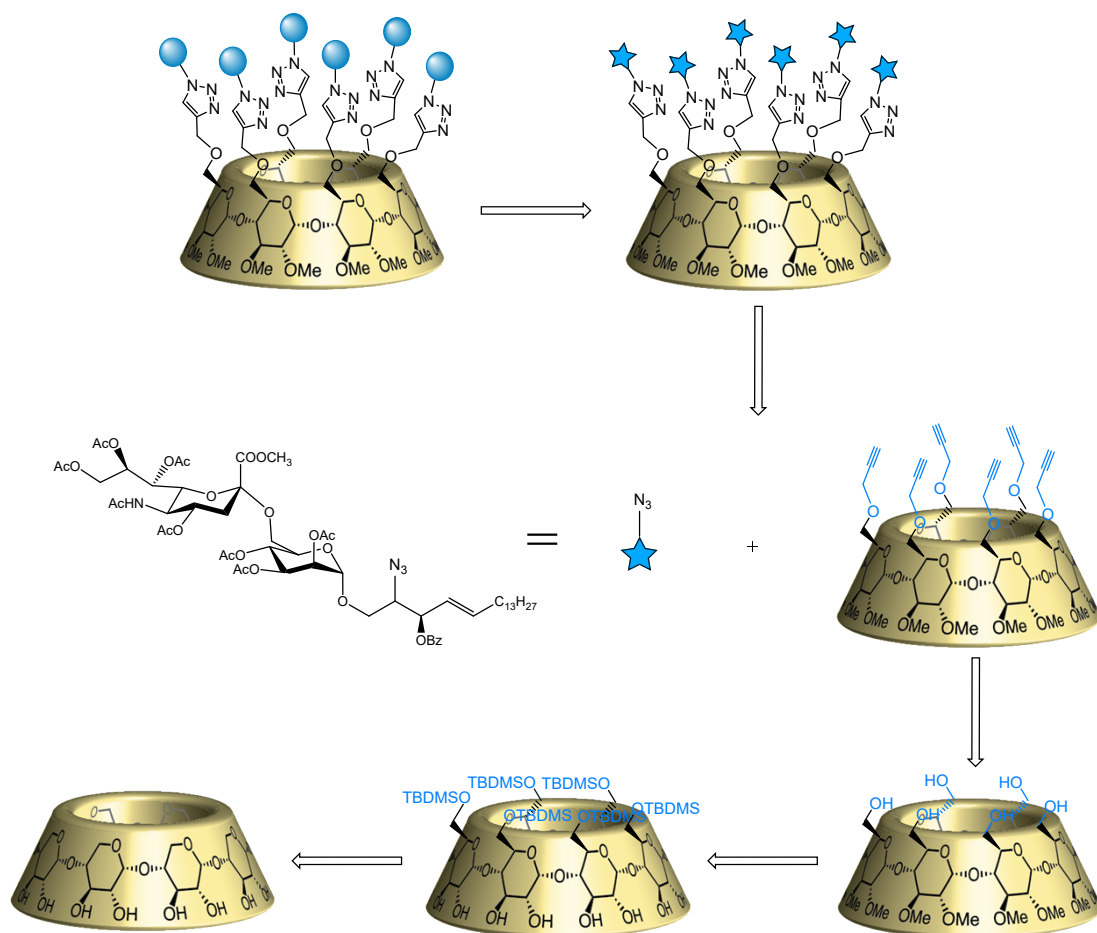


Figure V-2. Retrosynthetic plan for the synthesis of the hexamer of mannose-containing GM3 analogues.

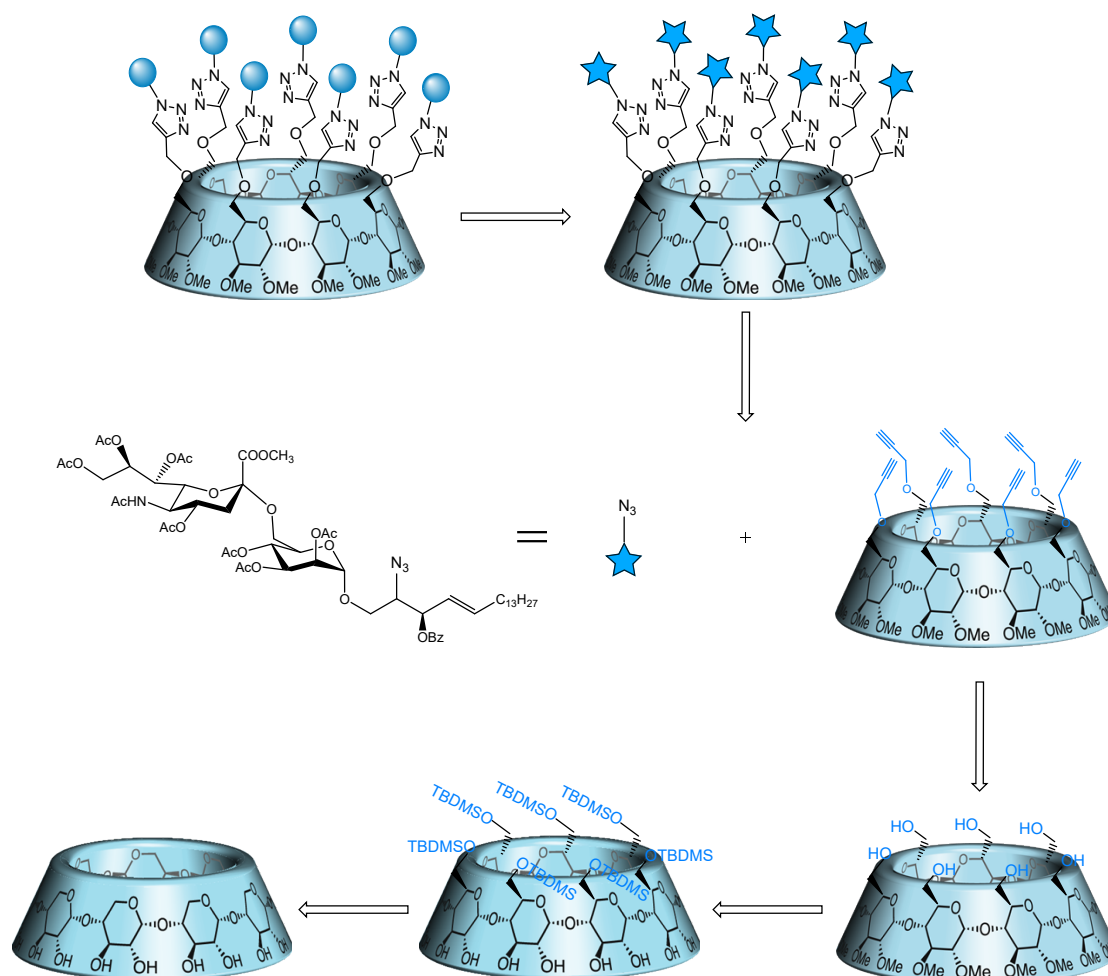


Figure V-3. Retrosynthetic plan for the synthesis of the heptamer of mannose-containing GM3 analogues.

5.3. Preparation of macromolecular skeletons

Cyclodextrins are cyclic oligosaccharides formed from D-glucose units linked by alpha-1,4 glycosidic bonds, of which the most studied and practically important are molecules containing 6, 7 and 8 glucose units, called alpha-, beta- and gamma-cyclodextrins, respectively [209],[210]. Since the glycosidic bonds connecting the glucose units are not free to rotate, cyclodextrins are distinctive slightly tapered rings that produce a hydrophilic outer surface and a nonpolar inner cavity. The multiple hydroxyl groups on the primary (C-6) and secondary (C-2, C-3) faces of cyclodextrins can be used as functional modification sites, so cyclodextrins can be used as molecular scaffolding to modify multiple functional groups onto the building blocks of cyclodextrins to generate cyclodextrin derivatives [211]. Due to their excellent structural characteristics and physicochemical properties, cyclodextrins and their derivatives have become excellent structural units for the construction of various functional compounds and have important applications in pharmaceuticals and other fields [212],[213]. It has been reported in the literature that cyclodextrin derivatives can bind to appropriately sized drug molecules to produce multivalent structural complexes [214],[215],[216],[217],[218],[219]. In

view of this, we used commercially available α and β cyclodextrins as starting materials for the synthesis of hexa- and heptavalent skeletons of cyclodextrin derivatives by alkyne group modification.

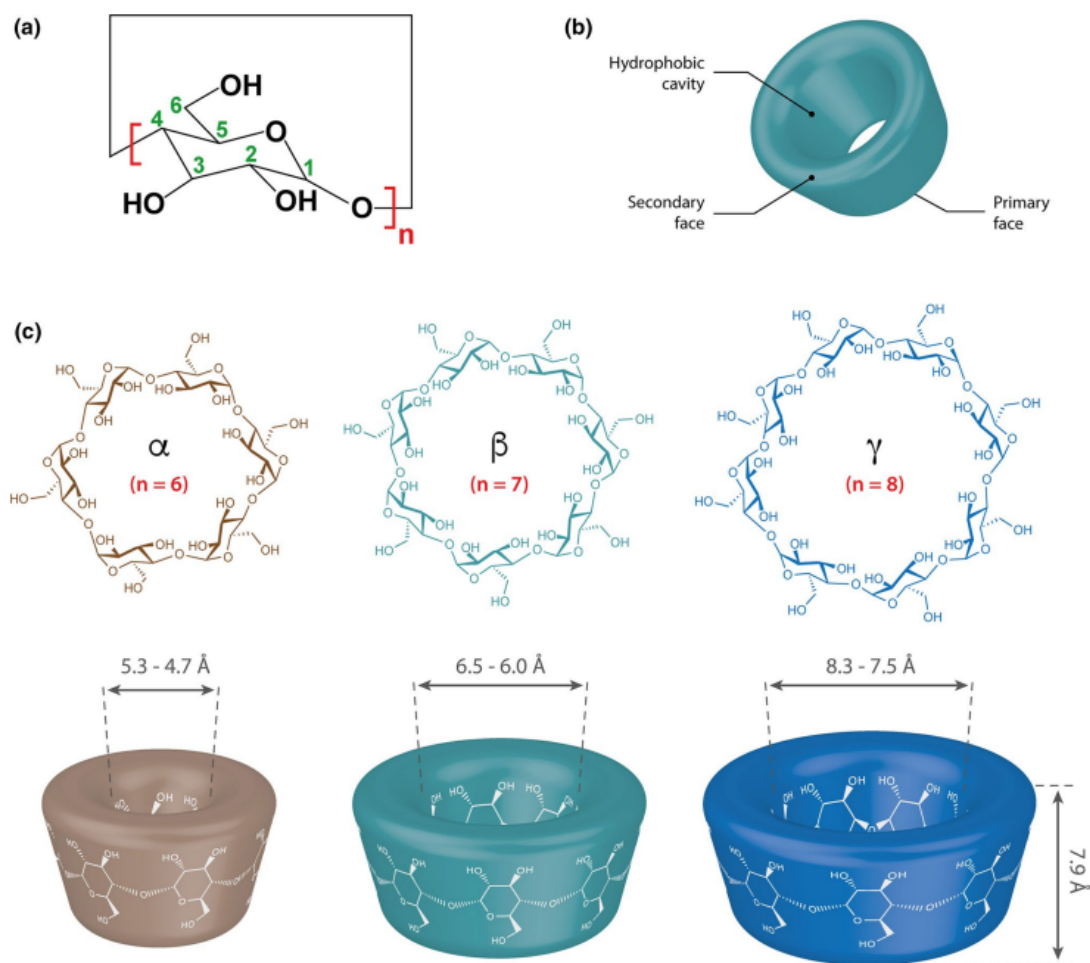
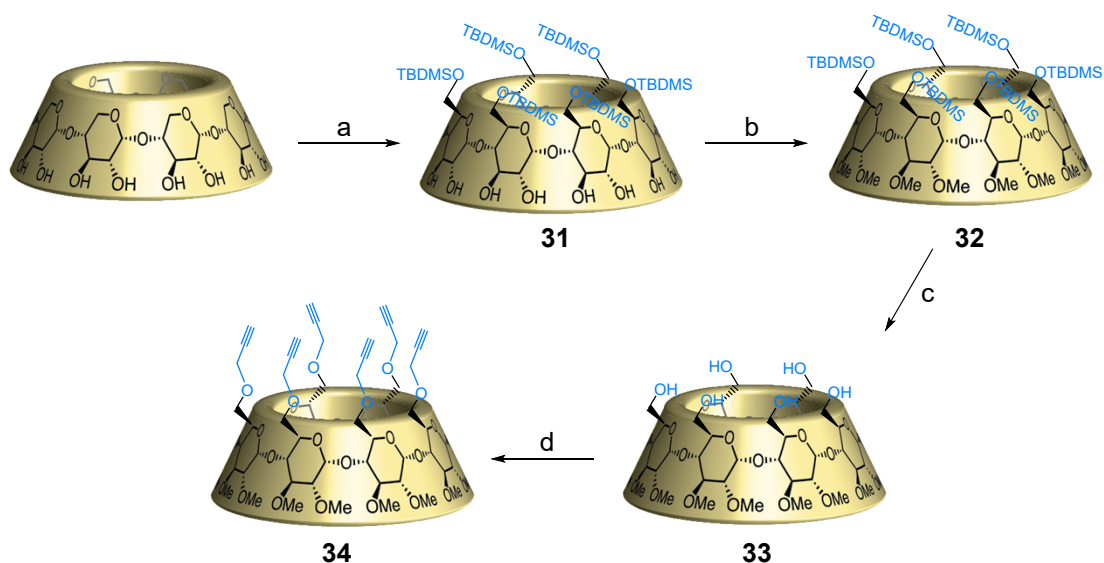


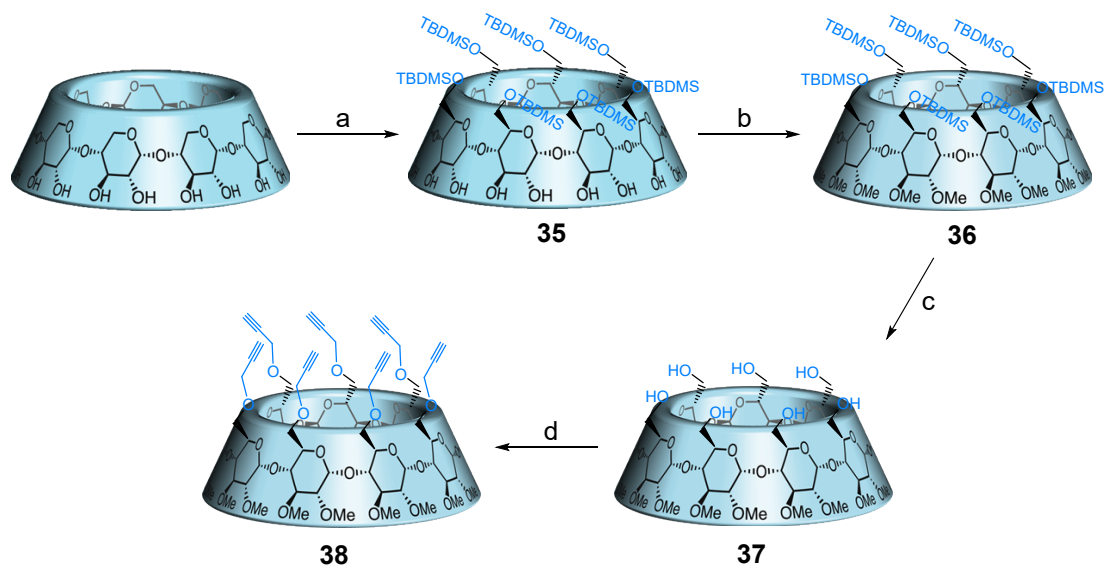
Figure V-4. (a) Schematic representations of the general chemical structure and (b) the tridimensional structure of cyclodextrins, and (c) chemical structure and dimensions for α -, β - and γ -cyclodextrin ($n=6$, 7 and 8 , respectively). [63]

At first, all the hydroxyl groups at the C-6 position of the main α -cyclodextrin rim were selectively protected by TBDMSCl in dry pyridine to give compound **31**, followed by methylation of the remaining hydroxyl groups at the C-2 and C-3 positions of the second rim in dry DMF with iodomethane and sodium hydride to get compound **32**, then refluxed in THF for 2 h in the presence of TBAF to remove the TBDMS group to obtain compound **33**, and finally, introduction of the alkyne groups to compound **33** was carried out with bromopropyne and sodium hydride in dry THF to yield α -cyclodextrin derivative **34**, which was used as a hexavalent skeleton for the subsequent click reaction[221],[222],[214]. as shown in **Scheme V-1**.



Scheme V-1. Reagents and conditions: (a) TBDMSCl, pyridine, 0 °C-r.t., 18 h, 71%; (b) Iodomethane, NaH, DMF, 0 °C-r.t., 14 h, 73%; (c) TBAF, THF, 80 °C, 2 h, 76%; (d) Bromopropyne, NaH, THF, 0 °C-r.t., 48 h, 72%.

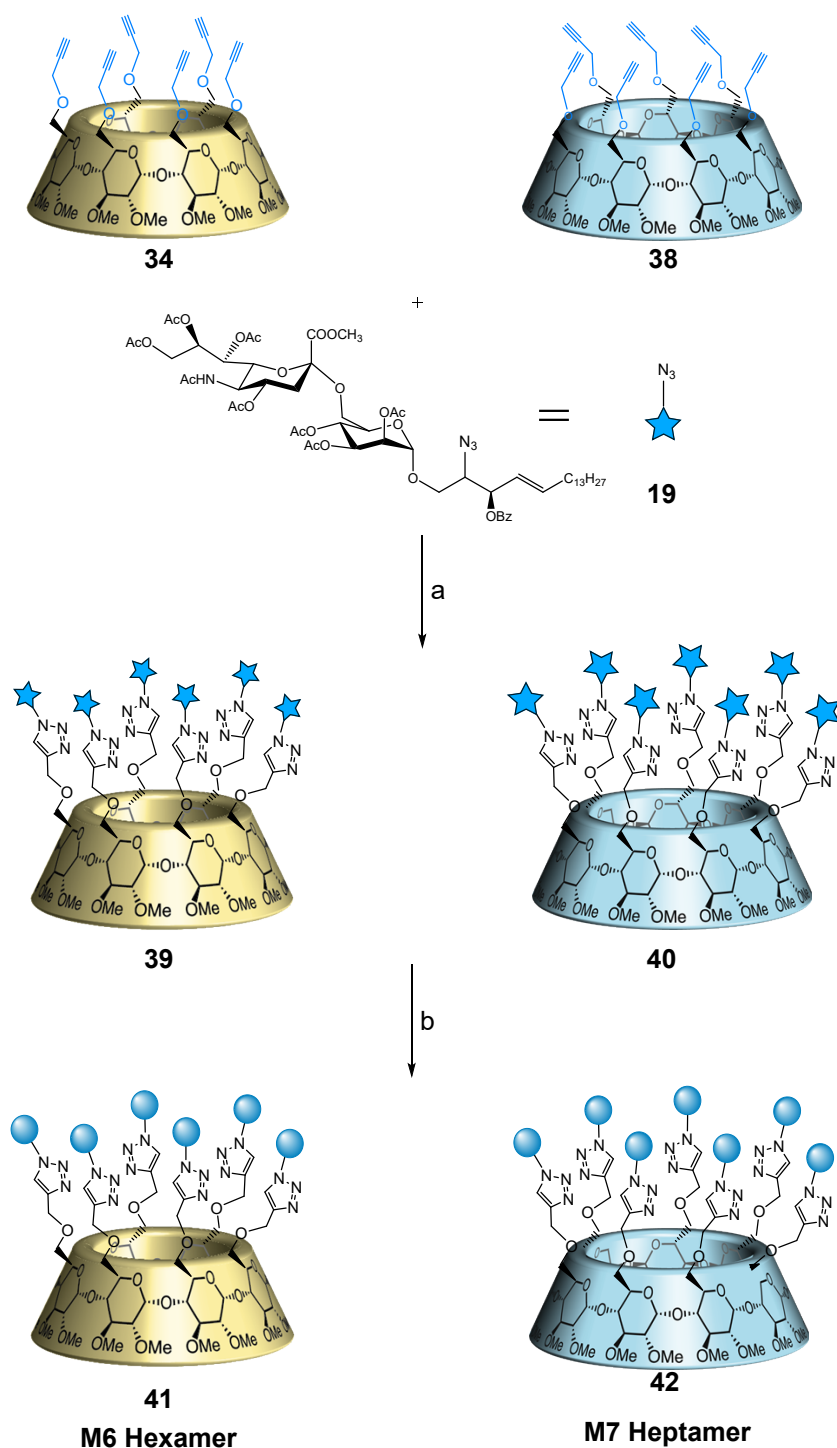
The synthetic strategy for the heptavalent skeleton β -cyclodextrin derivative **38** used for the subsequent click reaction took the same approach as described above for the synthesis of the α -cyclodextrin skeleton. As shown in **Scheme V-2**.



Scheme V-2. Reagents and conditions: (a) TBDMSCl, pyridine, 0 °C-r.t., 18 h, 70%; (b) Iodomethane, NaH, DMF, 0 °C-r.t., 14 h, 72%; (c) TBAF, THF, 80 °C, 2 h, 75%; (d) Bromopropyne, NaH, THF, 0 °C-r.t., 48 h, 69%.

5.4. Synthesis of hexamer and heptamer of mannose-containing GM3 analogues

For the synthesis of the hexamer, we still adopted the synthetic strategy of the copper-catalyzed cycloaddition reaction as shown in **Scheme V-3**, in which the monomer **19** containing the azide group was linked to the hexavalent skeleton α -cyclodextrin derivative with an alkyne group by click reaction. In the beginning, the monomer **19** and the hexavalent skeleton **34** or heptavalent skeleton **38** were dissolved in a mixture of tetrahydrofuran and deionized water, and then copper sulfate pentahydrate, which can be reduced to monovalent copper salts to play a catalytic role, and sodium ascorbate as the reducing agent were added, and the reaction system was reacted at 56 °C for 24 h to obtain the protected hexamer **39** or heptamer **40**. Finally, all protecting groups were removed under Zemplén transesterification (NaOMe/MeOH) conditions to achieve the target hexamer or heptamer of mannose-containing GM3 analogues **41** or **42** in good yields.



Scheme V-3. Reagents and conditions: (a) CuSO₄·5H₂O, Sodium ascorbate, THF, H₂O, 56 °C, 24 h, 56% of **39**, 55% of **40**; (b) NaOMe/MeOH, H₂O, r.t., 12 h, 66% of **41** (**M6**), 62% of **42** (**M7**).

To summarize: this section describes the synthesis of hexamer **M6** and heptamer **M7** of the mannose-containing GM3 analogue. Although the amounts synthesized so far are not sufficient to test for biological activity, by now we have prepared enough of the three blocks required to construct the monomer so that sufficient amounts of **M6** and **M7** will be prepared in the near future.

Chapter VI
Synthesis of GM3

6.1. Introduction

Numerous literatures we have mentioned before have reported that some GM3 derivatives have stronger antitumor activity than GM3 itself. Up to now, we have synthesized several oligomers of GM3 analogues, and for a more rigorous and complete assessment of their anticancer activity results, it is necessary to synthesize GM3 as a reference, therefore, this chapter describes the synthesis of GM3 by both chemoenzymatic and chemical synthesis routes. The structure of GM3 is shown in **Figure VI-1**.

Ganglioside GM3:

O-(5-Acetamido-3,5-dideoxy-D-glycero- α -D-galacto-2-nonulopyranosylonic acid)-(2 \rightarrow 3)-O-(β -D-galactopyranosyl)-(1 \rightarrow 4)-(β -D-glucopyranosyl)-(1 \rightarrow 1)-(2S,3R,4E)-2-octadecanamido-4-octadecene-1,3-diol.

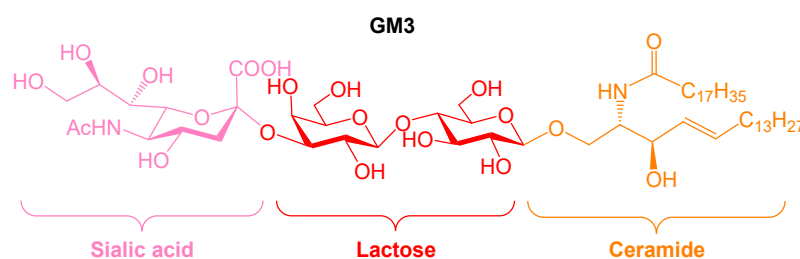


Figure VI-1. Structures of the GM3.

6.1.1. Retrosynthetic analysis of chemoenzymatic synthesis of GM3

The retrosynthetic analysis of the chemoenzymatic synthesis of GM3 is shown in **Figure VI-2**. Our synthetic strategy can be divided into three steps: first, we prepare the per-acetylated lactosyl trichloroacetimidate block, then we obtain lactosyl sphingosine by glycosylation of lactosyl residues and 3-O-benzoyl azidosphingosine **14**, and finally we complete the synthesis of GM3 using highly efficient one-pot multienzyme (OPME) sialylation systems.

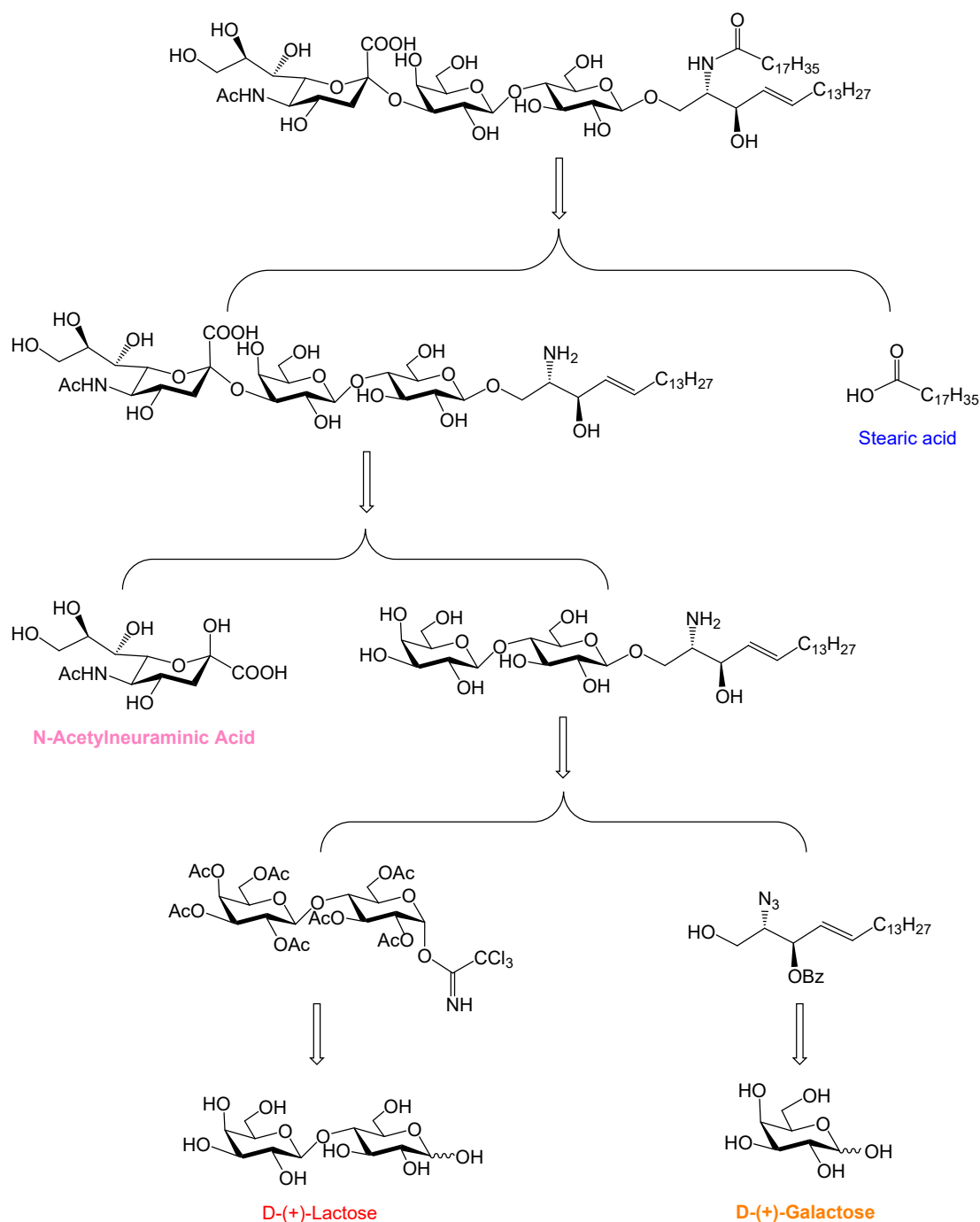
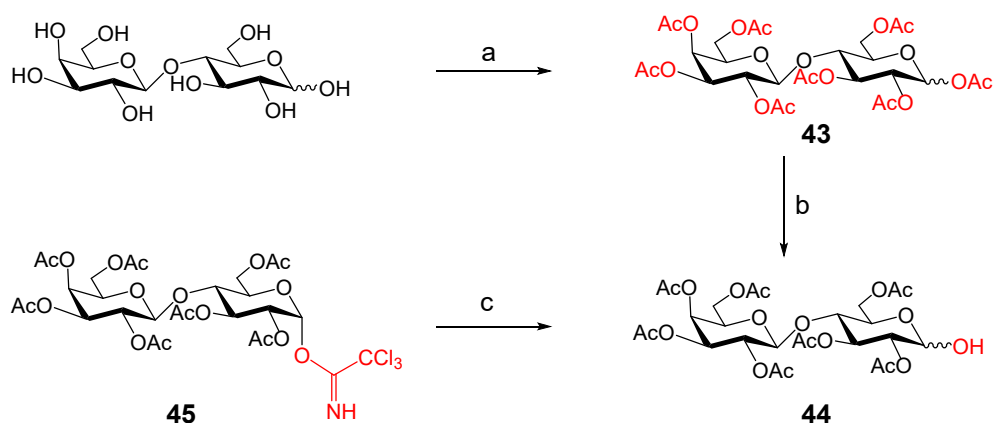


Figure VI-2. Retrosynthetic plan for the chemoenzymatic synthesis of GM3.

6.1.2. Preparation of the per-acetylated lactosyl trichloroacetimidate block

In the first step all hydroxyl groups on lactose were protected with acetic anhydride in pyridine to per-acetylated lactose **43**. In the second step, compound **43** was reacted in the presence of benzylamine in THF at room temperature overnight to selectively remove the acetyl group at the anomeric center, yielding compound **44** as a mixture of α and β . In the last step the reaction of trichloroacetonitrile with the compound **44** in the presence of DBU gave the fully

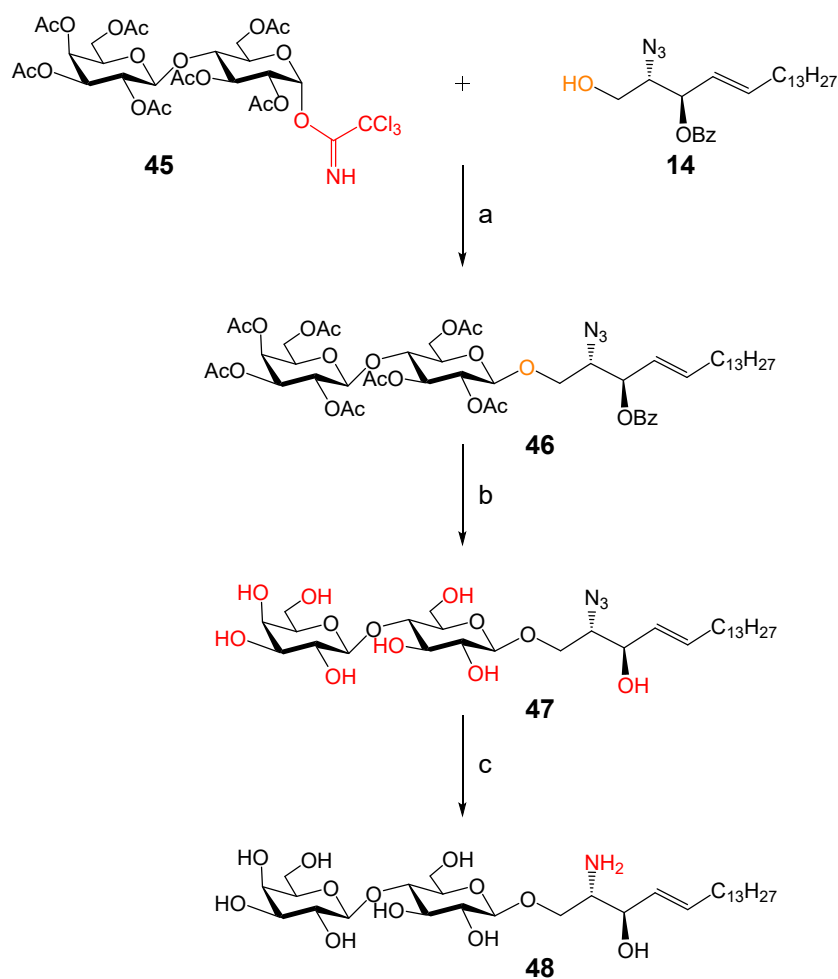
acetylated lactosyl trichloroacetimidate block **45** [223],[224]. as shown in **Scheme VI-1**.



Scheme VI-1. Reagents and conditions: (a) Acetic anhydride, pyridine, r.t., 12 h, 79%;
(b) PhCH₂NH₂, THF, r.t., 20 h, 88%; (c) CCl₃CN, DBU, CH₂Cl₂, -5 °C-0 °C, 12 h, 77%.

6.1.3. Preparation of the lactosyl sphingosine

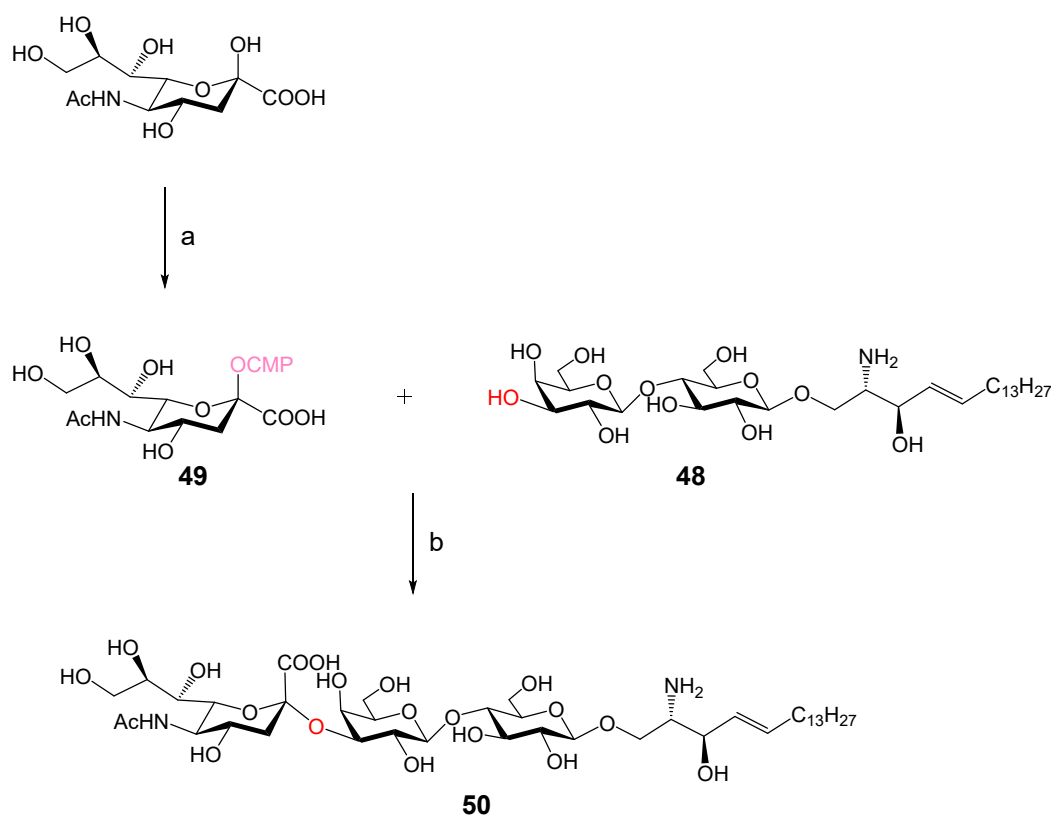
The glycosylation of the fully acetylated lactosyl trichloroacetimidate **45** to 3-O-benzoyl azidostigmine **14** was carried out using BF₃·Et₂O as a promoter at -18 °C for 3 h to give compound **46**. Subsequently, under Zemplén transesterification (NaOMe/MeOH) conditions, all protecting groups were removed and the resulting product was directly reduced for its azide group with 1,3-propanedithiol and triethylamine in a mixture of pyridine-water at 50 °C for 12 h without further purification to give the lactosyl sphingosine **48** [225] as shown in **Scheme VI-2**.



Scheme VI-2. Reagents and conditions: (a) $\text{BF}_3 \cdot \text{Et}_2\text{O}$, CH_2Cl_2 , molecular sieves, -18°C , 3 h, 78%; (b) NaOMe , MeOH , r.t., 14 h; H_2O , 0°C - r.t., 2 h; (c) 1,3-propanedithiol, Et_3N , pyridine-water, 50°C , 12 h, 80%.

6.1.4. Chemoenzymatic synthesis of GM3

To date, various methods have been explored for the synthesis of ganglioside GM3 [226],[227],[228],[229],[230],[231],[232]. In general, the routes for the total synthesis of GM3 by single chemical methods are tedious, involve repeated chemical synthesis steps of addition and removal of protection, are time-consuming, and, as previously described, the specificity of the complex structure of sialic acid makes chemical sialylation reactions usually more challenging than other glycosylation reactions. With the continuous development of advanced synthetic strategies, an efficient and simplified chemoenzymatic synthesis strategy has attracted our attention. Numerous studies have shown that chemoenzymatic synthesis simplifies the steps required for chemical synthesis, is more efficient, has better stereoselectivity and regioselectivity, and is a powerful method for the production of oligosaccharides, polysaccharides, glycoconjugates and their derivatives [233],[234],[235],[236],[237] so we decided to use the efficient one-pot multienzyme (OPME) sialylation system for the synthesis of GM3 [138].



Scheme VI-3. Reagents and conditions:

(a) CTP, MgCl₂, Tris-HCl buffer (100 mM, pH 8.5), NmCSS, 37 °C, 0.5h. (b) PmST1, 24 h.

The starting material **48**, sialic acid, was activated by *Neisseria meningitidis* CMP-sialic acid synthetase (NmCSS) to CMP-Neu5Ac intermediate **49** in Tris-HCl buffer (100 mM, pH 8.0) containing 20 mM MgCl₂ and CTP at 37 °C. Among the three CMP-sialic acid synthases cloned from *E. coli*, *Streptococcus agalactiae*, and *N. meningitidis*, the *Neisseria meningitidis* CMP-sialic acid synthetase (NmCSS) is the best in terms of expression level, activity and tolerance to substrate modification, and it has become an essential catalyst for the synthesis of sialosides [239]. Intermediates were then transferred to LacβSph by the multifunctional *Pasteurella multocida* sialyltransferase (PmST1) to yield lyso-GM3 **50** (**Scheme VI-3**). Of all bacterial SiaTs reported to date, PmST1 has the most flexible donor substrate specificity [138]. We monitored the progress of the enzymatic reaction by thin layer chromatography (TLC) and ESI mass spectrometry (ESI-MS) and found the molecular mass peak of lyso-GM3 on the mass spectrometry, but on the TLC we only saw the product point of the intermediate CMP but not the new point of lyso-GM3, analyzing that the yield was not satisfactory due to the low activity of PmST1 in this batch of fermentation we used, and we could not synthesize sufficient amount of GM3 based on the low activity of the enzyme in this batch, Even though we tried to adjust the enzyme equivalents, the reaction temperature, and the reaction time, there was no significant change. so we switched to the chemical method to complete the total synthesis of GM3.

6.1.5. Retrosynthetic analysis of chemical synthesis of GM3

The inverse synthesis analysis of GM3 chemical synthesis is shown in **Figure VI-3**. The work was broadly divided into three parts, firstly the lactoside block was prepared, then the lyso-GM3 was obtained by the sialylation reaction of sialic acid and lactoside followed by the glycosylation reaction with sphingosine and the subsequent azide reduction reaction, and finally the ganglioside GM3 was completed by the modification of stearic acid onto the lyso-GM3 through the condensation reaction.

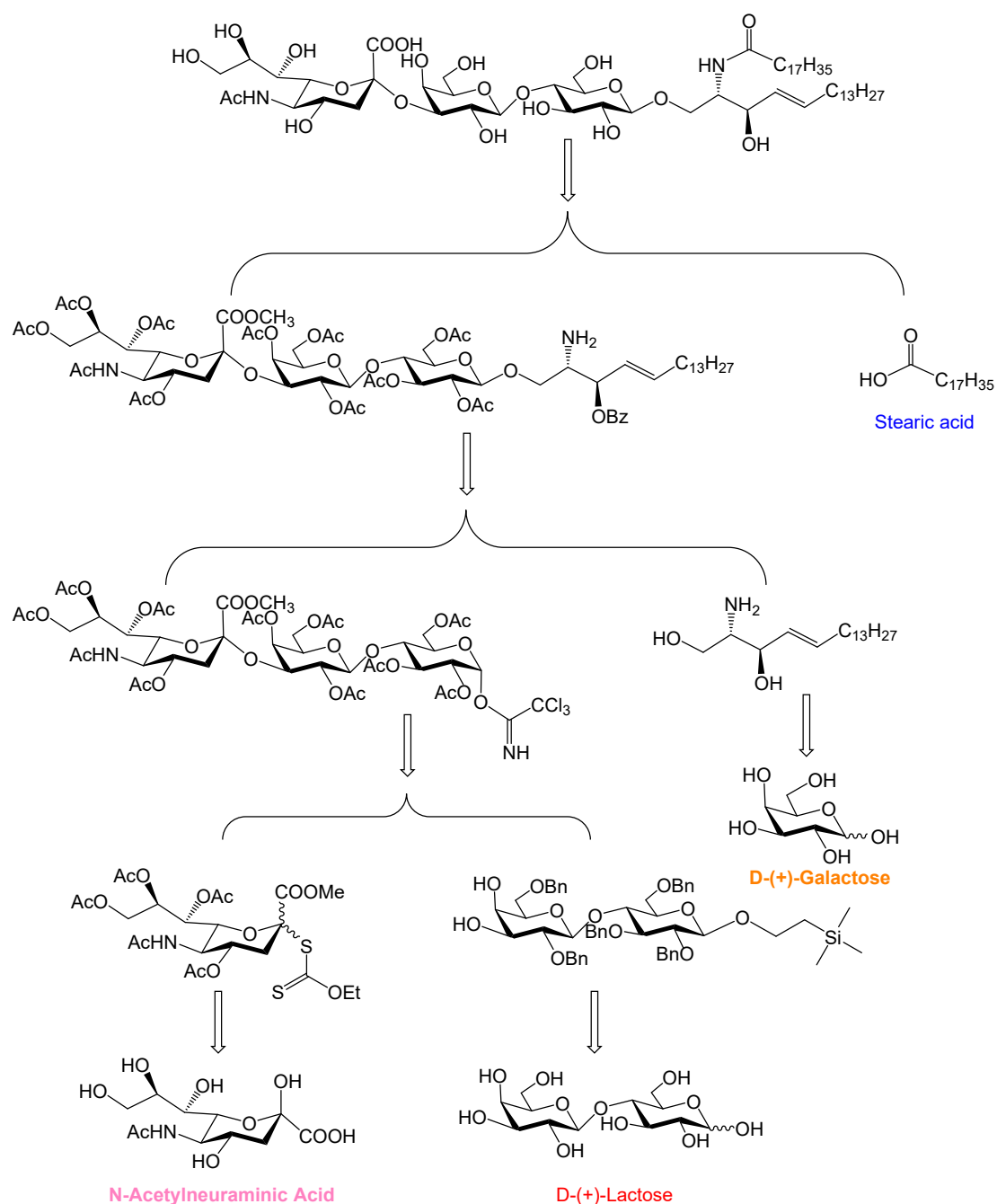
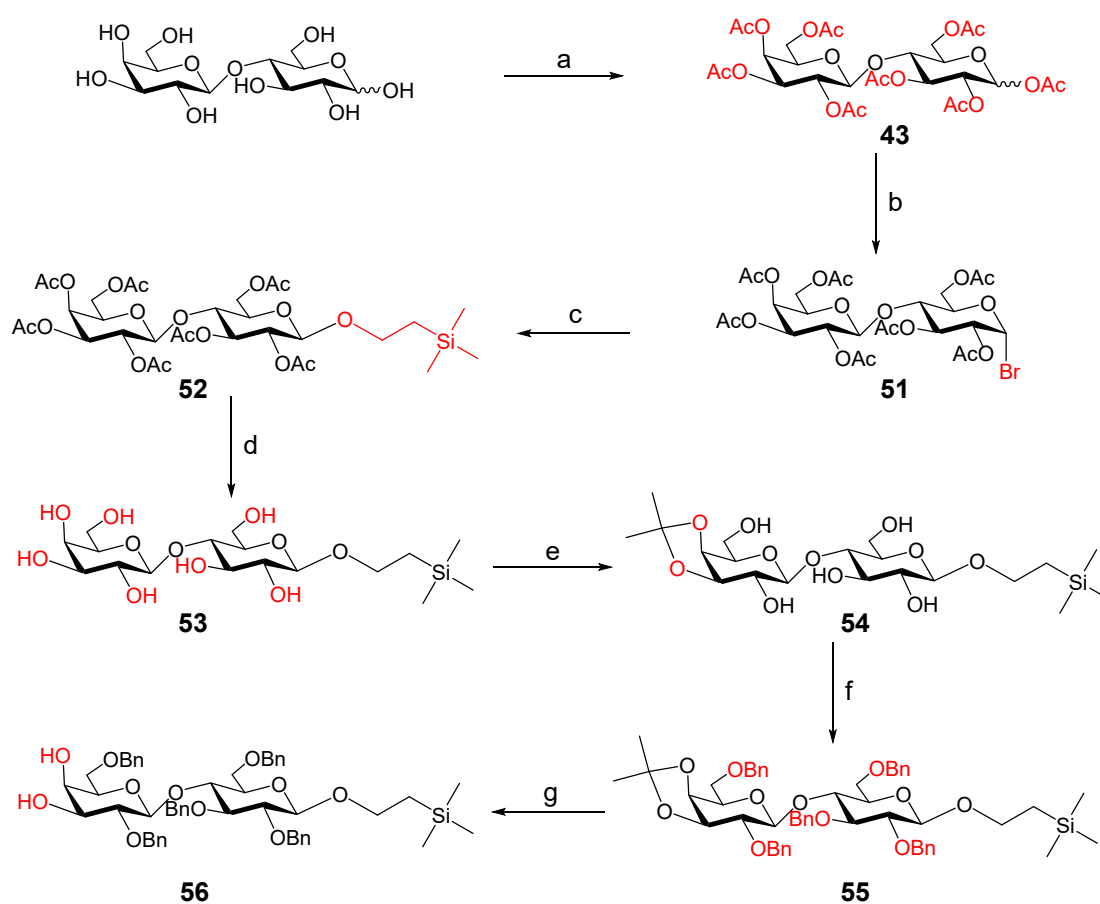


Figure VI-3. Retrosynthetic plan for the chemical synthesis of GM3.

6.1.6. Preparation of the lactoside block

All hydroxyl groups on lactose were protected with acetic anhydride in pyridine to give per-acetylated lactose **43**, which was then made into bromosaccharide **51** using HBr/AcOH in DCM and further converted to 2-(trimethylsilyl)ethyl glycoside **52** by using TMSEtOH, HgO and HgBr₂, followed by deacetylation to give compound **53**, and then the introduction of 3',4'-O-isopropylidene under catalytic amount of 10-d,1-camphorsulfonic acid to protect the 3' and 4' positions to get compound **54**, subsequent benzylation of compound **54** with benzyl bromide and sodium hydride in DMF to obtain fully protected compound **55**, and finally removal of the 3',4'-O-isopropylidene protection to yield the desired lactoside **56**.

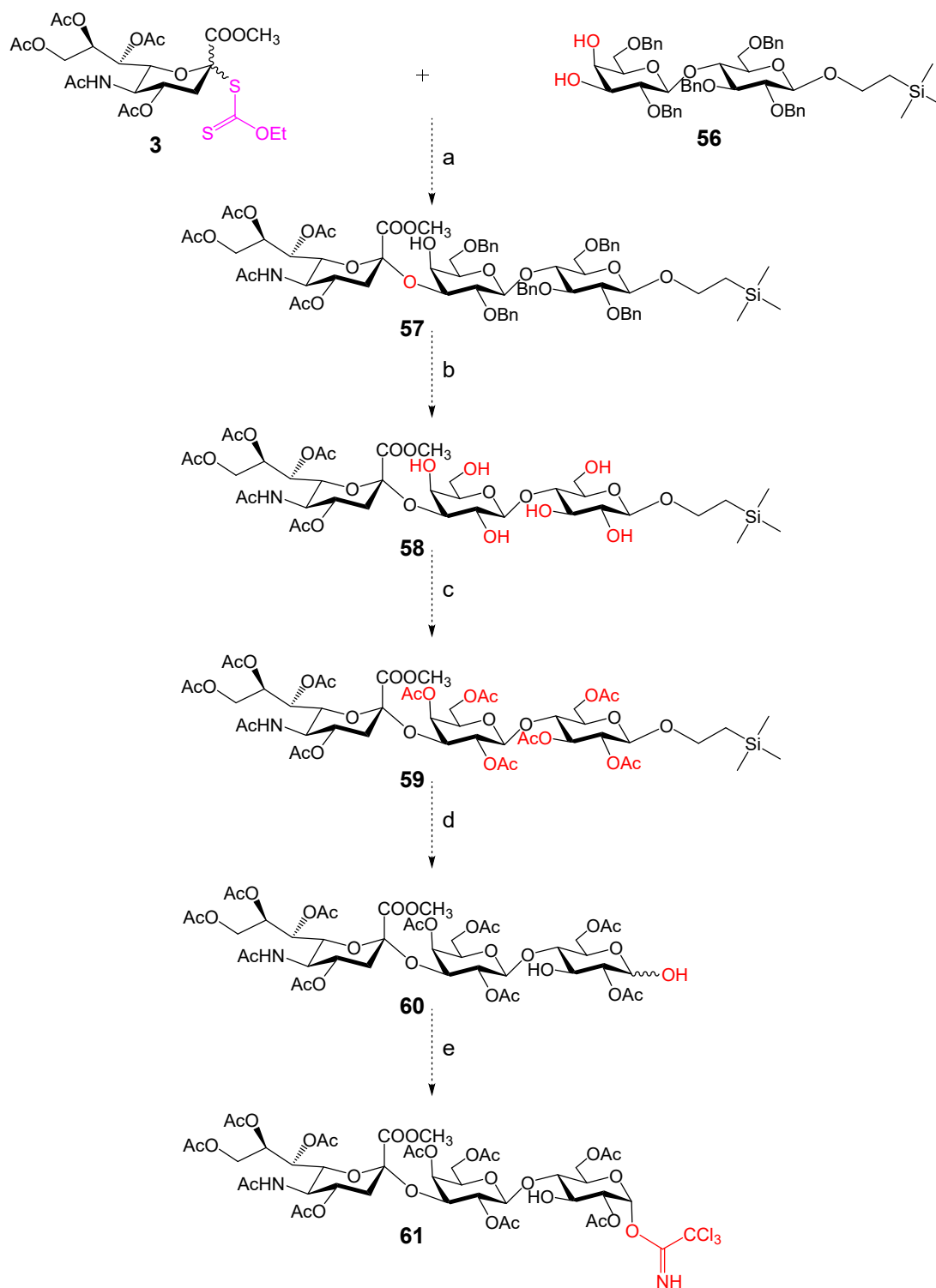


Scheme VI-4. Reagents and conditions: (a) Acetic anhydride, pyridine, r.t., 12 h, 79%; (b) HBr/AcOH, CH₂Cl₂, 0 °C - r.t. 1.5 h; (c) TMSEtOH, HgO, HgBr₂, r.t. 18 h, 76%; (d) NaOMe, MeOH, r.t., 14 h, quant.; (e) 2,2-dimethoxypropane, CSA, r.t., 14 h, 79%; (f) NaH, BnBr, DMF, 0 °C - r.t., overnight; (g) 80% AcOH, 80 °C, 1.5 h, 80%.

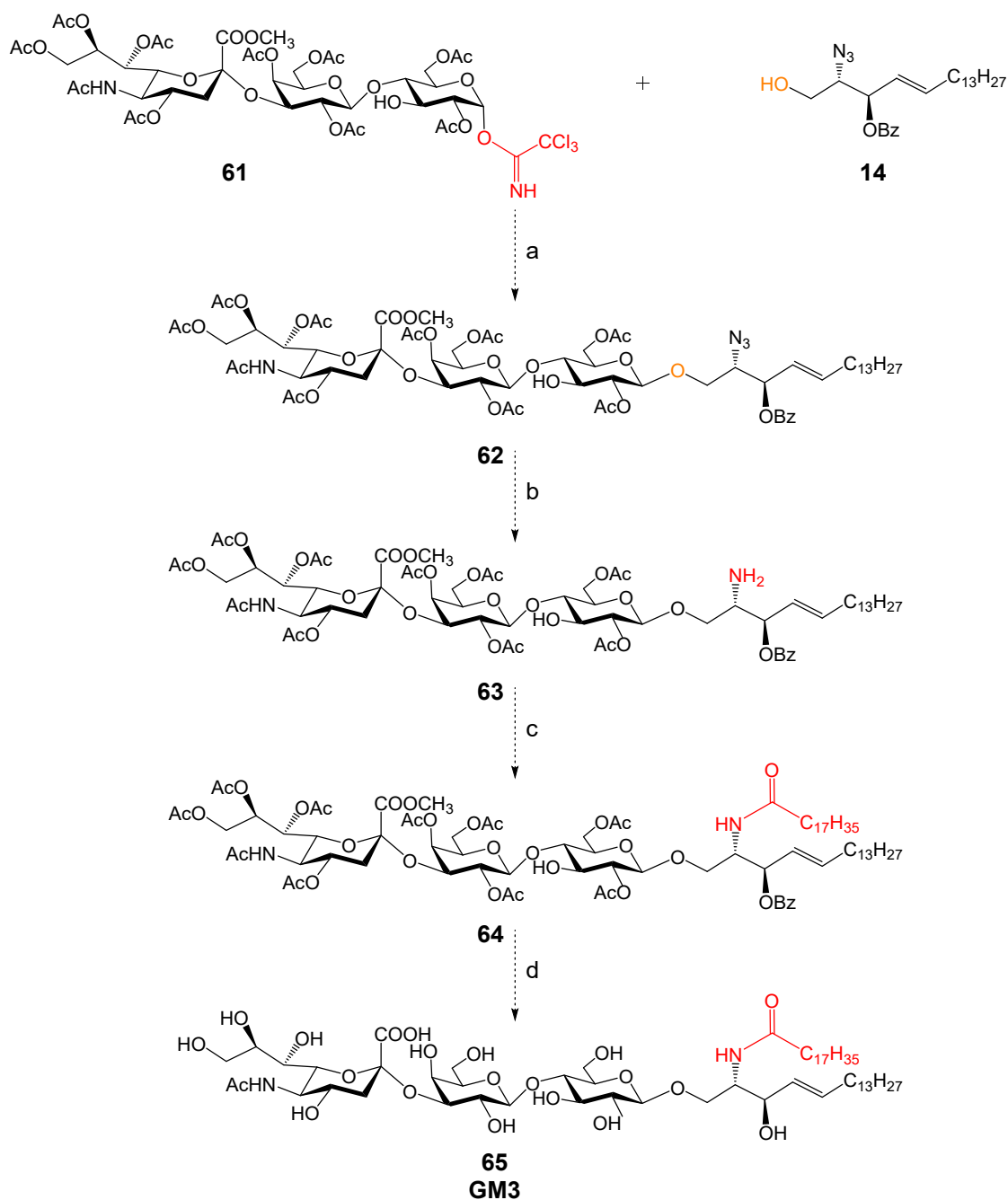
6.2. Construction of the GM3 by glycosylation of these three sugar units

The three main units involved in the synthesis of GM3 have been constructed. Next, we are constructing GM3 by glycosylation reactions according to the

following synthetic route (**Scheme VI-5** and **Scheme VI-6**) [240],[241],[229].



Scheme VI-5. Reagents and conditions: (a) MeCN, CH₂Cl₂, 4 Å powdered molecular sieves, 1 h, AgOTf, DTBP, -68 °C, PhSCL, 3 h; (b) Pd/C, MeOH, H₂, 40 °C, 5 h; (c) Pyr., Ac₂O, r.t., 18 h; (d) CF₃COOH, CH₂Cl₂, 0 °C, 1 h, r.t., 1 h; (e) CNCCl₃, DBU, CH₂Cl₂, -5 °C, 3 h.



Scheme VI-6. Reagents and conditions: (a) $\text{BF}_3 \cdot \text{Et}_2\text{O}$, CH_2Cl_2 , 4 Å powdered molecular sieves, -15°C , 2.5 h; (b) PPh_3 , toluene, H_2O , 45°C , 12 h; (c) Stearic acid, EDC, CH_2Cl_2 , r.t., 20 h; (d) NaOMe , MeOH , r.t., 14 h; H_2O , 0°C , 1 h.

To summarize: this section describes the synthesis of GM3. The loss of sialyltransferase activity led to a very low yield of Lyso-GM3 synthesis by chemoenzymatic methods, with only its molecular weight detected on mass spectrometry and no product spots visible on TLC plates, so we switched to a chemical synthesis route for GM3. The three blocks to construct GM3 have been prepared and the synthesis of GM3 will be completed at a later stage.

Summary and Perspective

Glycosphingolipids play an important role in various physiological and pathological processes such as cell growth, differentiation and apoptosis. In recent years, the biological role of GSLs structure and its structural changes related to biological functions in cancer and other diseases has been a hot topic of research. and the development of corresponding glycosphingolipid drugs is important for the early diagnosis and treatment of diseases. Ganglioside GM3 can significantly affect the growth of tumors or tumor-associated host cells by modulating cancer-related receptors or signalling pathways. Along with the in-depth research on its inhibition of tumor progression, it is of great medical-biological significance to modify its structure to develop anti-tumor agents with better biological activity.

In this work we report a concise protocol that can provide for the preparation of oligomers of a range of ganglioside GM3 analogues. The synthetic strategy for each GM3 analogue oligomer can be broadly divided into three parts: (i) synthesis of the GM3 analogue monomer; (ii) synthesis of the multivalent skeleton; and (iii) modification of the GM3 analogue monomer onto the multivalent skeleton to complete the preparation of the target oligomer. The key step in the synthesis of part (i) is the highly regioselective and stereoselective α -sialylation of mannose residue acceptors. In addition, enzymatic hydrolysis was applied in this part of the work to prepare the building block module (mannose residue block) of the GM3 analogue monomer. The multivalent skeletons in part (ii) include the small molecule skeletons obtained by one-step alkyne modification and the macromolecular skeletons based on cyclodextrin after selective protection and then alkyne modification. The key step in part (iii) is the multivalent modification between monomer and skeleton based on the click reaction. Finally, the monomer (M1) and oligomers (M2, M3, M4, M6, M7) of mannose-containing GM3 analogues were successfully synthesized as shown in **Figure VI-4**.

The effects of exogenous M1, M2, M3 and M4 on tumor cells were observed by in vitro assays and their anti-tumor activity was assessed. In MTT assays, cell colony assays and cell morphology assays, the oligomers exhibited stronger cytotoxicity than the monomers, indicating that they could have more potent anti-proliferative activity. In addition, the overall anti-proliferative effect was stronger on B16F10 and HCT116 cells than on K562 and BXPC-3 cells. In wound healing assays, Transwell migration and invasion assays, both M2 and M4 showed significant anti-migratory and anti-invasive activity against B16F10 and BXPC-3 cells compared to M1 and M3. From the results of the Western blot assay, M1, M2, M3 and M4 could inhibit the movement of tumor cells by suppressing the EMT process through inhibition of the EGFR/VEGFR- β -catenin signalling pathway. Moreover, in B16F10 and BXPC-3 cells, the expression levels of EMT-related proteins were more strongly inhibited by M2 and M4, further indicated that M2 and M4 could have more potent anti-migration and anti- invasion activities.

This research work will contribute to the construction of various novel oligomers of GM3 analogues, and it is encouraging to observe that some oligomers show stronger anti-tumor effects than the monomer to a certain extent in tumor cells, indicating that there is a good research prospect in the direction of synthesizing oligomers of glycosphingolipid-like agents, and these information can provide new ideas and valuable references for exploring the development of new glycosphingolipid-like anticancer agents.

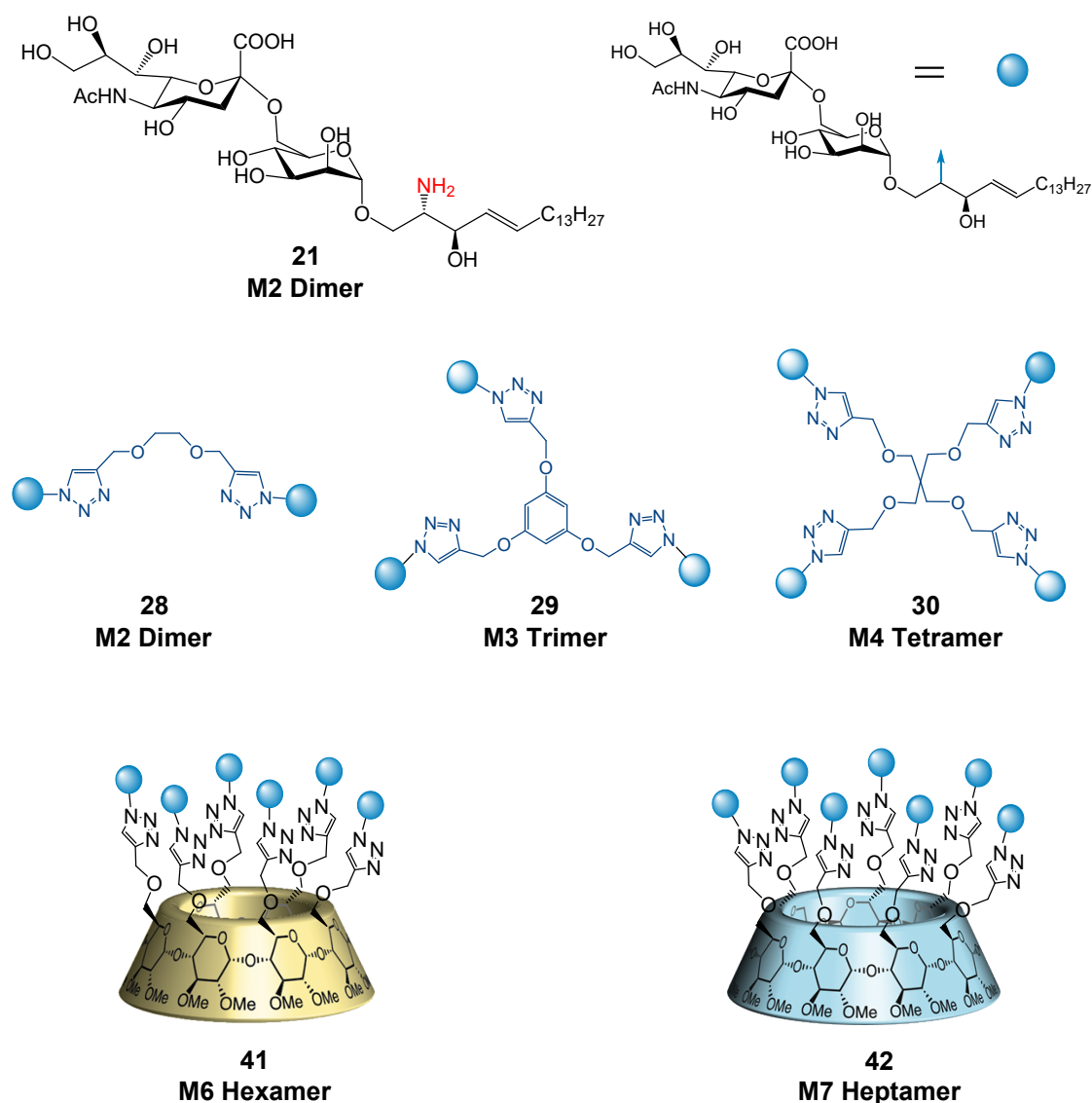


Figure VI-4. Synthesis of five novel oligomers and one known monomer.

Experimental section

7.1. General methods

All chemical reactions were carried out under Argon atmosphere and in the anhydrous conditions with fresh solvents, unless otherwise noted. The solvents were evaporated under reduced pressure and below 45 °C (water bath), followed by removal of residual solvent at high vacuum (< 0.2 mbar).

Reagents were purchased from Sigma-Aldrich, Fluorochem or Alfa Aesar. Dry solvents used in the reaction as following conditions: CH₂Cl₂, pyridine and acetonitrile were freshly distilled each time over CaH₂. Tetrahydrofuran (THF) was refluxed with sodium and benzophenone each time. DMF, MeOH and Et₃N were stored for several days over a bed of molecular sieves (4 Å, beads, 8-12 mesh) before use. All the mixture of solvents is presented in v/v.

Thin Layer Chromatographie (TLC) was performed on Merck silica gel 60 F 254 and revealed with a UV lamp ($\lambda = 254$ nm) and charring with 5% H₂SO₄/EtOH or Hanessian's Stain. Column Chromatographies were conducted on silica Geduran® Si 60Å (40–63 μ m) or silica Geduran® Si 60Å (63–200 μ m), typically using a 30:1 to 100:1 weight ratio of silica gel to crude product.

ESI-High-resolution mass spectra (ESI-HRMS) were recorded on a Bruker Micro-TOF spectrometer in electrospray ionization (ESI) mode, using Tuning-Mix as a reference.

¹H NMR and ¹³C NMR spectra were recorded at Bruker Avance 400 or Bruker Avance 600 MHz spectrometer. 2D COSY, TOCSY, NOESY, HSQC and HMBC experiments were used to assist NMR assignments. The chemical shifts were referenced to the solvent peaks, $\delta = 7.26$ ppm (¹H) and $\delta = 77.16$ ppm (¹³C) for CDCl₃; $\delta = 3.31$ ppm (¹H) and $\delta = 49.00$ ppm (¹³C) for CD₃OD; $\delta = 4.78$ ppm (¹H) for D₂O; $\delta = 3.33$ ppm (¹H) and $\delta = 39.52$ ppm (¹³C) for DMSO-d₆; at 300 K, and the coupling constants were given in Hz.

Optical rotations were measured at 589 nm (Na line) at 20 °C with a Perkin-Elmer Model 343 digital polarimeter using a 10 cm, 1 mL cell.

7.2. Molecule numbering

Preview of main monomer modules and intermediates and target product structure numbers are shown in **Figure VII-1**.

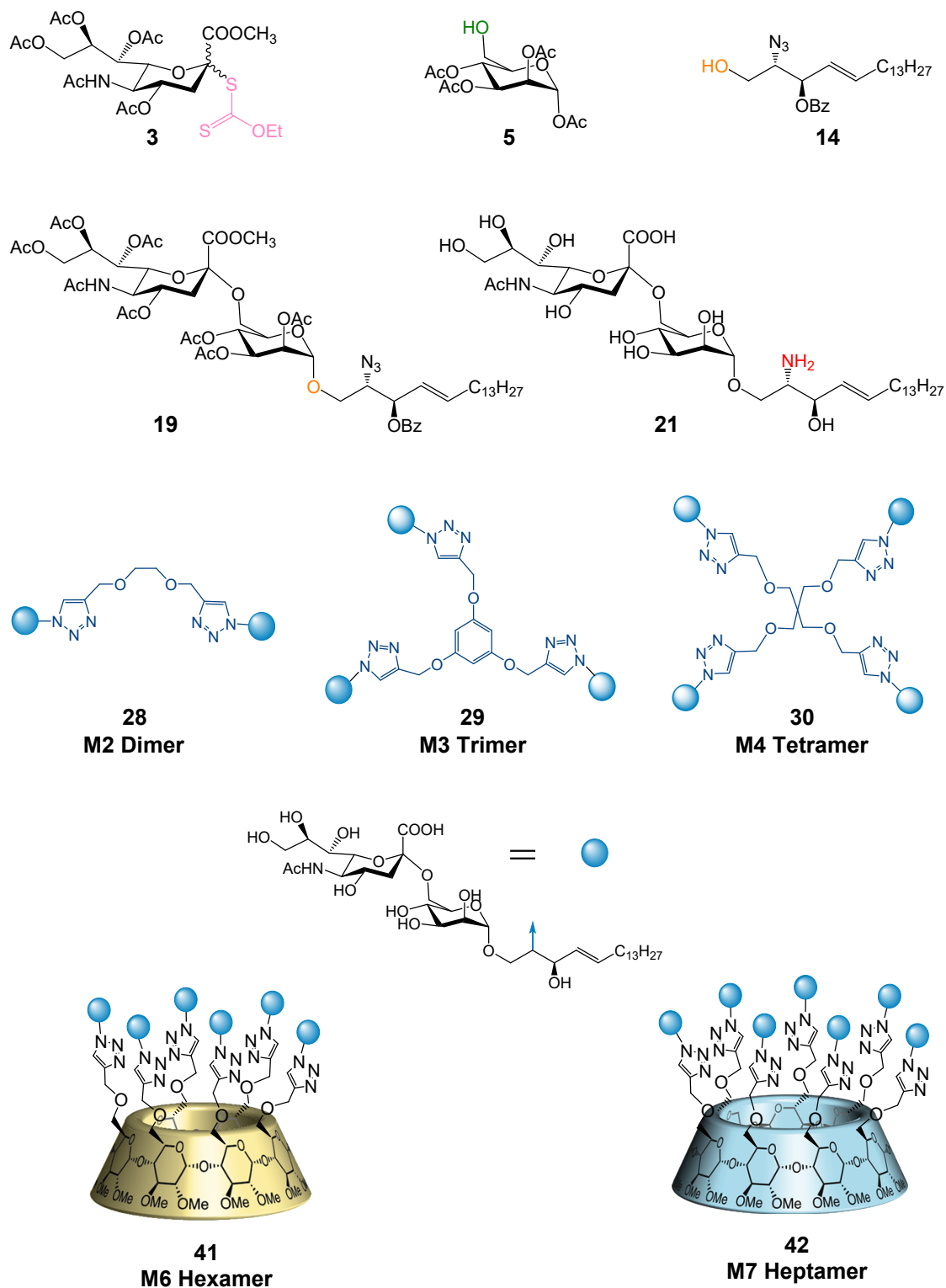
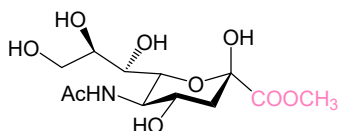


Figure VII-1. Molecule numbering

7.3. Preparation of sialic acid block

Methyl 5-acetamido-3,5-dideoxy-D-glycero- β -D-galacto-2-nonulopyranosonate (**1**)

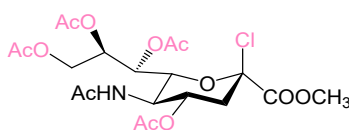


The N-acetyl neuraminic acid (5.0 g, 16.17 mmol) was added to a solution of Amberlyst-H⁺ resin (3.75 g) in methanol (160 mL) and stirred at 45 °C overnight. The progress of the reaction was monitored by thin-layer chromatography, and the color of the solution changed from milky white to clear and colorless. Finally, the solution was filtered and the resin was washed several times with methanol. The filtrate was then evaporated. The methyl ester **1** was obtained as a white solid (4.96 g, 95%) [242].

R_f = 0.33 (CH₂Cl₂-MeOH 3:1).

¹H NMR (400 MHz, CD₃OD): δ (ppm) = 4.11-3.99 (m, 2H, H-6, H-4), 3.86-3.81 (m, 2H, H-5, Ha-9), 3.80 (s, 3H, COOCH₃), 3.72 (dd, J = 9.0, 2.9 Hz, H-8), 3.64 (dd, J = 11.2, 5.7 Hz, 1H, Hb-9), 3.50 (dd, J = 9.1, 1.3 Hz, 1H, H-7), 2.24 (dd, J = 12.9, 4.9 Hz, 1H, H-3eq), 2.03 (d, J = 5.7 Hz, 3H, NHAc), 1.91 (dd, J = 12.8, 11.4 Hz, 1H, H-3ax).

Methyl 5-acetamido-2-chloro-4,7,8,9-tetra-O-acetyl-3,5-dideoxy-D-glycero- β -D-galacto-2-nonulopyranosonate (**2**)



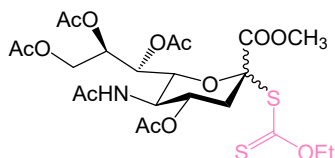
To a suspension of sialic acid methyl ester **1** (4.95 g, 15.31 mmol) in acetyl chloride (306 mL) cooled to 0 °C was slowly added absolute MeOH (3.7 mL). The mixture was allowed to warm to room temperature, and stirring was continued for about 3 days, during which time a clear solution was obtained. The reaction mixture was concentrated and purified by silica gel column, eluting with EtOAc. Concentration in vacuo afforded sialyl chloride **2** as a white foam (6.87 g, 88%) [243].

R_f = 0.38 (CHCl₃-EtOAc 1:5).

¹H NMR (400 MHz, CDCl₃): δ (ppm) = 5.47 (d, J = 5.9 Hz, 1H, H-7), 5.38 (dd, J = 10.5,

4.4 Hz, 1H, H-4), 5.17 (t, $J = 4.9$ Hz, 1H, H-8), 4.42 (dd, $J = 12.5, 2.3$ Hz, 1H, Ha-9), 4.35 (d, $J = 10.3$ Hz, 1H, H-6), 4.20 (dd, $J = 10.5, 10.3$ Hz, 1H, H-5), 4.06 (dd, $J = 12.5, 5.9$ Hz, 1H, Hb-9), 3.87 (s, 3H, COOCH₃), 2.78 (dd, $J = 13.9, 4.5$ Hz, 1H, H-3eq), 2.27 (dd, $J = 13.7, 11.3$ Hz, 1H, H-3ax). 2.11 (s, 3H, OAc), 2.07 (s, 3H, OAc), 2.05 (s, 3H, OAc), 2.04 (s, 3H, OAc), 1.90 (s, 3H, NHAc).

O-ethyl S-[methyl (5-acetamido-4,7,8,9-tetra-O-acetyl-3,5-dideoxy-D-glycero- α/β -D-galacto-2-nonulopyranosyl)onate] dithiocarbonate (α/β -3)



A solution of O-ethyl S-potassium dithiocarbonate (3.23 g, 20.15 mmol) in dry EtOH (103 mL) was added slowly for 15 min at 0 °C to a stirred solution of compound **2** (6.85 g, 13.43 mmol) in dry EtOH (172 mL). The mixture was stirred under N₂ in the dark at 0 °C for 12 h and then at room temperature for additional 12 h. The reaction mixture was diluted with pentane (206 mL), filtered, and concentrated under reduced pressure. The residue was dissolved in dichloromethane and washed with H₂O, saturated NaHCO₃ solution and brine. After drying over MgSO₄ and concentration, the residue was purified by silica gel column, eluting with CH₂Cl₂-EtOAc 1:4. The eluent was concentrated to afford a mixture of α -**3** and β -**3** in molar ratio 16:1 contaminated with known sialyl glycal **3'** (5.92 g, 74% of α/β -**3**, 15% of **3'**). This mixture was used for the sialylations [244].

α -3

R_f = 0.22 (CH₂Cl₂-EtOAc 1:4).

¹H NMR (400 MHz, CDCl₃): δ (ppm) = 5.33-5.29 (m, 2H, H-7, H-8), 5.24 (d, $J = 9.5$ Hz, 1H, NH), 4.89 (td, $J = 11.4, 4.6$ Hz, 1H, H-4), 4.84-4.76 (m, 1H, OCH_aCH₃), 4.60-4.51 (m, 2H, OCH_bCH₃, H-6), 4.33 (dd, $J = 12.4, 2.3$ Hz, 1H, Ha-9), 4.19 (dd, $J = 12.4, 5.1$ Hz, 1H, Hb-9), 4.02 (dd, $J = 20.7, 10.4$ Hz, 1H, H-5), 3.80 (s, 3H, COOCH₃), 2.63 (dd, $J = 13.0, 4.7$ Hz, 1H, H-3eq), 2.14 (s, 3H, OAc), 2.12 (s, 3H, OAc), 2.08-2.05 (m, 1H, H-3ax), 2.03 (t, $J = 3.1$ Hz, 6H, 2 × OAc), 1.88 (d, $J = 5.6$ Hz, 3H, NAc), 1.37 (t, $J = 7.1$ Hz, 3H, CH₃).

¹³C NMR (100 MHz, CDCl₃): δ (ppm) = 207.12 (C=S), 170.74 (C=O), 170.45 (C=O), 170.19 (C=O), 170.16 (C=O), 169.99 (C=O), 168.60 (C=O), 86.44 (C-2), 75.08, 70.15, 68.77, 67.67 (C-4,6,7,8), 70.37 (OCH₂CH₃), 61.98 (C-9), 53.21 (COOCH₃), 49.02 (C-5), 37.03 (C-3), 23.03 (CH₃, NAc), 20.98 (CH₃, OAc), 20.72 (CH₃, OAc), 20.69 (CH₃, OAc), 20.66 (CH₃, OAc), 13.23 (OCH₂CH₃).

β -3

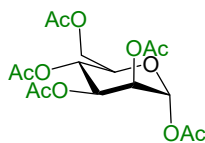
$R_f = 0.29$ (CH_2Cl_2 -EtOAc 1:4).

$^1\text{H NMR}$ (400 MHz, CDCl_3): δ (ppm) = 5.58 (bd, $J = 10.1$ Hz, 1H, NH), 5.33 (dd, $J = 4.1, 2.1$ Hz, 1H, H-7), 5.21 (ddd, $J = 8.0, 4.1, 2.8$ Hz, 1H, H-8), 4.83 (dt, $J = 12.7, 4.6$ Hz, 1H, H-4), 4.77 (m, 1H, OCH_aCH_3), 4.63 (dd, $J = 10.7, 2.1$ Hz, 1H, H-6), 4.53 (m, 1H, OCH_bCH_3), 4.01 (q, $J = 10.4$ Hz, 1H, H-5), 4.01 (dd, $J = 12.1, 2.8$ Hz, 1H, Ha-9), 3.79 (s, 3H, COOCH_3), 3.51 (dd, $J = 12.2, 8.0$ Hz, 1H, Hb-9), 2.57 (dd, $J = 12.9, 4.6$ Hz, 1H, H-3eq), 2.13 (s, 3H, OAc), 2.11 (s, 6H, $2 \times$ OAc), 2.00 (s, 3H, OAc), 1.94 (t, $J = 12.6$ Hz, 1H, H-3ax), 1.85 (s, 3H, NAc), 1.36 (t, $J = 7.1$ Hz, 3H, CH_3).

$^{13}\text{C NMR}$ (100 MHz, CDCl_3): δ (ppm) = 206.92 (C=S), 170.77 (C=O), 170.21 (C=O), 170.03 (C=O), 168.72 (C=O), 86.41 (C-2), 73.41, 70.89 (OCH_2CH_3), 68.61, 53.37 (COOCH_3), 49.05 (C-5), 36.89 (C-3), 23.08 (CH_3 , NAc), 20.89 (CH_3 , OAc), 20.83 (CH_3 , OAc), 20.75 (CH_3 , OAc), 20.68 (CH_3 , OAc), 13.26 (OCH_2CH_3).

7.4. Preparation of mannose block with a free 6-OH

1,2,3,4,6-penta-*O*-acetyl- α -D-mannopyranose (**4**)

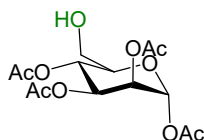


D-(+)-Mannose (3.0 g, 16.65 mmol) was dissolved in pyridine (60 mL) and acetic anhydride (60 mL) was added slowly. The mixture was stirred at room temperature overnight. To the resulting reaction mixture was added dichloromethane and extracted from cooled HCl solution (1.0 M). The combined organic phases were then washed with saturated NaHCO₃ solution and brine, dried over MgSO₄ and concentrated under reduced pressure. The residue was purified by column eluting with Cy-EtOAc 1:1 to give per-acetylated mannose **4** (4.68 g, 72%) as a thick colorless oil [245].

R_f = 0.55 (Cy-EtOAc 1:1).

¹H NMR (400 MHz, CDCl₃): δ (ppm) = 6.38 (d, J = 2.8 Hz, 1H, H-1), 5.50 (t, J = 8.7 Hz, 1H, H-4), 5.34 (m, 2H, H-2, H-3), 4.43-4.01 (m, 3H, H-5, H₂-6), 2.27-1.92 (5s, 15H, 5 \times OAc).

1,2,3,4-tetra-*O*-acetyl- α -D-mannopyranose (**5**)



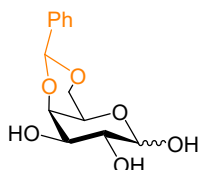
At room temperature, per-acetylated mannose **4** (1.2 g, 3.07 mmol) was added into 166 mL 50 mM phosphate buffer containing 20% acetonitrile at pH 5, and 5 g of biocatalyst CRL was added to initiate the reaction. The hydrolysis reaction was carried out under mechanical stirring, and the pH value was controlled by manual titration. After 4 h, the reaction was stopped by filtering the enzyme. The mixture was extracted with ethyl acetate, washed with water, dried over MgSO₄, and concentrated under reduced pressure. Column separation, eluting with Cy-EtOAc 1:1, gave compound **5** (835 mg, 78%) as a white foam [153].

R_f = 0.30 (Cy-EtOAc 1:1).

¹H NMR (400 Hz, CDCl₃): δ (ppm) = 6.37 (d, J = 2.8 Hz, 1H, H-1), 5.49 (t, J = 8.7 Hz, 1H, H-4), 5.32 (m, 2H, H-2, H-3), 4.33 (t, J = 6.5 Hz, 1H, H-5), 4.04-4.16 (m, 2H, H₂-6), 2.15-1.98 (4s, 12H, 4 \times OAc).

7.5. Preparation of azidosphingosine block

4,6-O-benzylidene- α/β -D-galactose (α/β -6)



D-(+)-galactose (6.0 g, 33.30 mmol) was dissolved in dry DMF (90 mL). Then α , α -dimethoxytoluene (6 mL, 39.82 mmol) and PTSA (210 mg, 1.10 mmol) were added. The resulting methanol was evaporated from the reaction mixture at 40°C. After 3 h, it was neutralized with Et₃N and concentrated under reduced pressure. The residue was purified by silica gel column (EtOAc-MeOH 95:5). Compound **6** (7.05 g, 79%) was obtained as a white amorphous solid [162].

R_f = 0.39 (CH₂Cl₂-MeOH 9:1).

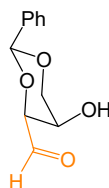
α -6

¹H NMR (400 MHz, DMSO-d₆): δ (ppm) = 7.50-7.30 (m, 5H, Ar-H), 6.26 (d, J = 4.2 Hz, 1H, 1-OH), 5.53 (s, 1H, CHPh), 5.05 (dd, 1H, J = 4.2, 3.4 Hz, H-1), 4.59 (d, J = 6.2 Hz, 1H, 3-OH), 4.41 (d, J = 6.7 Hz, 1H, 2-OH), 4.11 (d, J = 2.6 Hz, 1H, H-4), 4.05 (d, J = 12.1 Hz, 1H, Hb-6), 3.96 (d, J = 12.1 Hz, 1H, Ha-6), 3.77 (s, 1H, H-5), 3.76-3.74 (m, 1H, H-3), 3.62 (ddd, J = 9.4, 6.7, 3.4 Hz, 1H, H-2).

β -6

¹H NMR (400 MHz, DMSO-d₆): δ (ppm) = 7.50-7.30 (m, 5H, Ar-H), 6.56 (d, J = 6.9 Hz, 1H, 1-OH), 5.55 (s, 1H, CHPh), 4.77 (d, J = 5.2 Hz, 1H, 2-OH), 4.76 (d, J = 6.4 Hz, 1H, 3-OH), 4.34 (dd, J = 7.5, 6.9 Hz, 1H, H-1), 4.10-4.00 (m, 3H, H-4, H₂-6), 3.46-3.40 (m, 1H, H-3), 3.45 (br s, 1H, H-5), 3.34-3.28 (m, 1H, H-2).

4,6-O-benzylidene-D-threose (**7**)

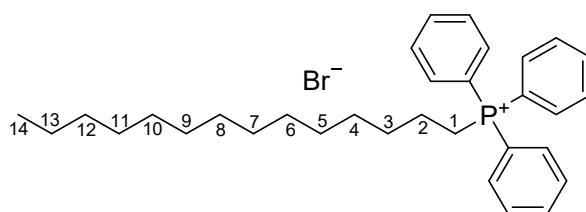


A solution of **6** (5.0 g, 18.64 mmol) in phosphate buffer (pH = 7.6, 214 mL, 0.1 M) was stirred vigorously and NaIO₄ (9.97 g, 46.60 mmol) was added at room

temperature. The pH was maintained above 7.6 by adding saturated sodium bicarbonate solution. After 2 hours, the mixture was concentrated under reduced pressure. The off-white solid residue was dissolved in cooled THF, filtered through filter paper, the solvent was removed, and the residue was dried in vacuo for 4 h to afford crude intermediate **7** (2.64 g, 68%) as a yellow foam. This crude intermediate, which was not separated and further characterized at this stage, was directly engaged in the following step [162].

$R_f = 0.51$ (CH₂Cl₂-MeOH 9:1).

Tetradecyltriphenylphosphonium bromide (**8**)

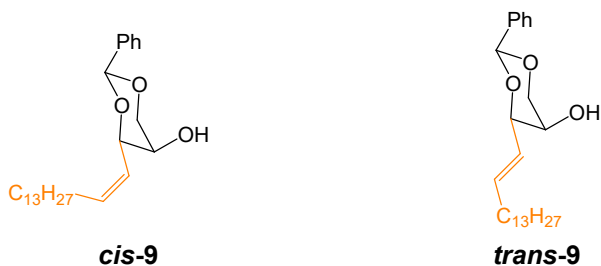


A mixture of tetradecylbromide (3.60 mL, 13.20 mmol) and triphenylphosphine (3.12 g, 11.88 mmol) were heated at 140 °C for 7 h, then dissolved in 7.5 mL of warm Me₂CO and the product crystallized by the addition of 500 mL of anhydrous Et₂O. A second crystallization from Me₂CO/Et₂O gave **8** (5.39 g, 84%) as a white crystalline solid, which was free of alkyl halide and triphenylphosphine [165].

$R_f = 0.35$ (Me₂CO).

¹H NMR (400 MHz, CDCl₃): δ (ppm) = 7.90-7.70 (m, 15H, Ar-H), 3.74 (m, 2H, H₂-1), 1.68-1.55 (m, 4H, H₂-2, H₂-3), 1.42-1.25 (m, 20H, 10 × CH₂), 0.87 (t, *J* = 6.5 Hz, 3H, CH₃).

(2*R*,3*R*,4*Z*)-1,3-*O*-benzylidene-4-octadecene-1,2,3-triol (*cis/trans*-**9**)



The tetradecyltriphenylphosphonium bromide **8** (5.25 g, 9.73 mmol) in 24 mL of anhydrous THF was cooled to -30 °C with mechanical stirring, then the *n*-

butyllithium solution (10.23 mL, 2.5 M in hexanes) was added dropwise over 15 min. The reaction mixture was stirred for an additional 30 min, and then a solution of **7** (1.5 g, 7.20 mmol) in 7.5 mL of anhydrous THF was added over 8 min. The reaction mixture was stirred at -30 °C overnight. The reaction was then quenched with 20 mL of MeOH and 30 mL of H₂O and stirred at room temperature for 1 h. After that, it was extracted with dichloromethane and dried over MgSO₄, filtered and concentrated under reduced pressure. Separation of trans and cis isomers by silica gel column (gradient elution: Cy-DCM 1:3 to 1:6) gave **trans-9** (1.28 g, 46%) and **cis-9** (448 mg, 16%) both as white powder [246].

cis-9

R_f = 0.58 (CH₂Cl₂-EtOAc 25:1).

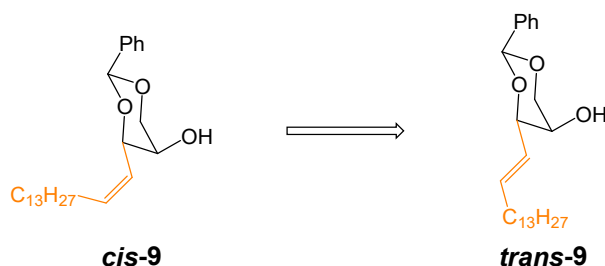
¹H NMR (300 MHz, CDCl₃): δ (ppm) = 7.52 (dd, *J* = 6.7, 3.0 Hz, 2H, Ar-H), 7.37 (dd, *J* = 5.0, 1.9 Hz, 3H, Ar-H), 5.69 (dd, *J* = 5.3, 3.3 Hz, 2H, H-5, H-4), 5.66 (s, 1H, CHPh), 4.73 (d, *J* = 5.0 Hz, 1H, H-3), 4.25 (dd, *J* = 11.9, 1.8 Hz, 1H, Ha-1), 4.11 (d, *J* = 11.8 Hz, 1H, Hb-1), 3.49 (d, *J* = 11.2 Hz, 1H, H-2), 2.75 (d, *J* = 11.2 Hz, 1H, OH), 2.25-2.01 (m, 2H, H₂-6), 1.27 (m, 22H, 11 × CH₂), 0.89 (t, *J* = 6.3 Hz, 3H, CH₃).

trans-9

R_f = 0.60 (CH₂Cl₂-EtOAc 25:1).

¹H NMR (400 MHz, CDCl₃): δ (ppm) = 7.57-7.50 (m, 2H, Ar-H), 7.42-7.33 (m, 3H, Ar-H), 5.88 (dtd, *J* = 15.4, 6.7, 1.0 Hz, 1H, H-5), 5.72-5.64 (m, 1H, H-4), 5.62 (s, 1H, CHPh), 4.41 (d, *J* = 6.1 Hz, 1H, H-3), 4.25 (dd, *J* = 11.8, 1.9 Hz, 1H, Ha-1), 4.08 (dd, *J* = 11.8, 1.3 Hz, 1H, Hb-1), 3.53 (dd, *J* = 10.4, 1.3 Hz, 1H, H-2), 2.66 (d, *J* = 10.4 Hz, 1H, OH), 2.09 (q, *J* = 7.1 Hz, 2H, H₂-6), 1.44-1.36 (m, 2H, H₂-7), 1.27 (s, 20H, 10 × CH₂), 0.89 (t, *J* = 6.9 Hz, 3H, CH₃).

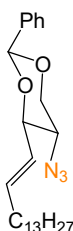
(2*R*,3*R*,4*Z*)-1,3-*O*-benzylidene-4-octadecene-1,2,3-triol (*trans-9*)



The **cis-9** (0.85 g, 2.21 mmol) and diphenyldisulfide (0.43 g, 1.03 mmol) were dissolved in a mixture of cyclohexane (12 mL) and dioxane (3 mL) was irradiated with

a 100 W high-pressure mercury lamp for 5 h. The solvent is removed by evaporation under reduced pressure, the residue was purified by chromatography (gradient elution: Cy-EtOAc 1:3 to 1:6) to yield **trans-9** (399.2 mg, 48%) as a pale yellow solid [246].

(2*S*,3*R*,4*E*)-2-azido-1,3-benzylidene-4-octadecene-1,3-diol (10)

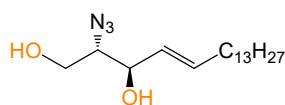


Trifluoromethanesulfonic anhydride (0.8 mL, 4.48 mmol) was added to a solution of **trans-9** (1.2 g, 3.09 mmol) in dry dichloromethane (15 mL) and pyridine (0.7 mL) at -15 °C. After 15 min, the DMF (20 mL) and sodium azide (1.2 g, 18.53 mmol) were added, stirring at -15 °C for 3 h. Further, gradually warmed to room temperature and stirred overnight. Finally, water was added and then extracted with dichloromethane, washed with brine, dried over MgSO₄, filtered and concentrated under reduced pressure. The residue was purified by silica gel column (Cy-CH₂Cl₂ 3:1) to yield **10** (1.02 g, 78%) as a white solid [246].

R_f = 0.34 (Cy-CH₂Cl₂ 3:2).

¹H NMR (400 MHz, CDCl₃): δ (ppm) = 7.49 (dd, *J* = 5.5, 2.5 Hz, 2H, Ar-H), 7.40-7.34 (m, 3H, Ar-H), 6.05-5.96 (m, 1H, H-5), 5.60 (dd, *J* = 15.5, 7.4 Hz, 1H, H-4), 5.50 (s, 1H, *CHPh*), 4.34 (dd, *J* = 11.0, 5.1 Hz, 1H, Ha-1), 4.10-4.03 (m, 1H, H-3), 3.62 (t, *J* = 10.9 Hz, 1H, Hb-1), 3.47 (td, *J* = 10.1, 5.1 Hz, 1H, H-2), 2.12 (dd, *J* = 14.4, 7.1 Hz, 2H, H₂-6), 1.43 (dt, *J* = 14.4, 7.2 Hz, 2H, H₂-7), 1.27 (s, 20H, 10 × CH₂), 0.89 (t, *J* = 6.7 Hz, 3H, CH₃).

(2*S*,3*R*,4*E*)-2-azido-4-octadecene-1,3-diol (11)



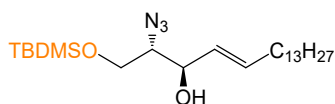
A solution of benzylidene azidosphingosine **10** (1.02 g, 2.47 mmol) in 45 mL of 1:2 CH₂Cl₂/MeOH was stirred vigorously at room temperature and a solution of

PTSA (281 mg, 1.48 mmol) in 52 mL of MeOH was added dropwise. The solution was stirred at room temperature overnight, then quenched with Et₃N. The mixture was concentrated and purified by column chromatography (Cy-EtOAc 2:1) to give azidosphingosine **11** (738 mg, 92%) as a pale-yellow solid [246].

R_f = 0.35 (Cy-EtOAc 2:1).

¹H NMR (400 MHz, CDCl₃): δ (ppm) = 5.85-5.75 (m, 1H, H-5), 5.51 (ddd, *J* = 15.4, 7.3, 1.2 Hz, 1H, H-4), 4.23 (t, *J* = 6.3 Hz, 1H, H-3), 3.83-3.71 (m, 2H, H₂-1), 3.48 (q, *J* = 5.2 Hz, 1H, H-2), 2.16-2.01 (m, 4H, H₂-6, 2 × OH), 1.41-1.32 (m, 2H, H₂-7), 1.24 (s, 20H, 10 × CH₂), 0.86 (t, *J* = 6.6 Hz, 3H, CH₃).

(2*S*,3*R*,4*E*)-2-azido-1-*O*-tertbutyldimethylsilyl-4-octadecene-1,3-diol (**12**)

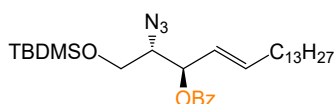


TBDMSCl (683 mg, 4.53 mmol) was added at 0 °C to a solution of compound **11** (738 mg, 2.27 mmol) in dry pyridine (8.6 mL). The mixture was stirred at room temperature for 3 h, quenched with methanol and then concentrated under reduced pressure. The residue was purified by silica gel chromatography (Cy-DCM 2:3) to yield **12** (937 mg, 94%) as a colorless oil [158].

R_f = 0.58 (Cy-EtOAc 4:1).

¹H NMR (400 MHz, CDCl₃): δ (ppm) = 5.82-5.72 (m, 1H, H-5), 5.54-5.44 (m, 1H, H-4), 4.21 (dd, *J* = 11.7, 5.3 Hz, 1H, H-3), 3.82-3.77 (m, 2H, H₂-1), 3.41 (dd, *J* = 10.7, 5.3 Hz, 1H, H-2), 2.36 (d, *J* = 5.0 Hz, 1H, OH), 2.06 (q, *J* = 6.9 Hz, 2H, H₂-6), 1.42-1.34 (m, 2H, H₂-7), 1.26 (s, 20H, 10 × CH₂), 0.92-0.85 (m, 12H, (CH₃)₃C, CH₃), 0.11-0.07 (m, 6H, (CH₃)₂Si).

(2*S*,3*R*,4*E*)-2-azido-3-*O*-benzoyl-1-*O*-tertbutyldimethylsilyl-4-octadecene-1,3-diol (**13**)



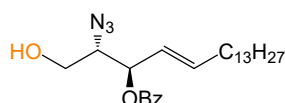
The compound **12** (930 mg, 2.11 mmol) in the dry pyridine (13 mL) was cooled to 0 °C, and benzoyl chloride (0.49 mL, 4.22 mmol) was added. After stirring at room temperature overnight, the mixture was diluted with dichloromethane and washed successively with saturated aqueous NaHCO₃ solution, and H₂O, then dried over MgSO₄, filtered and concentrated under reduced pressure. The residue

was chromatographed (Cy-EtOAc 40:1) to give **13** (1.15 g, quantitative) as a colorless oil [158].

$R_f = 0.35$ (Cy-EtOAc 40:1).

$^1\text{H NMR}$ (400 MHz, CDCl_3): δ (ppm) = 8.09-8.05 (m, 2H, Ar-H), 7.60-7.54 (m, 1H, Ar-H), 7.49-7.43 (m, 2H, Ar-H), 5.92 (dt, $J = 14.7, 6.8$ Hz, 1H, H-5), 5.59 (ddd, $J = 23.0, 11.5, 6.2$ Hz, 2H, H-4, H-3), 3.80 (dt, $J = 7.0, 4.9$ Hz, 1H, H-2), 3.71 (qd, $J = 10.3, 6.1$ Hz, 2H, H₂-1), 2.07 (dd, $J = 14.4, 7.0$ Hz, 2H, H₂-6), 1.41-1.20 (m, 22H, 11 \times CH₂), 0.94-0.85 (m, 12H, (CH₃)₃C, CH₃), 0.07 (d, $J = 0.6$ Hz, 6H, (CH₃)₂Si).

(2*S*,3*R*,4*E*)-2-azido-3-*O*-benzoyl-4-octadecene-1,3-diol (14**)**



To a stirred solution of **13** (1.15 g, 2.11 mmol) in dichloromethane (18 mL) was added $\text{BF}_3 \cdot \text{Et}_2\text{O}$ (0.63 mL, 5.07 mmol) dropwise over 5 min at 0 °C. After 4 h at room temperature, the reaction was quenched and neutralized by the addition of saturated aqueous NaHCO_3 followed by adding dichloromethane. The organic phase was washed with H_2O , dried over MgSO_4 , filtered and concentrated under reduced pressure. The residue was chromatographed (Cy-EtOAc 5:1) to give 3-*O*-benzoyl azidosphingosine **14** (745 mg, 82%) as a colorless oil [154],[157].

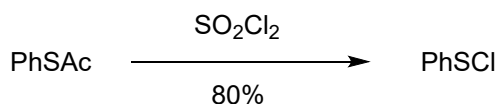
$R_f = 0.28$ (Cy-EtOAc 5:1).

$^1\text{H NMR}$ (400 MHz, CDCl_3): δ (ppm) = 8.14-8.04 (m, 2H, Ar-H), 7.64-7.56 (m, 1H, Ar-H), 7.49-7.43 (m, 2H, Ar-H), 6.03-5.90 (m, 1H, H-5), 5.68-5.55 (m, 2H, H-4, H-3), 3.86-3.73 (m, 2H, H-2, Ha-1), 3.64 (dd, $J = 11.6, 7.1$ Hz, 1H, Hb-1), 2.15-2.01 (m, 2H, H₂-6), 1.41-1.21 (m, 22H, 11 \times CH₂), 0.88 (t, $J = 6.9$ Hz, 3H, CH₃).

$^{13}\text{C NMR}$ (100 MHz, CDCl_3): δ (ppm) = 165.52 (C=O), 133.37 (Ar-C), 129.84 (3Ar-C), 128.53 (2Ar-C), 138.83 (C-5), 123.38 (C-4), 74.62 (C-3), 66.26 (C-2), 62.05 (C-1), 32.39 (C-6), 31.95-28.72 (10 \times CH₂), 22.71 (C-17), 14.13 (CH₃).

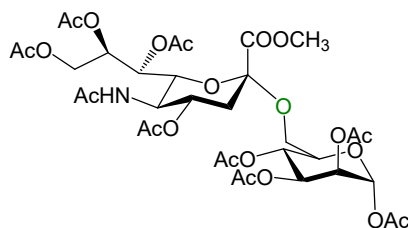
7.6. Synthesis of mannose-containing analogues

Benzenesulfenyl chloride (15)



To a solution of phenyl thioacetate (10g, 65.6 mmol) in CCl_4 (5 mL) cooled to 0°C was added SO_2Cl_2 (5.3 mL, 65.5 mmol) within 10 min. The mixture was stirred at room temperature for 30 min, concentrated, and distilled. The crude benzenesulfenyl chloride **15** (7.63 g, 80%) as a red liquid without further purification [247].

O-(methyl 5-acetamido-4,7,8,9-tetra-*O*-acetyl-3,5-dideoxy-*D*-glycero- α -*D*-galacto-2- nonulopyranosylonate)-(2 \rightarrow 6)-1,2,3,4-tetra-*O*-acetyl- α -*D*-mannopyranose (16)



A solution of the mannose derivative **5** (0.83 g, 2.38 mmol) and the sialyl xanthate **3** (2.13 mg, 3.57 mmol) in dry dichloromethane (25 mL) was added to a mixture of 4\AA powdered molecular sieves (4.7 g) in the dry CH_3CN (50 mL), the mixture was stirred at room temperature for 1 h. AgOTf (1.41 g, 5.48 mmol) and DTBP (1.09 g, 5.72 mmol) were then added, and the reaction system was protected from light and cooled to -68°C . Then PhSCI (1.12 g, 7.74 mmol) in the dry dichloromethane (0.8 mL) was added by running the solution down the cold wall of the reaction flask and the mixture was stirred for 3 h at -68°C . After the reaction was over, the mixture was diluted with a suspension of silica gel (12.5 g) in EtOAc (75 mL), filtered through celite, washed with saturated aqueous NaHCO_3 and water, dried with MgSO_4 , and concentrated under reduced pressure. The residue was chromatographed (Cy-EtOAc 1:3) to give the compound **16** (1.02 g, 52%) as a white foam [147].

$R_f = 0.31$ (Cy-EtOAc 1:3, twice).

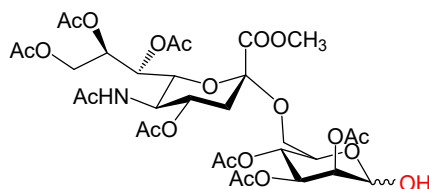
$[\alpha]_D^{20} = -10.8$ (c 1.0 in CHCl_3).

¹H NMR (400 MHz, CDCl₃): δ (ppm) = 6.05 (d, *J* = 1.8 Hz, 1H, H-1'), 5.46 (t, *J* = 9.5 Hz, 1H, H-3'), 5.34-5.29 (m, 4H, H7, H8, H-5', NH), 5.23-5.21 (m, 1H, H-2'), 4.91-4.85 (m, 1H, H-4), 4.36 (dd, *J* = 11.3, 2.7 Hz, 1H, Ha-9), 4.07-3.97 (m, 5H, H-6, Hb-9, H-4', H-5, Ha-6'), 3.79 (s, 3H, COOCH₃), 3.43 (dd, *J* = 11.2, 2.6 Hz, 1H, Hb-6'), 2.64 (dd, *J* = 11.4, 3.7 Hz, 1H, H-3eq), 2.18 (s, 3H, OAc), 2.15 (s, 6H, 2 × OAc), 2.14 (s, 3H, OAc), 2.08 (s, 3H, OAc), 2.04 (s, 3H, OAc), 2.03 (s, 3H, OAc), 2.02 (s, 3H, OAc), 1.89 (t, *J* = 9.8 Hz, 1H, H-3ax), 1.87 (s, 3H, NAc).

¹³C NMR (100 MHz, CDCl₃): δ (ppm) = 170.97 (C=O), 170.57 (C=O), 170.17 (C=O), 170.09 (C=O), 170.04 (C=O), 170.02 (C=O), 169.88 (C=O), 168.94 (C=O), 168.16 (C=O), 167.53 (C=O), 98.42 (C-2), 90.74 (C-1'), 72.31, 71.13, 69.22, 69.09, 68.56, 67.99, 67.21, 65.39 (C-4, C-6, C-7, C-8, C-2', C-3', C-4', C-5'), 62.62 (C-9), 62.37 (C-6'), 52.84 (COOCH₃), 49.41 (C-5), 37.66 (C-3), 23.21 (CH₃, NAc), 21.13 (CH₃, OAc), 20.91 (CH₃, OAc), 20.83 (CH₃, OAc), 20.82 (CH₃, OAc), 20.78 (CH₃, OAc), 20.71 (CH₃, OAc), 20.69 (CH₃, OAc), 20.67 (CH₃, OAc).

ESI-HRMS (*m/z*) calcd for C₃₄H₄₇NO₂₂Na [M+Na]⁺: 844.2487, found: 844.2495.

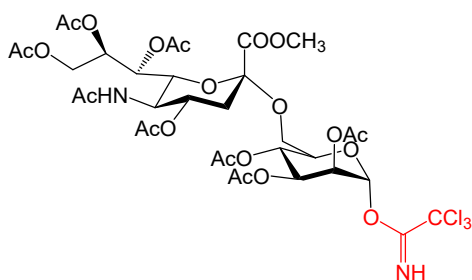
***O*-(methyl 5-acetamido-4,7,8,9-tetra-*O*-acetyl-3,5-dideoxy-*D*-glycero- α -*D*-galacto-2- nonulopyranosylonate)-(2 \rightarrow 6)-2,3,4-tri-*O*-acetyl- α / β -*D*-mannopyranose (17)**



PhCH₂NH₂ (180 mg, 1.68 mmol) was added to a solution of compound **16** (862 mg, 1.05 mmol) in THF (8.6 mL). The mixture was stirred at room temperature overnight. The solvent was evaporated under reduced pressure and the residue was taken into dichloromethane and washed progressively with 1.0 M HCl, saturated aqueous NaHCO₃, and water. The organic layer was dried over MgSO₄ and concentrated. The residue was chromatographed (EtOAc) to give the compound **17** (587 mg, 72%) as a white foam [147].

R_f = 0.29 (EtOAc).

***O*-(methyl 5-acetamido-4,7,8,9-tetra-*O*-acetyl-3,5-dideoxy-*D*-glycero- α -*D*-galacto-2- nonulopyranosylonate)-(2 \rightarrow 6)-2,3,4-tri-*O*-acetyl- α -*D*-mannopyranosyl trichloro- acetimidate (18)**



The solution of intermediate **17** (669 mg, 0.86 mmol) in 25 mL of dry dichloromethane was added trichloroacetonitrile (2.5 mL) and cooled to -5 °C. After that, 250 μ L of DBU was added dropwise and the mixture was stirred at 0 °C overnight. After concentration, the residue was applied to a column chromatography eluted with Cy-EtOAc (with 0.5 % Et₃N) 1:4 to give the product **18** (554 mg, 70%) as a pale-yellow foam [147].

R_f = 0.33 (EtOAc).

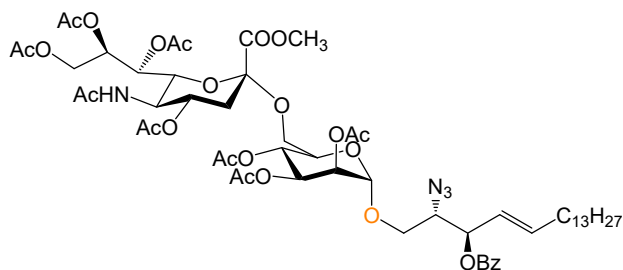
$[\alpha]_D^{20}$ = +2.8 (c 1.0 in CHCl₃).

¹H NMR (400 MHz, CDCl₃): δ (ppm) = 8.74 (s, 1H, NH), 6.25 (d, J = 1.9 Hz, 1H, H-1'), 5.47 (t, J = 11.8 Hz, 1H, H-3'), 5.42 (m, 1H, H-5'), 5.36 (dd, J = 10.2, 3.6 Hz, 1H, H-2'), 5.32-5.29 (m, 3H, H-7, H-8, NH), 4.91-4.85 (m, 1H, H-4), 4.26 (dd, J = 11.3, 3.2 Hz, 1H, Ha-9), 4.05-3.93 (m, 5H, H-5, H-6, Hb-9, H-4', Ha-6'), 3.78 (s, 3H, COOCH₃), 3.47 (dd, J = 11.4, 1.9 Hz, 1H, Hb-6'), 2.60 (dd, J = 11.4, 4.7 Hz, 1H, H-3eq), 2.19 (s, 3H, OAc), 2.14 (s, 3H, OAc), 2.12 (s, 3H, OAc), 2.07 (s, 3H, OAc), 2.03 (s, 3H, OAc), 2.02 (s, 3H, OAc), 1.99 (s, 3H, OAc), 1.94 (t, J = 9.8 Hz, 1H, H-3ax), 1.86 (s, 3H, NAc).

¹³C NMR (100 MHz, CDCl₃): δ (ppm) = 170.79 (C=O), 170.39 (C=O), 170.02 (C=O), 169.88 (C=O), 169.77 (C=O), 169.74 (C=O), 169.62 (C=O), 168.82 (C=O), 167.48 (C=O), 159.63 (C=NH), 98.23 (C-2), 94.65 (C-1'), 90.38 (CCl₃), 72.20, 71.69, 69.04, 68.88, 68.03, 67.78, 67.06, 65.05 (C-4, C-6, C-7, C-8, C-2', C-3', C-4', C-5'), 62.46 (C-9), 62.13 (C-6'), 52.64 (COOCH₃), 49.24 (C-5), 37.47 (C-3), 23.02 (CH₃, NAc), 20.92 (CH₃, OAc), 20.86 (CH₃, OAc), 20.67 (CH₃, OAc), 20.65 (CH₃, OAc), 20.62 (CH₃, OAc), 20.54 (CH₃, OAc), 20.46 (CH₃, OAc).

ESI-HRMS (m/z) calcd for C₃₄H₄₅N₂Cl₃O₂₁Na [M+Na]⁺: 945.1478, found: 945.1460.

***O*-(methyl 5-acetamido-4,7,8,9-tetra-*O*-acetyl-3,5-dideoxy-D-glycero- α -D-galacto- 2-nonulopyranosylonate)-(2 \rightarrow 6)-*O*-(2,3,4-tri-*O*-acetyl- α -D-mannosyl)-(1 \rightarrow 1)-(2*S*,3*R*,4*E*)-2-azido-3-*O*-benzoyl-4-octadecene-1,3-diol(19)**



4Å powdered molecular sieves (0.31 g) was added to a solution of compound **18** (578 mg, 0.62 mmol) and 3-*O*-benzoyl azidosphingosine **14** (376 mg, 0.87 mmol) in dry DCM (30 mL) and stirred at room temperature for 1 h. The mixture was then cooled to -15 °C, and BF₃·Et₂O (394 μL, 3.19 mmol) was added dropwise, stirred at -15 °C for 2.5 h and filtered through Celite. The filtrate was washed with saturated aqueous NaHCO₃ and water, dried over MgSO₄, and concentrated under reduced pressure. The residue was purified by column chromatography (Cy-EtOAc 1:5) to yield compound **19** (402 mg, 54%) as an amorphous solid [147].

R_f = 0.47 (EtOAc).

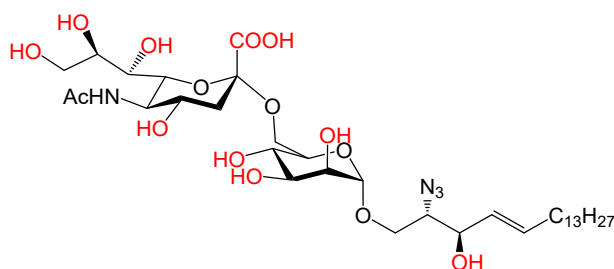
[α]_D²⁰ = -24.5 (*c* 1.0 in CHCl₃).

¹H NMR (400 MHz, CDCl₃): δ (ppm) = 8.06-8.03 (m, 5H, Ar-H), 5.82-5.75 (m, 1H, H-5''), 5.53-5.48 (m, 2H, H-3'', H-4''), 5.38-5.31 (m, 6H, H-4, H-7, H-8, NH, H-2', H-3'), 4.91-4.87 (m, 1H, H-4'), 4.86 (d, *J* = 2.0 Hz, 1H, H-1'), 4.36 (m, 1H, Ha-9), 4.28 (dd, *J* = 12.4, 2.7 Hz, 1H, Hb-9), 3.98-3.92 (m, 5H, H-5, H-5', H-6', H-2''), 3.86 (dd, *J* = 10.4, 3.6 Hz, 1H, Ha-1''), 3.76 (s, 3H, COOCH₃), 3.52-3.44 (m, 2H, H-6, Hb-1''), 2.59 (dd, *J* = 12.7, 4.6 Hz, 1H, H-3eq), 2.17-2.15 (m, 2H, H₂-6''), 2.14 (s, 3H, OAc), 2.13 (s, 3H, OAc), 2.11 (s, 3H, OAc), 2.05 (s, 3H, OAc), 2.02 (s, 3H, OAc), 1.99 (s, 3H, OAc), 1.98 (s, 3H, OAc), 1.90 (t, *J* = 11.2 Hz, 1H, H-3ax), 1.85 (s, 3H, NHAc), 1.39-1.36 (m, 2H, H₂-7''), 1.24 (s, 20H, 10 × CH₂), 0.87 (t, *J* = 6.8 Hz, 3H, CH₃).

¹³C NMR (100 MHz, CDCl₃): δ (ppm) = 170.86 (C=O), 170.57 (C=O), 170.22 (C=O), 170.07 (C=O), 169.99 (C=O), 169.86 (C=O), 169.79 (C=O), 169.14 (C=O), 167.83 (C=O), 165.13 (PhC=O), 138.67 (C-5''), 133.29 (C, CH aromatic), 133.25 (C aromatic), 129.81 (C, CH aromatic), 129.78 (C, CH aromatic), 129.76 (C, CH aromatic), 123.29 (C-4''), 98.45 (C-1'), 98.36 (C-2), 74.55 (C-3''), 72.45 (C-6), 69.64 (C-4'), 69.49 (C-3'), 69.19 (C-2'), 69.06 (C-4), 68.22 (C-8), 67.88 (C-1''), 67.29 (C-5'), 66.76 (C-7), 63.81 (C-2''), 62.36 (C-6'), 61.93 (C-9), 52.73 (COOCH₃), 49.37 (C-5), 37.89 (C-3), 32.36 (C-6''), 29.63, 29.58, 29.41, 29.34 (CH₂), 22.68 (CH₃, NHAc), 21.09 (CH₃, OAc), 20.89 (CH₃, OAc), 20.85 (CH₃, OAc), 20.79 (CH₃, 2 × OAc), 20.71 (CH₃, 2 × OAc), 20.67 (CH₃, OAc), 14.11 (CH₃).

ESI-HRMS (*m/z*) calcd for C₅₇H₈₂N₄O₂₃Na [M+Na]⁺: 1213.5268, found: 1213.5259.

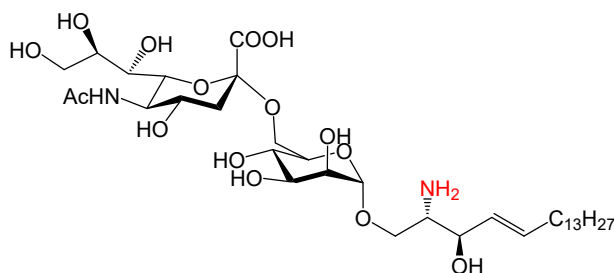
***O*-(5-acetamido-3,5-dideoxy-D-glycero- α -D-galacto-2-nonulopyranosylonate)-(2 \rightarrow 6)-*O*-(α -D-mannosyl)-(1 \rightarrow 1)-(2*S*,3*R*,4*E*)-2-azido-4-octadecene-1,3-diol (**20**)**



The compound **19** (66 mg, 0.055 mmol) was dissolved in 4.5 mL of NaOMe/MeOH (0.1 M) and stirred at room temperature overnight. Then added a few drops of water under 0 °C and stirred for 2 h at room temperature, Further, the mixture was neutralized by Amberlite IR 120/H⁺ ion exchange resin. After filtration and concentration, the crude residue **20** was used in the next step without further purification [147].

$R_f = 0.43$ (EtOAc-*i*PrOH-H₂O 3:2:1).

***O*-(5-acetamido-3,5-dideoxy-D-glycero- α -D-galacto-2-nonulopyranosylonate)-(2 \rightarrow 6)-*O*-(α -D-mannosyl)-(1 \rightarrow 1)-(2*S*,3*R*,4*E*)-2-amino-4-octadecene-1,3-diol (**21**)**



To the crude intermediate **20** (43 mg, 0.055 mmol) in pyridine-water (1:1 v/v, 0.42 mL), 1,3-propanedithiol (0.052 mL, 0.52 mmol) and Et₃N (0.055 mL) were added and the mixture was stirred at 50 °C for 12 h. The reaction mixture was concentrated and purified by silica gel chromatography using CHCl₃-MeOH-H₂O 5:4:0.2 as an eluent to afford **21** (34 mg, 82%) as a white amorphous solid [147].

$R_f = 0.28$ (EtOAc-*i*PrOH-H₂O 3:2:1).

$[\alpha]_D^{20} = -3.1$ (*c* 1.0 in CHCl₃-MeOH 1:1).

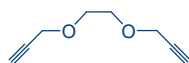
¹H NMR (400 MHz, CD₃OD): δ (ppm) = 5.90-5.85 (m, 1H, H-5''), 5.53-5.48 (m, 1H, H-4''), 4.76 (d, *J* = 1.8 Hz, 1H, H-1'), 4.01-3.78 (m, 8H, H-4, H-5, H-3', H-4', Ha-6', H-1'', H-3''), 3.72-3.6 (m, 7H, H-6, H-8, H₂-9, H-2', Hb-6', H-2''), 3.52 (dd, *J* = 9.1, 1.5 Hz, 1H, H-7), 3.44-3.40 (m, 1H, H-5'), 2.83 (dd, *J* = 12.1, 4.9 Hz, 1H, H-3eq), 2.15-2.08 (m, 2H, H₂-6''), 2.00 (s, 3H, NHAc), 1.79 (t, *J* = 12.1 Hz, 1H, H-3ax), 1.43-1.41 (m, 2H, H₂-7''), 1.30 (s, 20H, 10 × CH₂), 0.90 (t, *J* = 7.4 Hz, 3H, CH₃).

¹³C NMR (100 MHz, CD₃OD): δ (ppm) = 175.56 (C=O), 175.53 (C=O), 136.32 (C-5''), 128.71 (C-4''), 102.59 (C-1'), 101.46 (C-2), 74.42, 73.48, 72.96, 72.42, 71.66, 71.35, 71.20, 70.30, 69.45, 68.33 (C-4, C-6, C-7, C-8, C-2', C-3', C-4', C-5', C-1'', C-3''), 64.74 (C-6'), 64.51 (C-9), 58.46 (C-2''), 54.20 (C-5), 42.45 (C-3), 33.06, 30.81, 30.78, 30.73, 30.45 (CH₂), 23.72 (CH₃, NHAc), 14.42 (CH₃).

ESI-HRMS (*m/z*) calcd for C₃₅H₆₃N₂O₁₅ [M-H]⁻: 751.4234, found: 751.4209.

7.7. Synthesis of small molecule multivalent skeletons

1,2-bis(prop-2-yn-1-yloxy)ethane (**22**)



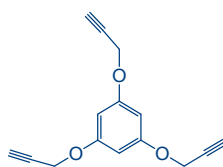
Ethylene glycol (500 mg, 8.06 mmol) was dissolved in DMF (10 mL) and KOH (2.26 g, 40.28 mmol) was added under an ice bath, followed by slow addition of bromopropyne (3.83 g, 32.22 mmol) and restored to room temperature overnight. The reaction was detected by TLC. After completion of the reaction, the solvent was removed under reduced pressure and the residue was taken up in dichloromethane. The organic layer was washed with water and brine and dried over MgSO₄, and concentrated under reduced pressure. The residue was separated by silica gel chromatography and eluted with Cy-EtOAc 5:1 to give compound **22** (532 mg, 48%) as a yellow oily compound [181].

$R_f = 0.31$ (Cy-EtOAc 4:1).

¹H NMR (400 MHz, CDCl₃): δ (ppm) = 4.21 (d, $J = 2.4$ Hz, 2H), 3.72 (s, 4H), 2.48 (d, $J = 2.4$ Hz, 4H).

¹³C NMR (100 MHz, CDCl₃): δ (ppm) = 79.5, 74.7, 68.7, 58.2.

1,3,5-tris(prop-2-yn-1-yloxy) benzene (**23**)



Phloroglucinol (500 mg, 3.96 mmol) was dissolved in DMF (10 mL) and K₂CO₃ (2.74 g, 19.82 mmol) was added under an ice bath, followed by slow addition of bromopropyne (2.83 g, 23.79 mmol) and restored to room temperature overnight. The reaction was detected by TLC. After completion of the reaction, the solvent was removed under reduced pressure and the residue was taken up in dichloromethane. The organic layer was washed with water and brine and dried over MgSO₄, and concentrated under reduced pressure. The residue was separated by silica gel chromatography and eluted with Cy-EtOAc 4:1 to give compound **23** (723 mg, 75%) as a yellow solid [181].

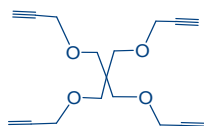
$R_f = 0.34$ (Cy-EtOAc 4:1).

¹H NMR (400 MHz, CDCl₃): δ (ppm) = 6.19 (s, 3H), 4.57 (d, $J = 2.4$ Hz, 3H), 2.46 (s,

6H).

^{13}C NMR (100MHz, CDCl_3): δ (ppm) = 159.3, 95.4, 78.2, 75.7, 55.9.

3-(3-(prop-2-yn-1-yloxy)-2,2-bis((prop-2-yn-1-yloxy) methyl) propoxy) prop-1-yne (24)



Pentaerythritol (500 mg, 3.67 mmol) was dissolved in DMF (10 mL) and sodium hydride (881 mg, 36.73 mmol) was added under an ice bath, followed by slow addition of bromopropyne (3.5 g, 29.38 mmol) and restored to room temperature overnight. The reaction was detected by TLC. After completion of the reaction, the solvent was removed under reduced pressure and the residue was taken up in dichloromethane. The organic layer was washed with water and brine and dried over MgSO_4 , and concentrated under reduced pressure. The residue was separated by silica gel chromatography and eluted with Cy-EtOAc 4:1 to give compound **24** (689 mg, 65%) as a yellow solid [181].

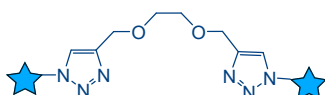
R_f = 0.38 (Cy-EtOAc 4:1).

^1H NMR (400 MHz, CDCl_3): δ (ppm) = 4.12 (d, J = 2.4 Hz, 4H), 3.53 (s, 8H), 2.41 (t, J = 2.4 Hz, 8H).

^{13}C NMR (100MHz, CDCl_3): δ (ppm) = 80.0, 74.1, 69.0, 58.7, 44.7.

7.8. Synthesis of mannose-containing GM3 analogue oligomers with small molecule multivalent skeletons based on "click chemistry"

1,2-Di-{1-[O-(methyl 5-acetamido-4,7,8,9-tetra-O-acetyl-3,5-dideoxy-D-glycero- α -D-galacto-2-nonulopyranosylonate)-(2 \rightarrow 6)-O-(2,3,4-tri-O-acetyl- α -D-mannosyl)-(1 \rightarrow 1)-(2S,3R,4E)-2-azido-3-O-benzoyl-4-octadecene-1,3-diol]-1H-1,2,3-triazole-4-ylmethoxy} ethane (25).



A mixture of compound **22** (8 mg, 0.057 mmol) and compound **19** (173 mg, 0.144 mmol) was dissolved in 2.9 mL of tetrahydrofuran and 2.9 mL of deionized water under argon gas. Then, $\text{CuSO}_4 \cdot 5\text{H}_2\text{O}$ (29 mg, 0.115 mmol) and sodium ascorbate (115 mg, 0.579 mmol) were added sequentially to the reaction system and the mixture was stirred at 56 °C for 24 h. Afterwards, the reaction was detected by TLC and mass spectrometry, extracted with EtOAc and brine, dried with MgSO_4 , and concentrated under reduced pressure. The residue was applied to a chromatography eluted with MeOH-EtOAc 1:50 to give the crude product, which was then further purified with Sephadex LH-20 (MeOH-DCM 1:1) to give the compound **25** (90 mg, 62%) as a white foam.

$R_f = 0.25$ (EtOAc-MeOH 50:1).

$[\alpha]_D^{20} = 25.40$ (c 0.5 in CHCl_3).

$^1\text{H NMR}$ (600 MHz, CDCl_3): δ (ppm) = 7.98 (d, $J = 7.7$ Hz, 4H, Ar-H), 7.69 (s, 2H, triazole), 7.60 (t, $J = 7.3$ Hz, 4H, Ar-H), 7.47 (t, $J = 7.5$ Hz, 4H, Ar-H), 5.91-5.84 (m, 4H, H-5'', H-3''), 5.45-5.39 (m, 2H, H-4''), 5.35-5.26 (m, 6H, H-8, H-7, H-4'), 5.21-5.16 (m, 4H, NH, H-3'), 5.09-5.05 (m, 4H, H-2', H-2''), 4.94-4.87 (m, 2H, H-4), 4.72 (s, 2H, H-1'), 4.71 (m, 4H, Skeleton CH_2), 4.28-4.22 (m, 6H, H-1'', Ha-9), 4.09-4.03 (m, 6H, Hb-9, H-6, H-5), 3.94 (dd, $J = 11.3, 5.1$ Hz, 2H, H-6'), 3.85-3.81 (m, 2H, H-5'), 3.79 (s, 6H, COOCH_3), 3.66 (m, 4H, Skeleton CH_2), 3.44 (d, $J = 10.7$ Hz, 2H, H-6'), 2.60 (dd, $J = 12.8, 4.4$ Hz, 2H, H-3eq), 2.16 (s, 6H, OAc), 2.14 (s, 6H, OAc), 2.12 (s, 6H, OAc), 2.07 (s, 6H, OAc), 2.05 (s, 6H, OAc), 2.03 (s, 6H, OAc), 1.99-1.96 (m, 12H, H-3eq, H-6'', OAc), 1.89 (s, 6H, NAc), 1.27-1.22 (m, 44H, CH_2), 0.89 (t, $J = 6.9$ Hz, 6H, CH_3).

$^{13}\text{C NMR}$ (150 MHz, CDCl_3): δ (ppm) = 171.04 (C=O), 170.68 (C=O), 170.30 (C=O), 170.21 (C=O), 169.97 (C=O), 169.94 (C=O), 169.86 (C=O), 169.24 (C=O), 167.93 (COOCH_3), 165.01 (C=O, OBz), 145.13 (C, triazole), 139.48 (C-5''), 133.56 (C, OBz), 129.81 (C, OBz), 129.65 (C, OBz), 128.71 (C, OBz), 123.72 (CH, triazole), 122.53 (C-4''), 98.65 (C-1'), 98.57 (C-2), 73.95 (C-3''), 72.61 (C-5), 69.91 (C-5'), 69.62 (CH_2).

Skeleton), 69.34 (C-3'), 69.23 (C-2'), 69.12 (C-4), 68.41 (C-8), 67.41 (C-7), 66.67 (C-1'), 65.92 (C-4'), 64.62 (CH₂, Skeleton), 63.29 (C-2''), 63.16 (C-6'), 62.47 (C-9), , 52.93 (COOCH₃), 49.55 (C-6), 37.77 (C-3), 32.34, 32.02, 29.78, 29.77, 29.76, 29.75, 29.74, 29.68, 29.51, 29.45, 29.24, 28.75 (CH₂), 23.30 (CH₃, NHAc), 22.78, 21.20, 20.94, 20.90, 20.82, 20.81, 20.75 (CH₃, OAc), 14.22 (CH₃).

ESI-HRMS (*m/z*) calcd for C₁₂₂H₁₇₄N₈O₄₈ [M+Na]⁺: 2543.1345, found: 2543.1379.

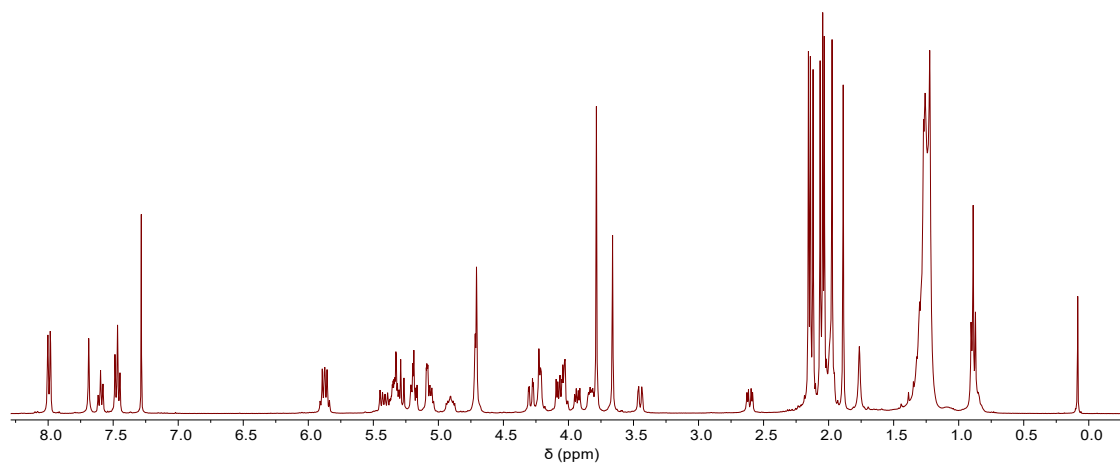


Figure VII-2. ¹H NMR spectrum (600 MHz, CDCl₃, 300 K) of compound **25**.

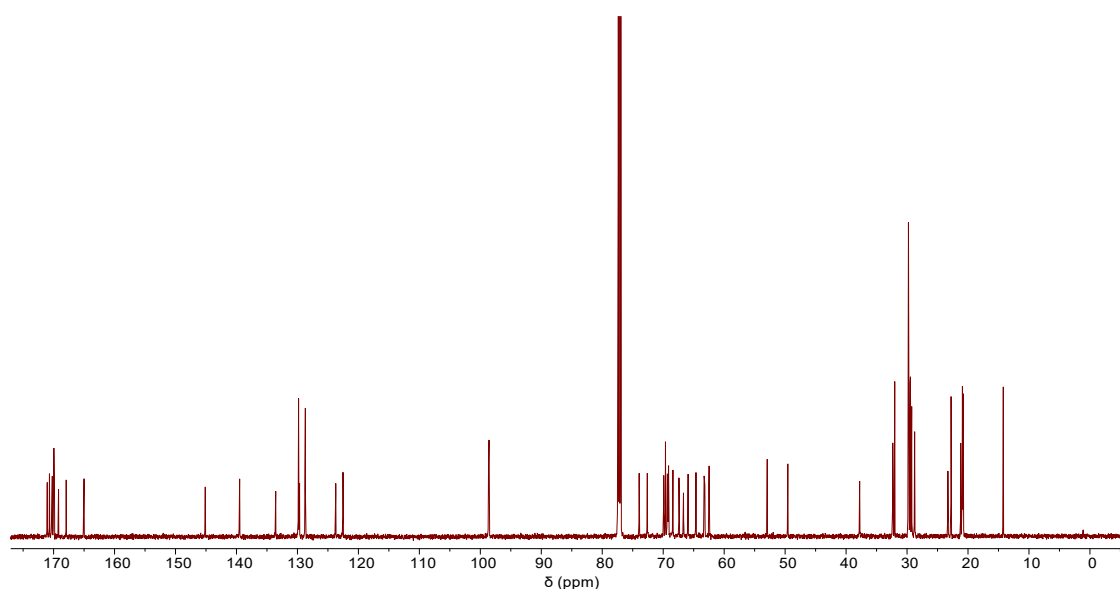


Figure VII-3. ¹³C NMR spectrum (150 MHz, CDCl₃, 300 K) of compound **25**.

Display Report

Analysis Info

Analysis Name D:\Data\GOBS\FANG\2+1-SMS-OAc-20211012.d
 Method tune_high.m
 Sample Name 2+1-SMS-OAc-20211012
 Comment

Acquisition Date 10/13/2021 7:01:16 PM

Operator BDAL@DE
 Instrument / Ser# micrOTOF 235

Acquisition Parameter

Source Type	ESI	Ion Polarity	Positive	Set Nebulizer	5.8 psi
Focus	Active			Set Dry Heater	180 °C
Scan Begin	50 m/z	Set Capillary	4500 V	Set Dry Gas	4.0 l/min
Scan End	3500 m/z	Set End Plate Offset	-500 V	Set Divert Valve	Waste

Meas. m/z	#	Formula	m/z	err [ppm]	mSigma	err [mDa]
1282.5643	1	C 122 H 174 N 8 Na 2 O 48	1282.5602	-3.2	15.1	-4.1
2542.1343	1	C 122 H 174 N 8 Na O 48	2542.1313	-1.2	60.5	-3.0

Meas. m/z	#	Formula	m/z	err [ppm]	mSigma	err [mDa]
2543.1345	1	C 122 H 174 N 8 Na O 48	2542.1313	0.0	1.0	0.0
	2	C 122 H 174 N 8 Na O 48	2542.1313	0.0	1.0	0.0
	3	C 122 H 174 N 8 Na O 48	2542.1313	0.0	1.0	0.0
	4	C 122 H 174 N 8 Na O 48	2542.1313	0.0	1.0	0.0
	5	C 122 H 174 N 8 Na O 48	2542.1313	0.0	1.0	0.0
	6	C 122 H 174 N 8 Na O 48	2542.1313	0.0	1.0	0.0
	7	C 122 H 174 N 8 Na O 48	2542.1313	0.0	1.0	0.0
	8	C 122 H 174 N 8 Na O 48	2542.1313	0.0	1.0	0.0
	9	C 122 H 174 N 8 Na O 48	2542.1313	0.0	1.0	0.0
	10	C 122 H 174 N 8 Na O 48	2542.1313	0.0	1.0	0.0
	11	C 122 H 174 N 8 Na O 48	2542.1313	0.0	1.0	0.0

Meas. m/z	#	Formula	m/z	err [ppm]	mSigma	err [mDa]
1283.0619	1	C 122 H 174 N 8 Na 2 O 48	1282.5602	0.0	1.0	0.0
	2	C 122 H 174 N 8 Na 2 O 48	1282.5602	0.0	1.0	0.0
	3	C 122 H 174 N 8 Na 2 O 48	1282.5602	0.0	1.0	0.0
	4	C 122 H 174 N 8 Na 2 O 48	1282.5602	0.0	1.0	0.0
	5	C 122 H 174 N 8 Na 2 O 48	1282.5602	0.0	1.0	0.0
	6	C 122 H 174 N 8 Na 2 O 48	1282.5602	0.0	1.0	0.0
	7	C 122 H 174 N 8 Na 2 O 48	1282.5602	0.0	1.0	0.0

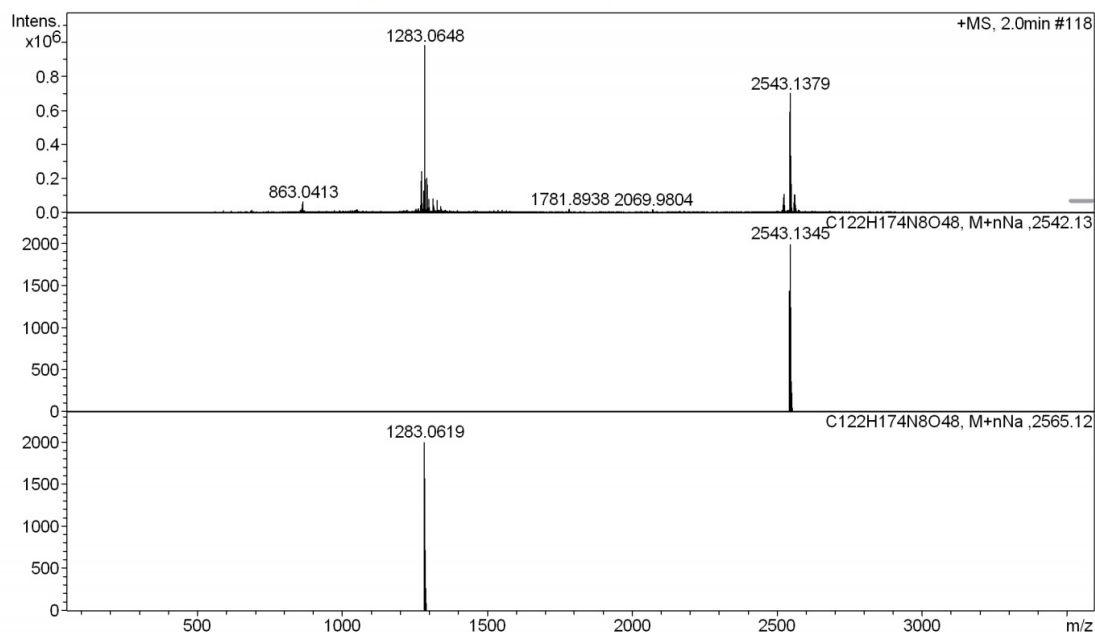
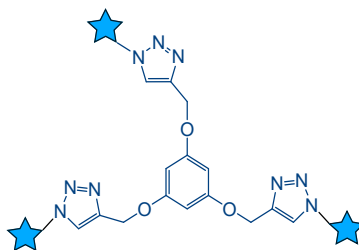


Figure VII-4. HRMS spectrum of compound 25.

1,3,5-Tri-{1-[O-(methyl5-acetamido-4,7,8,9-tetra-O-acetyl-3,5-dideoxy-D-glycero- α -D-galacto-2-nonulopyranosylonate)-(2 \rightarrow 6)-O-(2,3,4-tri-O-acetyl- α -D-mannosyl)-(1 \rightarrow 1)-(2S,3R,4E)-3-O-benzoyl-4-octadecene-1,3-diol]-1H-1,2,3-triazole-4-ylmethoxy} benzene (26).



A mixture of compound **23** (7.3 mg, 0.03 mmol) and compound **19** (135 mg, 0.113 mmol) was dissolved in 2.3 mL of tetrahydrofuran and 2.3 mL of deionized water under argon gas. Then, $\text{CuSO}_4 \cdot 5\text{H}_2\text{O}$ (15.2 mg, 0.06 mmol) and sodium ascorbate (60.19 mg, 0.303 mmol) were added sequentially to the reaction system and the mixture was stirred at 56 °C for 24 h. Afterwards, the reaction was detected by TLC and mass spectrometry, extracted with EtOAc and brine, dried with MgSO_4 , and concentrated under reduced pressure. The residue was applied to a silica gel column chromatography eluted with MeOH-EtOAc 1:50 to give the crude product, which was then further purified with Sephadex LH-20 (MeOH- CH_2Cl_2 1:1) to give the compound **26** (63 mg, 55%) as a white foam.

$R_f = 0.21$ (EtOAc-MeOH 50:1).

$[\alpha]_D^{20} = 18.35$ (c 0.5 in CHCl_3).

$^1\text{H NMR}$ (600 MHz, CDCl_3): δ (ppm) = 7.97 (d, $J = 7.7$ Hz, 6H, Ar-H), 7.78 (s, 3H, triazole), 7.58 (t, $J = 7.3$ Hz, 3H, Ar-H), 7.44 (t, $J = 7.5$ Hz, 6H, Ar-H), 6.31 (s, 3H, Skeleton Ar-H), 5.91-5.85 (m, 6H, H-5'', H-3''), 5.44-5.40 (m, 3H, H-4''), 5.33 (m, 3H, H-8), 5.30 (d, $J = 8.2$ Hz, 3H, H-7), 5.27 (d, $J = 9.9$ Hz, 3H, H-4'), 5.22-5.18 (m, 6H, NH, H-3'), 5.16-5.11 (m, 6H, Skeleton CH_2), 5.10-5.09 (m, 3H, H-2'), 5.07-5.05 (m, 3H, H-2''), 4.92-4.87 (m, 3H, H-4), 4.72 (s, 3H, H-1'), 4.29-4.22 (m, 9H, Ha-9, H-1''), 4.08-4.00 (m, 9H, Hb-9, H-6, H-5), 3.92 (dd, $J = 11.3, 5.1$ Hz, 3H, H-6'), 3.84-3.81 (m, 3H, H-5'), 3.76 (s, 9H, COOCH_3), 3.44 (d, $J = 10.7$ Hz, 3H, H-6''), 2.59 (dd, $J = 12.8, 4.4$ Hz, 3H, H-3eq), 2.13 (s, 9H, OAc), 2.11 (s, 9H, OAc), 2.10 (s, 9H, OAc), 2.03 (s, 9H, OAc), 2.02 (s, 9H, OAc), 2.01 (s, 9H, OAc), 2.00-1.96 (m, 6H, H-3eq, H-6''), 1.95 (s, 9H, OAc), 1.87 (s, 9H, NAc), 1.29-1.20 (m, 66H, CH_2), 0.87 (t, $J = 6.9$ Hz, 9H, CH_3).

$^{13}\text{C NMR}$ (150 MHz, CDCl_3): δ (ppm) = 171.07 (C=O), 170.72 (C=O), 170.34 (C=O), 170.25 (C=O), 170.05 (C=O), 169.97 (C=O), 169.91 (C=O), 169.24 (C=O), 167.98 (COOCH_3), 165.13 (C=O, OBz), 160.46 (C, Skeleton aromatic), 144.06 (C, triazole), 139.52 (C-5''), 133.65 (C, OBz), 129.86 (C, OBz), 129.65 (C, OBz), 128.77 (C, OBz),

124.54 (CH, triazole), 122.46 (C-4''), 98.69 (C-1'), 98.61 (C-2), 94.97 (CH, Skeleton aromatic), 73.77 (C-3''), 72.57 (C-5), 70.01 (C-5'), 69.32 (C-3'), 69.27 (C-2'), 69.13 (C-4), 68.35 (C-8), 67.42 (C-7), 66.63 (C-1''), 65.95 (C-4'), 63.42 (C-2''), 63.20 (C-6'), 62.51 (C-9), 62.25 (CH₂, Skeleton), 52.97 (COOCH₃), 49.59 (C-6), 37.81 (C-3), 32.38, 32.06, 29.84, 29.83, 29.82, 29.81, 29.79, 29.72, 29.54, 29.48, 29.27, 28.78 (CH₂), 23.34 (CH₃, NHAc), 22.82, 21.24, 20.99, 20.96, 20.86, 20.84, 20.80 (CH₃, OAc), 14.27 (CH₃).

ESI-HRMS (*m/z*) calcd for C₁₈₆H₂₅₈N₁₂O₇₂ [M+H+Na]³⁺: 1294.2250, found: 1294.2212.

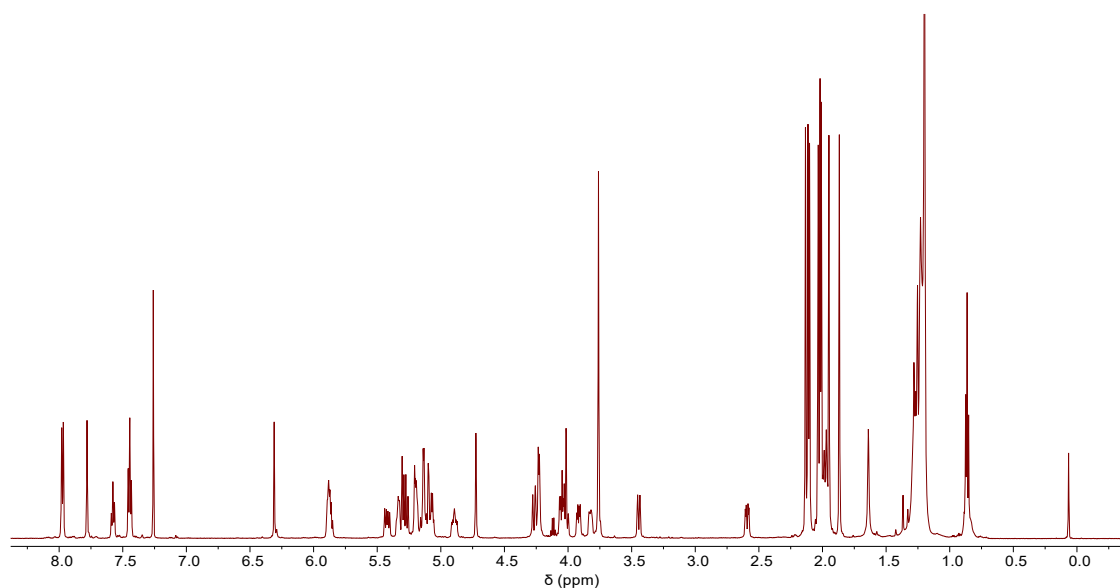


Figure VII-5. ¹H NMR spectrum (600 MHz, CDCl₃, 300 K) of compound 26.

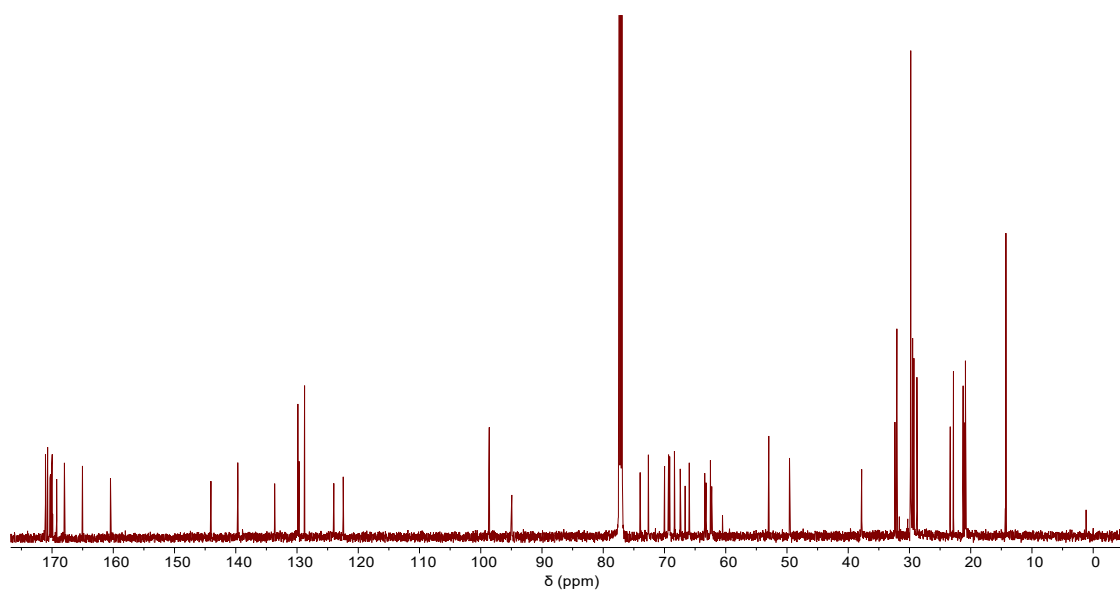


Figure VII-6. ¹³C NMR spectrum (150 MHz, CDCl₃, 300 K) of compound 26.

Display Report

Analysis Info

Analysis Name D:\Data\GOBS\FANG\2-SMS-OAc-20211012.d
Method tune_high.m
Sample Name 2-SMS-OAc-20211012
Comment

Acquisition Date 10/12/2021 7:34:10 PM

Operator BDAL@DE
Instrument / Ser# micrOTOF 235

Acquisition Parameter

Source Type	ESI	Ion Polarity	Positive	Set Nebulizer	5.8 psi
Focus	Active			Set Dry Heater	180 °C
Scan Begin	50 m/z	Set Capillary	4500 V	Set Dry Gas	4.0 l/min
Scan End	3500 m/z	Set End Plate Offset	-500 V	Set Divert Valve	Waste

Meas. m/z	#	Formula	m/z	err [ppm]	mSigma	err [mDa]
1293.5573	1	C 186 H 258 N 12 Na 3 O 72	1293.5524	-3.8	51.5	-4.9
1928.8367	1	C 186 H 258 N 12 Na 2 O 72	1928.8340	-1.4	30.2	-2.7

Meas. m/z	#	Formula	m/z	err [ppm]	mSigma	err [mDa]
-----------	---	---------	-----	-----------	--------	-----------

Meas. m/z	#	Formula	m/z	err [ppm]	mSigma	err [mDa]
-----------	---	---------	-----	-----------	--------	-----------

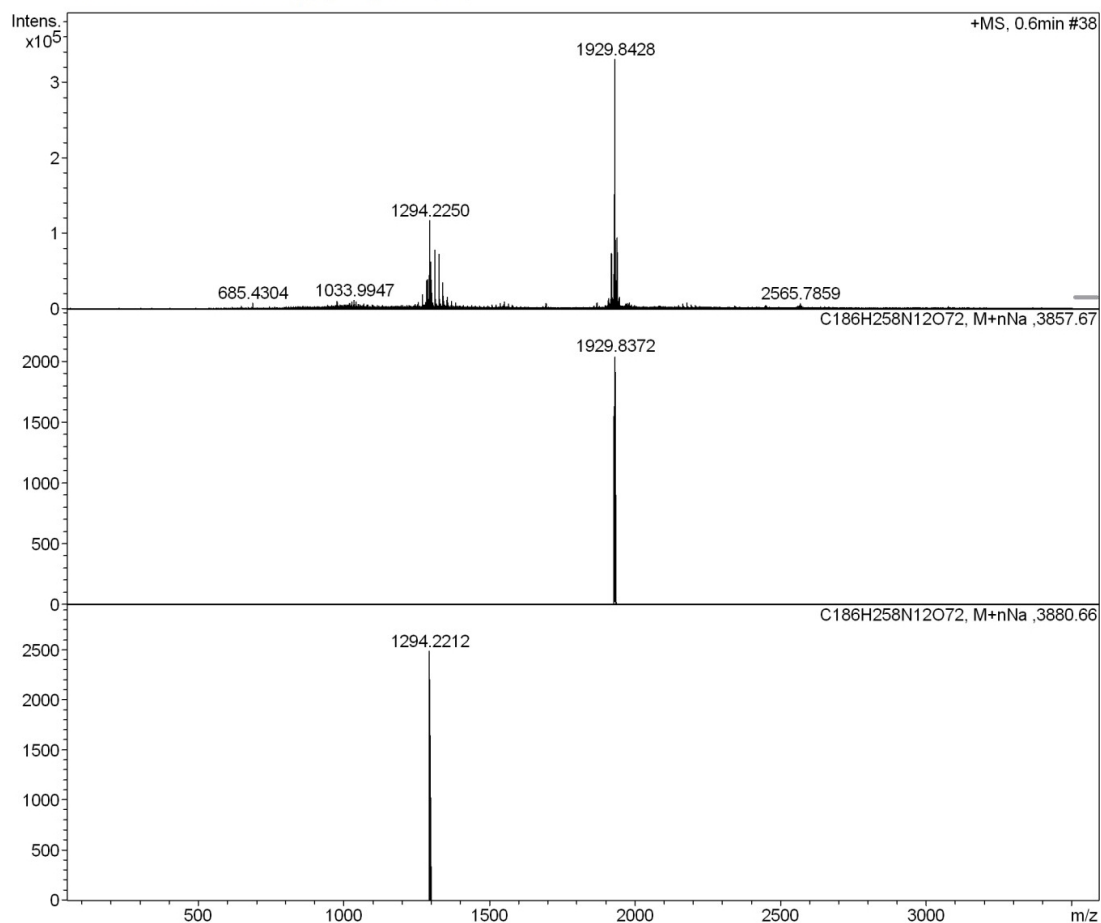
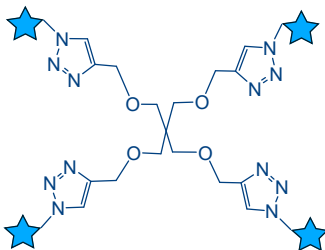


Figure VII-7. HRMS spectrum of compound 26.

Tetrakis- {1-[O-(methyl 5-acetamido-4,7,8,9-tetra-O-acetyl-3,5-dideoxy-D-glycero- α -D-galacto-2-nonulopyranosylonate)-(2 \rightarrow 6)-O-(2,3,4-tri-O-acetyl- α -D-mannosyl)-(1 \rightarrow 1)-(2S,3R,4E)-2-azido-3-O-benzoyl-4-octadecene-1,3-diol]-1H-1,2,3-triazole-4-ylmethoxy}pentaerythritol (27).



A mixture of compound **24** (6.9 mg, 0.23 mmol) and compound **19** (142 mg, 0.119 mmol) was dissolved in 2.4 mL of tetrahydrofuran and 2.4 mL of deionized water under argon gas. Then, $\text{CuSO}_4 \cdot 5\text{H}_2\text{O}$ (12.12 mg, 0.048 mmol) and sodium ascorbate (47.41 mg, 0.239 mmol) were added sequentially to the reaction system and the mixture was stirred at 56 °C for 24 h. Afterwards, the reaction was detected by TLC and mass spectrometry, extracted with EtOAc and brine, dried with MgSO_4 , and concentrated under reduced pressure. The residue was applied to a silica gel column chromatography eluted with MeOH-EtOAc 1:30 to give the crude product, which was then further purified with Sephadex LH-20 (MeOH- CH_2Cl_2 1:1) to give the compound **27** (58 mg, 48%) as a white foam.

$R_f = 0.22$ (EtOAc-MeOH 20:1).

$[\alpha]_D^{20} = 23.65$ (c 0.5 in CHCl_3).

$^1\text{H NMR}$ (600 MHz, CDCl_3): δ (ppm) = 7.95 (d, $J = 7.7$ Hz, 8H, Ar-H), 7.72 (s, 4H, triazole), 7.58 (t, $J = 7.3$ Hz, 4H, Ar-H), 7.41 (t, $J = 7.5$ Hz, 8H, Ar-H), 5.88-5.85 (m, 8H, H-5'', H-3''), 5.47-5.41 (m, 4H, H-4''), 5.34—5.25 (m, 16H, H-8, H-7, H-4', NH), 5.19-5.16 (m, 4H, H-3'), 5.12-5.07 (m, 8H, H-2'), 5.07-5.05 (m, 4H, H-2''), 4.92-4.86 (m, 4H, H-4), 4.75 (s, 4H, H-1'), 4.50 (m, 8H, Skeleton CH_2), 4.29-4.18 (m, 12H, H-1'', Ha-9), 4.08-4.01 (m, 12H, Hb-9, H-6, H-5), 3.94-3.87 (m, 8H, H-6', H-5'), 3.76 (s, 12H, COOCH_3), 3.44 (m, 12H, H-6', Skeleton CH_2), 2.59 (dd, $J = 12.8, 4.4$ Hz, 4H, H-3eq), 2.14 (s, 12H, OAc), 2.12 (s, 12H, OAc), 2.09 (s, 12H, OAc), 2.04 (s, 12H, OAc), 2.02 (s, 12H, OAc), 2.00 (s, 12H, OAc), 1.97-1.94 (m, 12H, H-3eq, H-6''), 1.93 (s, 12H, OAc), 1.86 (s, 12H, NAc), 1.28-1.19 (m, 88H, CH_2), 0.86 (t, $J = 6.9$ Hz, 12H, CH_3).

$^{13}\text{C NMR}$ (150 MHz, CDCl_3): δ (ppm) = 171.01 (C=O), 170.72 (C=O), 170.38 (C=O), 170.21 (C=O), 169.95 (C=O), 169.92 (C=O), 169.87 (C=O), 169.21 (C=O), 167.99 (COOCH_3), 164.95 (C=O, OBz), 144.88 (C, triazole), 139.26 (C-5''), 133.64 (C, OBz), 129.84 (C, OBz), 129.69 (C, OBz), 128.78 (C, OBz), 124.34 (CH, triazole), 122.59 (C-4''), 98.73 (C-1'), 98.63 (C-2), 74.24 (C-3''), 72.59 (C-5), 69.94 (C-5'), 69.47 (CH_2 ,

Skeleton), 69.41 (C-3'), 69.28 (C-2'), 69.21 (C-4), 68.37 (C-8), 67.44 (C-7), 66.52 (C-1''), 65.95 (C-4'), 64.79 (CH₂, Skeleton), 63.52 (C-2''), 63.14 (C-6'), 62.48 (C-9), 53.01 (COOCH₃), 49.54 (C-6), 37.79 (C-3), 32.43, 32.04, 29.84, 29.83, 29.82, 29.81, 29.79, 29.72, 29.54, 29.48, 29.34, 28.89 (CH₂), 23.32 (CH₃, NHAc), 22.82, 21.24, 20.98, 20.94, 20.86, 20.83, 20.75 (CH₃, OAc), 14.27 (CH₃).

ESI-HRMS (*m/z*) calcd for C₂₄₅H₃₄₈N₁₆O₉₆ [M+2H+Na]³⁺: 1707.4206, found: 1707.4197.

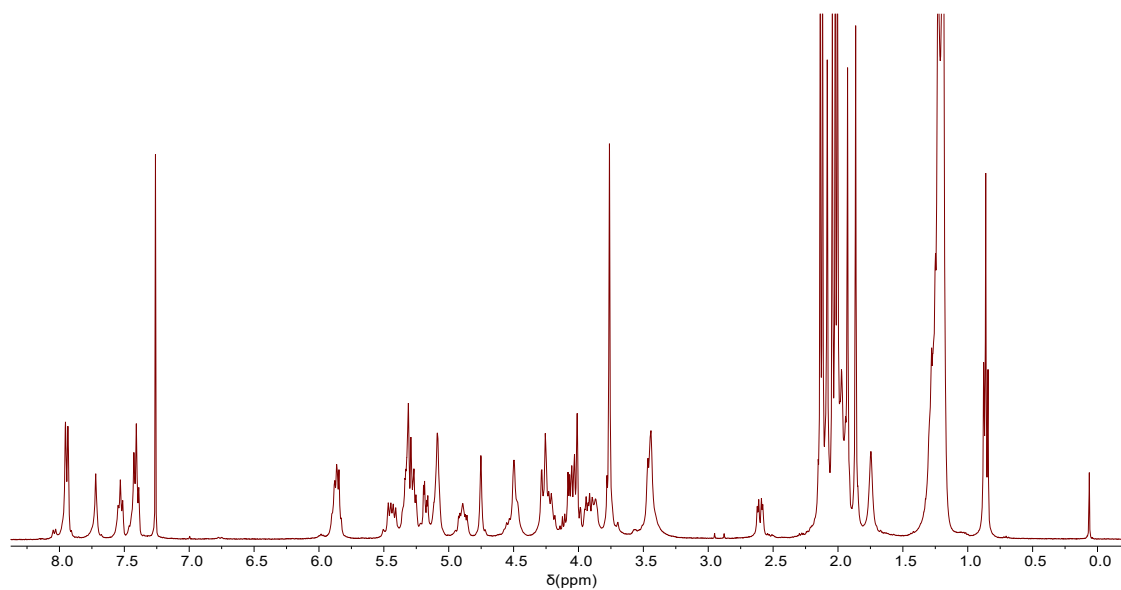


Figure VII-8. ¹H NMR spectrum (600 MHz, CDCl₃, 300 K) of compound 27.

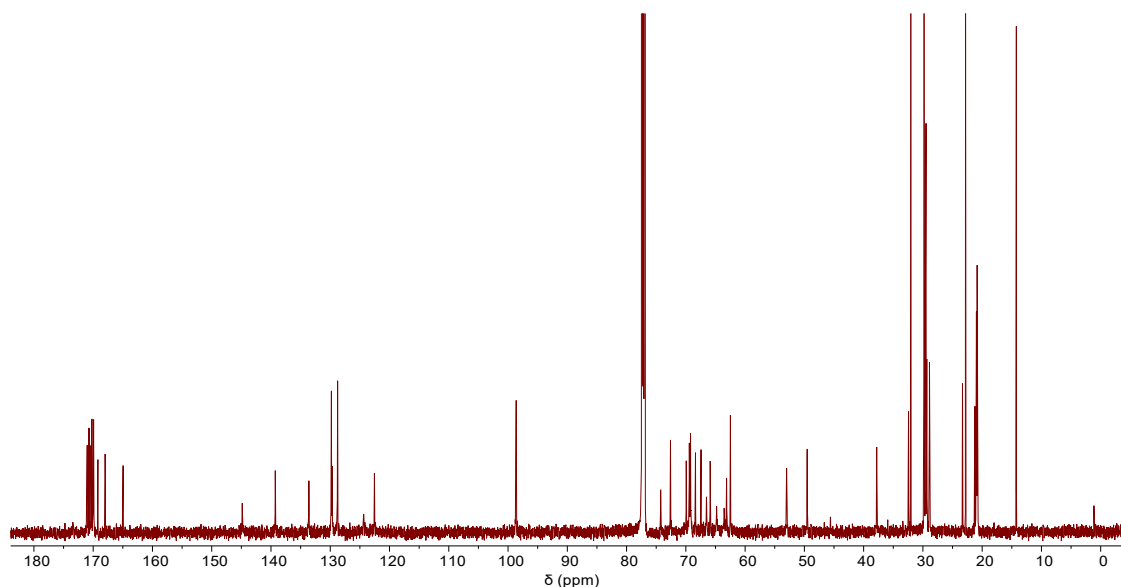


Figure VII-9. ¹³C NMR spectrum (150 MHz, CDCl₃, 300 K) of compound 27.

Display Report

Analysis Info

Analysis Name D:\Data\GOBS\FANG4-2-SMS-OAc-20211015.d
Method tune_high.m
Sample Name 4-2-SMS-OAc-20211015
Comment

Acquisition Date 10/15/2021 12:29:53 PM

Operator BDAL@DE
Instrument / Ser# micrOTOF 235

Acquisition Parameter

Source Type	ESI	Ion Polarity	Positive	Set Nebulizer	5.8 psi
Focus	Active			Set Dry Heater	180 °C
Scan Begin	50 m/z	Set Capillary	4500 V	Set Dry Gas	4.0 l/min
Scan End	3500 m/z	Set End Plate Offset	-500 V	Set Divert Valve	Waste

Meas. m/z	#	Formula	m/z	err [ppm]	mSigma	err [mDa]
1706.4162	1	C 245 H 348 N 16 Na 3 O 96	1706.4173	0.6	76.3	1.0

Meas. m/z	#	Formula	m/z	err [ppm]	mSigma	err [mDa]
-----------	---	---------	-----	-----------	--------	-----------

Meas. m/z	#	Formula	m/z	err [ppm]	mSigma	err [mDa]
-----------	---	---------	-----	-----------	--------	-----------

Meas. m/z	#	Formula	m/z	err [ppm]	mSigma	err [mDa]
-----------	---	---------	-----	-----------	--------	-----------

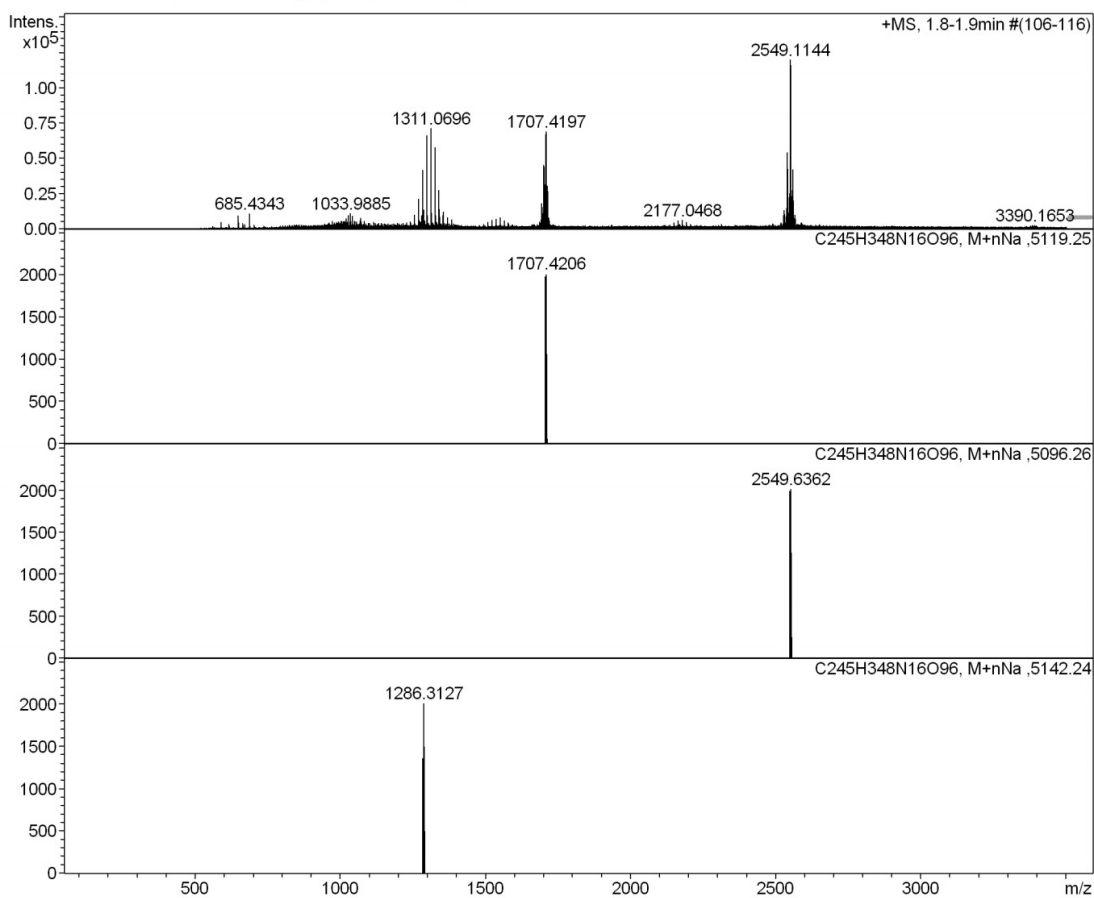
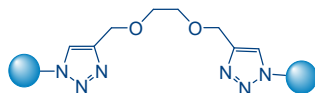


Figure VII-10. HRMS spectrum of compound 27.

1,2-Di-{1-[O-(5-acetamido-3,5-dideoxy-D-glycero- α -D-galacto-2-nonulopyranosylonate)-(2 \rightarrow 6)-O-(α -D-mannosyl)-(1 \rightarrow 1)-(2S,3R,4E)-2-amino-4-octadecene-1,3-diol]-1H-1,2,3-triazole-4-ylmethoxy} ethane (28).



The compound **25** (90 mg, 0.035 mmol) was dissolved in 14.28 mL of NaOMe/MeOH (0.04 M) and stirred overnight at room temperature. After addition of a few drops of water at 0 °C and the mixture was neutralized with Amberlite IR 120/H⁺ ion exchange resin stirring for 2 h at room temperature. After filtration and concentration, the residue was purified by silica gel chromatography (CHCl₃-MeOH-H₂O 5:4:0.3) and Sephadex LH-20 (MeOH-H₂O 1:1) to afford compound **28** (49 mg, 83%) as a white powder.

R_f = 0.36 (CHCl₃-MeOH-H₂O 5:4:0.3).

[α]_D²⁰ = 13.06 (c 0.5 in CHCl₃-MeOH-H₂O 5:4:1).

¹H NMR (600 MHz, CDCl₃-CD₃OD-D₂O 5:4:1): δ (ppm) = 7.64 (s, 2H, triazole), 5.26-5.18 (m, 2H, H-5''), 5.01-4.93 (m, 2H, H-4''), 4.38-4.33 (m, 8H, H-2'', H-1', CH₂ x 2-Skeleton), 4.13-4.08 (m, 2H, H-3''), 3.91-3.88 (m, 2H, H-1''), 3.78-3.74 (m, 2H, H-1''), 3.67-3.64 (m, 2H, H-6'), 3.54-3.51 (m, 4H, H-9, H-8), 3.41-3.26 (m, 20H, H-4, H-5, H-6, H-9, H-2', H-4', H-5', H-6', CH₂ x 2-Skeleton), 3.23 (m, 2H, H-7), 3.15 (m, 2H, H-3'), 2.47-2.43 (m, 2H, H-3eq), 1.71 (s, 6H, NHAc), 1.58-1.53 (m, 4H, H-6''), 1.42-1.36 (m, 2H, H-3ax), 1.01-0.88 (m, 44H, H-7''--17''), 0.56 (t, *J* = 7.4 Hz, 6H, CH₃).

¹³C NMR (150 MHz, CDCl₃-CD₃OD-D₂O 5:4:1): δ (ppm) = 174.21 (C=O, NHAc), 174.20 (C=O, COOH), 143.01 (C, triazole), 136.29 (C-5''), 128.13 (C-4''), 124.07 (CH, triazole), 101.63 (C-1'), 101.62 (C-2), 70.01 (CH₂, Skeleton), 72.58, 71.43, 71.24, 71.14, 70.46, 69.77, 68.94, 68.44, 67.53, 66.43, 65.32, 65.52, 63.56, 62.81, 62.53, 52.17, (C-4, C-5, C-6, C-7, C-8, C-9, C-2', C-3', C-4', C-5', C-6', C-1'', C-2'', C-3'') 67.61 (C-1''), 64.62 (CH₂, Skeleton), 41.17 (C-3), 32.77 (C-6''), 22.75 (NHAc), 32.58, 31.77, 31.52, 29.3, 29.25, 29.11, 28.95, 28.8, 28.64, 22.25, 21.74 (C-7''--17''), 13.48 (C-18'').

ESI-HRMS (*m/z*) calcd for C₇₈H₁₃₂N₈O₃₂ [M+Na-2H]⁻: 1715.8851, found: 1715.8781.

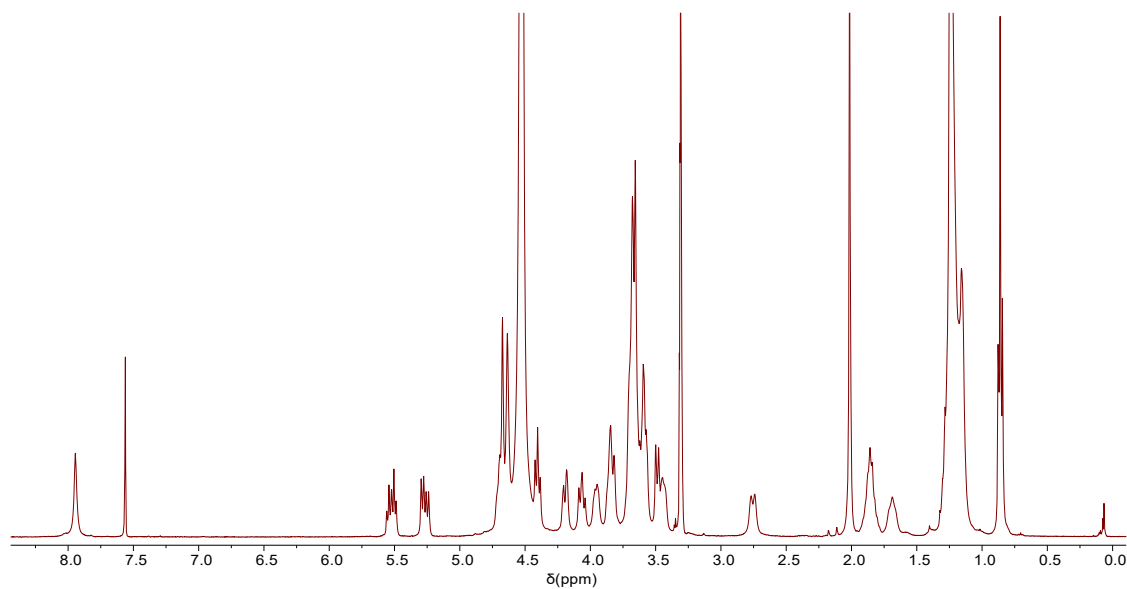


Figure VII-11. ¹H NMR spectrum (600 MHz, CDCl₃-CD₃OD-D₂O 5:4:1, 300 K) of compound **28**.

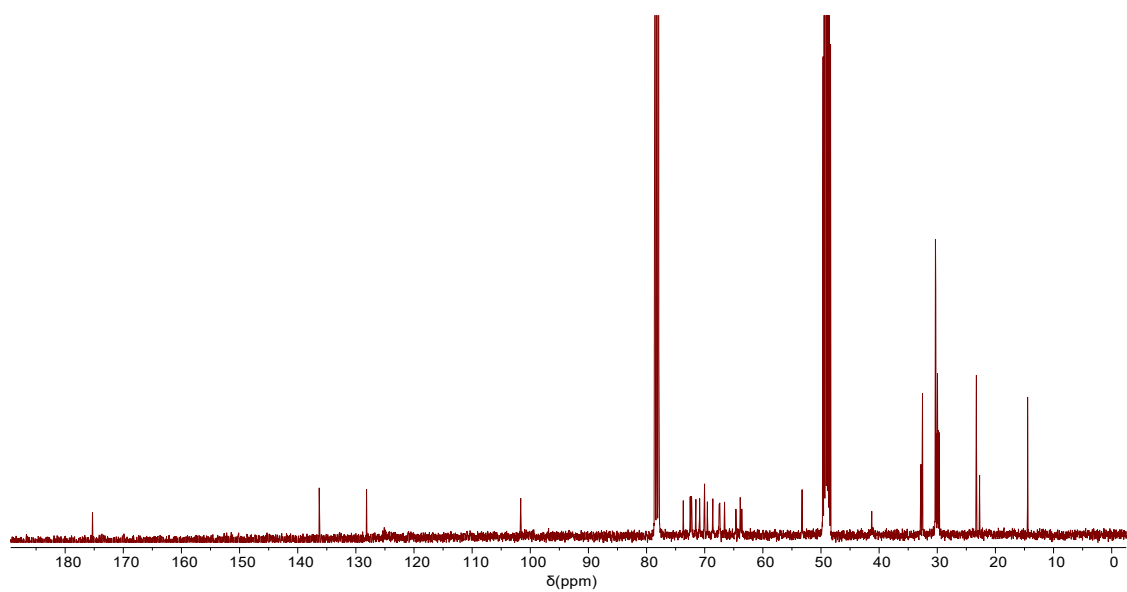


Figure VII-12. ¹³C NMR spectrum (150 MHz, CDCl₃-CD₃OD-D₂O 5:4:1, 300 K) of compound **28**.

Display Report

Analysis Info

Analysis Name D:\Data\GOBS\FANGV2-1-SMS-OH-20211115.d
Method tune_high_neg.m
Sample Name 2-1-SMS-OH-20211115
Comment

Acquisition Date 11/15/2021 6:28:45 PM

Operator BDAL@DE
Instrument / Ser# micrOTOF 235

Acquisition Parameter

Source Type	ESI	Ion Polarity	Negative	Set Nebulizer	5.8 psi
Focus	Active			Set Dry Heater	180 °C
Scan Begin	50 m/z	Set Capillary	4000 V	Set Dry Gas	4.0 l/min
Scan End	3000 m/z	Set End Plate Offset	-500 V	Set Divert Valve	Waste

Meas. m/z	#	Formula	m/z	err [ppm]	mSigma	err [mDa]
1715.8781	1	C 78 H 132 N 8 Na O 32	1715.8845	3.7	66.4	6.4

Meas. m/z	#	Formula	m/z	err [ppm]	mSigma	err [mDa]
-----------	---	---------	-----	-----------	--------	-----------

Meas. m/z	#	Formula	m/z	err [ppm]	mSigma	err [mDa]
-----------	---	---------	-----	-----------	--------	-----------

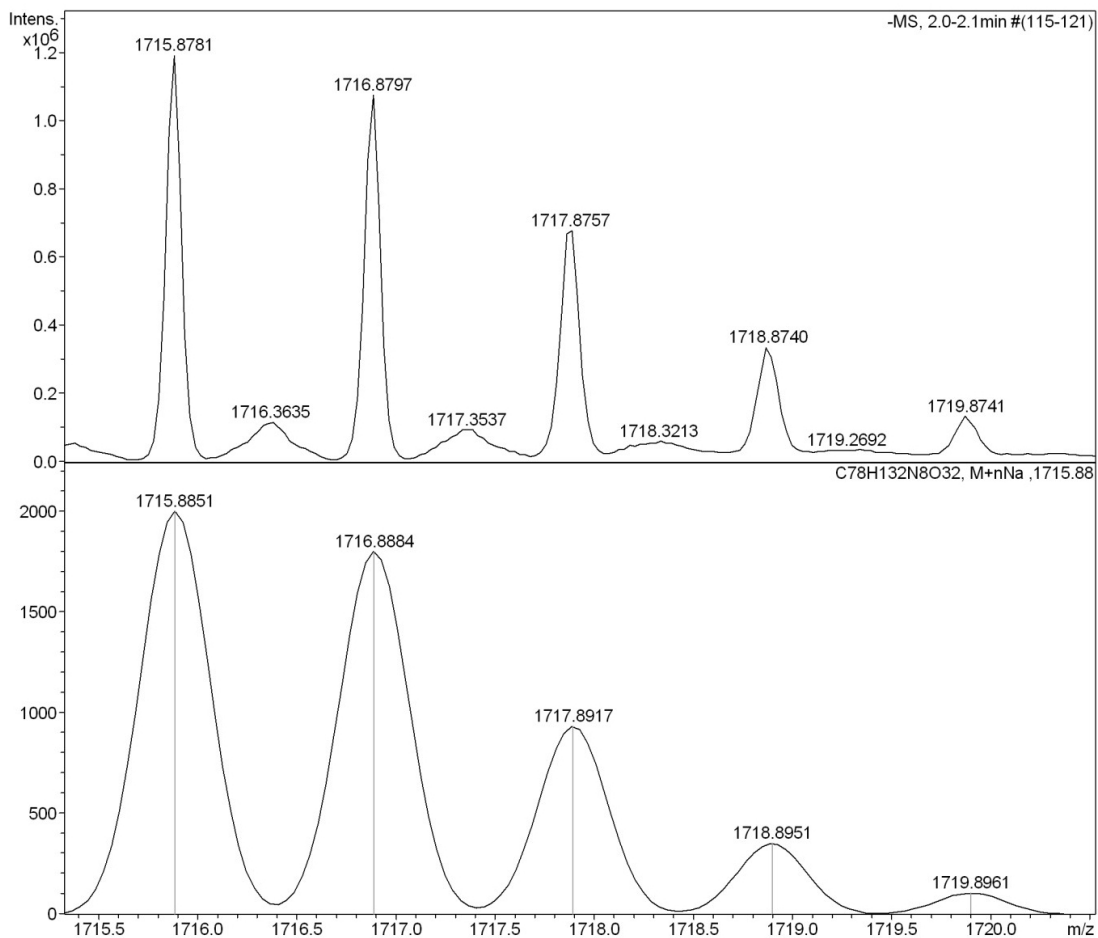
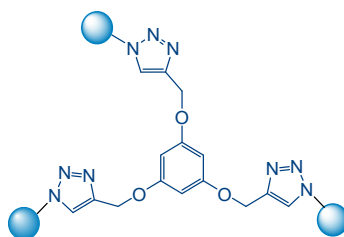


Figure VII-13. HRMS spectrum of compound 28.

1,3,5-Tri-{1-[O-(5-acetamido-3,5-dideoxy-D-glycero- α -D-galacto-2-nonulopyranosylonate)-(2 \rightarrow 6)-O-(α -D-mannosyl)-(1 \rightarrow 1)-(2S,3R,4E)-4-octadecene-1,3-diol]-1H-1,2,3-triazole-4-ylmethoxy} benzene (29).



The compound **26** (63 mg, 0.016 mmol) was dissolved in 9.92 mL of NaOMe/MeOH (0.04 M) and stirred overnight at room temperature. After addition of a few drops of water under 0 °C and the mixture was neutralized with Amberlite IR 120/H⁺ ion exchange resin after stirring for 2 h at room temperature. After filtration and concentration, the residue was purified by silica gel chromatography (CHCl₃-MeOH-H₂O 5:4:0.4) and Sephadex LH-20 (MeOH-H₂O 1:1) to afford compound **29** (36 mg, 85%).

R_f = 0.23 (CHCl₃-MeOH-H₂O 5:4:0.4).

[α]_D²⁰ = 10.72 (c 0.5 in CHCl₃-MeOH-H₂O 5:4:1).

¹H NMR (600 MHz, CDCl₃-CD₃OD-D₂O 5:4:1): δ (ppm) = 7.69 (s, 3H, triazole), 6.02 (s, 3H, Skeleton Ar-H), 5.25-5.20 (m, 3H, H-5''), 5.02-4.96 (m, 3H, H-4''), 4.86 (s, 6H, Skeleton 3 x CH₂), 4.40 (m, 6H, H-2'', H-1'), 4.17 (m, 3H, H-3''), 3.94-3.91 (m, 3H, H-1''), 3.80-3.75 (m, 3H, H-1''), 3.68-3.65 (m, 3H, H-6'), 3.57-3.53 (m, 6H, H-9, H-8), 3.43-3.31 (m, 24H, H-4, H-5, H-6, H-9, H-2', H-4', H-5', H-6'), 3.23 (m, 3H, H-7), 3.15 (m, 3H, H-3'), 2.48 (m, 3H, H-3eq), 1.74 (s, 9H, NHAc), 1.57 (m, 6H, H-6''), 1.39 (m, 3H, H-3ax), 1.01-0.88 (m, 66H, H-7''--17''), 0.59 (t, J = 7.4 Hz, 9H, CH₃).

¹³C NMR (150 MHz, CDCl₃-CD₃OD-D₂O 5:4:1): δ (ppm) = 175.31 (C=O, NHAc), 175.30 (C=O, COOH), 160.56 (C, Skeleton aromatic), 143.01 (C, triazole), 135.41 (C-5''), 127.08 (C-4''), 124.41 (CH, triazole), 100.51 (C-1'), 100.51 (C-2), 95.17 (CH, Skeleton aromatic), 72.57, 71.37, 71.24, 71.23, 70.46, 69.77, 68.41, 67.60, 67.60, 66.45, 65.52, 62.72, 63.72, 62.55, 52.17, (C-4, C-5, C-6, C-7, C-8, C-9, C-2', C-3', C-4', C-5', C-6', C-1'', C-2'', C-3'') 67.49 (C-1''), 62.19 (CH₂, Skeleton aromatic), 41.17 (C-3), 32.77 (C-6''), 22.75 (NHAc), 32.58, 31.77, 31.52, 29.3, 29.25, 29.11, 28.95, 28.8, 28.64, 22.25, 21.74 (C-7''--17''), 13.48 (C-18'').

ESI-HRMS (*m/z*) calcd for C₁₂₀H₁₉₆N₁₂O₄₈ [M+K-2H]⁺: 2613.2940, found: 2613.2871.

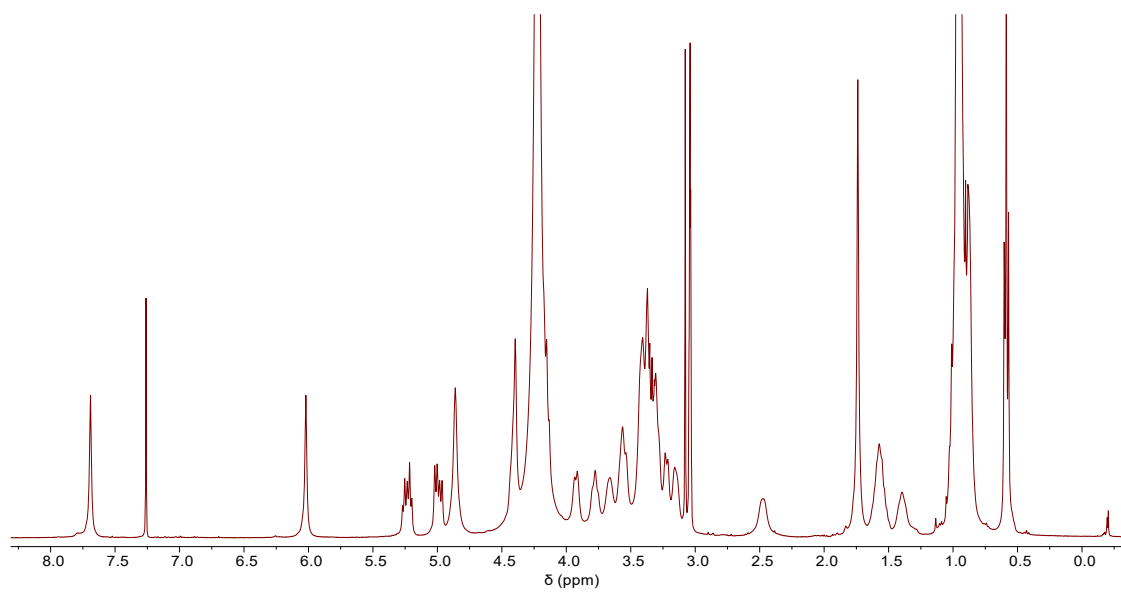


Figure VII-14. ¹H NMR spectrum (600 MHz, CDCl₃-CD₃OD-D₂O 5:4:1, 300 K) of compound **29**.

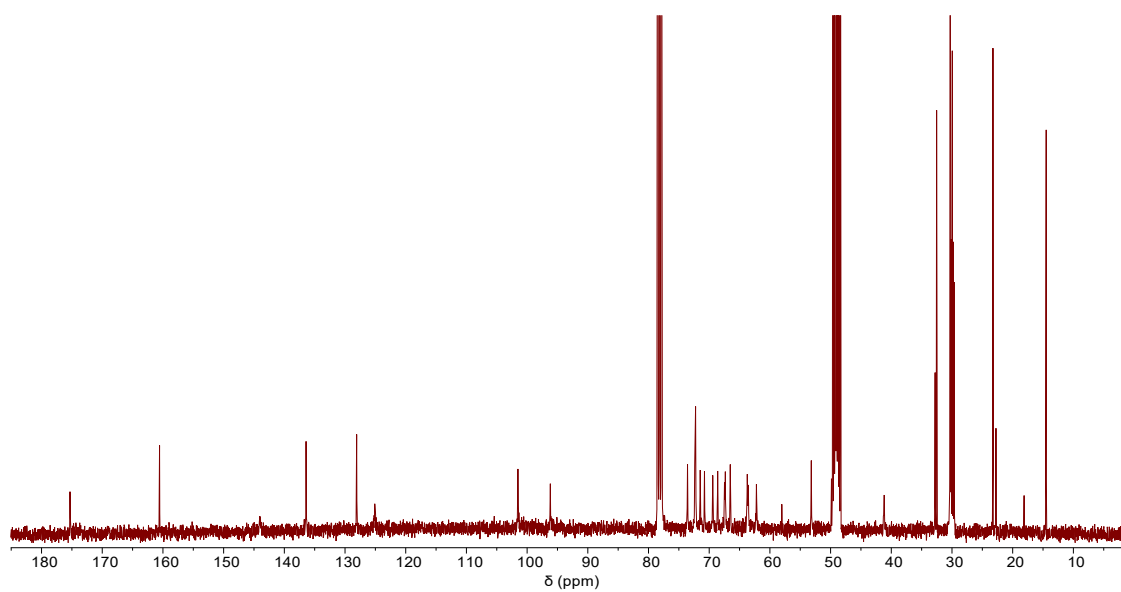


Figure VII-15. ¹³C NMR spectrum (150 MHz, CDCl₃-CD₃OD-D₂O 5:4:1, 300 K) of compound **29**.

Display Report

Analysis Info

Analysis Name D:\Data\GOBS\FANG\3-SMS-OH-20211115.d
Method tune_high_neg.m
Sample Name 3-SMS-OH-20211115
Comment

Acquisition Date 11/15/2021 7:07:24 PM

Operator BDAL@DE
Instrument / Ser# micrOTOF 235

Acquisition Parameter

Source Type	ESI	Ion Polarity	Negative	Set Nebulizer	5.8 psi
Focus	Active			Set Dry Heater	180 °C
Scan Begin	50 m/z	Set Capillary	4000 V	Set Dry Gas	4.0 l/min
Scan End	3000 m/z	Set End Plate Offset	-500 V	Set Divert Valve	Waste

Meas. m/z	#	Formula	m/z	err [ppm]	mSigma	err [mDa]
2612.2815	1	C 120 H 196 K N 12 O 48	2612.2908	3.5	130.9	9.2

Meas. m/z	#	Formula	m/z	err [ppm]	mSigma	err [mDa]
-----------	---	---------	-----	-----------	--------	-----------

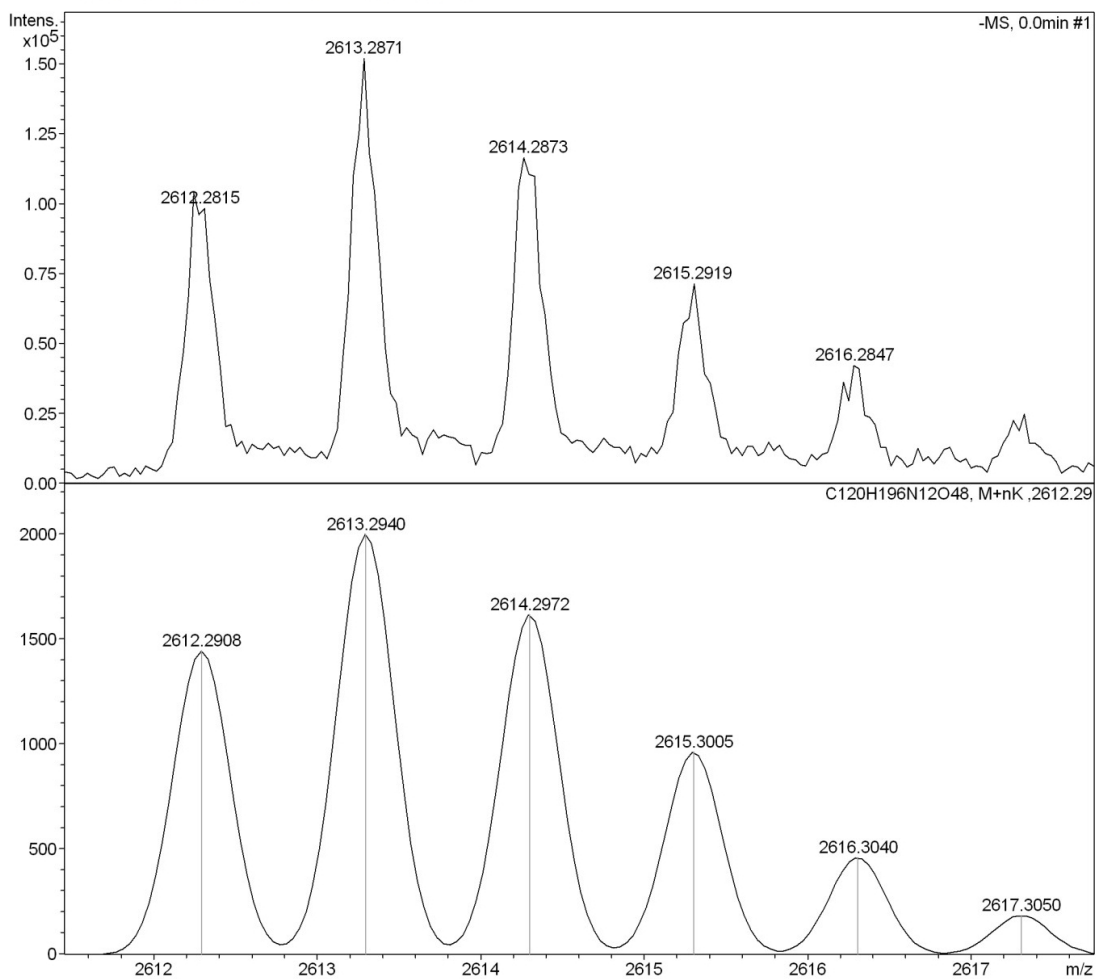
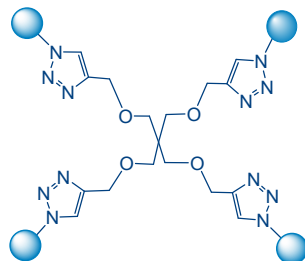


Figure VII-16. HRMS spectrum of compound 29.

Tetrakis- {1-[O-(5-acetamido-3,5-dideoxy-D-glycero- α -D-galacto-2-nonulopyranosylonate)-(2 \rightarrow 6)-O-(α -D-mannosyl)-(1 \rightarrow 1)-(2S,3R,4E)-2-amino-4-octadecene-1,3-diol]-1H-1,2,3-triazole-4-ylmethoxy} pentaerythritol (30).



The compound **27** (58 mg, 0.011 mmol) was dissolved in 9.18 mL of NaOMe/MeOH (0.04 M) and stirred overnight at room temperature. After addition of a few drops of water under 0 °C and the mixture was neutralized with Amberlite IR 120/H⁺ ion exchange resin after stirring for 2 h at room temperature. After filtration and concentration, the residue was purified by silica gel chromatography (CHCl₃-MeOH-H₂O 5:4:0.5) and Sephadex LH-20 (MeOH-H₂O 1:1) to afford compound **30** (33 mg, 84%).

$R_f = 0.27$ (CHCl₃-MeOH-H₂O 5:4:0.7).

$[\alpha]_D^{20} = 9.26$ (*c* 0.5 in CHCl₃-MeOH-H₂O 5:4:1).

¹H NMR (600 MHz, CDCl₃-CD₃OD-D₂O 5:4:1): δ (ppm) = 7.67 (s, 4H, triazole), 5.26-5.18 (m, 4H, H-5''), 5.02-4.95 (m, 4H, H-4''), 4.43-4.39 (m, 8H, H-2'', H-1'), 4.27-4.23 (m, 8H, CH₂ x 2- Skeleton), 4.18-4.13 (m, 4H, H-3''), 3.96-3.91 (m, 4H, H-1''), 3.79-3.74 (m, 4H, H-1''), 3.69-3.64 (m, 4H, H-6'), 3.54-3.52 (m, 8H, H-9, H-8), 3.40-3.18 (m, 48H, H-4, H-5, H-6, H-7, H-9, H-2', H-3', H-4', H-5', H-6', CH₂ x 2- Skeleton), 2.48-2.44 (m, 4H, H-3eq), 1.71 (s, 12H, NHAc), 1.57-1.53 (m, 8H, H-6''), 1.42-1.36 (m, 4H, H-3ax), 1.01-0.88 (m, 88H, H-7''--17''), 0.56 (t, *J* = 7.4 Hz, 12H, CH₃).

¹³C NMR (150 MHz, CDCl₃-CD₃OD-D₂O 5:4:1): δ (ppm) = 174.38 (C=O, NHAc), 174.20 (C=O, COOH), 144.08 (C, triazole), 135.11 (C-5''), 127.11 (C-4''), 123.68 (CH, triazole), 100.49 (C-1'), 100.48 (C-2), 69.60 (CH₂, Skeleton), 72.58, 71.43, 71.24, 71.14, 70.46, 69.77, 68.94, 68.44, 67.53, 66.43, 65.32, 65.52, 63.56, 62.81, 62.53, 52.17 (C-4, C-5, C-6, C-7, C-8, C-9, C-2', C-3', C-4', C-5', C-6', C-1'', C-2'', C-3'') 67.61 (C-1''), 65.24 (CH₂, Skeleton), 41.34 (C-3), 32.96 (C-6''), 22.75 (NHAc), 32.58, 31.77, 31.52, 29.3, 29.25, 29.11, 28.95, 28.8, 28.64, 22.25, 21.74 (C-7''--17''), 14.59 (C-18'').

ESI-HRMS (*m/z*) calcd for C₁₅₇H₂₆₈N₁₆O₆₄ [M+NH₄-H]²⁺:1719.4469, found:1719.4094.

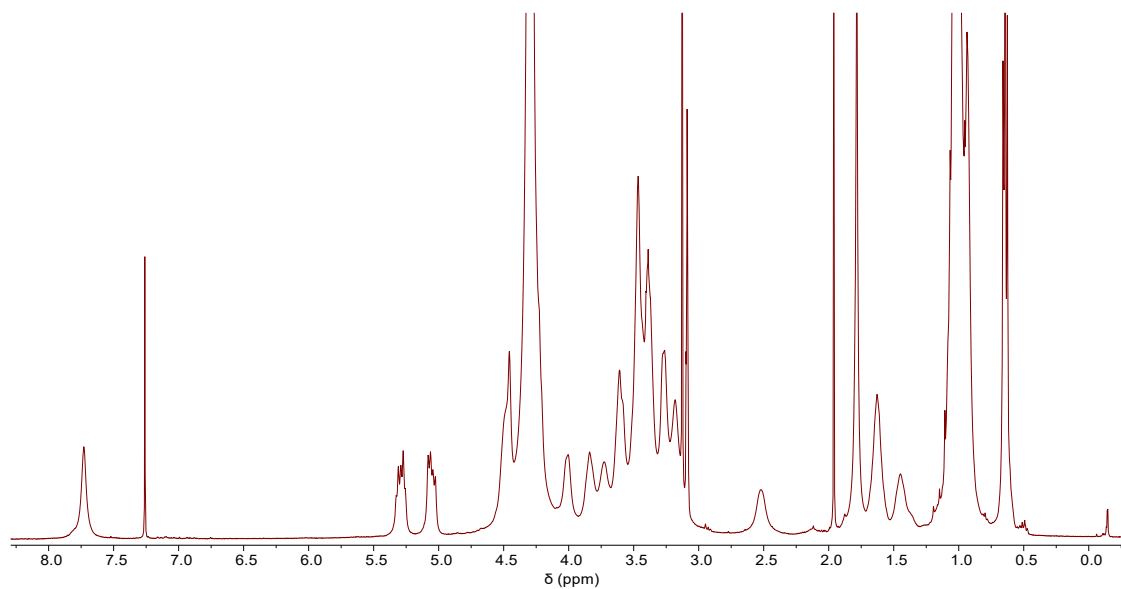


Figure VII-17. ¹H NMR spectrum (600 MHz, CDCl₃-CD₃OD-D₂O 5:4:1, 300 K) of compound **30**.

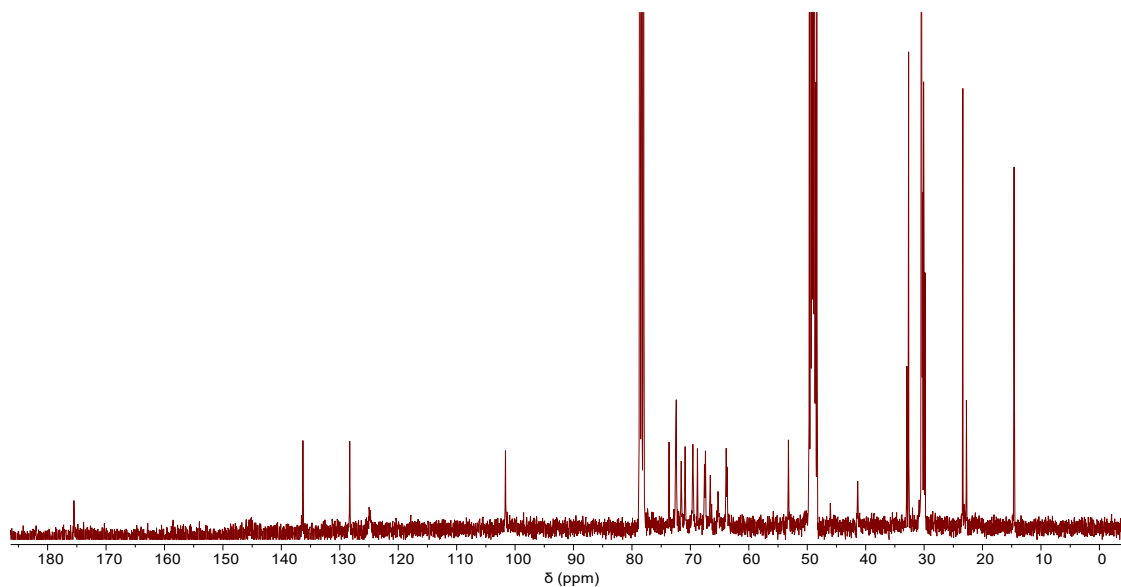


Figure VII-18. ¹³C NMR spectrum (150 MHz, CDCl₃-CD₃OD-D₂O 5:4:1, 300 K) of compound **30**.

Display Report

Analysis Info

Analysis Name D:\Data\GOBS\FANG\4-SMS-OH-20211115.d
Method tune_high_neg.m
Sample Name 4-SMS-OH-20211115
Comment

Acquisition Date 11/15/2021 8:00:51 PM

Operator BDAL@DE
Instrument / Ser# micrOTOF 235

Acquisition Parameter

Source Type	ESI	Ion Polarity	Negative	Set Nebulizer	5.8 psi
Focus	Active			Set Dry Heater	180 °C
Scan Begin	50 m/z	Set Capillary	4000 V	Set Dry Gas	4.0 l/min
Scan End	4000 m/z	Set End Plate Offset	-500 V	Set Divert Valve	Waste

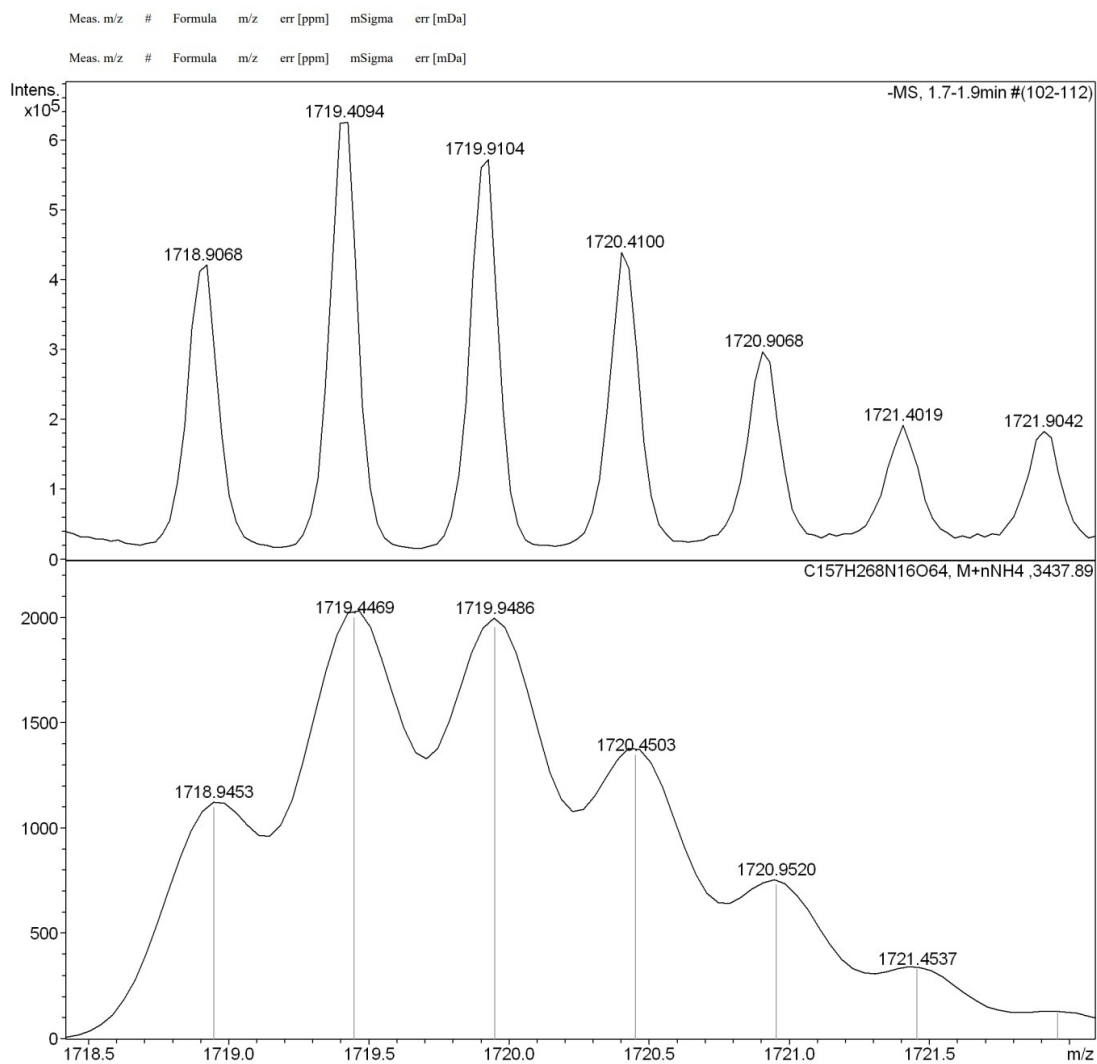
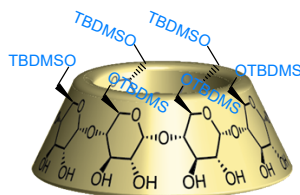


Figure VII-19. HRMS spectrum of compound 30.

7.9. Synthesis of macromolecular multivalent skeletons

Hexakis(6-O-tert-butylidimethylsilyl)cyclomaltohexaose (**31**)



α -Cyclodextrin (3 g, 3.08 mmol) was dissolved in dry pyridine (30 mL) and cooled to 0 °C in an ice bath, and then a solution of TBDMSCl (4.65 g, 30.8 mmol) in dry pyridine (50 mL) was added dropwise. After 3 h in the ice bath, the mixture was stirred at room temperature for 18 h. Afterwards, the solvent was removed under reduced pressure and the residue was extracted with dichloromethane, washed with 3% hydrochloric acid and brine, dried over MgSO₄, and concentrated under reduced pressure. The residue was separated on a silica gel column and eluted with chloroform-methanol 8:1 to obtain compound **31** (3.6 g, 71%) as a white powder [222].

R_f = 0.31 (CHCl₃-MeOH 6:1).

¹H NMR (400 MHz, CDCl₃): δ (ppm) = 4.86 (s, 6H, H-1), 4.00 (t, J = 9.0 Hz, 6H, H-4), 3.86 (dd, J = 28.6, 10.3 Hz, 12H, H-6), 3.76 – 3.56 (m, 18H, H-5, H-3, H-2), 0.87 (s, 54H, SiC(CH₃)₃), 0.03 (s, 36H, Si(CH₃)₃).

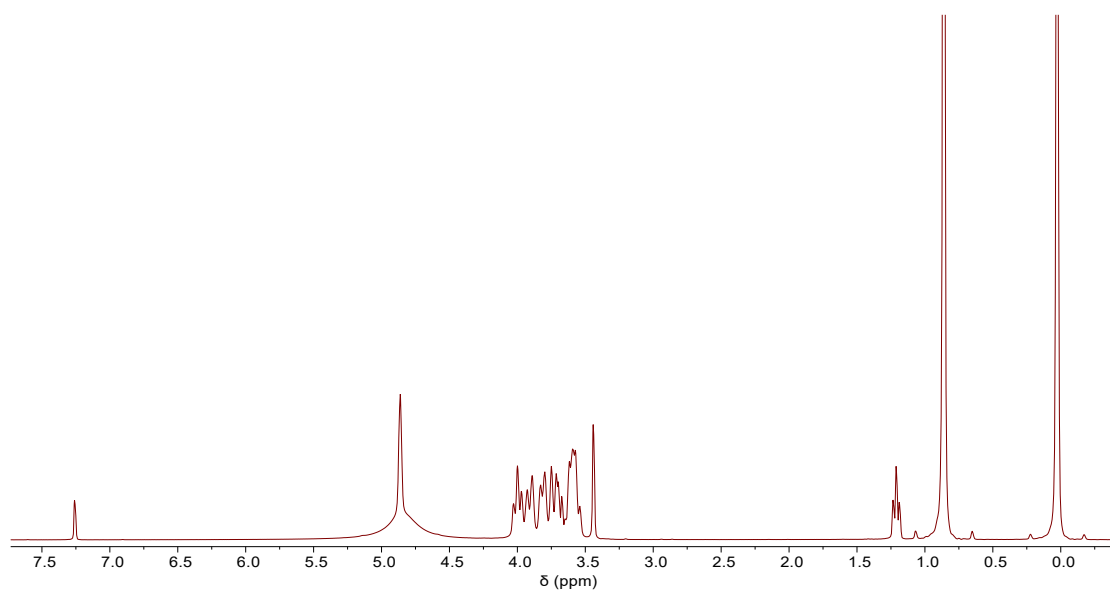
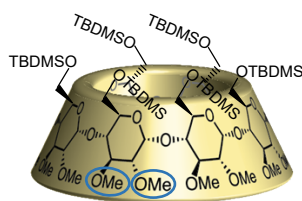


Figure VII-20. ¹H NMR spectrum (400 MHz, CDCl₃, 300 K) of compound **31**.

**Hexakis(6-O-tert-butyl dimethylsilyl-2,3-di-O-methyl)cyclomaltohexaose
(32)**



Sodium hydride (2.6 g, 60% mineral oil) was added to a solution of **31** (3 g, 1.81 mmol) in DMF (86 mL) at 0 °C and the mixture was stirred for 1 h at 0 °C. Iodomethane (4.73 mL) was added dropwise and the mixture was stirred at 0 °C for 1 h, then warmed to room temperature and stirred overnight. After that, the mixture was cooled to 0 °C again and MeOH was added dropwise to quench the remaining sodium hydride and methyl iodide. The solvent was removed under reduced pressure and the residue was taken up in dichloromethane. The organic layer was washed with brine, dried with MgSO₄, and concentrated. The residue was chromatographed (Cy-EtOAc 4:1) to give compound **32** (2.41 g, 73%) as a white powder [222].

$R_f = 0.26$ (Cy-EtOAc 2:1).

¹H NMR (400 MHz, CDCl₃): δ (ppm) = 5.02 (d, $J = 3.3$ Hz, 6H, H-1), 4.06 (dd, $J = 11.3, 2.7$ Hz, 6H, H-6a), 3.68 (d, $J = 9.0$ Hz, 6H, H-4), 3.64 – 3.54 (m, 36H, OCH₃, H-6b, H-5, H-3), 3.48 (s, 18H, OCH₃), 3.03 (dd, $J = 9.8, 3.2$ Hz, 6H, H-2), 0.85 (s, 54H, SiCC(CH₃)₃), 0.01 (d, $J = 3.7$ Hz, 36H, SiC(CH₃)₃).

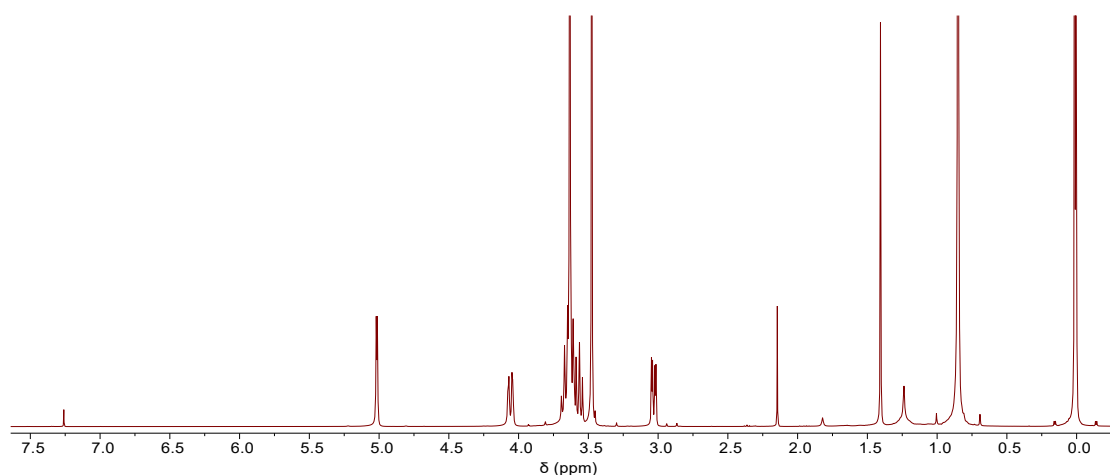
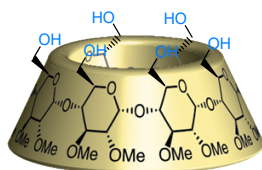


Figure VII-21. ¹H NMR (400 MHz, CDCl₃, 300 K) of compound **32**.

Hexakis(2,3-di-O-methyl)cyclomaltohexaose (**33**)



TBAF (1.1 M solution in THF, 7 mL, 7.63 mmol) was added dropwise to a solution of **32** (2 g, 1.09 mmol) in THF (22 mL). The mixture was heated to reflux for 2 h and then concentrated under reduced pressure. The residue was extracted by dichloromethane, washed with brine, dried over MgSO_4 , and concentrated under reduced pressure. The residue was separated by silica gel column, eluted with chloroform-methanol 4:1 to obtain compound **33** (950 mg, 76%) as a white foam [222].

$R_f = 0.27$ (CHCl_3 -MeOH 4:1).

$^1\text{H NMR}$ (400 MHz, CDCl_3): δ (ppm) = 4.99 (d, $J = 3.6$ Hz, 6H, H-1), 4.77 (s, 6H, OH), 3.97 (d, $J = 10.0$ Hz, 6H, H-6a), 3.72 (d, $J = 8.4$ Hz, 12H, H-5, H-6b), 3.58 (s, 18H, OCH_3), 3.48 (d, $J = 9.1$ Hz, 6H, H-3), 3.44 (s, 18H, OCH_3), 3.37 (t, $J = 8.9$ Hz, 6H, H-4), 3.09 (dd, $J = 9.9, 3.3$ Hz, 6H, H-2).

$^{13}\text{C NMR}$ (100 MHz, CDCl_3): δ (ppm) = 99.12 (C-1), 82.08 (C-4), 81.90 (C-2), 81.78 (C-3), 72.86 (C-5), 61.9 (C-6), 61.70 (OCH_3), 58.07 (OCH_3).

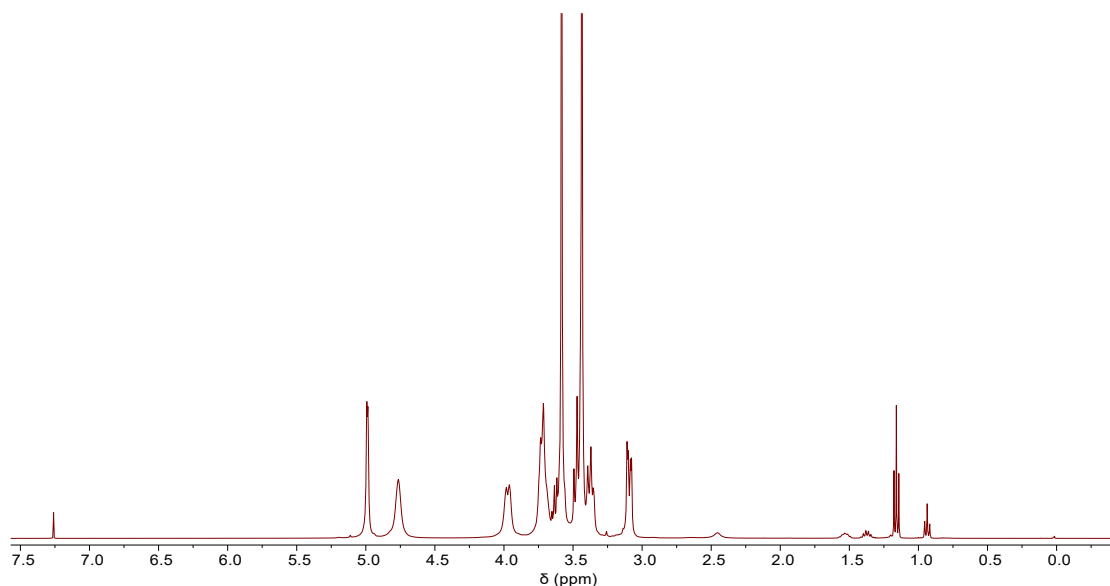


Figure VII-22. $^1\text{H NMR}$ spectrum (400 MHz, CDCl_3 , 300 K) of compound **33**.

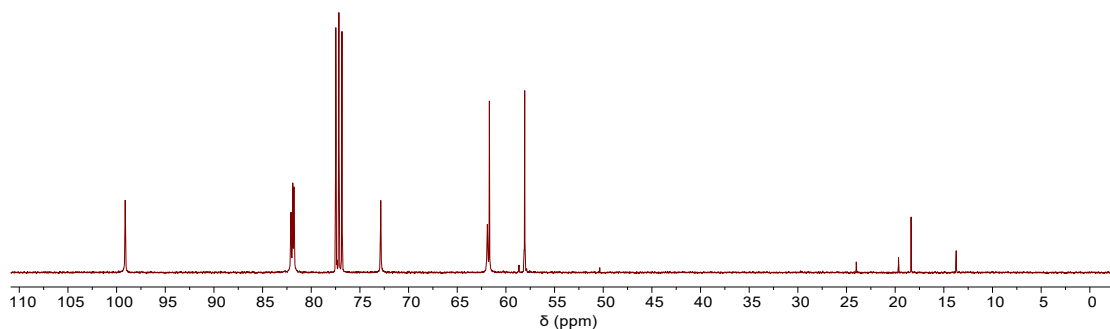
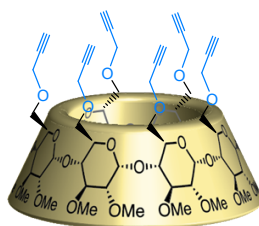


Figure VII-23. ^{13}C NMR spectrum (100 MHz, CDCl_3 , 300 K) of compound **33**.

Hexakis(2,3-di-O-methyl-6-O-propargyl)cyclomaltohexaose (**34**)



A suspension of NaH (60% dispersion in mineral oil, 4 equiv. per OH group) (0.47 g, 11.79 mmol) in anhydrous THF (11 mL) was added dropwise to a cooled (0 °C) solution of compound **33** (547 mg, 0.49 mmol) in anhydrous THF (16 mL). The suspension was then stirred at 0 °C for 1 hour. After that, a solution of propyne bromide (80% in toluene, 5 equiv. per OH group) (1.75 g, 14.74 mmol) in THF (1.67 mL) was added dropwise at 0 °C. The resulting mixture was first stirred at 0 °C for 2 h and then at r.t. for 48 h. The reaction was quenched by adding methanol (16 mL). The solvent was removed by evaporation under reduced pressure. The residue was extracted with ethyl acetate. The organic layer was washed with brine, dried over MgSO_4 and evaporated. The residue was purified by silica gel chromatography (DCM-MeOH 50:1) to give compound **34** (479 mg, 72%) as a white foam.

$R_f = 0.23$ (DCM-MeOH 50:1).

^1H NMR (400 MHz, CDCl_3): δ (ppm) = 5.03 (d, $J = 3.0$ Hz, 7H, H-1)), 4.35 – 4.28 (m, 7H, CH_2), 4.24 – 4.17 (m, 7H, CH_2), 4.03 (d, $J = 9.7$ Hz, 7H, H-6a), 3.83 (t, $J = 9.1$ Hz, 14H, H-5), 3.62 (s, 21H, OCH_3), 3.57 (t, $J = 8.9$ Hz, 7H, H-4), 3.53 – 3.49 (m, 7H, H-3), 3.47 (d, $J = 1.8$ Hz, 21H, OCH_3), 3.16 (dd, $J = 9.8, 3.2$ Hz, 7H, H-2), 2.47 (t, $J = 2.3$

Hz, 7H, C≡CH).

^{13}C NMR (100 MHz, CDCl_3): δ (ppm) = 100.38 (C-1), 82.75 (C-4), 82.20 (C-2), 81.31 (C-3), 79.98 (C≡CH), 75.05 (C≡CH), 71.06 (C-5), 68.88 (C-6), 61.96 (OCH₃), 58.67 (CH₂), 57.92 (OCH₃).

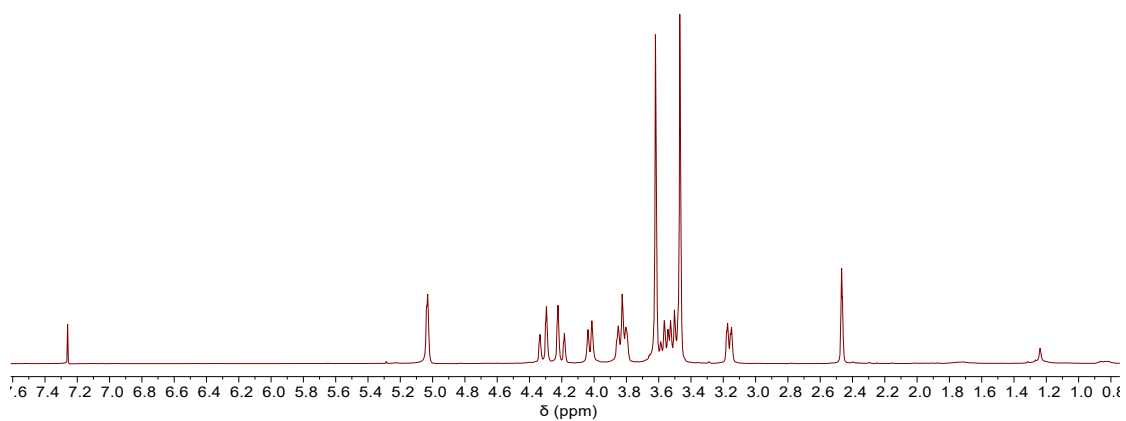


Figure VII-24. ^1H NMR spectrum (400 MHz, CDCl_3 , 300 K) of compound 34.

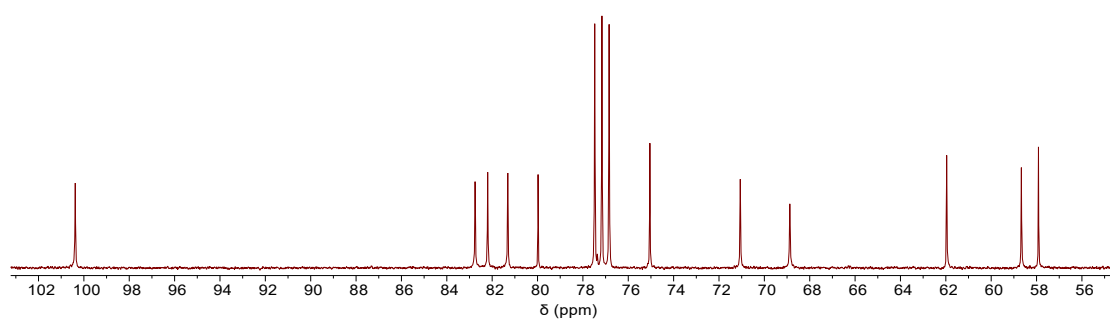
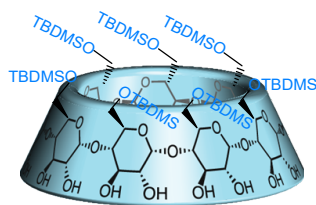


Figure VII-25. ^{13}C NMR spectrum (100 MHz, CDCl_3 , 300 K) of compound 34.

Heptakis(6-O-tert-butylidimethylsilyl)cyclomaltoheptaose (35)



β -Cyclodextrin (3 g, 2.64 mmol) was dissolved in dry pyridine (30 mL) and cooled to 0 °C in an ice bath, and then a solution of TBDMSCl (4.65 g, 30.82 mmol) in dry pyridine (50 mL) was added dropwise. After 3 h in the ice bath, the mixture was stirred at room temperature for 18 h. Afterwards, the solvent was removed under reduced pressure and the residue was extracted with dichloromethane, washed with 3% hydrochloric acid and brine, dried over MgSO_4 , and concentrated under reduced pressure. The residue was separated on a silica gel column and eluted with chloroform-methanol 8:1 to obtain compound **35** (3.94 g, 70%) as a white powder [248].

$R_f = 0.28$ (CHCl_3 -MeOH 6:1).

$^1\text{H NMR}$ (400 MHz, CDCl_3): δ (ppm) = 4.89 (s, 7H, H-1), 4.04 (t, $J = 9.1$ Hz, 7H, H-4), 3.90 (dd, $J = 11.4, 3.1$ Hz, 7H, Ha-6), 3.71 (d, $J = 10.7$ Hz, 7H, Hb-6), 3.67 – 3.60 (m, 14H, H-5, H-3), 3.56 (t, $J = 9.2$ Hz, 7H, H-2), 0.87 (s, 63H, $\text{SiC}(\text{CH}_3)_3$), 0.04 (s, 21H, $\text{Si}(\text{CH}_3)$), 0.03 (s, 21H, $\text{Si}(\text{CH}_3)$).

$^{13}\text{C NMR}$ (100 MHz, CDCl_3): δ (ppm) = 102.16 (C-1), 81.91 (C-2), 73.76 (C-3), 73.55 (C-4), 72.70 (C-5), 61.78 (C-6), 26.05 ($\text{SiC}(\text{CH}_3)_3$), 18.42 ($\text{SiC}(\text{CH}_3)_3$), -4.92 ($\text{Si}(\text{CH}_3)$), -5.04 ($\text{Si}(\text{CH}_3)$).

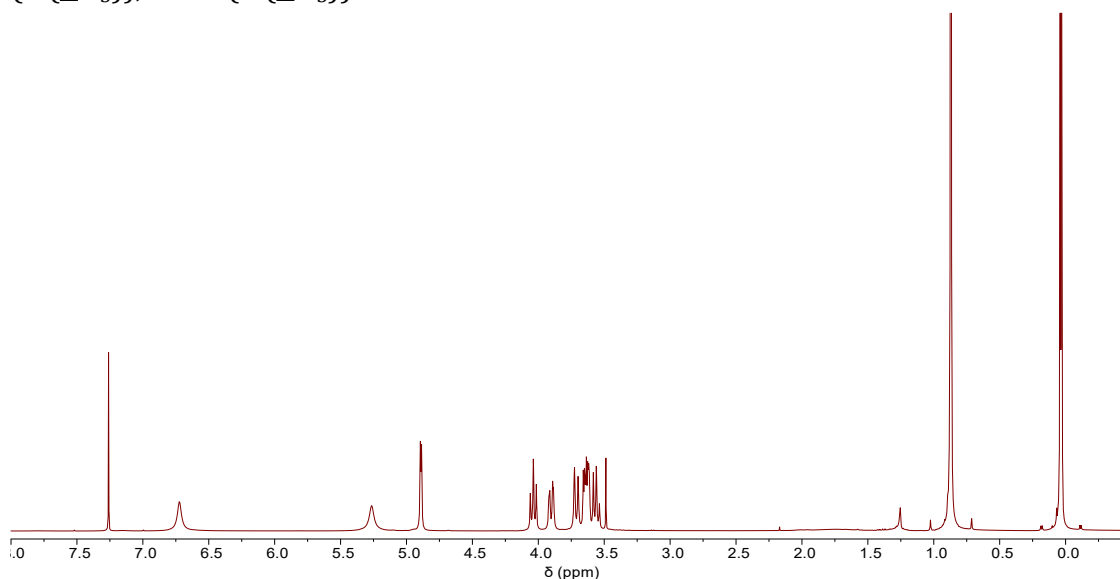


Figure VII-26. $^1\text{H NMR}$ spectrum (400 MHz, CDCl_3 , 300 K) of compound **35**.

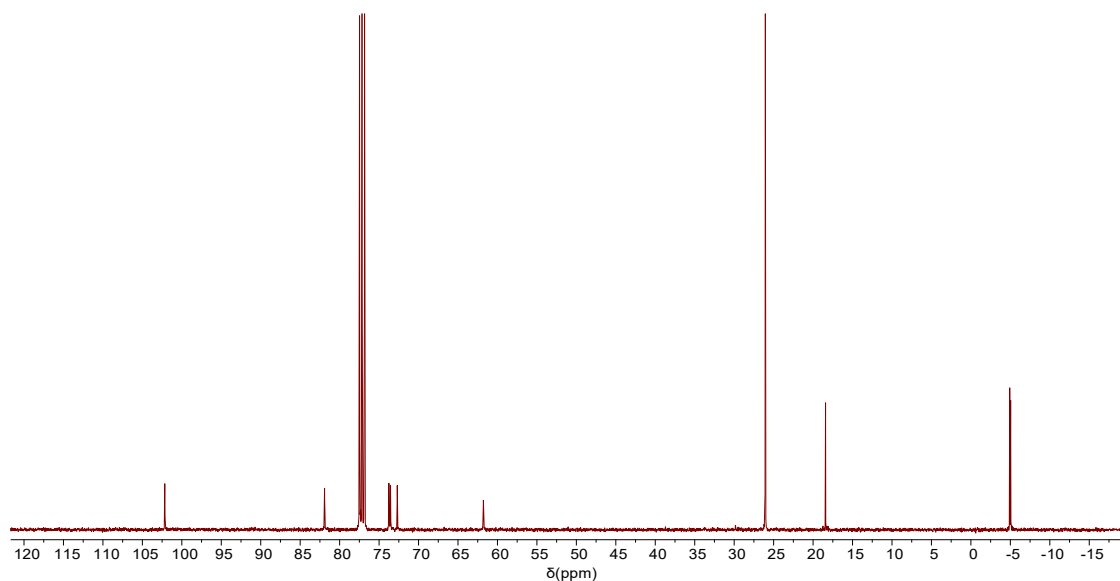
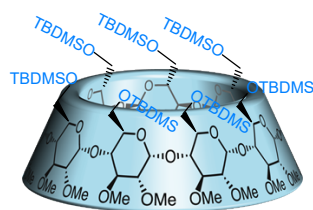


Figure VII-27. ^{13}C NMR spectrum (100 MHz, CDCl_3 , 300 K) of compound **35**.

Heptakis(6-O-tert-butyldimethylsilyl-2,3-di-O-methyl)cyclomaltoheptaose (**36**)



Sodium hydride (2.6 g, 60% mineral oil) was added to a solution of **35** (3 g, 1.55 mmol) in DMF (50 mL) at 0 °C and the mixture was stirred for 1 h at 0 °C. Iodomethane (4.73 mL) was added dropwise and the mixture was stirred at 0 °C for 1 h, then warmed to room temperature and stirred overnight. After that, the mixture was cooled to 0 °C again and MeOH was added dropwise to quench the remaining sodium hydride and methyl iodide. The solvent was removed under reduced pressure and the residue was taken up in dichloromethane. The organic layer was washed with brine, dried with MgSO_4 , and concentrated. The residue was chromatographed (Cy-EtOAc 4:1) to give compound **36** (2.37 g, 72%) as a white powder [248].

R_f = 0.25 (Cy-EtOAc 2:1).

^1H NMR (400 MHz, CDCl_3): δ (ppm) = 5.15 (d, J = 3.5 Hz, 7H, H-1), 4.08 (dd, J = 11.7, 2.7 Hz, 7H, H-6), 3.69 (t, J = 9.2 Hz, 7H, H-4), 3.63 (s, 21H, OCH_3), 3.61 – 3.48 (m, 21H, H-6, H-5, H-3), 3.47 (s, 21H, OCH_3), 3.02 (dd, J = 9.8, 3.5 Hz, 7H, H-2), 0.84 (s, 63H, $\text{SiCC}(\text{CH}_3)_3$), -0.02 (s, 42H, $\text{Si}(\text{CH}_3)_3$).

^{13}C NMR (100 MHz, CDCl_3): δ (ppm) = 98.26 (C-1), 82.36 (C-2), 82.13 (C-3), 78.83

(C-4), 72.28 (C-5), 62.42 (C-6), 61.55 (OCH₃), 58.68 (OCH₃), 25.99 (SiC(CH₃)₃), 18.37 (SiC(CH₃)₃), -4.78 (Si(CH₃)), -5.13 (Si(CH₃)).

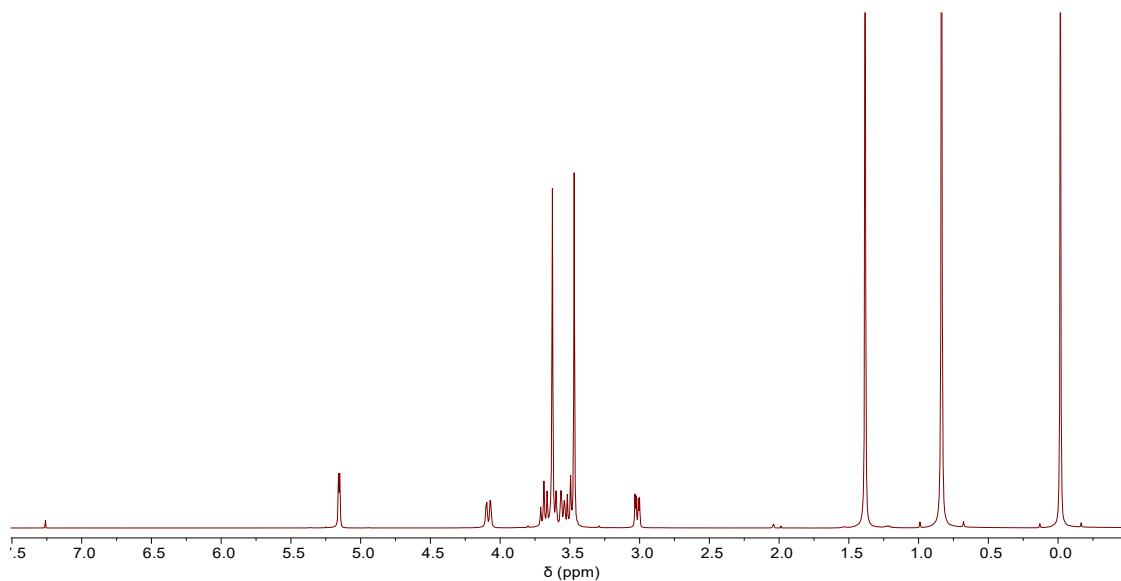


Figure VII-28. ¹H NMR spectrum (400 MHz, CDCl₃, 300 K) of compound **36**.

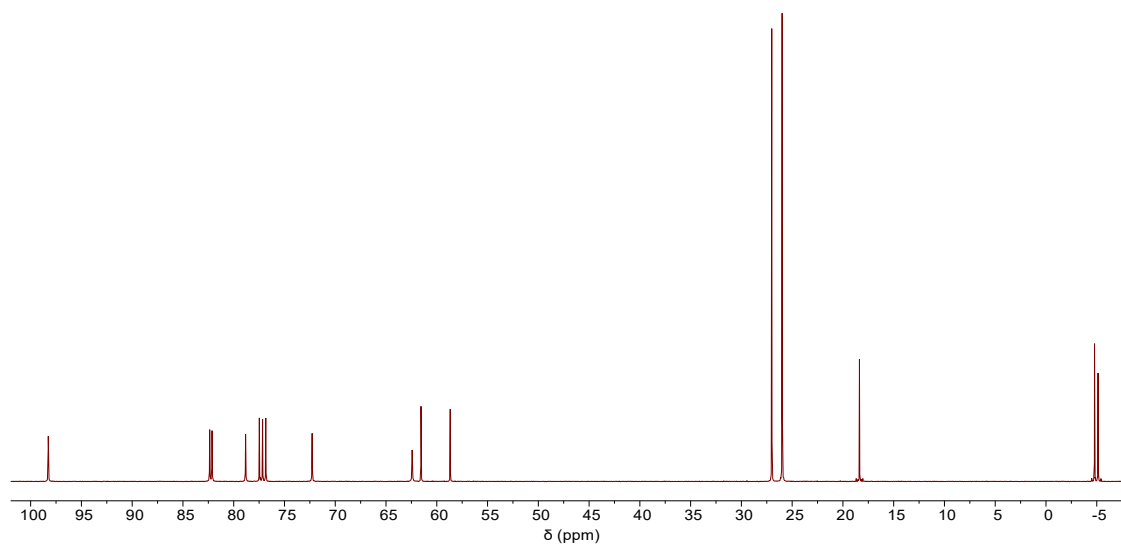
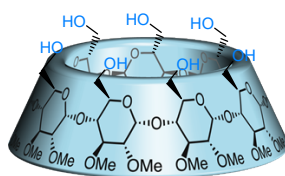


Figure VII-29. ¹³C NMR spectrum (100 MHz, CDCl₃, 300 K) of compound **36**.

Heptakis(2,3-di-O-methyl)cyclomaltoheptaose (**37**)

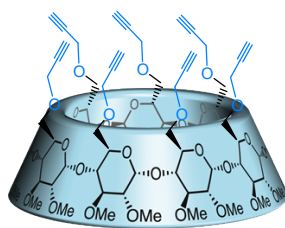


TBAF (1.1 M solution in THF, 7 mL, 7.7 mmol) was added dropwise to a

solution of **36** (2 g, 0.938 mmol) in THF (20 mL). The mixture was heated to reflux for 2 h and then concentrated under reduced pressure. The residue was extracted by dichloromethane, washed with brine, dried over MgSO_4 , and concentrated under reduced pressure. The residue was separated by silica gel column, eluted with chloroform-methanol 4:1, to obtain compound **37** (938 mg, 75%) as a white foam [248].

$R_f = 0.21$ (CHCl_3 -MeOH 4:1).

Heptakis(2,3-di-O-methyl-6-O-propargyl)cyclomaltoheptaose (**38**)



A suspension of NaH (60% dispersion in mineral oil, 4 equiv. per OH group) (0.44 g, 11.02 mmol) in anhydrous THF (10 mL) was added dropwise to a cooled (0 °C) solution of compound **37** (524 mg, 0.393 mmol) in anhydrous THF (15 mL). The suspension was then stirred at 0 °C for 1 hour. After that, a solution of propyne bromide (80% in toluene, 5 equiv. per OH group) (1.64 g, 13.78 mmol) in THF (1.56 mL) was added dropwise at 0 °C. The resulting mixture was first stirred at 0 °C for 2 h and then at r.t. for 48 h. The reaction was quenched by adding methanol (15 mL). The solvent was removed by evaporation under reduced pressure. The residue was extracted with ethyl acetate. The organic layer was washed with brine, dried over MgSO_4 and evaporated. The residue was purified by silica gel chromatography (DCM-MeOH 50:1) to give compound **38** (433 mg, 69%) as a white foam [248].

$R_f = 0.19$ (DCM-MeOH 50:1).

$^1\text{H NMR}$ (400 MHz, CDCl_3): δ (ppm) = 5.10 (d, $J = 3.6$ Hz, 7H, H-1), 4.27 (dd, $J = 15.9, 2.4$ Hz, 7H, CH_2), 4.19 (dd, $J = 15.8, 2.4$ Hz, 7H, CH_2), 3.90 – 3.82 (m, 21H, H-6, H-5), 3.62 (s, 21H, OCH_3), 3.56 (t, $J = 9.0$ Hz, 7H, H-4), 3.51 – 3.45 (m, 28H, H-3, OCH_3), 3.17 (dd, $J = 9.6, 3.6$ Hz, 7H, H-2), 2.48 (t, $J = 2.3$ Hz, 7H, $\text{C}\equiv\text{CH}$).

$^{13}\text{C NMR}$ (100 MHz, CDCl_3): δ (ppm) = 99.22 (C-1), 82.15 (C-2), 81.82 (C-3), 80.78 (C-4), 79.90 ($\underline{\text{C}}\equiv\text{CH}$), 74.99 ($\text{C}\equiv\text{C}\underline{\text{H}}$), 70.84 (C-5), 68.96 (C-6), 61.59 (OCH_3), 58.62 (OCH_3), 58.57 (CH_2).

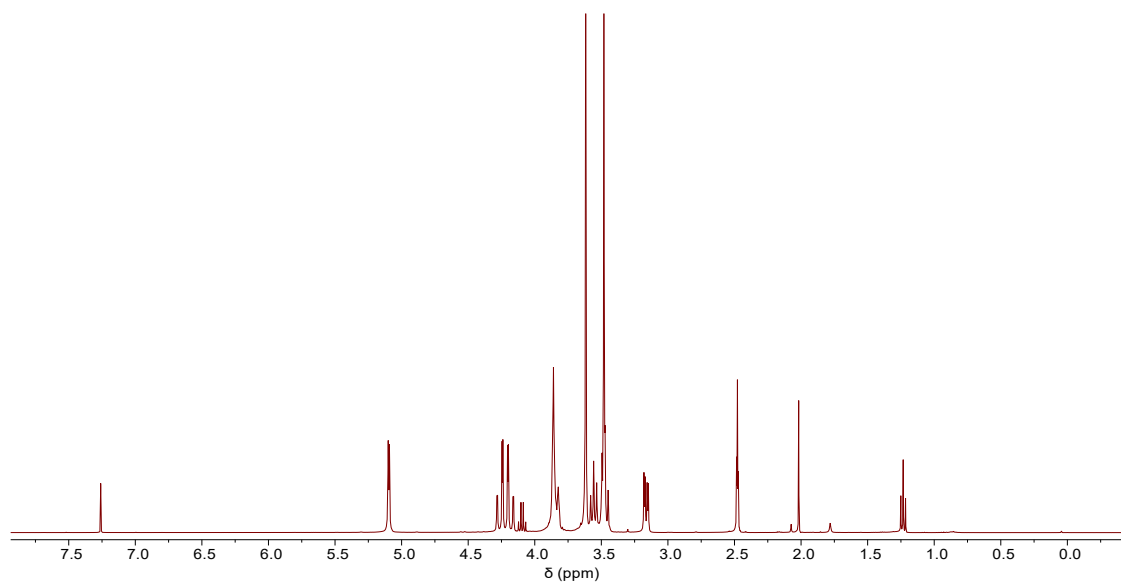


Figure VII-30. ¹H NMR spectrum (400 MHz, CDCl₃, 300 K) of compound **38**.

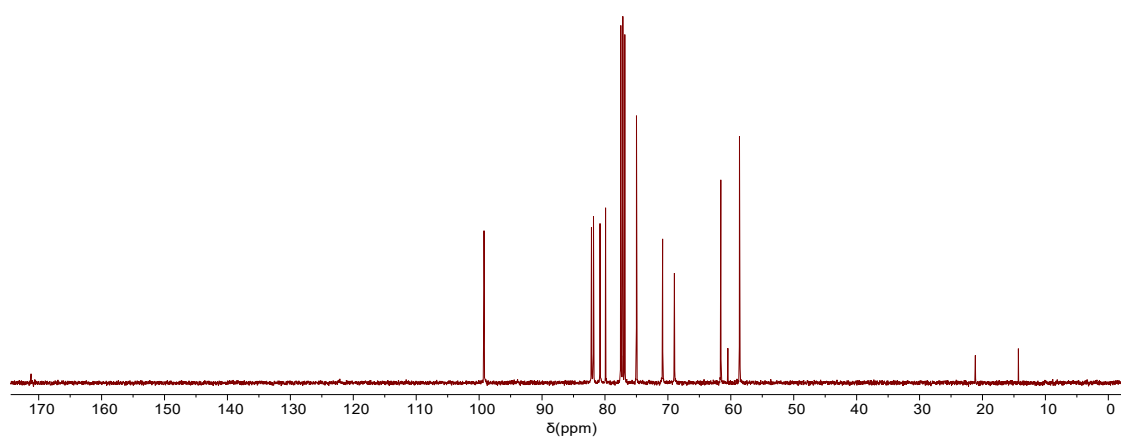
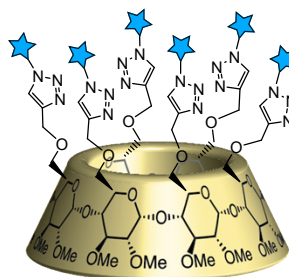


Figure VII-31. ¹³C NMR spectrum (100 MHz, CDCl₃, 300 K) of compound **38**.

7.10. Synthesis of mannose-containing GM3 analogue oligomers with macromolecular multivalent skeletons based on "click chemistry"

Hexakis {2,3-di-O-methyl-6-[O-(methyl 5-acetamido-4,7,8,9-tetra-O-acetyl-3,5-dideoxy-D-glycero- α -D-galacto-2-nonulopyranosylate)-(2 \rightarrow 6)-O-(2,3,4-tri-O-acetyl- α -D-mannosyl)-(1 \rightarrow 1)-(2S,3R,4E)-3-O-benzoyl-4-octadecene-1,3-diol)]-1H-1,2,3-triazole-4-ylmethoxy} cyclomaltohexaose (39)



A mixture of compound **34** (24 mg, 0.017 mmol) and compound **19** (158 mg, 0.132 mmol) was dissolved in 2.6 mL of tetrahydrofuran and 2.6 mL of deionized water under argon. Then, $\text{CuSO}_4 \cdot 5\text{H}_2\text{O}$ (9 mg, 0.035 mmol) and sodium ascorbate (35.08 mg, 0.177 mmol) were added sequentially to the reaction system and the mixture was stirred at 56 °C for 24 h. Afterwards, the reaction was detected by TLC, extracted with EtOAc and brine, dried with MgSO_4 , and concentrated under reduced pressure. The residue was applied to a silica gel column chromatography eluted with MeOH-EtOAc 1:10 to give the crude product, which was then further purified with Sephadex LH-20 (MeOH-DCM 1:1) to give compound **39** (84 mg, 56%) as colorless foam.

$R_f = 0.32$ (MeOH-EtOAc 1:10).

$[\alpha]_D^{20} = 39.24$ (c 0.5 in CHCl_3).

$^1\text{H NMR}$ (400 MHz, CDCl_3): δ (ppm) = 7.90 (d, $J = 7.4$ Hz, 12H, Ar-H), 7.76 (s, 6H, triazole), 7.44 (dd, $J = 26.7, 7.4$ Hz, 18H, Ar-H), 5.87 (dd, $J = 15.1, 7.8$ Hz, 12H, H-5'', H-3''), 5.39 (d, $J = 9.6$ Hz, 6H, H-4''), 5.31 (d, $J = 7.4$ Hz, 18H, H-7, H-8, H-4'), 5.20 – 4.98 (m, 24H, H-3', H-CD1, H-2', H-2''), 4.92 – 4.85 (m, 6H, H-4), 4.74 (s, 18H, H-1', H-CDCH₂), 4.25 (d, $J = 12.4$ Hz, 12H, Ha-1'', Ha-9), 4.16 – 3.97 (m, 30H, Hb-1'', Ha-CD6, H-5, H-6, Hb-9), 3.97 – 3.83 (m, 18H, H-5', Ha-6', H-CD4), 3.83 – 3.72 (m, 24H, H-CD5, COOCH₃), 3.59 (s, 30H, Hb-CD6, H-CDOMe, H3), 3.41 (d, $J = 29.5$ Hz, 24H, Hb-6', H-CDOMe), 3.01 (d, $J = 9.7$ Hz, 6H, H-CD2), 2.59 (dd, $J = 13.1, 4.6$ Hz, 6H, H-3eq), 2.13 (s, 18H, OAc), 2.11 (s, 18H, OAc), 2.06 (s, 18H, OAc), 2.04 (s, 18H, OAc), 2.00 (m, 36H, OAc x 2), 1.97 (s, 18H, H-3eq, H-6''), 1.91 (s, 18H, OAc), 1.85 (s, 18H, OAc), 1.23 (m, 132H, CH₂), 0.85 (t, $J = 6.7$ Hz, 18H, CH₃).

¹³C NMR (100 MHz, CDCl₃): δ (ppm) = 170.94 (C=O), 170.57 (C=O), 170.22 (C=O), 170.10 (C=O), 169.76 (C=O x 3), 169.04 (C=O), 167.82 (PhC=O), 164.81 (C=O), 144.78 (Click ring C), 139.33 (C-5''), 133.36 (C-Ar), 129.65 (C-Ar x 2), 128.65 (C-Ar x 2), 123.90 (Click ring CH), 122.38 (C-4''), 100.25 (C-CD1), 98.44 (C-1), 98.32 (C-1'), 82.04 (C-CD2), 81.22 (C-CD3), 77.24 (C-CD4), 74.30 (C-3''), 72.42 (C-6), 71.71 (C-CD5), 70.01 (C-5'), 69.71 (C-CD6), 69.49 (C-3'), 69.32 (C-2'), 69.11 (C-4), 68.15 (C-8), 67.25 (C-7), 66.21 (C-1''), 65.68 (C-4'), 64.98 (C-CDCH₂), 62.82 (C-6'), 62.72 (C-2''), 62.33 (C-9), 61.66 (C-CDOMe), 57.81 (C-CDOMe), 52.87 (COOCH₃), 49.40 (C-5), 37.65 (C-3), 32.34 (C-6''), 31.91, 29.70, 29.66, 29.51, 29.35, 29.26, 28.85, 23.19, 22.67 (11 x CH₂), 21.10, 20.85, 20.82, 20.72, 20.62 (CH₃, 8 x OAc), 14.11 (CH₃).

ESI-HRMS: calcd for C₄₀₈H₅₈₈N₂₄O₁₆₈ [M+H]⁴⁺: 2130.2164, found: 2130.2108.

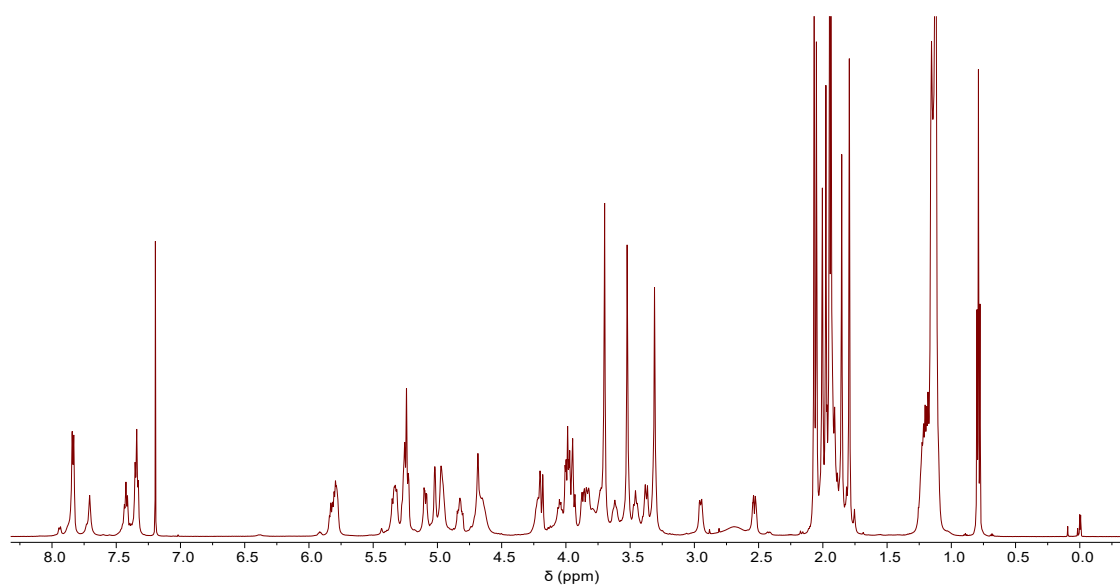


Figure VII-32. ¹H NMR spectrum (600 MHz, CDCl₃, 300 K) of compound **39**.

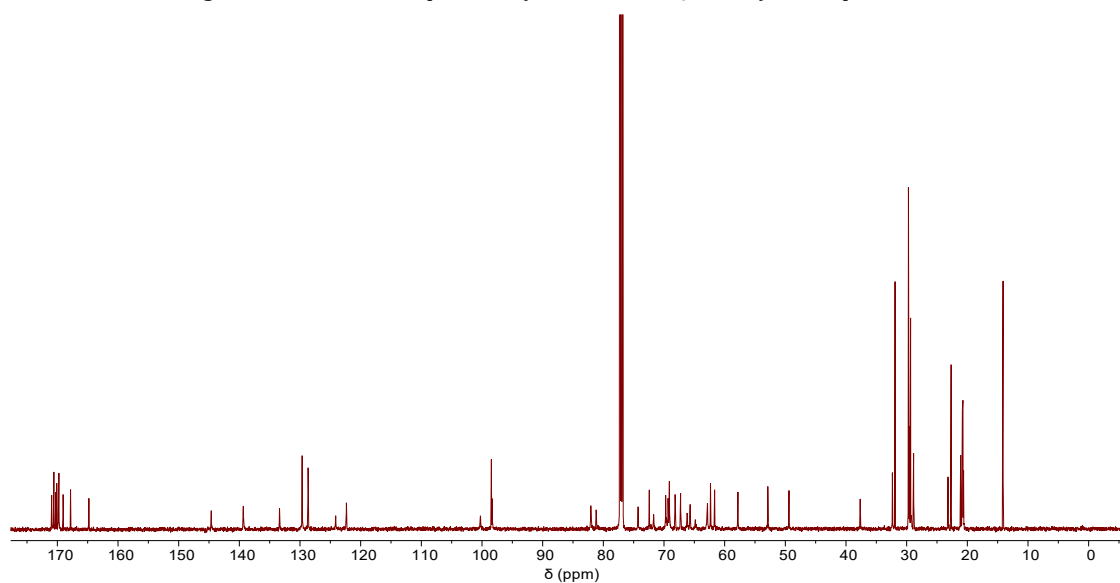
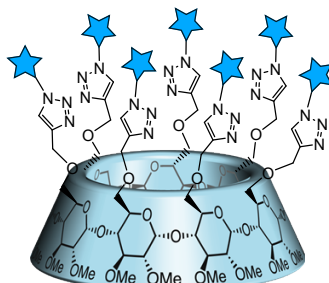


Figure VII-33. ¹³C NMR spectrum (150 MHz, CDCl₃, 300 K) of compound **39**.

Heptakis {2,3-di-O-methyl-6-[O-(methyl 5-acetamido-4,7,8,9-tetra-O-acetyl-3,5-dideoxy-D-glycero- α -D-galacto-2-nonulopyranosylonate)-(2 \rightarrow 6)-O-(2,3,4-tri-O-acetyl- α -D-mannosyl)-(1 \rightarrow 1)-(2S,3R,4E)-3-O-benzoyl-4-octadecene-1,3-diol)]-1H-1,2,3-triazole-4-ylmethoxy} cyclomaltoheptaose (40)



A mixture of compound **38** (17 mg, 0.01 mmol) and compound **19** (112 mg, 0.093 mmol) was dissolved in 1.9 mL of tetrahydrofuran and 1.9 mL of deionized water under argon. Then, $\text{CuSO}_4 \cdot 5\text{H}_2\text{O}$ (5.37 mg, 0.021 mmol) and sodium ascorbate (21.08 mg, 0.106 mmol) were added sequentially to the reaction system and the mixture was stirred at 56 °C for 24 h. Afterwards, the reaction was detected by TLC and mass spectrometry, extracted with EtOAc and brine, dried with MgSO_4 , and concentrated under reduced pressure. The residue was applied to a silica gel column chromatography eluted with MeOH-EtOAc 1:10 to give the crude product, which was then further purified with Sephadex LH-20 (MeOH-DCM 1:1) to give compound **40** as colorless foam (58 mg, 55%).

$R_f = 0.31$ (MeOH-EtOAc 1:10).

$[\alpha]_D^{20} = 38.07$ (c 0.5 in CHCl_3).

$^1\text{H NMR}$ (400 MHz, CDCl_3): δ (ppm) = 7.91 (d, $J = 7.6$ Hz, 14H, Ar-H), 7.76 (s, 7H, triazole), 7.50 (t, $J = 7.4$ Hz, 7H, Ar-H), 7.41 (t, $J = 7.6$ Hz, 14H, Ar-H), 5.89-5.84 (m, 14H, H-5'', H-3''), 5.42-5.38 (m, 7H, H-4''), 5.33-5.29 (m, 21H, H-7, H-8, H-4'), 5.19 - 5.14 (m, 14H, H-3', H-CD1), 5.09 (s, 7H, H-2'), 5.01 (d, $J = 8.0$ Hz, 7H, H-2''), 4.92 - 4.87 (m, 7H, H-4), 4.76 (s, 7H, H-1'), 4.72 - 4.64 (m, 14H, H-CDCH₂), 4.29-4.25 (m, 14H, Ha-1'', Ha-9), 4.13 (s, 7H, Hb-1''), 4.08-4.00 (m, 28H, Ha-CD6, H-5, H-6, Hb-9), 3.94 - 3.89 (m, 14H, H-5', Ha-6'), 3.81 (s, 14H, H-CD4, H-CD5), 3.76 (s, 21H, COOCH₃), 3.73 (s, 7H, Hb-CD6), 3.60 (s, 21H, H-CDOMe), 3.55 (d, $J = 9.3$ Hz, 7H, H-CD3), 3.44 (d, $J = 10.5$ Hz, 7H, Hb-6'), 3.38 (s, 21H, H-CDOMe), 3.05 (d, $J = 9.9$ Hz, 7H, H-CD2), 2.60 (d, $J = 8.8$ Hz, 7H, H-3eq), 2.14 (s, 21H, OAc), 2.12 (s, 21H, OAc), 2.07 (s, 21H, OAc), 2.05 (s, 21H, OAc), 2.02 - 2.00 (m, 42H, OAc x 2), 1.99 - 1.94 (m, 21H, H-3eq, H-6''), 1.93 (s, 21H, OAc), 1.86 (s, 21H, OAc), 1.26 - 1.19 (m, 154H, CH₂), 0.86 (t, $J = 7.0$ Hz, 21H, CH₃).

$^{13}\text{C NMR}$ (100 MHz, CDCl_3): δ (ppm) = 171.08 (C=O), 170.71 (C=O), 170.39 (C=O), 170.25 (C=O), 169.88 (C=O x 3), 169.19 (C=O), 167.99 (PhC=O), 164.96 (C=O),

144.95 (Click ring C), 139.41(C-5''), 133.51 (C, C aromatic), 129.80 (C, 2 x C aromatic), 128.81(C, 2 x C aromatic), 124.11 (Click ring CH), 122.55 (C-4''), 98.83 (C-CD1), 98.60 (C-1), 98.52 (C-1'), 82.33 (C-CD2), 81.76 (C-CD3), 79.55 (C-CD4), 74.48 (C-3''), 72.58 (C-6), 71.77 (C-CD5), 69.84 (C-5'), 69.70 (C-CD6), 69.47 (C-3'), 69.33 (C-2'), 69.25 (C-4), 68.32 (C-8), 67.40 (C-7), 66.45 (C-1''), 65.83 (C-4'), 65.18 (C-CDCH₂), 62.98(C-6'), 62.92 (C-2''), 62.48 (C-9), 61.30 (C-CDOMe), 58.62 (C-CDOMe), 53.02 (COOCH₃), 49.54 (C-5), 37.81 (C-3), 32.49 (C-6''), 32.05, 31.65, 31.58, 30.45, 30.34, 30.28, 29.85, 29.81, 29.67, 29.49, 29.41, 29.00, 23.32, 22.82 (11 x CH₂), 21.24, 20.99, 20.96, 20.87, 20.76(CH₃, 8 x OAc), 14.25(CH₃).

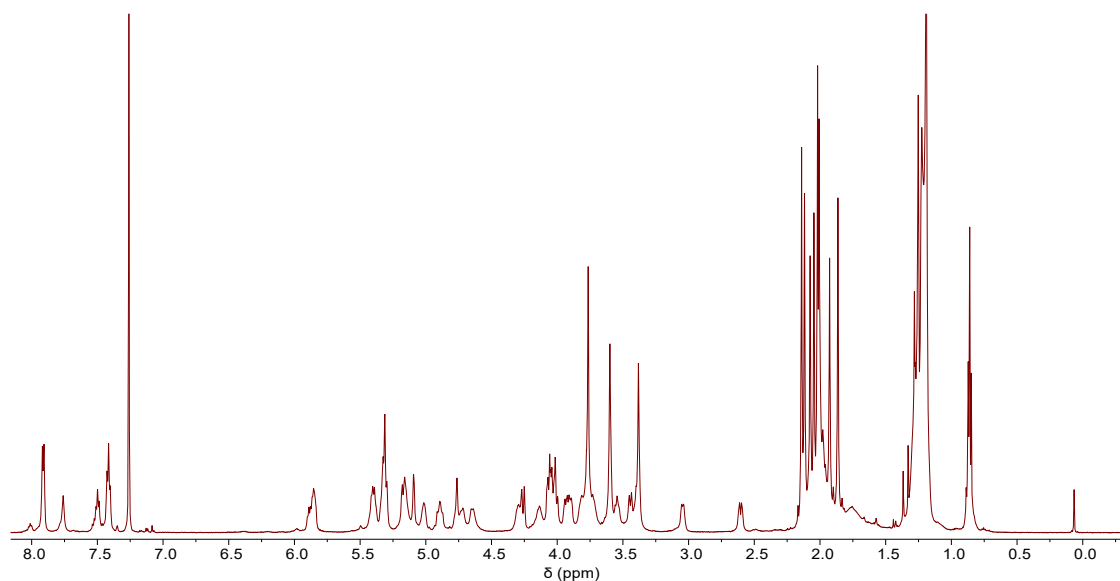


Figure VII-34. ¹H NMR spectrum (600 MHz, CDCl₃, 300 K) of compound **40**.

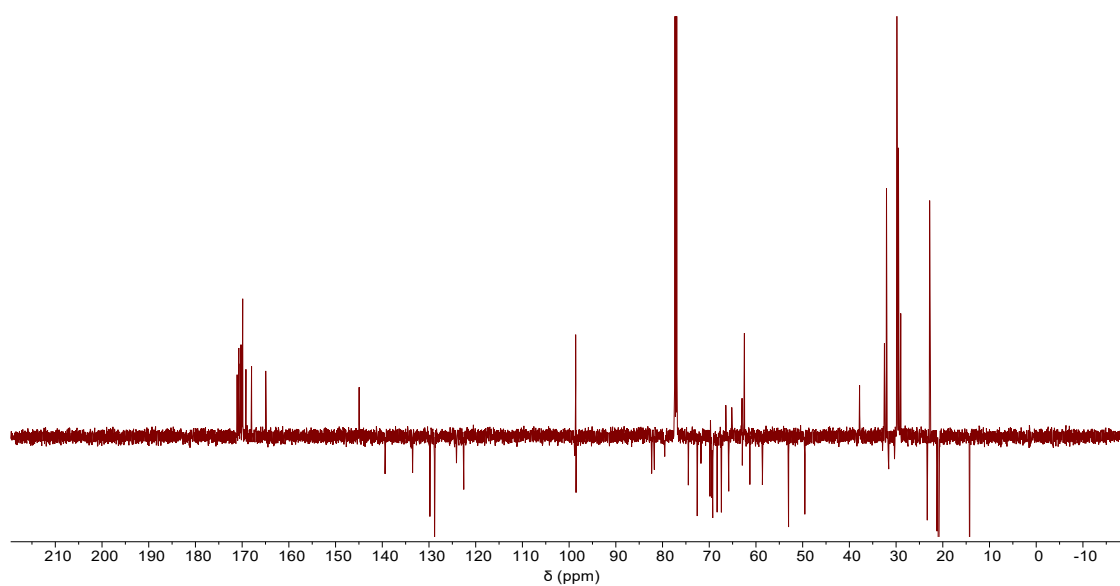
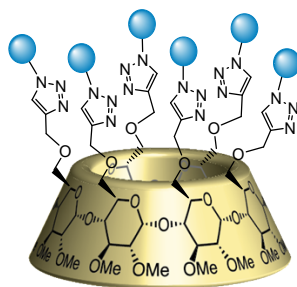


Figure VII-35. ¹³C NMR spectrum (150 MHz, CDCl₃, 300 K) of compound **40**.

Hexakis {2,3-di-O-methyl-6-[O-(5-acetamido-3,5-dideoxy-D-glycero- α -D-galacto-2-nonulopyranosylonate)-(2 \rightarrow 6)-O-(α -D-mannosyl)-(1 \rightarrow 1)-(2S,3R,4E)-4-octadecene-1,3-diol.]-1H-1,2,3-triazole-4-ylmethoxy} cyclomaltohexaose (41**)**



The compound **39** (12 mg, 0.001 mmol) was dissolved in 1.69 mL of NaOMe/MeOH (0.04 M) and stirred overnight at room temperature. Then was added a few drops of water under 0 °C and the mixture was neutralized with Amberlite IR 120/H⁺ ion exchange resin after stirring for 2 hours at room temperature. After filtration and concentration, the residue was purified by silica gel chromatography (CHCl₃-MeOH-H₂O 5:4:1) and Sephadex LH-20 (MeOH-H₂O 1:1) to afford compound **41** as white solid (5.6 mg, 66%).

R_f = 0.38 (CHCl₃-MeOH-H₂O 5:4:1).

ESI-HRMS: calcd for C₂₇₆H₄₆₈N₂₄O₁₂₀ [M-OH-4H]⁴⁺ : 1509.5025, found: 1509.5097.

¹H NMR (400 MHz, CDCl₃-CD₃OD-D₂O 5:4:1): δ (ppm) = 7.68 (s, 6H, triazole), 5.26-5.18 (m, 6H, H-5''), 5.02-4.95 (m, 6H, H-4''), 4.73-4.68 (m, 6H, H-CD1), 4.43-3.17 (m, 186H, H-4, H-5, H-6, H-7, H-8, H-9, H-1', H-2', H-3', H-4', H-5', H-6', H-1'', H-2'', H-3'', H-CD3, H-CD4, H-CD5, H-CD6, H-CDOMe, H-CDCH₂), 2.78-2.75 (m, 6H, H-CD2), 2.46-2.41 (m, 6H, H-3eq), 1.67 (s, 18H, NHAc), 1.57-1.52 (m, 12H, H-6''), 1.35-1.31 (m, 6H, H-3ax), 0.94-0.87 (m, 132H, H-7'''-17'''), 0.51 (t, J = 7.4 Hz, 18H, CH₃).

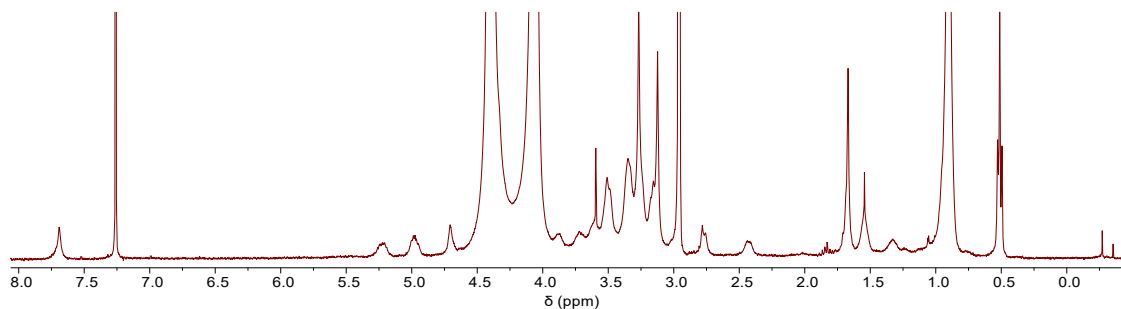


Figure VII-36. ¹H NMR spectrum (400 MHz, CDCl₃-CD₃OD-D₂O 5:4:1, 300 K) of compound **41**.

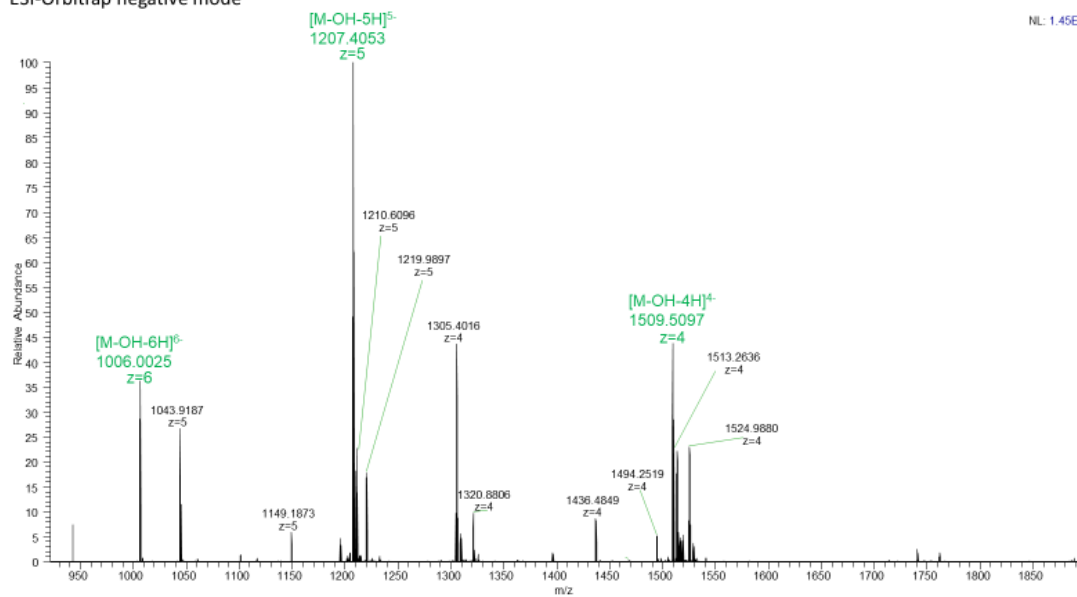
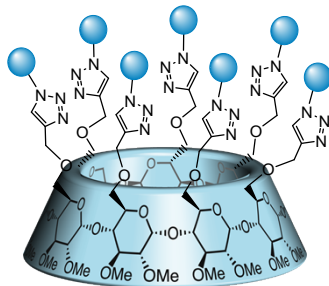


Figure VII-37. HRMS spectrum of compound 41.

Heptakis {2,3-di-O-methyl-6-[O-(5-acetamido-3,5-dideoxy-D-glycero- α -D-galacto-2-nonulopyranosylate)-(2 \rightarrow 6)-O-(α -D-mannosyl)-(1 \rightarrow 1)-(2S,3R,4E)-4-octadecene-1,3-diol.]-1H-1,2,3-triazole-4-ylmethoxy} cyclomaltoheptaose (42**)**



The compound **40** (12 mg, 0.001 mmol) was dissolved in 1.69 mL of NaOMe/MeOH (0.04 M) and stirred overnight at room temperature. Then was added a few drops of water under 0 °C and the mixture was neutralized with Amberlite IR 120/H⁺ ion exchange resin after stirring for 2 hours at room temperature. After filtration and concentration, the residue was purified by silica gel chromatography (CHCl₃-MeOH-H₂O 5:4:1) and Sephadex LH-20 (MeOH-H₂O 1:1) to afford compound **42** as white solid (5.3 mg, 62%).

R_f = 0.33 (CHCl₃-MeOH-H₂O 5:4:1).

ESI-HRMS: calcd for C₃₂₂H₅₄₆N₂₈O₁₄₀ [M-6H]⁶⁻: 1173.7662, found: 1173.7687.

¹H NMR (400 MHz, CDCl₃-CD₃OD-D₂O 5:4:1): δ (ppm) = 7.68 (s, 7H, triazole), 5.26-5.18 (m, 7H, H-5''), 5.02-4.95 (m, 7H, H-4''), 4.73-4.68 (m, 7H, H-CD1), 4.43-3.17 (m, 217H, H-4, H-5, H-6, H-7, H-8, H-9, H-1', H-2', H-3', H-4', H-5', H-6', H-1'', H-2'', H-3'', H-CD3, H-CD4, H-CD5, H-CD6, H-CDCH₂, H-CDOMe), 2.78-2.75 (m, 7H, H-CD2), 2.46-2.41 (m, 7H, H-3eq), 1.67 (s, 21H, NHAc), 1.57-1.52 (m, 14H, H-6''), 1.35-1.31 (m, 7H, H-3ax), 0.94-0.87 (m, 154H, H-7'''-17'''), 0.51 (t, J = 7.4 Hz, 21H, CH₃).

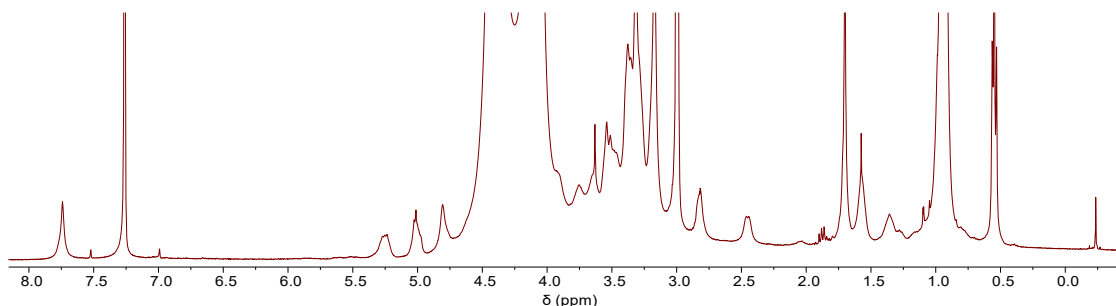


Figure VII-38. ¹H NMR spectrum (400 MHz, CDCl₃-CD₃OD-D₂O 5:4:1, 300 K) of compound **42**.

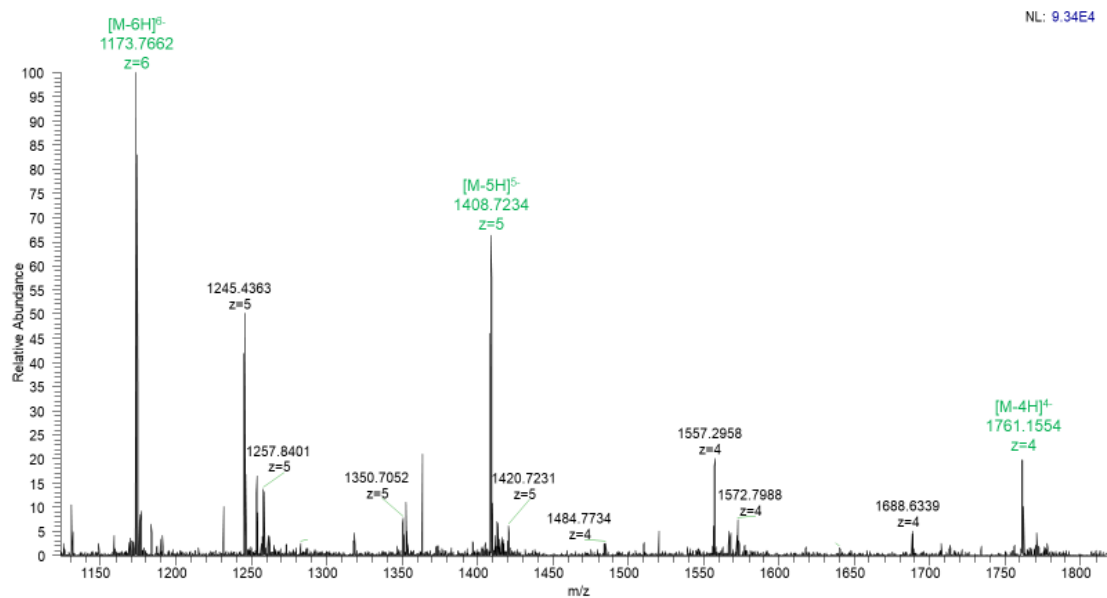
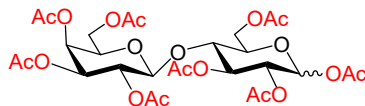


Figure VII-39. HRMS spectrum of compound **42**.

7.11. Synthesis of GM3

1,2,3,6-Tetra-O-acetyl-4-O-(2,3,4,6-tetra-O-acetyl- β -D-galactopyranosyl)-D-glucopyranose (**43**)

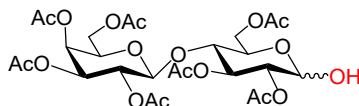


Lactose (5.00 g, 1.0 equiv.) was dissolved in pyridine (100 mL), and acetic anhydride (100 mL) was added slowly. The mixture was stirred at room temperature overnight. To the resulting reaction mixture, CH_2Cl_2 was added, and extracted from a chilled solution of HCl (1.0 M). The combined organic phases were then washed with saturated NaHCO_3 solution and brine, dried over MgSO_4 , and concentrated under reduced pressure. The residue was purified by column chromatography, eluted with Cy-EtOAc 1:1 to give compound **43** (8.31 g, 79%) as a white solid [249].

Rf = 0.55 (Cy-EtOAc 1:1)

The product was confirmed by comparison with the literature [249].

2,3,6-Tri-O-acetyl-4-O-(2,3,4,6-tetra-O-acetyl- β -D-galactopyranosyl)-D-glucopyranose (**44**)

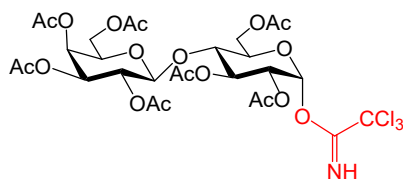


Benzyl amine (1.5 g, 2.0 equiv) was added to a solution of compound **43** (5.00 g, 1.0 equiv.) in 50 mL THF. The solution was stirred at room temperature for 20 h before removing the solvent. DCM was added to dissolve the residue and the solution was washed three times with 1.0 M HCl, followed by saturated NaHCO_3 , then brine, and finally dried over anhydrous sodium sulfate. After concentration, the crude product was purified by flash column chromatography (Cy-EtOAc 1:1 to 1:2), giving the desired product **44** (4.1 g, 88%) as a white solid [249].

Rf = 0.38 (Cy-EtOAc 1:1)

The product was confirmed by comparison with the literature [249].

α -D-glucopyranose-4-O-(2,3,4,6-tetra-Oacetyl- β -D-glucopyranosyl)-2,3,6-triacetyl-1-Otrichloroacetimidate (**45**)

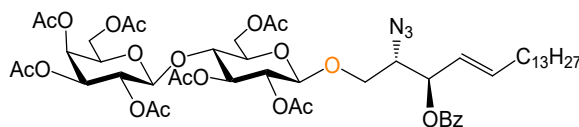


Product **44** (4.5 g, 1.0 equiv.) was placed in a flame-dried round bottom flask. After evacuating and refilling with nitrogen for three times, 30 mL of anhydrous DCM was injected, followed by trichloroacetonitrile (5.12 g, 5.0 equiv.). The solution was cooled in an ice bath for 5 min before adding a catalytic amount of DBU (0.11 g, 0.1 equiv.). The solution was allowed to warm to room temperature over 12 h, and the solvent removed and the crude product purified by flash column chromatography (Cy-EtOAc 3:2), giving product **45** (4.3g, 77%) as a light yellow foam [249].

$R_f = 0.23$ (Cy-EtOAc 3:2)

The product was confirmed by comparison with the literature [249].

O-(2,3,4,6-Tetra-O-acetyl- β -D-galactopyranosyl)-(1 \rightarrow 4)-(2,3,6-tri-O-acetyl- β -D-glucopyranosyl)-(1 \rightarrow 1)-(2S, 3R, 4E)-2-azido-3-O-benzoyloxy-octadec-4-ene (46)

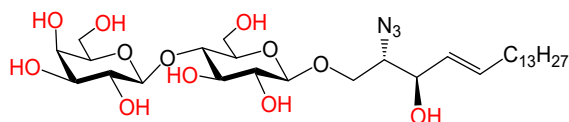


To a solution of per-acetylated lactosyl trichloroacetimidate **45** (0.5 g, 0.65 mmol) and acceptor **14** (209 mg, 0.5 mmol) in 18 mL of dry CH_2Cl_2 , powdered molecular sieves (4 Å, 0.5 g) were added. The mixture was stirred under argon at r.t. for 1 h. The reaction mixture was cooled down to -18°C and $\text{BF}_3 \cdot \text{OEt}_2$ (85 μL , 0.65 mmol) was added. The reaction mixture was then stirred at -18°C until TLC analysis (Cy-EtOAc 4:1) showed fully conversion of the acceptor. The reaction was quenched with Et_3N , and the solid was filtered off. The filtrate was concentrated under vacuum, and the residue was purified by silica gel chromatography using Cy-EtOAc 2:1 as an eluent to produce compound **46** (0.51 g, 78%) as a colorless oil [138].

$R_f = 0.41$ (Cy-EtOAc 2:1).

The product was confirmed by comparison with the literature [138].

O-(β -D-galactopyranosyl)-(1 \rightarrow 4)-(β -D-glucopyranosyl)-(1 \rightarrow 1)-(2S, 3R, 4E)-2-2-azido-4-ene-1,3-diol (47)

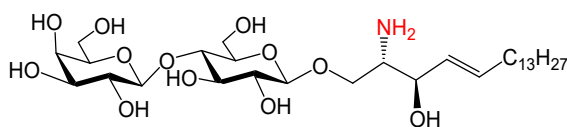


To a solution of **46** (0.51 g, 0.52 mmol) in dry MeOH (10 mL), NaOMe (48 mg) was added. After being stirred at r.t. for overnight, Using ESI-MS to track the reaction until all the starting materials were converted into product. the reaction mixture was neutralized with Dowex50W (H⁺), filtered and concentrated under reduced pressure. The intermediate **47** was used in the next step without further purification [138].

$R_f = 0.38$ (EtOAc MeOH 3:1).

The product was confirmed by comparison with the literature [138].

O-(β-D-galactopyranosyl)-(1→4)-(β-D-glucopyranosyl)-(1→1)-(2S, 3R, 4E)-2-aminooctadec-4-ene-1,3-diol (48)

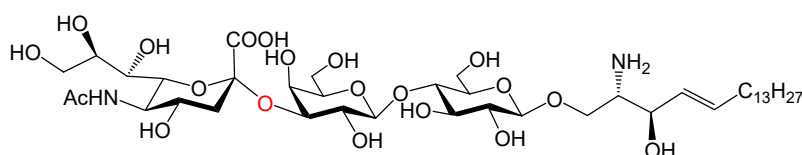


To the dry intermediate **47** (310 mg, 0.5 mmol) in pyridine-water (1:1 v/v, 3 mL), 1,3-propanedithiol (0.47 mL, 4.7 mmol) and Et₃N (0.5 mL) were added and the mixture was stirred at 50 °C for 12 h. Using ESI-MS and TLC to track the reaction until all the starting materials were converted into product. The reaction mixture was concentrated and purified by silica gel chromatography using EtOAc-MeOH 1:1 as an eluent to afford **48** (237 mg, 80%) as a white amorphous powder [138].

$R_f = 0.32$ (CHCl₃-MeOH-H₂O 5:4:0.6).

The product was confirmed by comparison with the literature [138].

O-(5-Acetamido-3,5-dideoxy-D-glycero-α-D-galacto-2- nonulopyranosylonic acid)-(2 → 3)-(β-D-galactopyranosyl) -(1 → 4)-(β-Dglucopyranosyl)-(1 → 1)-(2S, 3R, 4E)-2-aminooctadec-4-ene-1,3-diol (50)



The acceptor **48** (34 mg, 0.054 mmol), sialic acid (33 mg, 0.12 mmol) and CTP (57 mg, 2 equiv.) were dissolved in water in a 15 mL centrifuge tube containing Tris-HCl buffer (100 mM, pH 8.5) and MgCl₂ (20 mM). NmCSS (1 mg) and PmST1 (1 mg) were added, and water was added to bring the total volume of the reaction mixture to 10 mL. The reaction mixture was incubated at 37 °C for 12 h with agitation at 200 rpm in an isotherm incubator. The product formation was monitored by TLC (EtOAc:MeOH:H₂O:AcOH 4:2:1:0.5, v/v/v/v) and stained with p-anisaldehyde sugar stain. The reaction was stopped by adding 10 mL of ice-cold EtOH followed by incubation at 4 °C for 30 min. The precipitates were removed by centrifugation and the supernatant was concentrated. The target product **50** was too few in amount and was only detected by ESI-MS and ¹H NMR [138].

$R_f=0.33$ (Cy-EtOAc 1:1).

¹H NMR (400 MHz, CDCl₃-CD₃OD-D₂O 5:4:1): δ (ppm) = 5.39–5.44 (m, 1H), 5.06–5.02 (m, 1H), 4.51–2.83 (m, 21H), 2.38 (dd, $J = 13.5, 6.4$ Hz, 1H), 1.66–1.58 (m, 3H), 1.43 (m, 1H), 1.31 (m, 2H), 1.17 (m, 2H), 0.97–0.73 (m, 24H), 0.45 (t, $J = 6.2$ Hz, 3H).

ESI-MS m/z calcd for C₄₁H₇₄N₂O₂₀, [M-H]⁻: 913.4762; found: 913.6486.

The product was confirmed by comparison with the literature [138].

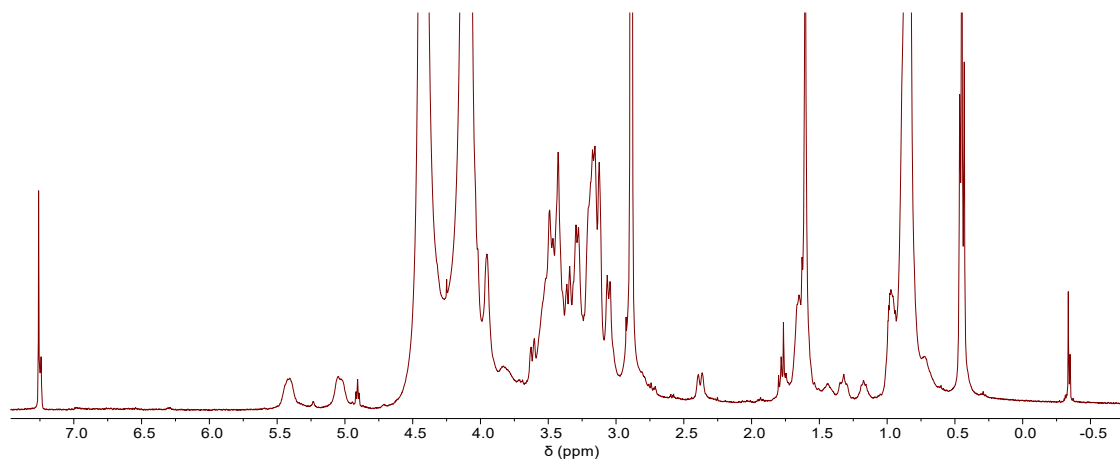


Figure VII-40. ¹H NMR spectrum (400 MHz, CDCl₃-CD₃OD-D₂O 5:4:1, 300 K) of compound **50**.

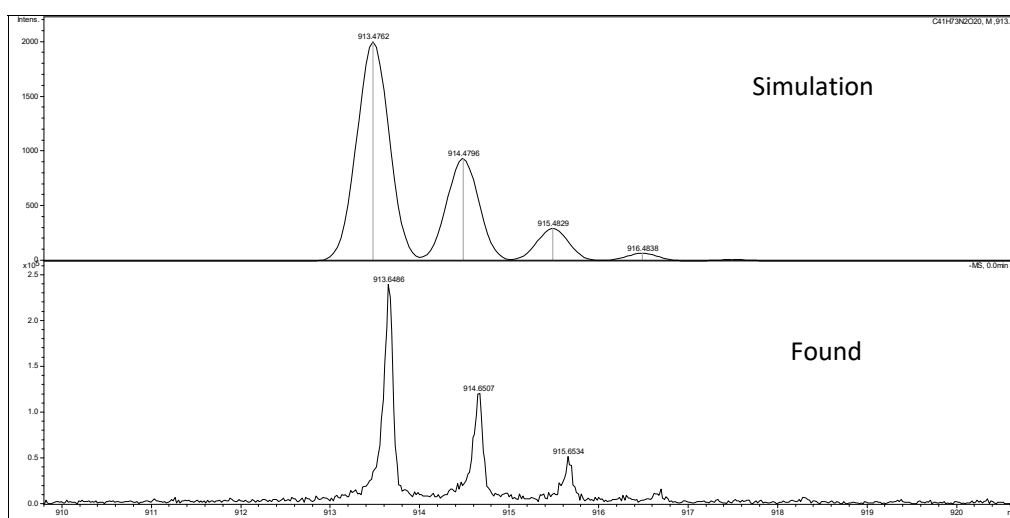
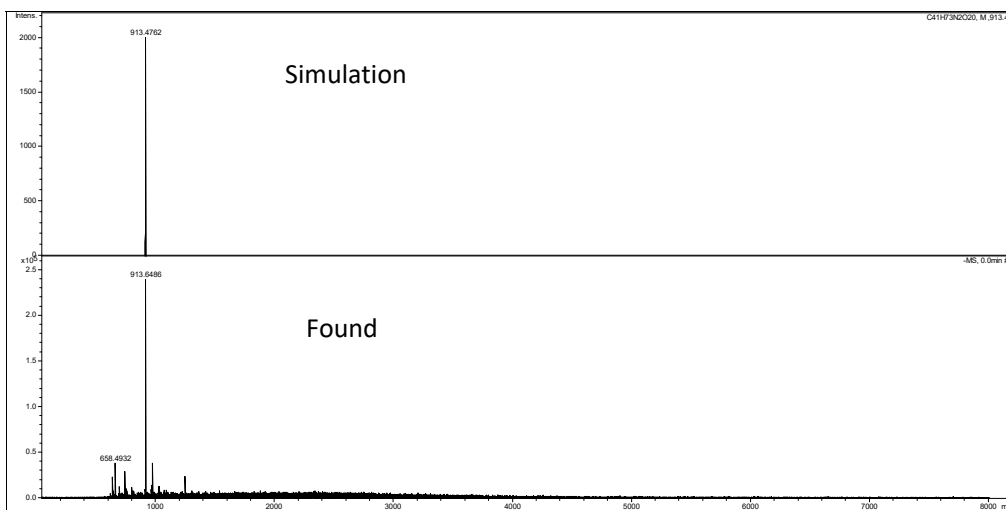
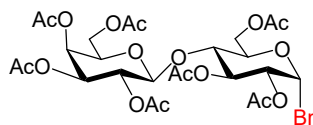


Figure VII-41. MS spectrum of compound 50.

2,3,4,6-Tetra-O-acetyl- β -D-galactopyranosyl-(1 \rightarrow 4)-2,3,6-tri-O-acetyl- α -D-glucopyranosyl bromide (51)

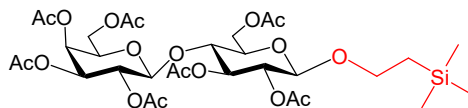


To a stirred, ice-cold solution of **43** (3.00 g, 4.42 mmol) in CH_2Cl_2 (30 mL) was added dropwise HBr in acetic acid (33 wt%, 10 mL, 57.92 mmol). The mixture was allowed to gradually warm to room temperature and was stirred for 1.5 h. The reaction mixture was neutralized by careful addition of NaHCO_3 and iced-water, and the aqueous solution was extracted three times with CH_2Cl_2 . The combined organic extracts were dried over MgSO_4 and concentrated to give crude intermediate **51** as a yellow amorphous foam. This crude intermediate, which was not separated and further characterized at this stage, was directly engaged in the following step [250].

$R_f = 0.31$ (Cy-EtOAc 1:1).

The product was confirmed by comparison with the literature [250].

2-(Trimethylsilyl)ethyl (2,3,4,6-tetra-O-acetyl- β -D-galactopyranosyl)-(1 \rightarrow 4)-2,3,6-tri-O-acetyl- β -D-glucopyranoside (52)



The crude intermediate **51** was dissolved in dry CH_2Cl_2 (30 mL), and 2-(trimethylsilyl)ethanol (1.9 mL, 13.26 mmol), mercury (II) oxide (1.05 g, 4.86 mmol) and mercury (II) bromide (264.4 mg, 0.734 mmol) were added. The resulting suspension was stirred for 18 h at room temperature. The reaction mixture was then diluted with CH_2Cl_2 , stirred with KI and NaHCO_3 solution for 2 h at room temperature, and filtered through a pad of Celite. The aqueous eluate was extracted three times with CH_2Cl_2 , and the combined organic extracts were washed with brine, dried over MgSO_4 and concentrated under reduced pressure. The resulting residue was purified by flash column chromatography (Cy-EtOAc 4:3). Compound **52** was obtained (2.47 g, 76% for two steps from **43**) as a white amorphous solid [250].

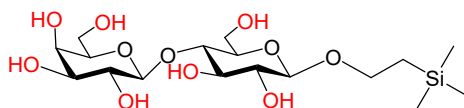
$R_f = 0.33$ (Cy-EtOAc 1:1).

$^1\text{H NMR}$ (400 MHz, CDCl_3): δ (ppm) = 5.35 (dd, $J = 3.4, 1.0$ Hz, 1H, H-4'), 5.19 (t, $J = 9.3$ Hz, 1H, H-3), 5.11 (dd, $J = 10.5, 7.8$ Hz, 1H, H-2'), 4.95 (dd, $J = 10.5, 3.4$ Hz, 1H, H-3'), 4.88 (dd, $J = 9.5, 7.8$ Hz, 1H, H-2), 4.48 (d, $J = 7.8$ Hz, 1H, H-1), 4.47 (d, $J = 7.8$ Hz, 1H, H-1'), 4.10 (m, 4H, H₂-6, H₂-6'), 3.94 (m, 1H, $\text{OCH}_a\text{CH}_2\text{Si}$), 3.87 (dt, $J = 7.6, 1.0$ Hz, 1H, H-5'), 3.79 (t, $J = 9.8$ Hz, 1H, H-4), 3.60 (ddd, $J = 9.8, 5.1, 2.0$ Hz, 1H, H-

5), 3.55 (m, 1H, OCH_bCH_2Si), 2.15 – 1.97 (7×s, 21H, OAc), 0.91 (m, 2H, OCH_2CH_2Si), 0.00 (s, 9H, $Si(CH_3)_3$).

The product was confirmed by comparison with the literature [250].

2-(Trimethylsilyl)ethyl 4-O- β -D-galactopyranosyl- β -D-glucopyranoside (53)



A solution of product **52** (2.00 g, 2.71 mmol) in 25 mL of NaOMe/MeOH (0.04 M) was stirred overnight at room temperature. Then the reaction mixture was neutralized by Amberlite IR 120/H⁺ ion exchange resin. After filtration and concentration, the residue obtained was purified by short silica gel column chromatography (CH_2Cl_2 -MeOH 3:1) to give **53** (1.20 g, quantitative) as a white foam [250].

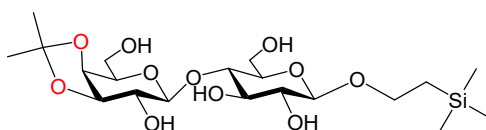
R_f = 0.34 (CH_2Cl_2 -MeOH 3:1).

¹H NMR (400 MHz, CD_3OD): δ (ppm) = 4.41 (d, J = 7.5 Hz, 1H, H-1), 4.35 (d, J = 7.8 Hz, 1H, H-1'), 4.04 (ddd, J = 11.5, 9.6, 5.8 Hz, 1H), 3.95 (dd, J = 12.1, 2.5 Hz, 1H), 3.92 – 3.79 (m, 5H), 3.79 – 3.48 (m, 11H), 3.48 – 3.43 (m, 1H), 3.36 (dd, J = 3.2, 1.6 Hz, 1H), 3.30 – 3.25 (m, 1H), 1.16 – 0.97 (m, 2H, OCH_2CH_2Si), 0.08 (s, 9H, $Si(CH_3)_3$).

ESI-HRMS (m/z) calcd for $C_{17}H_{34}O_{11}SiNa$ [$M+Na$]⁺: 465.1768, found: 465.1791.

The product was confirmed by comparison with the literature [250].

2-(Trimethylsilyl)ethyl (3,4-O-isopropylidene- β -D-galactopyranosyl)-(1→4)- β -D-glucopyranoside (54)



Product **53** (1.20 g, 2.71 mmol) was put in 2,2-dimethoxypropane (40 mL) containing 10-d,1-camphorsulfonic acid (25.2 mg, 0.108 mmol). The mixture was stirred at room temperature for 14 h then neutralized with Et_3N , concentrated and co-evaporated with toluene. The mixture obtained, diluted in a mixture of solvents methanol/water (40 mL, 10/1) with two drops of acetic acid was fluxed until TLC indicated one major product. The mixture was then concentrated, and then purified by silica gel column chromatography (CH_2Cl_2 -MeOH 10:1) to give product **54** (1.03 g, 79%) as a white amorphous solid [250].

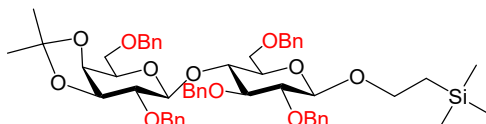
R_f = 0.33 (CH_2Cl_2 -MeOH 10:1).

$^1\text{H NMR}$ (400 MHz, D_2O): δ (ppm) = 4.36 (d, J = 8.2 Hz, 1H, H-1'), 4.30 (d, J = 8.1 Hz, 1H, H-1), 1.45 (s, 3H, CH_3), 1.33 (s, 3H, CH_3), 0.04 (s, 9H, $\text{Si}(\text{CH}_3)_3$).

ESI-HRMS (m/z) calcd for $\text{C}_{20}\text{H}_{38}\text{O}_{11}\text{SiNa}$ [$\text{M}+\text{Na}$] $^+$: 505.2081, found: 505.2074.

The product was confirmed by comparison with the literature [250].

2-(Trimethylsilyl)ethyl (2,6-di-*O*-benzyl-3,4-*O*-isopropylidene- β -D-galactopyranosyl)-(1 \rightarrow 4)-2,3,6-tri-*O*-benzyl- β -D-glucopyranoside (55)



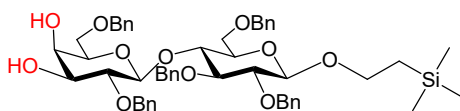
Product **54** (1.11 g, 2.30 mmol) was dissolved in dry DMF (30 ml), the benzyl bromide (1.5 mL, 12.54 mmol) was added, and the mixture was cooled to 0 °C. NaH (60% in oil, 852.8 mg, approximately 21.32 mmol) was then added to the mixture by small successive additions. The reaction mixture is allowed to warm to room temperature and stirred for 1 h, quenched by careful addition of MeOH, and diluted with diethyl ether and water. The aqueous layer was extracted four times with diethyl ether. The combined organic extracts were washed with brine, dried over MgSO_4 and concentrated under reduced pressure. This resulting intermediate **55**, which was not separated and further characterized at this stage, was directly engaged in the following step [244].

R_f = 0.43 (Cy-EtOAc 4:1).

ESI-HRMS (m/z) calcd for $\text{C}_{55}\text{H}_{68}\text{O}_{11}\text{SiNa}$ [$\text{M}+\text{Na}$] $^+$: 955.4429, found: 955.4443.

The product was confirmed by comparison with the literature [244].

2-(Trimethylsilyl)ethyl (2,6-di-*O*-benzyl- β -D-galactopyranosyl)-(1 \rightarrow 4)-2,3,6-tri-*O*-benzyl- β -D-glucopyranoside (56)



The crude intermediate **55** was dissolved in 80% AcOH (30 mL) and heated to 80 °C. The reaction was complete after stirring for 1.5 h, and then the solution was allowed to cool to room temperature. The solution was then concentrated, and the residue was chromatographed (Cy-EtOAc 2:1) to give **56** as white powder (1.64 g, 80%) [244].

R_f = 0.32 (Cy-EtOAc 2:1).

$^1\text{H NMR}$ (400 MHz, CDCl_3): δ (ppm) = 7.42 – 7.18 (m, 25H, Ar-H), 4.98 (d, J = 11.0

Hz, 1H, CH_2Ph), 4.92 (d, $J = 11.0$ Hz, 1H, CH_2Ph), 4.83 (d, $J = 11.6$ Hz, 1H, CH_2Ph), 4.79 (d, $J = 11.0$ Hz, 1H, CH_2Ph), 4.73 (d, $J = 11.0$ Hz, 1H, CH_2Ph), 4.68 (d, $J = 11.6$ Hz, 1H, CH_2Ph), 4.60 (d, $J = 12.1$ Hz, 1H, CH_2Ph), 4.47 (d, $J = 7.7$ Hz, 1H, H-1'), 4.45 (d, $J = 12.1$ Hz, 1H, CH_2Ph), 4.44 (d, $J = 7.8$ Hz, 1H, H-1), 4.42 – 4.36 (m, 2H, CH_2Ph), 4.07 – 3.93 (m, 3H, OCH_aCH_2Si , H-3, H-4'), 3.85 – 3.75 (m, 2H, H₂-6), 3.66 – 3.56 (m, 3H, Ha-6', OCH_bCH_2Si , H-4), 3.50 (dd, $J = 9.9, 5.0$ Hz, 1H, Hb-6'), 3.47 – 3.38 (m, 4H, H-2', H-3', H-2, H-5), 3.36 (t, $J = 5.8$ Hz, 1H, H-5'), 2.47 (d_{large} , $J = 3.6$ Hz, 1H, OH), 2.40 (d_{large} , $J = 4.4$ Hz, 1H, OH), 1.10 – 0.99 (m, 2H, OCH_2CH_2Si), 0.04 (s, 9H, $Si(CH_3)_3$).

The product was confirmed by comparison with the literature [244].

Bibliography

- [1] R. A. Flynn *et al.*, "Small RNAs are modified with N-glycans and displayed on the surface of living cells," *Cell*, **2021**, *184*, 3109-3124.
- [2] J. L. W. Thudichum, "A treatise on the chemical constitution of the brain.," *JAMA*, **1963**, *184*, 840-840.
- [3] T. Wennekes, R. J. B. H. N. van den Berg, R. G. Boot, G. A. van der Marel, H. S. Overkleeft, and J. M. F. G. Aerts, "Glycosphingolipids—Nature, Function, and Pharmacological Modulation," *Angew. Chem. Int. Ed.*, **2009**, *48*, 8848–8869.
- [4] E. Chiricozzi, "Plasma membrane glycosphingolipid signaling: a turning point," *Glycoconj. J.*, **2022**, *39*, 99–105.
- [5] T. Zhang, A. A. de Waard, M. Wuhrer, and R. M. Spaapen, "The Role of Glycosphingolipids in Immune Cell Functions," *Front. Immunol.*, **2019**, *10*, 90.
- [6] G. D'Angelo, S. Capasso, L. Sticco, and D. Russo, "Glycosphingolipids: synthesis and functions," *FEBS J.*, **2013**, *280*, 6338–6353.
- [7] "Inhibition of human neuroblastoma cell proliferation and EGF receptor phosphorylation by gangliosides GM1, GM3, GD1A and GT1B", *Cell proliferation*, **2002**, *35*, 105-115.
- [8] "Regulation of human EGF receptor by lipids." *Proc. Natl. Acad. Sci. U. S. A.*, **2011**, *108*, 9044-9048.
- [9] Y. Liu, Y. Su, M. Wiznitzer, O. Epifano, and S. Ladisch, "Ganglioside depletion and EGF responses of human GM3 synthase-deficient fibroblasts," *Glycobiology*, **2008**, *18*, 593–601.
- [10] S.-Y. Park, C.-Y. Kwak, J. A. Shayman, and J. H. Kim, "Globoside (Gb4) promotes activation of ERK by interaction with the epidermal growth factor receptor," *Biochim. Biophys. Acta*, **2012**, *1820*, 1141-1148.
- [11] F. Guan, K. Handa, and S. Hakomori, "Regulation of Epidermal Growth Factor Receptor Through Interaction of Ganglioside GM3 with GlcNAc of N-Linked Glycan of the Receptor: Demonstration in Id1D Cells," *Neurochem. Res.*, **2011**, *36*, 1645–1653.
- [12] X. Huang, Y. Li, J. Zhang, Y. Xu, Y. Tian, and K. Ma, "Ganglioside GM3 inhibits hepatoma cell motility via down-regulating activity of EGFR and PI3K/AKT signaling pathway," *J. Cell. Biochem.*, **2013**, *114*, 1616–1624.
- [13] S. Milani, E. Sottocornola, S. Zava, M. Galbiati, B. Berra, and I. Colombo, "Gangliosides influence EGFR/ErbB2 heterodimer stability but they do not modify EGF-dependent ErbB2 phosphorylation," *Biochim. Biophys. Acta BBA - Mol. Cell Biol. Lipids*, **2010**, *1801*, 617–624.
- [14] E. G. Bremer and S. Hakomori, "GM3 ganglioside induces hamster fibroblast growth inhibition in chemically-defined medium: Ganglioside may regulate growth factor receptor function," *Biochem. Biophys. Res. Commun.*, **1982**, *106*, 711–718.
- [15] M. S. Toledo, E. Suzuki, K. Handa, and S. Hakomori, "Cell Growth Regulation through GM3-enriched Microdomain (Glycosynapse) in Human Lung Embryonal Fibroblast WI38 and Its Oncogenic Transformant VA13", *J. Biol. Chem.*, **2004**, *279*, 34655-34664.
- [16] E. G. Bremer, S. I. Hakomori, D. F. Bowen-Pope, E. Raines, and R. Ross,

- “Ganglioside-mediated modulation of cell growth, growth factor binding, and receptor phosphorylation”, *J. Biol. Chem.*, **1984**, *259*, 6818-6825.
- [17] T. Farooqui, T. Kelley, K. M. Coggeshall, A. A. Rampersaud, and A. J. Yates, “GM1 inhibits early signaling events mediated by PDGF receptor in cultured human glioma cells,” *Anticancer Res.*, **1999**, *19*, 5007–5013.
- [18] T. Mutoh, A. Tokuda, T. Miyadai, M. Hamaguchi, and N. Fujiki, “Ganglioside GM1 binds to the Trk protein and regulates receptor function.,” *Proc. Natl. Acad. Sci.*, **1995**, *92*, 5087–5091.
- [19] M. Kimura, K. I. Hidari, T. Suzuki, D. Miyamoto, and Y. Suzuki, “Engagement of endogenous ganglioside GM1a induces tyrosine phosphorylation involved in neuron-like differentiation of PC12 cells,” *Glycobiology*, **2001**, *11*, 335–343.
- [20] N. Saha, M. V. Kolev, M. Semavina, J. Himanen, and D. B. Nikolov, “Ganglioside mediate the interaction between Nogo receptor 1 and LINGO-1,” *Biochem. Biophys. Res. Commun.*, **2011**, *413*, 92–97.
- [21] T.-W. Chung *et al.*, “Ganglioside GM3 inhibits VEGF/VEGFR-2-mediated angiogenesis: direct interaction of GM3 with VEGFR-2,” *Glycobiology*, **2009**, *19*, 229–239.
- [22] S. J. Kim *et al.*, “Ganglioside GM3 participates in the TGF- β 1-induced epithelial–mesenchymal transition of human lens epithelial cells,” *Biochem. J.*, **2012**, *449*, 241–251.
- [23] K. Kabayama *et al.*, “Dissociation of the insulin receptor and caveolin-1 complex by ganglioside GM3 in the state of insulin resistance,” *Proc. Natl. Acad. Sci. U. S. A.*, **2007**, *104*, 13678–13683.
- [24] S. Tagami *et al.*, “Ganglioside GM3 Participates in the Pathological Conditions of Insulin Resistance,” *J. Biol. Chem.*, **2002**, *277*, 3085–3092.
- [25] N. Sekino-Suzuki *et al.*, “Involvement of gangliosides in the process of Cbp/PAG phosphorylation by Lyn in developing cerebellar growth cones,” *J. Neurochem.*, **2013**, *124*, 514–522.
- [26] Y. Miura, M. Kainuma, H. Jiang, H. Velasco, P. K. Vogt, and S. Hakomori, “Reversion of the Jun-induced oncogenic phenotype by enhanced synthesis of sialosylactosylceramide (GM3 ganglioside),” *Proc. Natl. Acad.*, **2004**, *101*, 16204-16209.
- [27] S. Y. Park, S.-J. Yoon, L. Freire-de-Lima, J.-H. Kim, and S. Hakomori, “Control of cell motility by interaction of gangliosides, tetraspanins, and epidermal growth factor receptor in A431 versus KB epidermoid tumor cells,” *Carbohydr. Res.*, **2009**, *344*, 1479–1486.
- [28] M. S. Toledo, E. Suzuki, K. Handa, and S. Hakomori, “Effect of Ganglioside and Tetraspanins in Microdomains on Interaction of Integrins with Fibroblast Growth Factor Receptor ,” *J. Biol. Chem.*, **2005**, *280*, 16227–16234.
- [29] H. Nakayama, H. Ogawa, K. Takamori, and K. Iwabuchi, “GSL-Enriched Membrane Microdomains in Innate Immune Responses,” *Arch. Immunol. Ther. Exp. (Warsz.)*, **2013**, *61*, 217–228.
- [30] X.-Q. Wang, P. Sun, and A. S. Paller, “Ganglioside Induces Caveolin-1 Redistribution and Interaction with the Epidermal Growth Factor Receptor *,”

- J. Biol. Chem.*, **2002**, *277*, 47028–47034.
- [31] X. Wang *et al.*, “Suppression of Epidermal Growth Factor Receptor Signaling by Protein Kinase C- α Activation Requires CD82, Caveolin-1, and Ganglioside,” *Cancer Res.*, **2007**, *67*, 9986–9995.
- [32] J. Duan, J. Zhang, Y. Zhao, F. Yang, and X. Zhang, “Ganglioside GM2 modulates the erythrocyte Ca²⁺-ATPase through its binding to the calmodulin-binding domain and its ‘receptor,’” *Arch. Biochem. Biophys.*, **2006**, *454*, 155–159.
- [33] J. Wang, Z.-H. Lu, H.-J. Gabius, C. Rohowsky-Kochan, R. W. Ledeen, and G. Wu, “Cross-linking of GM1 ganglioside by galectin-1 mediates regulatory T cell activity involving TRPC5 channel activation: possible role in suppressing experimental autoimmune encephalomyelitis,” *J. Immunol. Baltim. Md 1950*, **2009**, *182*, 4036–4045.
- [34] C. Boscher *et al.*, “Galectin-3 Protein Regulates Mobility of N-cadherin and GM1 Ganglioside at Cell-Cell Junctions of Mammary Carcinoma Cells,” *J. Biol. Chem.*, **2012**, *287*, 32940–32952.
- [35] R. D. Lardone and I. Cely, “Immune Response Modulation by Tumor-Secreted Glycosphingolipids,” *J. Glycobiol.*, **2015**, *3*, 107-115.
- [36] Y. Fukushi, E. Nudelman, S. B. Lavery, T. Higuchi, and S. Hakomori, “A novel disialoganglioside (IV3NeuAcIII6NeuAcLc4) of human adenocarcinoma and the monoclonal antibody (FH9) defining this disialosyl structure,” *Biochemistry*, **1986**, *25*, 2859–2866.
- [37] M. R. Stroud *et al.*, “Extended type 1 chain glycosphingolipids: dimeric Lea (III4V4Fuc2Lc6) as human tumor-associated antigen,” *J. Biol. Chem.*, **1991**, *266*, 8439–8446.
- [38] J. L. Magnani *et al.*, “A monoclonal antibody-defined antigen associated with gastrointestinal cancer is a ganglioside containing sialylated lacto-N-fucopentaose II,” *J. Biol. Chem.*, **1982**, *257*, 14365–14369.
- [39] E. Nudelman, Y. Fukushi, S. B. Lavery, T. Higuchi, and S. Hakomori, “Novel fucolipids of human adenocarcinoma: disialosyl Lea antigen (III4FucIII6NeuAcIV3NeuAcLc4) of human colonic adenocarcinoma and the monoclonal antibody (FH7) defining this structure,” *J. Biol. Chem.*, **1986**, *261*, 5487–5495.
- [40] Y. W. Koh, H. J. Lee, J.-H. Ahn, J. W. Lee, and G. Gong, “Expression of Lewis X is associated with poor prognosis in triple-negative breast cancer,” *Am. J. Clin. Pathol.*, **2013**, *139*, 746–753.
- [41] E. H. Holmes, G. K. Ostrander, and S. Hakomori, “Enzymatic basis for the accumulation of glycolipids with X and dimeric X determinants in human lung cancer cells (NCI-H69),” *J. Biol. Chem.*, **1985**, *260*, 7619–7627.
- [42] S. Hakomori, E. Nudelman, S. B. Lavery, and R. Kannagi, “Novel fucolipids accumulating in human adenocarcinoma. I. Glycolipids with di- or trifucosylated type 2 chain,” *J. Biol. Chem.*, **1984**, *259*, 4672–4680.
- [43] S. B. Lavery *et al.*, “¹H-n.m.r. analysis of type-2 chain lacto-gangliosides. Confirmation of structure of a novel cancer-associated fucoganglioside, alpha-NeuAc-(2----6)- beta-D-Galp-(1----4)-beta-D-GlcpNAc-(1----3)-beta-D-

- Galp-(1----4)-[alp ha-L- Fucp-(1----3)]-beta-D-GlcpNAc-(1----3)-beta-D-Galp-(1----4)-beta -D-Glc p- (1----1)-Cer (VI6NeuAcIII3FucnLc6Cer)," *Carbohydr. Res.*, **1988**, *178*, 121–144.
- [44] K. Numahata *et al.*, "Sialosyl-Le(x) expression defines invasive and metastatic properties of bladder carcinoma," *Cancer*, **2002**, *94*, 673–685.
- [45] N. Hiraiwa, M. Hiraiwa, and R. Kannagi, "Human T-cell leukemia virus-1 encoded Tax protein transactivates alpha 1-->3 fucosyltransferase Fuc-T VII, which synthesizes sialyl Lewis X, a selectin ligand expressed on adult T-cell leukemia cells," *Biochem. Biophys. Res. Commun.*, **1997**, *231*, 183–186.
- [46] Y. Fukushi, R. Kannagi, S. Hakomori, T. Shepard, B. G. Kulander, and J. W. Singer, "Location and distribution of difucoganglioside (VI3NeuAcV3III3Fuc2nLc6) in normal and tumor tissues defined by its monoclonal antibody FH6," *Cancer Res.*, **1985**, *45*, 3711–3717.
- [47] K. Abe, J. M. McKibbin, and S. Hakomori, "The monoclonal antibody directed to difucosylated type 2 chain (Fuc alpha 1 leads to 2Gal beta 1 leads to 4[Fuc alpha 1 leads to 3]GlcNAc; Y Determinant)," *J. Biol. Chem.*, **1983**, *258*, 11793–11797.
- [48] M. Miyake, K. Zenita, O. Tanaka, Y. Okada, and R. Kannagi, "Stage-specific expression of SSEA-1-related antigens in the developing lung of human embryos and its relation to the distribution of these antigens in lung cancers," *Cancer Res.*, **1988**, *48*, 7150–7158.
- [49] Y. S. Kim *et al.*, "Lex and Ley antigen expression in human pancreatic cancer," *Cancer Res.*, **1988**, *48*, 475–482.
- [50] E. Nudelman *et al.*, "A glycolipid antigen associated with Burkitt lymphoma defined by a monoclonal antibody," *Science*, **1983**, *220*, 509–511.
- [51] H. Farkas-Himsley, R. Hill, B. Rosen, S. Arab, and C. A. Lingwood, "The bacterial colicin active against tumor cells in vitro and in vivo is verotoxin 1.," *Proc. Natl. Acad. Sci.*, **1995**, *92*, 6996–7000.
- [52] S. Zhang *et al.*, "Selection of tumor antigens as targets for immune attack using immunohistochemistry: I. Focus on gangliosides," *Int. J. Cancer*, **1997**, *73*, 42–49.
- [53] E. G. Bremer *et al.*, "Characterization of a glycosphingolipid antigen defined by the monoclonal antibody MBr1 expressed in normal and neoplastic epithelial cells of human mammary gland," *J. Biol. Chem.*, **1984**, *259*, 14773–14777.
- [54] R. Kannagi *et al.*, "New globoseries glycosphingolipids in human teratocarcinoma reactive with the monoclonal antibody directed to a developmentally regulated antigen, stage-specific embryonic antigen 3," *J. Biol. Chem.*, **1983**, *258*, 8934–8942.
- [55] S. Saito *et al.*, "Human alpha2,3-sialyltransferase (ST3Gal II) is a stage-specific embryonic antigen-4 synthase," *J. Biol. Chem.*, **2003**, *278*, 26474–26479.
- [56] M. Satoh *et al.*, "Disialosyl galactosylgloboside as an adhesion molecule expressed on renal cell carcinoma and its relationship to metastatic potential," *Cancer Res.*, **1996**, *56*, 1932–1938.

- [57] R. Chammas *et al.*, “De-N-acetyl-gangliosides in humans: unusual subcellular distribution of a novel tumor antigen,” *Cancer Res.*, **1999**, *59*, 1337–1346.
- [58] Y. N. Malykh, R. Schauer, and L. Shaw, “N-Glycolylneuraminic acid in human tumours,” *Biochimie*, **2001**, *83*, 623–634.
- [59] H. Higashi *et al.*, “Tumor-associated expression of glycosphingolipid Hanganutziu-Deicher antigen in human cancers,” *Gan*, **1984**, *75*, 1025–1029.
- [60] G. Marquina *et al.*, “Gangliosides expressed in human breast cancer,” *Cancer Res.*, **1996**, *56*, 5165–5171.
- [61] H. Higashi, T. Sasabe, Y. Fukui, M. Maru, and S. Kato, “Detection of gangliosides as N-glycolylneuraminic acid-specific tumor-associated Hanganutziu-Deicher antigen in human retinoblastoma cells,” *Jpn. J. Cancer Res. Gann*, **1988**, *79*, 952–956.
- [62] T. Tsuchida, R. E. Saxton, D. L. Morton, and R. F. Irie, “Gangliosides of human melanoma,” *J. Natl. Cancer Inst.*, **1987**, *78*, 45–54.
- [63] O. Nakamura, M. Iwamori, M. Matsutani, and K. Takakura, “Ganglioside GD3 shedding by human gliomas,” *Acta Neurochir. (Wien)*, **1991**, *109*, 34–36.
- [64] D. A. Cheresch, R. A. Reisfeld, and A. P. Varki, “O-acetylation of disialoganglioside GD3 by human melanoma cells creates a unique antigenic determinant,” *Science*, **1984**, *225*, 844–846.
- [65] S. M. Birks, J. O. Danquah, L. King, R. Vlasak, D. C. Gorecki, and G. J. Pilkington, “Targeting the GD3 acetylation pathway selectively induces apoptosis in glioblastoma,” *Neuro-Oncol.*, **2011**, *13*, 950–960.
- [66] R. X. Li and S. Ladisch, “Shedding of human neuroblastoma gangliosides,” *Biochim. Biophys. Acta*, **1991**, *1083*, 57–64.
- [67] F. Chang, R. Li, and S. Ladisch, “Shedding of gangliosides by human medulloblastoma cells,” *Exp. Cell Res.*, **1997**, *234*, 341–346.
- [68] J. Portoukalian, G. Zwingelstein, and J. F. Doré, “Lipid composition of human malignant melanoma tumors at various levels of malignant growth,” *Eur. J. Biochem.*, **1979**, *94*, 19–23.
- [69] J. Portoukalian, M. J. David, P. Gain, and M. Richard, “Shedding of GD2 ganglioside in patients with retinoblastoma,” *Int. J. Cancer*, **1993**, *53*, 948–951.
- [70] A. Vangsted, L. Drivsholm, E. Andersen, T. Pallesen, J. Zeuthen, and H. Wallin, “New serum markers for small-cell lung cancer. I. The ganglioside fucosyl-GM1,” *Cancer Detect. Prev.*, **1994**, *18*, 221–229.
- [71] S. Wickramasinghe and J. F. Medrano, “Primer on genes encoding enzymes in sialic acid metabolism in mammals,” *Biochimie*, **2011**, *93*, 1641–1646.
- [72] F. G. Blix, A. Gottschalk, and E. Klenk, “Proposed Nomenclature in the Field of Neuraminic and Sialic Acids,” *Nature*, **1957**, *179*, 1088–1088.
- [73] M. Cohen and A. Varki, “The sialome--far more than the sum of its parts,” *Omics J. Integr. Biol.*, **2010**, *14*, 455–464.
- [74] A. Varki, “Uniquely human evolution of sialic acid genetics and biology,” *Proc. Natl. Acad. Sci.*, **2010**, *107*, 8939–8946.
- [75] A. Varki and P. Gagneux, “Human-specific evolution of sialic acid targets:

- Explaining the malignant malaria mystery?," **2009**, *106*, 14739-14740.
- [76] S. Bi and L. G. Baum, "Sialic acids in T cell development and function," *Biochim. Biophys. Acta BBA - Gen. Subj.*, **2009**, *1790*, 1599–1610.
- [77] H. Nie, Y. Li, and X. L. Sun. "Recent advances in sialic acid-focused glycomics," *J. Proteomics*, **2012**, *75*, 3098-3112.
- [78] J. L. Daniotti, R. D. Lardone, and A. A. Vilcaes, "Dysregulated Expression of Glycolipids in Tumor Cells: From Negative Modulator of Anti-tumor Immunity to Promising Targets for Developing Therapeutic Agents," *Front. Oncol.*, **2015**, *5*, 300.
- [79] S. Cavdarli *et al.*, "Profiling of O-acetylated Gangliosides Expressed in Neuroectoderm Derived Cells," *Int. J. Mol. Sci.*, **2020**, *21*, 370.
- [80] A. H. Ali, W. Wei, and X. Wang, "A review of milk gangliosides: Occurrence, biosynthesis, identification, and nutritional and functional significance," *Int. J. Dairy Technol.*, **2022**, *75*, 21–45.
- [81] N. Berois and E. Osinaga, "Glycobiology of Neuroblastoma: Impact on Tumor Behavior, Prognosis, and Therapeutic Strategies," *Front. Oncol.*, **2023**, *4*, 114.
- [82] S. Cavdarli, S. Groux-Degroote, and P. Delannoy, "Gangliosides: The Double-Edge Sword of Neuro-Ectodermal Derived Tumors," *Biomolecules*, **2019**, *9*, 311.
- [83] J. L. Daniotti and R. Iglesias-Bartolomé, "Metabolic pathways and intracellular trafficking of gangliosides," *IUBMB Life*, **2011**, *63*, 513–520.
- [84] N. Sasaki, M. Toyoda, and T. Ishiwata, "Gangliosides as Signaling Regulators in Cancer," *Int. J. Mol. Sci.*, **2021**, *22*, 5076.
- [85] E. Chiricozzi *et al.*, "GM1 promotes TrkA-mediated neuroblastoma cell differentiation by occupying a plasma membrane domain different from TrkA," *J. Neurochem.*, **2019**, *149*, 231–241.
- [86] J. H. Hwang *et al.*, "Caveolin-1-dependent and -independent uPAR signaling pathways contribute to ganglioside GT1b induced early apoptosis in A549 lung cancer cells," *Am. J. Cancer Res.*, **2014**, *4*, 801–810.
- [87] A. Cazet *et al.*, "The ganglioside G(D2) induces the constitutive activation of c-Met in MDA-MB-231 breast cancer cells expressing the G(D3) synthase," *Glycobiology*, **2012**, *22*, 806–816.
- [88] S. Hyuga *et al.*, "Ganglioside GD1a inhibits HGF-induced motility and scattering of cancer cells through suppression of tyrosine phosphorylation of c-Met," *Int. J. Cancer*, **2001**, *94*, 328–334.
- [89] N. Sasaki *et al.*, "Ganglioside GM2, highly expressed in the MIA PaCa-2 pancreatic ductal adenocarcinoma cell line, is correlated with growth, invasion, and advanced stage," *Sci. Rep.*, **2019**, *9*, 19369.
- [90] C. Tringali *et al.*, "The plasma membrane sialidase NEU3 regulates the malignancy of renal carcinoma cells by controlling β 1 integrin internalization and recycling," *J. Biol. Chem.*, **2012**, *287*, 42835–42845.
- [91] R. De Maria *et al.*, "Requirement for GD3 ganglioside in CD95- and ceramide-induced apoptosis," *Science*, **1997**, *277*, 1652–1655.
- [92] K. Hamamura *et al.*, "Functional activation of Src family kinase yes protein is

- essential for the enhanced malignant properties of human melanoma cells expressing ganglioside GD3," *J. Biol. Chem.*, **2011**, *286*, 18526–18537.
- [93] Y. Makino *et al.*, "A therapeutic trial of human melanomas with combined small interfering RNAs targeting adaptor molecules p130Cas and paxillin activated under expression of ganglioside GD3," *Biochim. Biophys. Acta*, **2016**, *1860*, 1753–1763.
- [94] N. V. Prokazova, N. N. Samoilova, E. V. Gracheva, and N. K. Golovanova, "Ganglioside GM3 and its biological functions," *Biochem. Mosc.*, **2009**, *74*, 235–249.
- [95] S. I. Hakomori and W. T. Murakami, "Glycolipids of hamster fibroblasts and derived malignant-transformed cell lines," *Proc. Natl. Acad. Sci. U. S. A.*, **1968**, *59*, 254–261.
- [96] P. T. Mora, R. O. Brady, R. M. Bradley, and V. W. McFarland, "Gangliosides in DNA virus-transformed and spontaneously transformed tumorigenic mouse cell lines," *Proc. Natl. Acad. Sci. U. S. A.*, **1969**, *63*, 1290–1296.
- [97] S. I. Hakomori, J. A. Wyke, and P. K. Vogt, "Glycolipids of chick embryo fibroblasts infected with temperature-sensitive mutants of avian sarcoma viruses," *Virology*, **1977**, *76*, 485–493.
- [98] M. H. Ravindranath, T. Tsuchida, D. L. Morton, and R. F. Irie, "Ganglioside GM3:GD3 ratio as an index for the management of melanoma," *Cancer*, **1991**, *67*, 3029–3035.
- [99] A. Merzak, S. Koochekpour, and G. J. Pilkington, "Cell surface gangliosides are involved in the control of human glioma cell invasion in vitro," *Neurosci. Lett.*, **1994**, *177*, 44–46.
- [100] S. Kawamura *et al.*, "Glycolipid composition in bladder tumor: A crucial role of GM3 ganglioside in tumor invasion," *Int. J. Cancer*, **2001**, *94*, 343–347.
- [101] A. Prinetti *et al.*, "GM3 synthase overexpression results in reduced cell motility and in caveolin-1 upregulation in human ovarian carcinoma cells," *Glycobiology*, **2010**, *20*, 62–77.
- [102] M. Ono, K. Handa, S. Sonnino, D. A. Withers, H. Nagai, and S. Hakomori, "GM3 ganglioside inhibits CD9-facilitated haptotactic cell motility: coexpression of GM3 and CD9 is essential in the downregulation of tumor cell motility and malignancy," *Biochemistry*, **2001**, *40*, 6414–6421.
- [103] C. Tringali *et al.*, "Silencing of membrane-associated sialidase Neu3 diminishes apoptosis resistance and triggers megakaryocytic differentiation of chronic myeloid leukemic cells K562 through the increase of ganglioside GM3," *Cell Death Differ.*, **2009**, *16*, 164–174.
- [104] H. Zhao and Y. Ma, "Effects of ganglioside GM3 on proliferation and cell cycle of multiple myeloma cell line U266," *J. Leuk. Lymphoma*, **2017**, *12*, 457–460.
- [105] N. Hanai, G. A. Nores, C. MacLeod, C. R. Torres-Mendez, and S. Hakomori, "Ganglioside-mediated modulation of cell growth. Specific effects of GM3 and lyso-GM3 in tyrosine phosphorylation of the epidermal growth factor receptor," *J. Biol. Chem.*, **1988**, *263*, 10915–10921.

- [106] E. J. Meuillet *et al.*, "Sialidase gene transfection enhances epidermal growth factor receptor activity in an epidermoid carcinoma cell line, A431," *Cancer Res.*, **1999**, *59*, 234–240.
- [107] E. J. Meuillet, B. Mania-Farnell, D. George, J. I. Inokuchi, and E. G. Bremer, "Modulation of EGF receptor activity by changes in the GM3 content in a human epidermoid carcinoma cell line, A431," *Exp. Cell Res.*, **2000**, *256*, 74–82.
- [108] W. X. Song, M. F. Vacca, R. Welti, and D. A. Rintoul, "Effects of gangliosides GM3 and De-N-acetyl GM3 on epidermal growth factor receptor kinase activity and cell growth," *J. Biol. Chem.*, **1991**, *266*, 10174–10181.
- [109] Q. Zhou, S. Hakomori, K. Kitamura, and Y. Igarashi, "GM3 directly inhibits tyrosine phosphorylation and de-N-acetyl-GM3 directly enhances serine phosphorylation of epidermal growth factor receptor, independently of receptor-receptor interaction," *J. Biol. Chem.*, **1994**, *269*, 1959–1965.
- [110] E. A. Miljan *et al.*, "Interaction of the Extracellular Domain of the Epidermal Growth Factor Receptor with Gangliosides*," *J. Biol. Chem.*, **2002**, *277*, 10108–10113.
- [111] B. L. Mirkin, S. H. Clark, and C. Zhang, "Inhibition of human neuroblastoma cell proliferation and EGF receptor phosphorylation by gangliosides GM1, GM3, GD1A and GT1B," *Cell Prolif.*, **2002**, *35*, 105–115.
- [112] S. J. Yoon *et al.*, "Interaction of N-linked glycans, having multivalent GlcNAc termini, with GM3 ganglioside," *Glycoconj. J.*, **2006**, *23*, 639–649.
- [113] S. J. Yoon, K. Nakayama, T. Hikita, K. Handa, and S. Hakomori, "Epidermal growth factor receptor tyrosine kinase is modulated by GM3 interaction with N-linked GlcNAc termini of the receptor," *Proc. Natl. Acad. Sci. U. S. A.*, **2006**, *103*, 18987–18991.
- [114] N. Kawashima, S.-J. Yoon, K. Itoh, and K. Nakayama, "Tyrosine kinase activity of epidermal growth factor receptor is regulated by GM3 binding through carbohydrate to carbohydrate interactions," *J. Biol. Chem.*, **2009**, *284*, 6147–6155.
- [115] A. Prinetti, N. Loberto, V. Chigorno, and S. Sonnino, "Glycosphingolipid behaviour in complex membranes," *Biochim. Biophys. Acta*, **2009**, *1788*, 184–193.
- [116] M. Shibuya, "Vascular Endothelial Growth Factor (VEGF) and Its Receptor (VEGFR) Signaling in Angiogenesis: A Crucial Target for Anti- and Pro-Angiogenic Therapies," *Genes Cancer*, **2011**, *2*, 1097–1105.
- [117] V. Loizzi *et al.*, "Biological Pathways Involved in Tumor Angiogenesis and Bevacizumab Based Anti-Angiogenic Therapy with Special References to Ovarian Cancer," *Int. J. Mol. Sci.*, **2017**, *18*, 1967.
- [118] M. Ziche, G. Alessandri, and P. M. Gullino, "Gangliosides promote the angiogenic response," *Lab. Investig. J. Tech. Methods Pathol.*, **1989**, *61*, 629–634.
- [119] M. Ziche, L. Morbidelli, G. Alessandri, and P. M. Gullino, "Angiogenesis can be stimulated or repressed in vivo by a change in GM3:GD3 ganglioside ratio,"

- Lab. Investig. J. Tech. Methods Pathol.*, **1992**, 67, 711–715.
- [120] G. Alessandri, P. Cornaglia-Ferraris, and P. M. Gullino, “Angiogenic and angiostatic microenvironment in tumors--role of gangliosides,” *Acta Oncol. Stockh. Swed.*, **1997**, 36, 383–387.
- [121] L. E. Abate, P. Mukherjee, and T. N. Seyfried, “Gene-linked shift in ganglioside distribution influences growth and vascularity in a mouse astrocytoma,” *J. Neurochem.*, **2006**, 98, 1973–1984.
- [122] P. Mukherjee, A. C. Faber, L. M. Shelton, R. C. Baek, T. C. Chiles, and T. N. Seyfried, “Thematic review series: sphingolipids. Ganglioside GM3 suppresses the proangiogenic effects of vascular endothelial growth factor and ganglioside GD1a,” *J. Lipid Res.*, **2008**, 49, 929–938.
- [123] T. N. Seyfried and P. Mukherjee, “Ganglioside GM3 Is Antiangiogenic in Malignant Brain Cancer,” *J. Oncol.*, **2010**, 961243.
- [124] Y. Kawakami *et al.*, “Tetraspanin CD9 Is a ‘Proteolipid,’ and Its Interaction with $\alpha 3$ Integrin in Microdomain Is Promoted by GM3 Ganglioside, Leading to Inhibition of Laminin-5-dependent Cell Motility,” *J. Biol. Chem.*, **2002**, 277, 34349–34358.
- [125] Y. Kariya and K. Miyazaki, “The basement membrane protein laminin-5 acts as a soluble cell motility factor,” *Exp. Cell Res.*, **2004**, 297, 508–520.
- [126] K. Mitsuzuka, K. Handa, M. Satoh, Y. Arai, and S. Hakomori, “A Specific Microdomain (‘Glycosynapse 3’) Controls Phenotypic Conversion and Reversion of Bladder Cancer Cells through GM3-mediated Interaction of $\alpha 3\beta 1$ Integrin with CD9*,” *J. Biol. Chem.*, **2005**, 280, 35545–35553.
- [127] D. P. Choma, V. Milano, K. M. Pumiglia, and C. M. DiPersio, “Integrin $\alpha 3\beta 1$ -Dependent Activation of FAK/Src Regulates Rac1-Mediated Keratinocyte Polarization on Laminin-5,” *J. Invest. Dermatol.*, **2007**, 127, 31–40.
- [128] L. Wong *et al.*, “Coupled Motions in the SH2 and Kinase Domains of Csk Control Src Phosphorylation,” *J. Mol. Biol.*, **2005**, 351, 131–143.
- [129] M. S. Toledo, E. Suzuki, K. Handa, and S. Hakomori, “Cell Growth Regulation through GM3-enriched Microdomain (Glycosynapse) in Human Lung Embryonal Fibroblast WI38 and Its Oncogenic Transformant VA13,” *J. Biol. Chem.*, **2004**, 279, 34655–34664.
- [130] A. R. Todeschini, J. N. Dos Santos, K. Handa, and S. Hakomori, “Ganglioside GM2/GM3 complex affixed on silica nanospheres strongly inhibits cell motility through CD82/cMet-mediated pathway,” *Proc. Natl. Acad. Sci.*, **2008**, 105, 1925–1930.
- [131] Y. Zhang *et al.*, “Function of the c-Met receptor tyrosine kinase in carcinogenesis and associated therapeutic opportunities,” *Mol. Cancer*, **2018**, 17, 1–14.
- [132] S. Raj *et al.*, “Molecular mechanism(s) of regulation(s) of c-MET/HGF signaling in head and neck cancer,” *Mol. Cancer*, **2022**, 1, 1–16.
- [133] S. I. Hakomori and K. Handa, “GM3 and cancer,” *Glycoconj. J.*, **2015**, 32, 1–8.
- [134] A. Regina Todeschini and S. Hakomori, “Functional role of

- glycosphingolipids and gangliosides in control of cell adhesion, motility, and growth, through glycosynaptic microdomains," *Biochim. Biophys. Acta*, **2008**, *1780*, 421–433.
- [135] N. Kawashima *et al.*, "Efficient synthesis of chloro-derivatives of sialosyllactosylceramide, and their enhanced inhibitory effect on epidermal growth factor receptor activation," *Oncol. Lett.*, **2014**, *7*, 933–940.
- [136] Z. Y. Zhu, and Y. M. Zhang, "An Efficient Method for Ganglioside GM3 Preparation," *Acta Chim. Sin.*, **2007**, *65*, 2909.
- [137] M. Zheng and X.-S. Ye, "Synthesis of N-modified ganglioside GM3 derivatives," *Tetrahedron*, **2012**, *68*, 1475–1482.
- [138] T. Li, X. Wang, P. Dong, P. Yu, Y. Zhang, and X. Meng, "Chemoenzymatic synthesis and biological evaluation of ganglioside GM3 and lyso-GM3 as potential agents for cancer therapy," *Carbohydr. Res.*, **2021**, *509*, 108431.
- [139] A. Hasegawa, M. Ogawa, and M. Kiso, "Synthesis of a Ganglioside GM3 Position Isomer, N-Acetylneuraminosyl- α (2 \rightarrow 6)-lactosyl- β (1 \rightarrow 1)-ceramide," *Biosci., Biotechnol., Biochem.*, **1992**, *56*, 535-536.
- [140] G. Hirai, M. Kato, H. Koshino, E. Nishizawa, K. Oonuma, E. Ota, and M. Sodeoka, "Ganglioside GM3 Analogues Containing Monofluoromethylene-Linked Sialoside: Synthesis, Stereochemical Effects, Conformational Behavior, and Biological Activities" **2020**, *1*, 137-146.
- [141] Y. Haga, K. Hatanaka, and S. Hakomori, "Effect of lipid mimetics of GM3 and lyso-GM3 dimer on EGF receptor tyrosine kinase and EGF-induced signal transduction," *Biochim. Biophys. Acta*, **2007**, *1780*, 393–404.
- [142] Y. Murozuka, N. Watanabe, K. Hatanaka, and S. Hakomori, "Lyso-GM3, its dimer, and multimer: their synthesis, and their effect on epidermal growth factor-induced receptor tyrosine kinase," *Glycoconj. J.*, **2007**, *24*, 551–563.
- [143] J. J. Lundquist and E. J. Toone, "The Cluster Glycoside Effect," *Chem. Rev.*, **2002**, *102*, 555–578.
- [144] N. Horan, L. Yan, H. Isobe, G. M. Whitesides, and D. Kahne, "Nonstatistical binding of a protein to clustered carbohydrates," *Proc. Natl. Acad. Sci.*, **1999**, *96*, 11782–11786.
- [145] L. L. Kiessling, J. E. Gestwicki, and L. E. Strong, "Synthetic multivalent ligands in the exploration of cell-surface interactions," *Curr. Opin. Chem. Biol.*, **2000**, *4*, 696–703.
- [146] W. Wang and F. Kong, "New Synthetic Methodology for Regio- and Stereoselective Synthesis of Oligosaccharides via Sugar Ortho Ester Intermediates," *J. Org. Chem.*, **1998**, *63*, 5744–5745.
- [147] C. Zheng *et al.*, "Chemoenzymatically synthesized ganglioside GM3 analogues with inhibitory effects on tumor cell growth and migration," *Eur. J. Med. Chem.*, **2019**, *165*, 107–114.
- [148] H. Qu *et al.*, "Synthesis and cytotoxicity assay of four ganglioside GM3 analogues," *Eur. J. Med. Chem.*, **2014**, *75*, 247–257.
- [149] R. Šardžik, G. T. Noble, M. J. Weissenborn, A. Martin, S. J. Webb, and S. L. Flitsch, "Preparation of aminoethyl glycosides for glycoconjugation," *Beilstein*

- J. Org. Chem.*, **2010**, *6*, 699–703.
- [150] M. Baier, J. L. Ruppertz, M. M. Pfleiderer, B. S. Blaum, and L. Hartmann, "Synthesis of highly controlled carbohydrate-polymer based hybrid structures by combining heparin fragments and sialic acid derivatives, and solid phase polymer synthesis," *Chem. Commun.*, **2018**, *54*, 10487–10490.
- [151] M. Filice, J. M. Guisan, M. Terreni, and J. M. Palomo, "Regioselective monodeprotection of peracetylated carbohydrates," *Nat. Protoc.*, **2012**, *7*, 1783–1796.
- [152] M. Filice *et al.*, "Chemo-biocatalytic regioselective one-pot synthesis of different deprotected monosaccharides," *Catal. Today*, **2009**, *140*, 1–18.
- [153] T. Bavaro *et al.*, "Chemoenzymatic synthesis of neoglycoproteins driven by the assessment of protein surface reactivity," *RSC Adv*, **2014**, *4*, 56455–56465.
- [154] R. R. Schmidt and P. Zimmermann, "Synthesis of Glycosphingolipids and Psychosines," *Angew. Chem. Int. Ed. Engl.*, **1986**, *25*, 725–726.
- [155] T. Bär and R. R. Schmidt, "Glycosylimidate, 35 Synthese eines Cerebrosids mit (4E,8E)-Sphingadienin-Struktur aus *Tetragonia tetragonoides* mit antiulcerogener Aktivität," *Liebigs Ann. Chem.*, **1988**, *7*, 669–674.
- [156] Y. D. Vankar and R. R. Schmidt, "Chemistry of glycosphingolipids—carbohydrate molecules of biological significance," *Chem. Soc. Rev.*, **2000**, *29*, 201–216.
- [157] P. Zimmermann and R. R. Schmidt, "Synthese von erythro-Sphingosinen über die Azidoderivate," *Liebigs Ann. Chem.*, **1988**, *7*, 663–667.
- [158] Y. Ito, M. Kiso, and A. Hasegawa, "Studies on the Thioglycosides of *N*-Acetylneuraminic Acid. 6: Synthesis of Ganglioside GM₄ Analogs¹," *J. Carbohydr. Chem.*, **1989**, *8*, 285–294.
- [159] P. Kumar and R. R. Schmidt, "An Efficient Stereoselective Synthesis of Sphingosine," *Synthesis*, **1998**, *1*, 33–35.
- [160] P. M. Koskinen, "Sphingosine, an Enigmatic Lipid: A Review of Recent Literature Syntheses," *Synthesis*, **1998**, *8*, 1075–1091.
- [161] J. Ohlsson and G. Magnusson, "A short and practical route to 3-O-benzoyl azidosphingosine," *Carbohydr. Res.*, **2001**, *331*, 91–94.
- [162] R. J. B. H. N. van den Berg, C. G. N. Korevaar, G. A. van der Marel, H. S. Overkleeft, and J. H. van Boom, "A simple and low cost synthesis of d-erythro-sphingosine and d-erythro-azidosphingosine from d-ribo-phytosphingosine: glycosphingolipid precursors," *Tetrahedron Lett.*, **2002**, *43*, 8409–8412.
- [163] Y. Gao, X. He, F. Ding, and Y. Zhang, "Recent Progress in Chemical Syntheses of Sphingosines and Phytosphingosines," *Synthesis*, **2016**, *48*, 4017–4037.
- [164] R. R. Schmidt and P. Zimmermann, "Synthesis of d-erythro-sphingosines," *Tetrahedron Lett.*, **1986**, *27*, 481–484.
- [165] O. H. Abdelmageed, R. I. Duclos, E. Abushanab, and A. Makriyannis, "Chiroselective syntheses of 2H- and 13C-labeled 1-O-alkyl-2-O-alkyl'-sn-glycero-3-phosphoethanolamines and 1-O-alkyl-2-O-alkyl'-sn-glycero-3-

- phosphocholines," *Chem. Phys. Lipids*, **1990**, *54*, 49–59.
- [166] K.-H. Jung and R. Schmidt, "Synthesis of sphingosine, radiolabeled-sphingosine, 4-methyl-cis-sphingosine, and 1-amino derivatives of sphingosine via their azido derivatives," *Methods Enzymol.*, **2000**, *311*, 441–457.
- [167] D. G. Churchill, "Chemical Structure and Accidental Explosion Risk in the Research Laboratory," *J. Chem. Educ.*, **2006**, *83*, 1798.
- [168] M. von Itzstein and R. J. Thomson, "The synthesis of novel sialic acids as biological probes," in *Glycoscience Synthesis of Oligosaccharides and Glycoconjugates*, **2008**, *186*, 119–170.
- [169] D. Ress and R. Linhardt, "Sialic Acid Donors: Chemical Synthesis and Glycosylation," *Curr. Org. Synth.*, **2004**, *1*, 31–46.
- [170] C. De Meo and B. T. Jones, "Chemical Synthesis of Glycosides of N-Acetylneuraminic Acid," in *Advances in Carbohydrate Chemistry and Biochemistry*, **2018**, *75*, 215–316.
- [171] V. Martichonok and G. M. Whitesides, "Stereoselective α -Sialylation with Sialyl Xanthate and Phenylsulfenyl Triflate as a Promotor," *J. Org. Chem.*, **1996**, *61*, 1702–1706.
- [172] D. J. M. van der Vleugel, W. A. R. van Heeswijk, and J. F. G. Vliegthart, "A facile preparation of alkyl α -glycosides of the methyl ester of N-acetyl-d-neuraminic acid," *Carbohydr. Res.*, **1982**, *102*, 121–130.
- [173] K. Okamoto, T. Kondo, and T. Goto, "Glycosylation of 4,7,8,9-Tetra-O-acetyl-2-deoxy-2 β ,3 β -epoxy-N-acetylneuraminic Acid Methyl Ester," *Bull. Chem. Soc. Jpn.*, **1987**, *60*, 637–643.
- [174] U. Dabrowski, H. Friebolin, R. Brossmer, and M. Supp, "1H-NMR studies at N-acetyl-D-neuraminic acid ketosides for the determination of the anomeric configuration II.," *Tetrahedron Lett.*, **1979**, *20*, 4637–4640.
- [175] J. Haverkamp, H. Van Halbeek, L. Dorland, J. F. G. Vliegthart, R. Pfeil, and R. Schauer, "High-Resolution 1H-NMR Spectroscopy of Free and Glycosidically Linked O-Acetylated Sialic Acids," *Eur. J. Biochem.*, **1982**, *122*, 305–311.
- [176] H. Hori, T. Nakajima, Y. Nishida, H. Ohru, and H. Meguro, "A simple method to determine the anomeric configuration of sialic acid and its derivatives by 13C-NMR," *Tetrahedron Lett.*, **1988**, *29*, 6317–6320.
- [177] R. Christian, G. Schulz, H. H. Brandstetter, and E. Zbiral, "On the side-chain conformation of N-acetylneuraminic acid and its epimers at C-7, C-8, and C-7,8," *Carbohydr. Res.*, **1987**, *162*, 1–11.
- [178] S. Prytulla, J. Lambert, J. Lauterwein, M. Klessinger, and J. Thiem, "Configurational assignment in N-acetylneuraminic acid and analogues via the geminal C,H coupling constants," *Magn. Reson. Chem.*, **1990**, *28*, 888–901.
- [179] H. C. Kolb and K. B. Sharpless, "The growing impact of click chemistry on drug discovery," *Drug Discov. Today*, **2003**, *8*, 1128–1137.
- [180] S. André, B. Liu, H.-J. Gabius, and R. Roy, "First demonstration of differential inhibition of lectin binding by synthetic tri- and tetravalent

- glycoclusters from cross-coupling of rigidified 2-propynyl lactoside," *Org Biomol Chem*, **2003**, *1*, 3909–3916.
- [181] W.-Q. Zhang *et al.*, "Polyvalent effect enhances diglycosidic antiplasmodial activity," *Eur. J. Med. Chem.*, **2016**, *121*, 640–648.
- [182] Z.-L. Yang *et al.*, "Synthesis of multivalent difluorinated zanamivir analogs as potent antiviral inhibitors," *Tetrahedron Lett.*, **2016**, *57*, 2579–2582.
- [183] H. C. Kolb, M. G. Finn, and K. B. Sharpless, "Click Chemistry: Diverse Chemical Function from a Few Good Reactions," *Angew. Chem. Int. Ed.*, **2001**, *40*, 2004–2021.
- [184] H. C. Kolb, M. G. Finn, and K. B. Sharpless, "Click Chemistry: Diverse Chemical Function from a Few Good Reactions," *Angew. Chem. Int. Ed Engl.*, **2001**, *40*, 2004–2021.
- [185] J. E. Moses and A. D. Moorhouse, "The growing applications of click chemistry," *Chem. Soc. Rev.*, **2007**, *36*, 1249–1262.
- [186] P. Thirumurugan, D. Matosiuk, and K. Jozwiak, "Click Chemistry for Drug Development and Diverse Chemical–Biology Applications," *Chem. Rev.*, **2013**, *113*, 4905–4979.
- [187] W. H. Binder and C. Kluger, "Azide/Alkyne-‘Click’ Reactions: Applications in Material Science and Organic Synthesis," *Curr. Org. Chem.*, **2006**, *10*, 1791–1815.
- [188] X. Jiang *et al.*, "Recent applications of click chemistry in drug discovery," *Expert Opin. Drug Discov.*, **2019**, *14*, 779–789.
- [189] F. Musumeci, S. Schenone, A. Desogus, E. Nieddu, D. Deodato, and L. Botta, "Click chemistry, a potent tool in medicinal sciences," *Curr. Med. Chem.*, **2015**, *22*, 2022–2050.
- [190] R. Huisgen, "1,3-Dipolar Cycloadditions. Past and Future," *Angew. Chem. Int. Ed. Engl.*, **1963**, *2*, 565–598.
- [191] V. V. Rostovtsev, L. G. Green, V. V. Fokin, and K. B. Sharpless, "A Stepwise Huisgen Cycloaddition Process: Copper(I)-Catalyzed Regioselective ‘Ligation’ of Azides and Terminal Alkynes," *Angew. Chem. Int. Ed.*, **2002**, *41*, 2596–2599.
- [192] C. W. Tornøe, C. Christensen, and M. Meldal, "Peptidotriazoles on Solid Phase: [1,2,3]-Triazoles by Regiospecific Copper(I)-Catalyzed 1,3-Dipolar Cycloadditions of Terminal Alkynes to Azides," *J. Org. Chem.*, **2002**, *67*, 3057–3064.
- [193] V. O. Rodionov, S. I. Presolski, D. D. Díaz, V. V. Fokin, and M. G. Finn, "Ligand-accelerated Cu-catalyzed azide-alkyne cycloaddition: a mechanistic report," *J. Am. Chem. Soc.*, **2007**, *129*, 12705–12712.
- [194] J. E. Hein and V. V. Fokin, "Copper-catalyzed azide–alkyne cycloaddition (CuAAC) and beyond: new reactivity of copper (I) acetylides," *Chem. Soc. Rev.*, **2010**, *39*, 1302–1315.
- [195] "‘Click’-reaction: An alternative tool for new architectures of porphyrin based derivatives | Elsevier Enhanced Reader."
- [196] C. Zheng, M. Terreni, M. Sollogoub, and Y. Zhang, "Ganglioside GM3 and Its Role in Cancer," *Curr. Med. Chem.*, **2019**, *26*, 2933–2947.

- [197] P. Wang *et al.*, "GM3 Upregulation of Matrix Metalloproteinase-9 Possibly Through PI3K, AKT, RICTOR, RHOGDI-2, and TNF-A Pathways in Mouse Melanoma B16 Cells," in *The Molecular Immunology of Complex Carbohydrates-3*, Boston, MA, **2011**, 705, 335–348.
- [198] C. Wilson *et al.*, "Overcoming EMT-associated resistance to anti-cancer drugs via Src/FAK pathway inhibition," *Oncotarget*, **2014**, 5, 7328–7341.
- [199] J. Pijuan *et al.*, "In vitro Cell Migration, Invasion, and Adhesion Assays: From Cell Imaging to Data Analysis," *Front. Cell Dev. Biol.*, **2019**, 7, 107.
- [200] C. Zheng, R. Huang, T. Bavaro, M. Terreni, M. Sollogoub, J. Xu, and Y. Zhang, "Design, synthesis and biological evaluation of new ganglioside GM3 analogues as potential agents for cancer therapy," *Eur. J. Med. Chem.*, **2020**, 189, 112065.
- [201] Y. M. Yang and W. X. Yang, "Epithelial-to-mesenchymal transition in the development of endometriosis," *Oncotarget*, **2017**, 8, 41679–41689.
- [202] E. Tomaskovic-Crook, E. W. Thompson, and J. P. Thiery, "Epithelial to mesenchymal transition and breast cancer," *Breast Cancer Res.*, **2009**, 11, 1–10.
- [203] M. Li *et al.*, "Biological role of metabolic reprogramming of cancer cells during epithelial-mesenchymal transition," *Oncol. Rep.*, **2019**, 41, 727-741.
- [204] M. Li, X. Bu, B. Cai, P. Liang, K. Li, X. Qu, and L. Shen, "Biological role of metabolic reprogramming of cancer cells during epithelial - mesenchymal transition," *Oncol. Rep.*, **2019**, 41, 727-741.
- [205] A. Kazi *et al.*, "GSK3 suppression upregulates β -catenin and c-Myc to abrogate KRas-dependent tumors," *Nat. Commun.*, **2018**, 9, 5154.
- [206] X. Cheng, X. Xu, D. Chen, F. Zhao, and W. Wang, "Therapeutic potential of targeting the Wnt/ β -catenin signaling pathway in colorectal cancer," *Biomed. Pharmacother.*, **2019**, 110, 473-481.
- [207] P. Duda *et al.*, "Targeting GSK3 and Associated Signaling Pathways Involved in Cancer," *Cells*, **2020**, 9, 1110.
- [208] K. B. Cho, M. K. Cho, W. Y. Lee, and K. W. Kang, "Overexpression of c-myc induces epithelial mesenchymal transition in mammary epithelial cells," *Cancer Lett.*, **2010**, 293, 230–239.
- [209] Z. Guan, Y. Wang, Y. Chen, L. Zhang, and Y. Zhang, "Novel approach for synthesis of 2:1 permethylated β -cyclodextrin-C60 conjugate," *Tetrahedron*, **2009**, 65, 1125–1129.
- [210] G. Crini, S. Fourmentin, É. Fenyvesi, G. Torri, M. Fourmentin, and N. Morin-Crini, "Cyclodextrins, from molecules to applications," *Environ. Chem. Lett.*, **2018**, 16, 1361–1375.
- [211] J. Y. LIU, X. ZHANG, and B. R. TIAN, "Selective modifications at the different positions of cyclodextrins: a review of strategies," *Turk. J. Chem.*, **2020**, 44, 261–278.
- [212] S. S. Jambhekar and P. Breen, "Cyclodextrins in pharmaceutical formulations I: structure and physicochemical properties, formation of complexes, and types of complex," *Drug Discov. Today*, **2016**, 21, 356–362.

- [213] G. Rivero-Barbarroja, J. M. Benito, C. Ortiz Mellet, and J. M. García Fernández, "Cyclodextrin-Based Functional Glyconanomaterials," *Appl. Nanomater.*, **2020**, *10*, 2517.
- [214] A. Joshi *et al.*, "Structure-Based Design of a Heptavalent Anthrax Toxin Inhibitor," *Biomacromolecules*, **2011**, *12*, 791–796.
- [215] C. Decroocq, D. Rodríguez-Lucena, V. Russo, T. Mena Barragán, C. Ortiz Mellet, and P. Compain, "The Multivalent Effect in Glycosidase Inhibition: Probing the Influence of Architectural Parameters with Cyclodextrin-based Iminosugar Click Clusters," *Chem. – Eur. J.*, **2011**, *17*, 13825–13831.
- [216] S. Xiao *et al.*, "Synthesis and biological evaluation of novel pentacyclic triterpene α -cyclodextrin conjugates as HCV entry inhibitors," *Eur. J. Med. Chem.*, **2016**, *124*, 1–9.
- [217] P. Jiao *et al.*, "Facile preparation and characterization of novel oleanane-type triterpene functionalized β -cyclodextrin conjugates," *Chin. Chem. Lett.*, **2019**, *30*, 690–693.
- [218] Y. Chen *et al.*, "Synthesis of a Hexavalent Betulinic Acid Derivative as a Hemagglutinin-Targeted Influenza Virus Entry Inhibitor," *Mol. Pharm.*, **2020**, *17*, 2546–2554.
- [219] O. Kocabiyik *et al.*, "Non-Toxic Virucidal Macromolecules Show High Efficacy Against Influenza Virus Ex Vivo and In Vivo," *Adv. Sci.*, **2021**, *8*, 2001012.
- [220] G. Crini, S. Fourmentin, É. Fenyvesi, G. Torri, M. Fourmentin, and N. Morin-Crini, "Cyclodextrins, from molecules to applications," *Environ. Chem. Lett.*, **2018**, *16*, 1361–1375.
- [221] K. Takeo, K. Ueraura, and H. Mitoh, "Derivatives Of α -Cyclodextrin and the Synthesis of 6-O- α -D-Glucopyranosyl- α -Cyclodextrin," *J. Carbohydr. Chem.*, **1988**, *7*, 293–308.
- [222] O. Jurcek *et al.*, "Heads or Tails? Sandwich-Type Metallocomplexes of Hexakis(2,3-di-O-methyl)- α -cyclodextrin," *Cryst. Growth Des.*, **2020**, *20*, 4193–4199.
- [223] R. Wang, D. H. Steensma, Y. Takaoka, J. W. Yun, T. Kajimoto, and C. H. Wong, "A search for pyrophosphate mimics for the development of substrates and inhibitors of glycosyltransferases," *Bioorg. Med. Chem.*, **1997**, *5*, 661–672.
- [224] Y. Huang, Q. Chai, M. R. Warmin, and N. Ayres, "Lactose-containing hydrogels for enzyme stabilization," *J. Polym. Sci. Part Polym. Chem.*, **2016**, *54*, 2507–2514.
- [225] A. Santra, Y. Li, H. Yu, T. J. Slack, P. G. Wang, and X. Chen, "Highly efficient chemoenzymatic synthesis and facile purification of α -Gal pentasaccharyl ceramide Gal α 3nLc₄ β Cer," *Chem. Commun.*, **2017**, *53*, 8280–8283.
- [226] T. Murase, H. Ishida, M. Kiso, and A. Hasegawa, "A facile, regio- and stereo-selective synthesis of ganglioside GM3," *Carbohydr. Res.*, **1989**, *188*, 71–80.
- [227] Y. Ito and J. C. Paulson, "A novel strategy for synthesis of ganglioside GM3 using an enzymically produced sialoside glycosyl donor," *J. Am. Chem. Soc.*, **1993**, *115*, 1603–1605.

- [228] K. K. C. Liu and S. J. Danishefsky, "A striking example of the interfacing of glycal chemistry with enzymatically mediated sialylation: a concise synthesis of ganglioside GM3," *J. Am. Chem. Soc.*, **1993**, *115*, 4933–4934.
- [229] T. Tomoo, T. Kondo, H. Abe, S. Tsukamoto, M. Isobe, and T. Goto, "An efficient short-step total synthesis of ganglioside GM3: effective usage of the neighbouring group participation strategy," *Carbohydr. Res.*, **1996**, *284*, 207–222.
- [230] U. Zehavi and A. Tuchinsky, "Enzymic glycosphingolipid synthesis on polymer supports. III. Synthesis of GM3, its analog [NeuNAc α (2-3)Gal β (1-4)Glc β (1-3)Cer] and their lyso-derivatives," *Glycoconj. J.*, **1998**, *15*, 657–662.
- [231] L. Mauri, R. Casellato, G. Kirschner, and S. Sonnino, "A procedure for the preparation of GM3 ganglioside from GM1-lactone," *Glycoconj. J.*, **1999**, *16*, 197–203.
- [232] R. I. Duclos, "The total synthesis of ganglioside GM3," *Carbohydr. Res.*, **2000**, *328*, 489–507.
- [233] H. Yu *et al.*, "Chemoenzymatic Total Synthesis of GM3 Gangliosides Containing Different Sialic Acid Forms and Various Fatty Acyl Chains," *J. Org. Chem.*, **2021**, *86*, 8672–8682.
- [234] S. Huang, H. Yu, and X. Chen, "Chemoenzymatic synthesis of α 2-3-sialylated carbohydrate epitopes," *Sci. China Chem.*, **2011**, *54*, 117–128.
- [235] H. Yu *et al.*, "Streamlined chemoenzymatic total synthesis of prioritized ganglioside cancer antigens," *Org. Biomol. Chem.*, **2018**, *16*, 4076–4080.
- [236] H. Yu *et al.*, "Sequential One-Pot Multienzyme Chemoenzymatic Synthesis of Glycosphingolipid Glycans," *J. Org. Chem.*, **2016**, *81*, 10809–10824.
- [237] A. Santra, Y. Li, T. Ghosh, R. Li, H. Yu, and X. Chen, "Regioselective One-Pot Multienzyme (OPME) Chemoenzymatic Strategies for Systematic Synthesis of Sialyl Core 2 Glycans," *ACS Catal.*, **2019**, *9*, 211–215.
- [238] T. Li, X. Wang, P. Dong, P. Yu, Y. Zhang, and X. Meng, "Chemoenzymatic synthesis and biological evaluation of ganglioside GM3 and lyso-GM3 as potential agents for cancer therapy," *Carbohydr. Res.*, **2021**, *509*, 108431.
- [239] X. Chen and A. Varki, "Advances in the Biology and Chemistry of Sialic Acids," *ACS Chem. Biol.*, **2010**, *5*, 163–176.
- [240] L. F. Tietze and D. Gretzke, "Synthesis of Specifically Labelled Ganglioside [1c-13C]-GM3," *Eur. J. Org. Chem.*, **1998**, *9*, 1895–1899.
- [241] A. Hasegawa, T. Nagahama, H. Ohki, and M. Kiso, "Synthetic Studies on Sialoglycoconjugates 41: A Facile Total Synthesis of Ganglioside GM2," *J. Carbohydr. Chem.*, **1992**, *11*, 699–714.
- [242] R. Kuhn, P. Lutz, and D. L. Macdonald, "Synthese anomerer Sialinsäuremethylketoside," *Chem. Ber.*, **1966**, *99*, 611–617.
- [243] I. Carlescu, H. M. I. Osborn, J. Desbrieres, D. Scutaru, and M. Popa, "Synthesis of poly(aspartimide)-based bio-glycoconjugates," *Carbohydr. Res.*, **2010**, *345*, 33–40.
- [244] V. Martichonok and G. M. Whitesides, "A Practical Method for the Synthesis of Sialyl α -Glycosides," *J. Am. Chem. Soc.*, **1996**, *118*, 8187–8191.

- [245] I. Kalograiaki, M. Abellán-Flos, L. Á. Fernández, M. Menéndez, S. P. Vincent, and D. Solís, "Direct Evaluation of Live Uropathogenic *Escherichia coli* Adhesion and Efficiency of Antiadhesive Compounds Using a Simple Microarray Approach," *Anal. Chem.*, **2018**, *90*, 12314–12321.
- [246] K. Ohashi *et al.*, "Syntheses of D-erythro-1-deoxydihydroceramide-1-sulfonic acid and phosphosphingoglycolipid found in marine organisms via a common precursor," *Tetrahedron*, **1989**, *45*, 2557–2570.
- [247] L. Almasi and A. Hantz, "Die Arylschwefelchloride und ihre Molekularrefraktion," *Chem. Ber.*, **1961**, *94*, 725–728.
- [248] F. G. Calvo-Flores *et al.*, "1,3-Dipolar Cycloadditions as a Tool for the Preparation of Multivalent Structures," *Org. Lett.*, **2000**, *2*, 2499–2502.
- [249] H. A. Moynihan, J. A. Hayes, K. S. Eccles, S. J. Coles, and S. E. Lawrence, "Hydrogen bonding in crystal forms of primary amide functionalised glucose and cellobiose," *Carbohydr. Res.*, **2013**, *374*, 29–39.
- [250] K. Jansson *et al.*, "2-(Trimethylsilyl)ethyl glycosides. 3. Synthesis, anomeric deblocking, and transformation into 1,2-trans 1-O-acyl sugars," *J. Org. Chem.*, **1988**, *53*, 5629–5647.